Novel Stress T1-mapping Applications for the Assessment of Cardiovascular Disease

Matthew K. Burrage

BSc, MBBS, FRACP



Green Templeton College

Division of Cardiovascular Medicine

Radcliffe Department of Medicine

University of Oxford

A thesis submitted for the degree of

Doctor of Philosophy in Medical Sciences

Trinity Term 2021

Declaration

This Thesis is entirely my own work unless otherwise indicated. It has not been submitted, either wholly or substantially, for another degree at this university, or for a degree at any other institution. I have acknowledged assistance from colleagues and collaborators where relevant. Professor Vanessa Ferreira provided data on patients with end-stage renal disease (Chapter 3) and patients with coronary artery disease (Chapter 5). Dr Leo Yun (Mackay Memorial Hospital, Taipei, Taiwan) provided dipyridamole patient data (Chapter 7).

The total word count is 42,024 words (excluding bibliography).

Abstract

Cardiovascular disease (and particularly coronary artery disease and ischaemic heart disease) remains the leading cause of morbidity and mortality worldwide. There is increasing need for non-invasive imaging tests and biomarkers that could allow early therapeutic interventions and help risk-stratify and prognosticate to improve individual outcomes. Cardiovascular magnetic resonance (CMR) is a powerful non-invasive and radiation-free imaging tool that can comprehensively evaluate cardiac structure, function, and ischaemia, and allows advanced myocardial tissue characterisation. Stress T1-mapping is a promising contrast-free CMR application that assesses coronary vasodilatory reserve and has shown utility in the non-invasive assessment of cardiovascular disease during adenosine vasodilator stress. However, this field has not progressed beyond original proof-of-principle studies, is limited by method sensitivity and choice of pharmacological stress agent, and has not been validated against gold standard invasive coronary physiology. This Thesis addresses these issues by performing further clinical validation and method development work towards standardising the technique across a range of T1-mapping methods and stress agents.

I first built on the existing adenosine stress T1-mapping proof-of-principle groundwork by performing further clinical validation. This was done in a cohort of patients with end-stage renal disease (ESRD) referred for kidney transplantation, who are most likely to benefit from a non-invasive and contrast-free imaging assessment for cardiovascular disease. I demonstrated for the first time that stress T1-mapping has good diagnostic performance for the detection of obstructive coronary artery disease (CAD) in patients with ESRD, as validated against invasive coronary physiology in a systematic study.

I next explored the feasibility of stress T1-mapping using alternative pharmacological stress agents. I demonstrated that regadenoson (a 'coronary-specific', selective A_{2A} receptor agonist vasodilator) is a viable alternative for stress T1-mapping applications by modelling regadenoson stress T1 dynamics over time in healthy volunteers. I also directly compared the performance and variability of commonly used T1-mapping methods (ShMOLLI and MOLLI variants) for stress and post-contrast T1-mapping. I showed that ShMOLLI stress T1-mapping has the strongest relationship with quantitative myocardial blood flow and has a greater effect size with less variability compared to the other T1-mapping methods tested. I then applied this in a cohort of patients with CAD and showed that regadenoson stress T1-mapping has similar clinical efficacy to adenosine for detecting obstructive CAD and differentiating between normal, remote, ischaemic, and infarcted myocardium.

Finally, I demonstrated the suitability of alternative pharmacological stress agents (dobutamine and dipyridamole) for future stress T1-mapping applications, which included successful translation of the technique to an external international centre. I showed that dobutamine and dipyridamole are both viable and potentially cost-effective stress agents to use for stress T1-mapping.

Overall, this Thesis reports on further development of the highly promising and novel stress T1-mapping technique for the assessment of cardiovascular disease without contrast agents, including clinical validation against invasive coronary physiology, clinical application in patients with CAD, and method comparison across a range of commonly used pharmacological stress agents and T1-mapping techniques.

Publications

Manuscripts Contributing to DPhil Thesis

1. **Burrage MK**, Shanmuganathan M, Masi A, Hann E, Zhang Q, Popescu IA, Soundarajan R, Leal Pelado J, Chow K, Neubauer S, Piechnik SK, Ferreira VM. Cardiovascular magnetic resonance stress and rest T1-mapping using regadenoson for detection of ischemic heart disease compared to healthy controls. *Int J Cardiol*. 2021 Jun15;333:239-245. doi: 10.1016/j.ijcard.2021.03.

2. **Burrage MK**, Shanmuganathan M, Zhang Q, Hann E, Popescu IA, Soundarajan R, Chow K, Neubauer S, Ferreira VM, Piechnik SK. Cardiac stress T1-mapping response and extracellular volume stability of MOLLI-based T1-mapping methods. *Sci Rep.* 11, 13568 (2021). https://doi.org/10.1038/s41598-021-92923-4

Other Publications During DPhil

1. **Burrage MK***, Hundertmark M*, Valkovič L, Watson WD, Rayner J, Sabharwal N, Ferreira VM, Neubauer S, Miller JJ#, Rider OJ#, Lewis AJM#. Energetic basis for exercise-induced pulmonary congestion in heart failure with preserved ejection fraction. Circulation. (Ahead of Print) *contributed equally, #contributed equally

2. Zhang Q, **Burrage MK**, Lukaschuk E, Shanmuganathan M, Popescu IA, Nikolaidou C, Mills R, Werys K, Hann E, Barutçu A, Polat S, Salerno M, Jerosch-Herold M, Kwong R, Watkins H, Kramer C, Neubauer S, Ferreira VM, Piechnik SK. Towards replacing late gadolinium enhancement with artificial intelligence native enhancement for gadolinium-free cardiovascular magnetic resonance tissue characterization in hypertrophic cardiomyopathy. Circulation. (Ahead of Print).

3. Scarsini R, Shanmuganathan M, De Maria G, Borlotti A, Kotronias R, **Burrage MK**, Terentes-Printzios D, Langrish J, Lucking A, Fahrni G, Cuculi F, Ribichini F, Choudhury R, Kharbanda R, Ferreira VM, Channon KC, Banning AP, OxAMI Investigators. Coronary Microvascular Dysfunction Assessed by Pressure Wire and CMR After STEMI Predicts Long-Term Outcomes. JACC Cardiovasc Imaging. 2021 Apr 7;S1936-878X(21)00205-9. doi: 0.1016/j.jcmg.2021.02.023. (Ahead of Print).

4. Marin F, Scarsini R, Kotronias RA, Printzios DT, **Burrage MK**, Bray JJH, Ciofani JL, Venturi G, Pighi M, De Maria GL, Banning AP. Aortic Valve Disease and Associated Complex CAD: The Interventional Approach. J Clin Med. 2021 Mar 1;10(5):946. doi: 10.3390/jcm10050946

5. **Burrage MK**, Ferreira VM. Cardiovascular magnetic resonance for the differentiation of left ventricular hypertrophy. Curr Heart Fail Rep. 2020 Oct;17(5):192-204. doi: 10.1007/s11897-020-00481-z.

6. **Burrage MK**, Ferreira VM. The use of cardiovascular magnetic resonance as an early non-invasive biomarker for cardiotoxicity in cardio-oncology. Cardiovasc Diagn Ther 2020;10(3):610-624. doi: 10.21037/cdt-20-165

7. Lewis AJM, **Burrage MK**, Ferreira VM. Cardiovascular magnetic resonance imaging for inflammatory heart diseases. Cardiovasc Diagn Ther 2020;10(3):598-609. doi: 10.21037/cdt.2019.12.09

8. **Burrage MK**, Baker C, Nikolaidou C, Myerson S, Ferreira VM. Rare unicuspid pulmonary valve and pulmonary artery aneurysm in an elderly asymptomatic patient. Eur Heart J Cardiovasc Imaging. 2020;21(6):708.

9. Cutter DJ, Taylor CW, Rahimi R, McGale P, Ferreira V, **Burrage M**, Vivekanandan S, Hawkins M, Darby SC. Effects of radiation therapy on the cardiovascular system. In Cancer and the Heart (3rd Ed); Ewer MS, Yeh ET, Eds; PMPH USA, 2019.

10. Malek L, Barczuk-Falecka M, Werys K, Czajkowska A, Mroz A, Witek K, **Burrage M**, Bakalarski W, Nowicki D, Roik D, Brzewski M. Cardiovascular magnetic resonance with parametric mapping in long-term ultra-marathon runners. European Journal of Radiology. 2019; August (117):89-94

Prizes and Awards During DPhil

1. **Young Investigator Award – Runner-Up**

   "Impaired myocardial energetics as the basis for exercise-induced pulmonary congestion in heart failure with preserved ejection fraction"

   British Cardiovascular Society / British Atherosclerosis Society / British Society of Cardiovascular Research, June 2021

2. **Young Investigator Award in Clinical Cardiology – Winner**

   "Impaired myocardial energetics limits cardiac functional reserve and leads to exercise-induced pulmonary congestion in heart failure with preserved ejection fraction"

   European Society of Cardiology, August 2021

3. **Melvin Judkins Early Career Clinical Investigator Award – Winner**

   "Myocardial energetic impairment is the basis for reduced cardiac reserve and exercise-induced pulmonary congestion in heart failure with preserved ejection fraction: Insights from novel cardiopulmonary magnetic resonance imaging"

   American Heart Association, November 2021

Contents

Declaration **i**

Abstract **iii**

Publications **vii**

Contents **xiii**

List of Figures **xxi**

List of Tables **xxv**

List of Abbreviations **xxvii**

Acknowledgements **xxxi**

1 Introduction **1**

1.1 Overview 1

1.1.1 Imaging assessment of ischaemic heart disease 1

1.2 Pathophysiology of ischaemic heart disease 5

1.2.1 The coronary circulation 5

1.2.2 Coronary autoregulation and vasodilatory reserve 7

1.2.3 Effects of ischaemia and infarction on myocardial tissue composition changes and the importance of coronary vasodilatory reserve 8

1.3 Myocardial tissue characterisation using CMR 9

1.4 T1-mapping 11

1.4.1 Physics principles 13

1.4.2 T1-mapping methods 15

1.4.2.1 Original MOLLI 3(3)3(3)5 16

1.4.2.2 ShMOLLI 5(1)1(1)1 17

1.4.2.3 MOLLI 5(3)3 21

1.4.2.4 MOLLI 5s(3s)3s 24
1.5 Stress T1-mapping 24
1.5.1 Basic principles and the role of myocardial blood flow and myocardial blood volume 24
1.5.2 Clinical applications of stress T1-mapping 25
1.5.2.1 Patients with obstructive coronary artery disease 25
1.5.2.2 Patients without obstructive CAD 26
1.5.3 Pharmacological stress agents 28
1.5.3.1 Coronary vasodilators 28
1.5.3.2 Inotropes (dobutamine) 30
1.5.4 Stress T1-mapping pitfalls and method selection 33
1.6 Current knowledge gaps 37
1.7 Overview of Thesis 38
2 Methods 41
2.1 Ethical Considerations 41
2.2 Study Participants 41
2.2.1 Inclusion Criteria 43
2.2.2 Exclusion Criteria 44
2.3 Clinical Assessment 45
2.4 CMR Protocols 46
2.4.1 Cine imaging for cardiac volumes and function 47
2.4.2 Choice of short axis slice positions 48
2.4.3 T1-mapping (native) 49
2.4.4 Stress T1-mapping 53
2.4.5 Stress and rest perfusion 53
2.4.6 Late gadolinium enhancement imaging 58
2.4.7 Post-contrast T1-mapping and ECV estimation 59

2.5 Coronary Angiography 59

2.6 Summary 61

3 Adenosine stress T1-mapping to assess cardiovascular disease in kidney transplant candidates 63

3.1 Abstract 63

3.1.1 Background 63

3.1.2 Methods 64

3.1.3 Results 64

3.1.4 Conclusions 65

3.2 Introduction 66

3.3 Methods 70

3.3.1 Study population 70

3.3.2 Data acquisition 71

3.3.2.1 CMR image acquisition 71

3.3.2.2 Coronary angiography 72

3.3.2.3 Data blinding for analysis 72

3.3.3 Data analysis 73

3.3.3.1 CMR data analysis 73

3.3.3.2 Coronary angiography data analysis 74

3.3.4 Statistical analysis 75

3.4 Results 76

3.4.1 Study population 76

3.4.2 Myocardial stress T1-mapping 81

3.4.2.1 Myocardial stress T1 in normal controls and patients with ESRD with normal cardiac functional testing 81

3.4.2.2 Myocardial stress T1 to distinguish between obstructive and non-obstructive coronary arteries 81

3.4.2.3 Diagnostic performance of stress T1-mapping to detect obstructive CAD 85

3.5 Discussion 92

3.5.1 Stress T1-mapping to differentiate myocardial tissue profiles in patients with ESRD 92

3.5.1.1 Blunted stress T1 reactivity in patients with ESRD 93

3.5.2 Diagnostic performance of stress T1-mapping to detect obstructive coronary artery disease in patients with ESRD 95

3.5.2.1 Comparison of stress T1-mapping with other non-invasive imaging strategies 95

3.5.2.2 Microvascular dysfunction and myocardial fibrosis may explain blunted stress T1-reactivity in the absence of obstructive CAD 96

3.5.3 Limitations and future directions 100

3.6 Conclusions 103

4 Regadenoson stress T1-mapping and extracellular volume stability of MOLLI-based T1-mapping methods 105

4.1 Abstract 106

4.1.1 Background 106

4.1.2 Methods 106

4.1.3 Results 107

4.1.4 Conclusions 107

4.2 Introduction 108

4.3 Methods 110

4.3.1 Study population 110

4.3.2 Image acquisition 110

4.3.3 Image analysis 116

4.3.4 Data modelling and statistical analysis 116

4.4 Results 118

4.4.1 Study population 118

4.4.2 Effect of regadenoson stress on heart rate and MBF 118

4.4.3 Regadenoson stress T1 response between ShMOLLI and MOLLI variants 120

4.4.4 ECV measurement stability after dual gadolinium dose administration 122

4.4.5 Relationship between T1 measured by ShMOLLI and MOLLI variants 125

4.4.6 Intra-individual and intra-method variability between T1-mapping variants 130

4.5 Discussion 131

4.5.1 Dynamic response of T1-mapping during regadenoson stress 132

4.5.1.1 Dose-response relationships between T1-mapping and MBF. 134

4.5.1.2 Heart rate sensitivities between stress T1-mapping variants. 136

4.5.2 ECV quantification depends on gadolinium dosage, post-contrast time and T1 method 137

4.5.3 Pre-contrast, stress and post-contrast T1-mapping using different MOLLI variants 139

4.5.4 Intra-individual and intra-method variability between T1-mapping variants and their impact on power calculations for clinical studies 139

4.5.5 Limitations 140

4.6 Conclusions 143

5 Regadenoson stress and rest T1-mapping for the assessment of coronary artery disease 145

5.1 Abstract 146

5.1.1 Background 146

5.1.2 Methods 146

5.1.3 Results 147

5.1.4 Conclusions 147
5.2 Introduction 148
5.3 Methods 150
5.3.1 Study Population 150
5.3.2 Image acquisition 150
5.3.3 Image analysis 151
5.3.4 Statistical analysis 154
5.4 Results 154
5.4.1 Myocardial stress T1 reactivity to regadenoson in healthy controls 154
5.4.2 Myocardial stress T1 reactivity to regadenoson in patients with CAD 160
5.5 Discussion 163
5.5.1 Regadenoson stress T1 reactivity in healthy controls 163
5.5.2 Regadenoson stress T1 reactivity for the assessment of CAD 164
5.5.3 Limitations 166
5.6 Conclusions 168
6 Cardiac stress T1-mapping response to dobutamine 169
6.1 Abstract 169
6.1.1 Background 169
6.1.2 Methods 170
6.1.3 Results 170
6.1.4 Conclusions 170
6.2 Introduction 172
6.3 Methods 173
6.3.1 Study population 173
6.3.2 Image acquisition 173

6.3.3 Image analysis 176
6.3.4 Data modelling and statistical analysis 177
6.4 Results 178
6.4.1 Study population 178
6.4.2 Physiological effect of pharmacological stress 178
6.4.3 Dobutamine stress T1 response and relationship to the physiological response 180
6.4.3.1 Dobutamine stress T1 response 180
6.4.3.2 Dobutamine stress T1 response and its association with physiological variables 183
6.5 Discussion 186
6.5.1 Dynamic response of T1-mapping during dobutamine stress 186
6.5.1.1 Effect of dobutamine on myocardial blood flow 187
6.5.1.2 Effect of dobutamine on myocardial T1 190
6.5.1.3 Effect of physiological response on myocardial T1 with dobutamine 193
6.5.1.4 Clinical applications of dobutamine stress T1-mapping 195
6.5.2 Limitations 196
6.6 Conclusions 196
7 Cardiac stress T1-mapping response to dipyridamole 199
7.1 Abstract 199
7.1.1 Background 199
7.1.2 Methods 200
7.1.3 Results 200
7.1.4 Conclusions 201
7.2 Introduction 202
7.3 Methods 203

7.3.1 Study population 203
7.3.2 Method translation to an international centre 203
7.3.3 Image acquisition 204
7.3.3 Image analysis 207
7.3.4 Data modelling and statistical analysis 208
7.4 Results 209
7.4.1 Study population 209
7.4.2 Physiological effect of pharmacological stress 210
7.4.3 Dipyridamole stress T1 response between ShMOLLI and MOLLI variants 211
7.5 Discussion 214
7.5.1 Dynamic response of T1-mapping during dipyridamole stress 214
7.5.1.1 Dipyridamole stress T1 response for different T1-mapping sequences 215
7.5.2 Differences in stress T1-mapping response across different pharmacological stress agents 217
7.5.2.1 Myocardial blood flow and volume changes with dipyridamole compared to regadenoson 219
7.5.2.2 Myocardial blood flow and volume changes with dipyridamole compared to dobutamine 220
7.5.2.3 Myocardial stress T1-mapping and PET myocardial blood flow 221
7.5.2.4 Cost effectiveness for different pharmacological stress agents 222
7.5.3 Limitations 222
7.6 Conclusions 223
8 General conclusions and future directions 225
Bibliography 231

List of Figures

1.1: Components and function of the coronary circulation..... 6

1.2: Cardiovascular magnetic resonance techniques for myocardial tissue characterisation. 10

1.3: T1 relaxation curves for fat, myocardium, and blood at 1.5-Tesla.....14

1.4: Parametric T1-map example.....15

1.5: Example of the original MOLLI 3(3)3(3)5 sampling scheme. 17

1.6: Simulated recovery and signal plots for tissues with short T1 and long T1. 18

1.7: Example of an excellent quality parametric goodness-of-fit (R^2) map.....20

1.8: Schematic of the pitfalls of T1-mapping method using the MOLLI a-priori sequence selection for rest, stress, and post-contrast T1 applications.....23

1.9: Heart rate sensitivity of T1-mapping methods. 35

2.1: T1-map analysis from a mid-ventricular slice using MC-ROI software.....51

2.2: American Heart Association (AHA) 17 segment model of Left Ventricular Segmentation.....52

2.3: Pixel-wise perfusion maps for quantification of myocardial blood flow.....57

2.4: Quantitative flow reserve analysis. 61

3.1: Myocardial T1 tissue profiles at rest and during adenosine stress in healthy controls and patients with ESRD referred for kidney transplantation. 84

3.2: Myocardial stress T1 reactivity in healthy controls and patients with ESRD referred for kidney transplantation.....85

3.3: Diagnostic performance of CMR stress T1-mapping for detecting obstructive coronary artery disease in patients with end-stage renal disease referred for kidney transplantation.....86

3.4: Relationship between stress myocardial T1 reactivity and coronary physiology assessed by invasive fractional flow reserve (FFR) and quantitative flow reserve (QFR).....87

3.5: Stress T1-mapping as an up-front test to assess for obstructive coronary artery disease in patients with end-stage renal disease referred for renal transplant assessment.....88

3.6: Representative polar map example based on segmental stress T1 analysis. 90

3.7: Diagnostic performance of CMR stress T1-mapping for detecting obstructive coronary artery disease in patients with end-stage renal disease referred for kidney transplantation following polar map analysis.....91

3.8: Polar map example of a patient with significantly elevated myocardial T1 values and abolished stress T1 reactivity.....98

4.1: CMR scanning protocol for assessing T1 time dependencies.....113

4.2: Modified second CMR scanning protocol for assessing stress T1 and MBF. 115

4.3: Physiological effects of regadenoson stress. 119

4.4: Regadenoson stress effects on delta T1 with overlaid mono-exponential decay models.....120

4.5: Correlation between stress MBF and delta T1 during regadenoson stress.....121

4.6: Effect of time and gadolinium dose on ECV. 124

4.7: Relationship between T1-mapping variants. 127

4.8: Impacts of MOLLI choice on estimation of stress delta T1 and ECV. 129

4.9: Nonlinear logarithmic relationship between stress MBF and delta T1 during regadenoson stress. 134

4.10: Dose-response relationship between stress MBF and delta T1 during regadenoson stress. 135

5.1: Example image analysis of a patient with coronary artery disease. 153

5.2: Normal regadenoson stress T1 responses in healthy controls. 159

5.3: Regadenoson stress T1-mapping distinguishes between different myocardial tissue classes. 162

6.1: Dobutamine stress T1-mapping protocol for assessing time dependencies. 175

6.2: Effect of time and dobutamine dose on heart rate. 179

6.3: Change in LV myocardial T1 values with time and increasing dobutamine doses. 181

6.4: Inter-individual variability for physiological and stress T1 responses with IV dobutamine in healthy controls. 185

6.5: Effect of dobutamine on coronary artery luminal diameter. 188

7.1: Dipyridamole stress CMR protocol for assessing T1 time dependencies. 206

7.2: Average heart rate response to intravenous dipyridamole infusion over time. 211

7.3: Effects of dipyridamole on delta T1 over time. 213

7.4: Physiological and myocardial stress T1 responses for different pharmacological stress agents. 218

List of Tables

1.1: Pharmacological stress agents 32

3.2: Baseline characteristics of the study participants 77

3.3: CMR parameters and adenosine stress haemodynamic data 79

3.4: Invasive coronary angiography findings 80

3.5: Myocardial T1 tissue characteristics 83

3.6: Coronary microvascular dysfunction and stress T1 reactivity 97

4.1: Differences between methods for rest, stress, and post-contrast T1 122

4.2: Effect of gadolinium dose on ECV 125

4.3: Measures of intra-individual variability across different T1-mapping variants 131

5.1: Baseline characteristics of the study participants. 155

5.2: CMR parameters and angiographic data 156

5.3: Rest and regadenoson stress native T1-mapping myocardial tissue profiles 157

6.1: Dobutamine dosing protocol and time intervals 176

6.2: Myocardial T1 and relative change (delta T1) recorded at the end of each dobutamine dose epoch 183

7.1: Differences in myocardial T1 measurements between methods for rest and dipyridamole stress T1 212

List of Abbreviations

AIF	arterial input function
ANOVA	analysis of variance
AS	aortic stenosis
AUC	area under the curve
BMI	body mass index
bpm	beats per minute
bSSFP	balanced steady-state free precession
CABG	coronary artery bypass grafting
CAD	coronary artery disease
CFR	coronary flow reserve
CKD	chronic kidney disease
CMD	coronary microvascular dysfunction
CMR	cardiovascular magnetic resonance
CTCA	computed tomography coronary angiography
CTO	chronic total occlusion
CV	coefficient of variance
CVD	cardiovascular disease
DICOM	Digital Imaging and Communications in Medicine
ECG	electrocardiogram
ECV	extracellular volume
EDV	end-diastolic volume
EF	ejection fraction
ESV	end-systolic volume
ESRD	end-stage renal disease
FFR	fractional flow reserve
FOV	field of view

GBCA	gadolinium-based contrast agent
Gd	gadolinium
GRAPPA	generalized auto-calibrating partially parallel acquisition
HLA	horizontal long axis
HR	heart rate
ICA	invasive coronary angiography
IHD	ischaemic heart disease
IMR	index of microcirculatory resistance
IQR	interquartile range
IR	inversion recovery
IV	intravenous
LAD	left anterior descending
LCx	left circumflex
LGE	late gadolinium enhancement
LV	left ventricle/ventricular
LVEDVi	left ventricular end diastolic volume index
LVMi	left ventricular mass index
LVOT	left ventricular outflow tract
MBF	myocardial blood flow
MBV	myocardial blood volume
MOCO	motion correction
MOLLI	Modified Look-Locker Inversion recovery
MPHR	maximal predicted heart rate
MPI/MPS	myocardial perfusion imaging/scan
MR	magnetic resonance
MRI	magnetic resonance imaging
MT	magnetisation transfer
Mx,y	transverse magnetisation
Mz	longitudinal magnetisation
NHS	National Health Service

NMR	nuclear magnetic resonance
NPV	negative predictive value
Pa	aortic pressure
PCI	percutaneous coronary intervention
PET	positron emission tomography
Pd	distal pressure
PPV	positive predictive value
QFR	quantitative flow reserve
RCA	right coronary artery
RF	radiofrequency
ROC	receiver operating characteristic
ROI	region of interest
RMSE	root mean square error
SBP	systolic blood pressure
SCMR	Society for Cardiovascular Magnetic Resonance
SD	standard deviation
ShMOLLI	Shortened Modified Look-Locker Inversion recovery
SPECT	single-photon emission computed tomography
SPK	simultaneous pancreas-kidney
SV	stroke volume
T	Tesla
T1	longitudinal or spin-lattice relaxation
T2	transverse or spin-spin relaxation
TD	trigger delay
TE	echo time
TI	inversion time
TR	repetition time
T1DM	type 1 diabetes mellitus
T2DM	type 2 diabetes mellitus
VLA	vertical long axis

Acknowledgements

The work presented in this thesis would not have been possible without the expertise and support of an outstanding group of colleagues, collaborators, and mentors. I feel enormously privileged to have been able to work in such an inspiring and multi-disciplinary environment.

I am particularly grateful to my primary supervisor Prof Vanessa Ferreira, who has been a tremendous source of encouragement, insight, and direction. I am extremely appreciative of the time you have invested in me, from taking a chance on me and supporting my efforts to move to Oxford to pursue a DPhil, right through to the rigorous academic, scientific, and clinical training you have provided. I have learnt an enormous amount from you and I am truly grateful. I would also like to thank my co-supervisors Prof Stefan Piechnik and Prof Stefan Neubauer, who have been constant sources of support and wisdom throughout my DPhil. I am forever grateful for your support and guidance.

I am also extremely grateful to my close friends and colleagues within OCMR, without whom none of this would have been possible. I am particularly grateful to Prof Oliver Rider, for his support, good humour, and guidance, as well as providing me with the opportunity to branch out into other research

projects; I hugely enjoyed working on the LWE and VLED studies alongside Andrew Lewis, Moritz Hundertmark, Laci Valkovič, and Jack Miller. I would also like to thank Mayooran Shanmuganathan for his constant advice, support, and friendship, as well as Rebecca Chamley, Will Watson, and Valantou Nikolaidou. I am also grateful to Perry Green, Shveta Monga, Arjun Jayaswal, Marco Spartera, Andy Apps, Jenny Rayner, Ferenc Mózes, and Rohan Wijesurendra, as well as the Image Analysis team of Qiang Zhang, Elena Lukaschuk, Evan Hann, and Iulia Popescu; I have been truly fortunate to work with such a talented and inspiring group of people. I am grateful as well to the excellent clinicians and teachers (particularly Prof Saul Myerson) I have had throughout my clinical CMR training.

I sincerely thank the patients and volunteers who gave up their time to participate in these research studies, as well as the OCMR radiographer and nursing teams who have helped me to coordinate and run study visits. I also acknowledge the British Heart Foundation for supporting my research, as well as the Oxford British Heart Foundation Centre for Research Excellence and the National Institute for Health Research Oxford Biomedical Research Centre.

Finally, I would like to thank my parents for their lifelong love and unwavering support and encouragement. Above all, my deepest thanks to Emily for her endless love, patience, and support from across the world, which allowed me the opportunity to follow my dreams, and to whom this thesis is dedicated.

1 Introduction

1.1 Overview

Cardiovascular disease (CVD) remains the leading cause of morbidity and mortality worldwide (1). It is responsible for 27% of all deaths in the United Kingdom, with an estimated annual healthcare cost of £9 billion (2). Ischaemic heart disease (IHD) is the largest contributor to this burden and is an important cause of heart failure and sudden cardiac death if left untreated. It is a complex chronic disease that is categorised by pathological changes in the coronary arteries and the development of coronary atherosclerosis, with downstream effects on the left ventricular myocardium (3). Recent advances in cardiac imaging techniques have greatly improved our ability to diagnose and treat patients with CVD at different stages of these disease processes.

1.1.1 Imaging assessment of ischaemic heart disease

Multiple invasive and non-invasive imaging modalities are available to provide a comprehensive evaluation of coronary atherosclerosis and IHD. Particular strategies include the evaluation and visualisation of luminal stenoses within the coronary arteries, overall atherosclerotic plaque burden and high-risk plaque characteristics, and the downstream effects of myocardial perfusion, infarction, viability, and function (3,4).

Invasive coronary angiography (ICA) allows a direct luminal assessment of the epicardial coronary arteries, with the presence of significant stenoses in multiple vessels being associated with a stepwise increase in adverse outcomes (5). However, visual assessment of luminal stenosis alone correlates poorly with the haemodynamic significance of coronary stenoses of intermediate severity (6). The incorporation of newer anatomical (e.g., intravascular ultrasonography, IVUS; optical coherence tomography, OCT) and physiological (e.g., fractional flow reserve, FFR) assessments into conventional angiographic practices is increasingly used to guide revascularisation strategies but are time-consuming, expensive, and invasive.

Anatomical imaging with non-invasive computed tomography coronary angiography (CTCA) allows rapid and precise imaging of coronary atherosclerosis (calcium scoring, angiography, plaque burden, adverse plaque characteristics) (3) with excellent diagnostic performance compared with ICA (7). Large multi-centre randomised controlled trials in patients have demonstrated that CTCA provides effective risk stratification with improved diagnostic accuracy, better-targeted therapy, and reduced need for ICA (8,9). Novel CT-based biomarkers of coronary artery inflammation such as the perivascular fat attenuation index (FAI) and radiomic profiling of coronary artery perivascular tissue have further improved cardiac risk prediction and restratification (10–12), although they are not as yet able to perform advanced myocardial tissue characterisation. Importantly, anatomical imaging with

CTCA alone does not give a precise indication of ischaemia, which is better demonstrated using perfusion imaging. CT perfusion is currently limited in its clinical application by the need for significant additional radiation exposure.

Other functional imaging modalities such as single-photon emission computed tomography (SPECT) myocardial perfusion imaging (MPI), stress echocardiography (SE), and cardiovascular magnetic resonance (CMR) allow more detailed assessments of ventricular function, viability and infarction, myocardial perfusion, and tissue characterisation. Large-scale SPECT-MPI studies have established a stepwise increase in mortality with progressive ischaemic burden, leading to the widespread use of this technique to risk stratify patients and guide clinical decision making (4,13,14). While SPECT-MPI may also quantify ventricular function, it requires the use of radioactive tracers and ionising radiation, which may limit its use for serial evaluations.

SE is frequently used for the diagnosis of flow-limiting CAD as well as risk stratification and prognostication (15). Multiple studies have shown that a normal study is associated with a benign prognosis (16,17). The performance of SE is comparable to SPECT-MPI, has high accuracy in real-world large multi-centre studies (18), and may even be further improved with incorporation of artificial intelligence (AI) and machine learning technologies (19). Although cheap and widely available, SE may be limited in patients with poor acoustic windows and does not allow advanced myocardial tissue characterisation.

Finally, CMR is a potential "one-stop-shop" for the assessment of IHD. It is gold standard for reproducible assessment of ventricular volumes and function, is able to detect obstructive CAD and ischaemia using first pass perfusion imaging with greater accuracy (20–22) and cost-effectiveness (23) than SPECT-MPI, and can definitively assess for the presence of myocardial infarction and viability (24). CMR advanced tissue characterisation techniques (such as T1-mapping) may assess for myocardial inflammation, oedema, and fibrosis, and improve the diagnosis of acute cardiac pathologies in patients with myocardial infarction with non-obstructed coronary arteries (MINOCA) (25). It is radiation-free and is not limited by acoustic windows or imaging planes. Novel stress CMR imaging techniques that focus on changes in myocardial tissue properties using T1-mapping may be able to assess changes in myocardial blood volume, which is thought to be a more comprehensive and earlier marker of ischaemia than changes in perfusion and blood flow alone (26). CMR may therefore have additional benefit in that it can theoretically interrogate the autoregulatory properties of the coronary macro- and micro-circulations as a novel marker of ischaemia and vasodilatory reserve.

Thus, non-invasive CMR imaging biomarkers of cardiovascular disease severity, with emphasis on imaging at the tissue level, could allow early therapeutic interventions and help risk-stratify and prognosticate to improve individual outcomes above that seen with other non-invasive imaging modalities.

1.2 Pathophysiology of ischaemic heart disease

1.2.1 The coronary circulation

The coronary arterial vasculature may be broadly subdivided into the macro- and micro-circulations based on vessel size, capacitance, and resistance to myocardial blood flow (MBF) (27). The macro-circulation refers to the epicardial coronary vessels (>400 μm diameter), which are primarily conductive vessels with near negligible resistance, while the micro-circulation is comprised of the small arteries (<400 μm), arterioles (<100 μm), and capillaries (<10 μm) (**Figure 1.1**) (28). The intramural arterioles are highly autoregulated resistance vessels and are responsible for matching blood supply to myocardial oxygen consumption across a large range of perfusion pressures (29). The capillary system is made up of low-resistance capacitance vessels and accounts for up to 90% of total intramyocardial blood volume (28,30). The function of the macro-circulation and micro-circulation may be assessed using invasive coronary physiology measurements such as fractional flow reserve (FFR), coronary flow reserve (CFR), and the index of microcirculatory resistance (IMR).

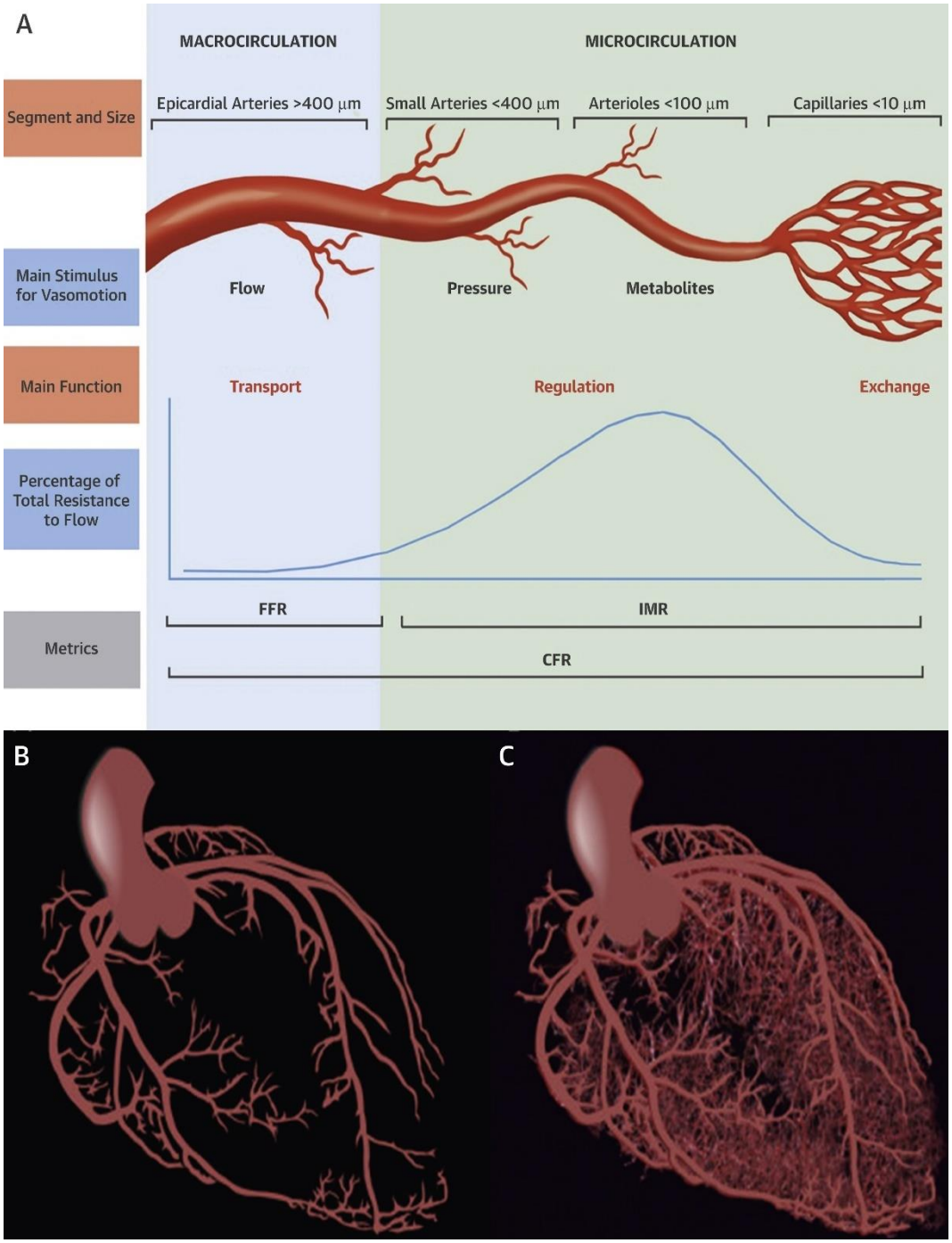


Figure 1.1: Components and function of the coronary circulation. *The individual components and their main function within the macro- and micro- coronary circulation (A) with schematics of the macrocirculation (B) and microcirculation (C). CFR = coronary flow reserve; FFR = fractional flow reserve; IMR = index of microcirculatory resistance. Reproduced with permission from: Mathew RC, Bourque JM, Salerno M, Kramer CM. Cardiovascular Imaging Techniques to Assess Microvascular Dysfunction. JACC Cardiovasc Imaging. 2020;13(7):1577–1590. (28)*

1.2.2 Coronary autoregulation and vasodilatory reserve

Stable coronary blood flow is maintained across a large range of perfusion pressures due to complex autoregulatory mechanisms in the pre-arteriolar and arteriolar microcirculation (28). For example, autoregulation reduces microvascular resistance in the setting of hypotension and reduced driving pressure so as to maintain adequate coronary blood flow.

The most common clinical manifestation of IHD is angina pectoris, typically due to the development of obstructive atherosclerotic plaque in an epicardial coronary artery and subsequent myocardial ischaemia. Under resting conditions, epicardial coronary stenoses of moderate severity do not cause ischaemia, as coronary autoregulation maintains adequate myocardial perfusion via compensatory reductions in microcirculatory resistance, and increased microvascular dilatation and capillary recruitment (31,32). However, as stenosis severity increases, microvascular compensatory mechanisms and vasodilatory reserve may become depleted. These compensatory mechanisms may thus become overwhelmed during exercise or pharmacological stress, where increased myocardial demand and wall stress results in supply-demand mismatch and subsequent myocardial ischaemia (33). It is not surprising that disorders of the microcirculation are also implicated, with microvascular dysfunction increasingly recognised as an important cause of angina and myocardial ischaemia (34).

1.2.3 Effects of ischaemia and infarction on myocardial tissue composition changes and the importance of coronary vasodilatory reserve

Myocardial ischaemia and infarction may both significantly affect ventricular structure and function via changes in tissue composition, such as the development of myocardial oedema or fibrosis (35). Subclinical changes in the myocardium and myocardial blood supply may lead to cardiac dysfunction, adverse remodelling, and progressive decompensation, and thus increase the risk of adverse cardiovascular events. Early detection of these changes is clearly of great diagnostic and prognostic value.

Myocardial oedema is central to disease processes such as myocardial inflammation, ischaemia or infarction, and is associated with development of left ventricular dysfunction (36). Myocardial fibrosis, a downstream correlate of myocardial injury and oedema, may result in increased wall stiffness, cardiac remodelling, and heart failure (37). Reactive interstitial fibrosis is reversible if recognised and treated promptly (35,38–40). Irreversible replacement fibrosis, typically induced by cardiomyocyte cell death following myocardial ischaemia or infarction, is also seen in advanced non-ischaemic processes and the terminal stages of heart failure (35). It is no surprise that fibrosis adversely impacts myocardial function and that the extent is associated with worse prognosis (41).

Determinants of progressive loss of function and disease decompensation likely reflect the ability of the heart (particularly the microcirculation) to respond to physiological stress. Depleted coronary vasodilatory reserve and microvascular dysfunction are seen in ischaemic (most commonly) and valvular heart disease, non-ischaemic cardiomyopathies, and heart failure, and portend a worse prognosis (27,42–46). Depletion of coronary vasodilatory reserve may thus represent a transition point towards decompensated disease states. Recent advances in CMR allow advanced myocardial tissue characterisation, with potential to detect these subclinical tissue composition changes, along with stress applications for assessment of coronary vasodilatory reserve.

1.3 Myocardial tissue characterisation using CMR

CMR is the current imaging gold-standard for accurate and reproducible assessment of cardiac mass, volumes and function (47–49). Its excellent spatial resolution allows evaluation of cardiac structure, image quality is not adversely affected by body habitus, and it does not involve ionising radiation or radioactive isotopes. The main strength of CMR is its advanced multiparametric myocardial tissue characterisation capabilities (**Figure 1.2**) such as late gadolinium enhancement (LGE), T1-mapping, and T2-mapping, which provide valuable diagnostic and prognostic information in the assessment of cardiovascular disease.

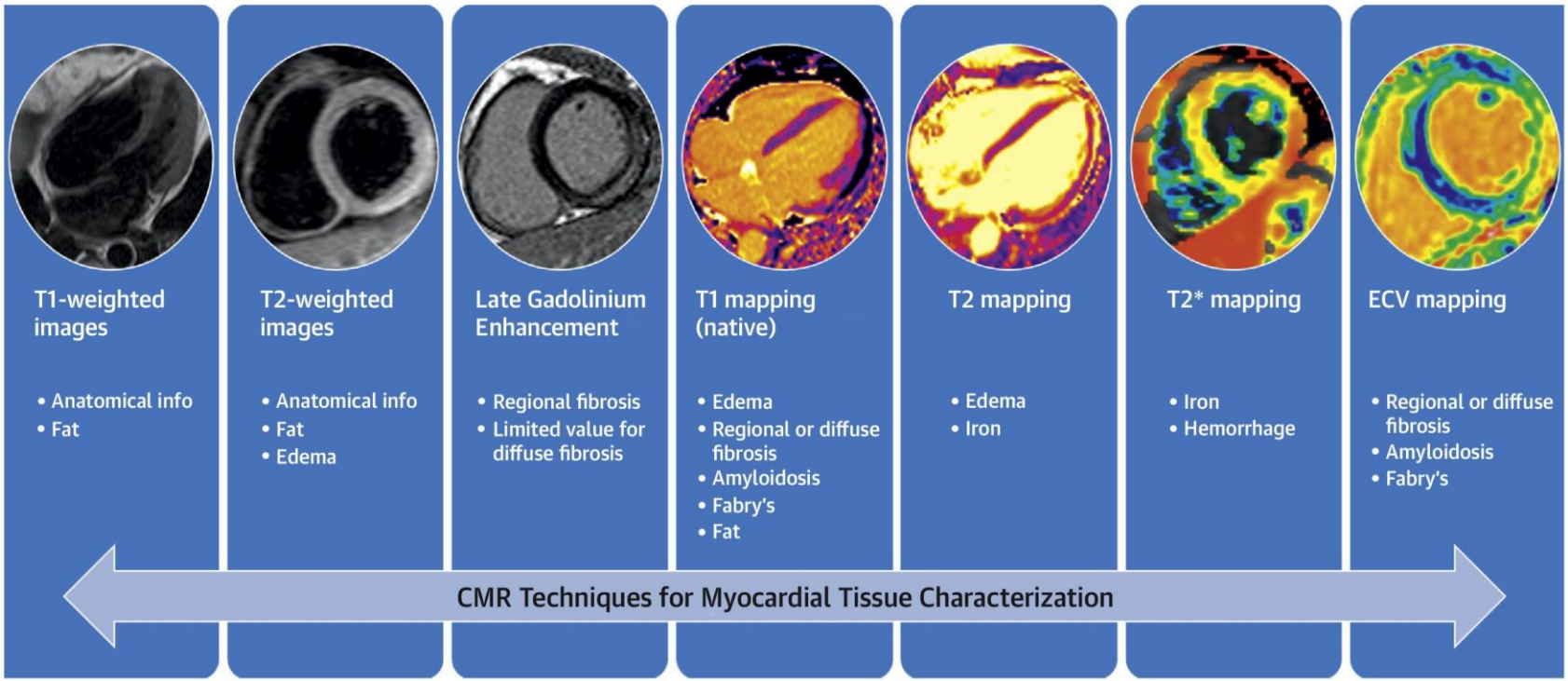


Figure 1.2: Cardiovascular magnetic resonance techniques for myocardial tissue characterisation. *Cardiovascular magnetic resonance allows comprehensive myocardial tissue characterisation, offering superior and well-validated biomarkers of important pathophysiological processes encountered in cardiac diseases (i.e., fibrosis, oedema, iron, or amyloid infiltration, and so on), via a variety of myocardial tissue characterisation techniques such as T1- and T2-weighted imaging, LGE, and parametric mapping. Reproduced with permission from: Karamitsos TD, Arvanitaki A, Karvounis H, Neubauer S, Ferreira VM. Myocardial tissue characterisation and fibrosis by imaging. J Am Coll Cardiol Img. 2020;13(5):1221-34. (35)*

LGE is the prototypical CMR myocardial tissue characterisation technique. It allows differentiation of ischaemic and non-ischaemic heart disease via characteristic enhancement patterns following injection of an intravenous gadolinium-based contrast agent (GBCA), and is excellent for detecting areas of focal scarring/fibrosis (50). However, to highlight areas of pathology, it relies on areas of presumed normal myocardium for nulling. Detection of diffuse myocardial fibrosis may thus be challenging, particularly if GBCA uptake is uniform (51). Furthermore, LGE imaging requires intravenous injection of a GBCA, which is relatively contra-indicated in certain populations (e.g., renal failure, contrast allergy, pregnancy), increases scan time, and may even lead to deposition in brain tissue (52), the clinical significance of which remains to be determined.

Novel parametric mapping techniques, such as T1- and T2-mapping, may address these limitations by allowing rapid advanced tissue characterisation via directly quantitative pixel-wise maps without the need for contrast agents (53). T1- and T2-mapping are often used in clinical practice to detect changes in diffuse myocardial fibrosis, inflammation, and oedema (54).

1.4 T1-mapping

Native (pre-contrast) T1-mapping reflects signal from the intra- and extra-cellular myocardial compartments. Each tissue-type exhibits a normal T1

range, deviation from which may indicate pathology or change in physiology (54). T1 values of imaged tissues are displayed on a pixel-by-pixel basis, enabling quantitative myocardial tissue characterisation. Native T1 values are sensitive to increased tissue free water content and are prolonged by myocardial inflammation and oedema, as well as areas of focal and diffuse fibrosis (35). Strictly speaking, T1 does not directly detect collagen fibres as a marker of fibrosis; rather it is the accumulation of free water content in the expanded interstitial space around fibrotic tissue which T1 is sensitive to. Conversely, T1 values are shortened by high tissue iron content, fat deposition, and GBCAs (55–57).

Focal and global T1 changes are sensitive biomarkers for diagnosing myocardial pathology. T1-mapping is well-validated in detecting acute myocardial injury and inflammation (58–67), myocardial fibrosis in cardiomyopathies and valvular heart disease (68–73), myocardial infiltration in amyloidosis (74–78) and Anderson-Fabry disease (79–81), and subclinical cardiac involvement in systemic diseases (82–84).

Additionally, there is increasing interest to perform post-contrast T1-mapping to quantify the myocardial extracellular volume (ECV) in these pathologies. ECV may act as a surrogate marker for diffuse interstitial fibrosis after exclusion of confounding factors (such as oedema, inflammation, and infiltrative diseases that expand the interstitial space) and has important

prognostic implications (85–88). Although T1-mapping shows clear promise for the assessment of cardiovascular disease, the field has been hindered by a lack of standardisation, particularly across different T1-mapping sequences (89).

1.4.1 Physics principles

The main principle behind nuclear magnetic resonance (NMR) and magnetic resonance imaging (MRI) is that certain atomic nuclei exhibit a property called *spin*, which describes the rotational motion of an odd-numbered nucleus (e.g., the proton ^{1}H) about an internal axis. These nuclei preferentially align with the direction of an externally applied magnetic field in either high-energy or low-energy states, resulting in a net magnetization vector. Although this is not directly detectable, protons may be excited into high-energy states by application of a radiofrequency (RF) pulse such that their magnetic moments are tipped into a different, e.g., transverse, plane. When the RF pulse is stopped, the protons will release that energy and return to their lower-energy state at equilibrium. T1, also known as spin-lattice, relaxation is the decay constant that governs the recovery of longitudinal magnetisation (Mz) towards the equilibrium, while T2, also known as spin-spin, relaxation, is the basic MR constant that governs the dephasing of transverse magnetisation (Mx,y) (53). Different tissues have different MR relaxation times, resulting in a key source of tissue contrast (**Figure 1.3**).

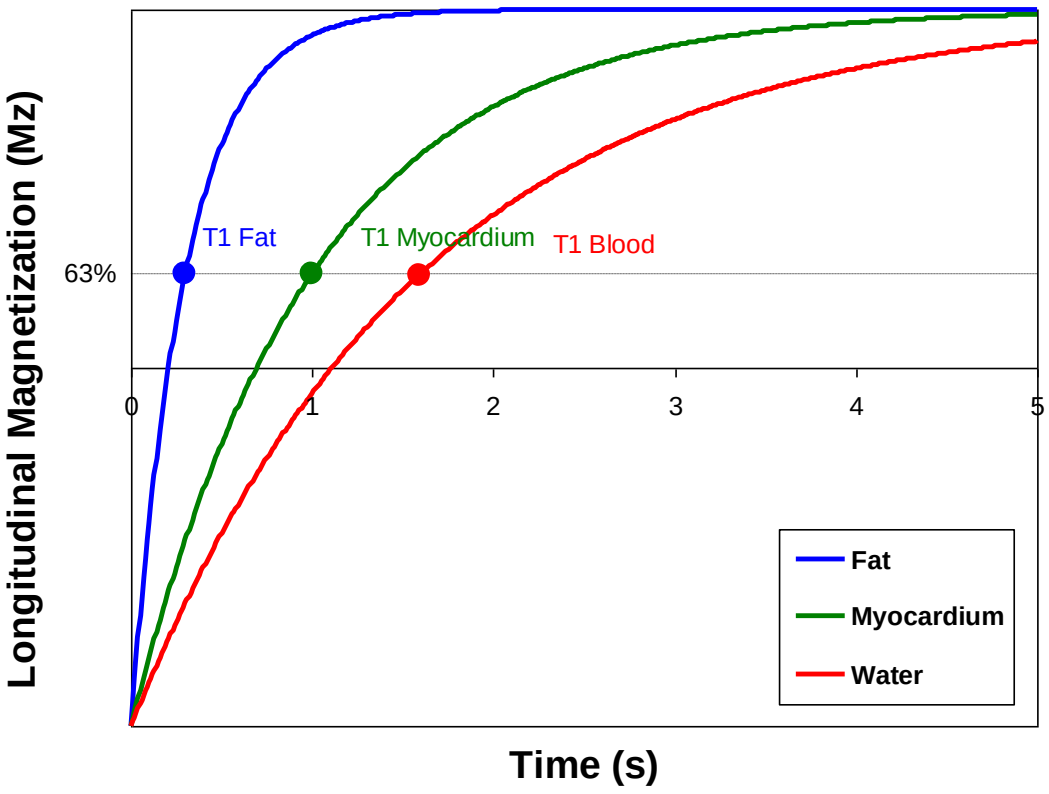


Figure 1.3: T1 relaxation curves for fat, myocardium, and blood at 1.5-Tesla. *Figure provided by Professor Vanessa M Ferreira.*

Traditionally these differences underpin T1/T2-weighted imaging, where the relaxation properties drive the contrast between various tissues in MR imaging. It is possible to calculate the underlying T1 or T2 relaxation times in the form of a quantitatively denominated value, a technique known as relaxometry. The general principle is that multiple signal intensity samples with different T1 weightings are acquired, with the different signal intensities fitted to a mathematical equation describing an appropriate MR recovery curve. Using the weighted images, T1 values may be derived on a pixel-by-pixel basis and expressed in the form of a parametric T1-map (**Figure 1.4**)(90).

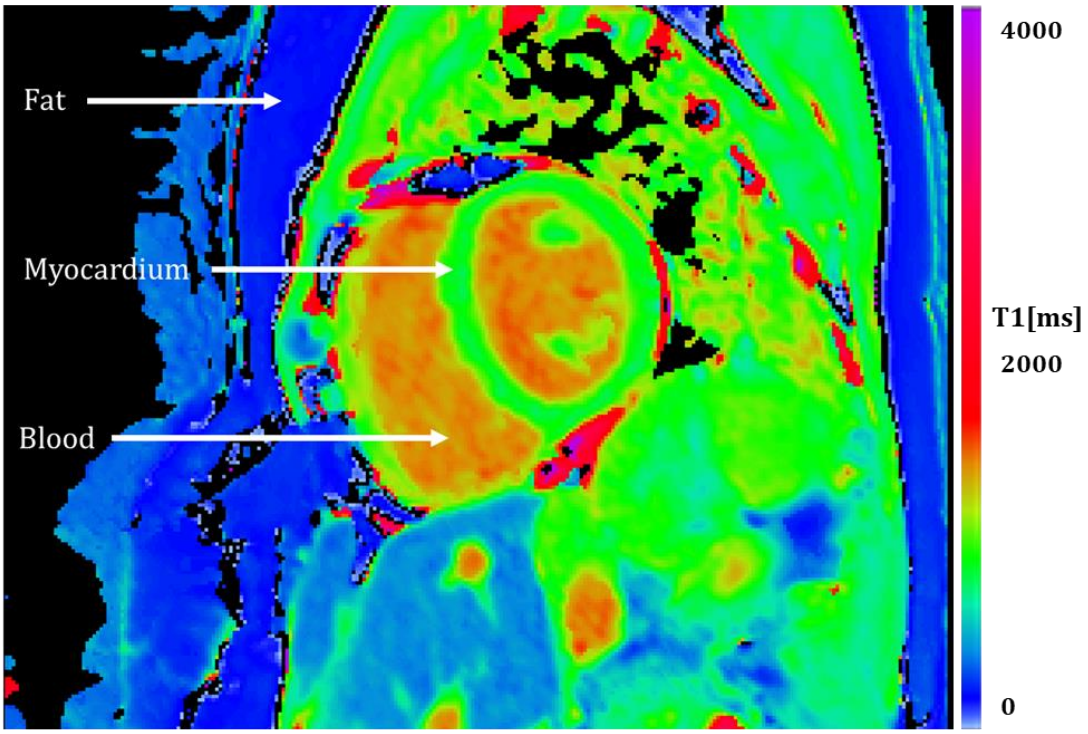


Figure 1.4: Parametric T1-map example. *There are clear tissue contrasts between fat (blue), myocardium (green), and blood (red).*

1.4.2 T1-mapping methods

Multiple different techniques for the quantification of myocardial T1 have been described (54). The majority of these techniques utilise multiple single-shot balanced steady-state free precession (bSSFP) acquisitions using inversion preparation (e.g., modified Look-Locker inversion recovery (MOLLI) (91), shortened MOLLI (ShMOLLI) (92)), saturation preparation (e.g., saturation recovery single-shot acquisition (SASHA) (93)), or a combination of the two (e.g., saturation pulse prepared heart rate independent inversion recovery (SAPPHIRE) (94)). This Thesis will mainly discuss MOLLI and ShMOLLI, the two most commonly used sequences worldwide.

1.4.2.1 Original MOLLI 3(3)3(3)5

The most commonly used T1-mapping sequences are based upon inversion preparation sequences and utilise single-shot image acquisitions at a fixed time in the cardiac cycle following each inversion pulse (95). Each group of inversion pulse, image acquisition, and relaxation recovery period is termed a Look-Locker cycle (96). The modified Look-Locker inversion recovery (MOLLI) family are the most widely used and validated techniques for myocardial T1-mapping. The original MOLLI sequence was based on a 3(3)3(3)5 sampling scheme, referring to acquisition of 3, 3, and 5 images after each inversion preparation and separated by three heartbeat long recovery epochs after the first and second inversions (91). T1 values are derived from each set of image acquisitions, which may be plotted along a T1 recovery curve to generate a parametric map (**Figure 1.5**). MOLLI offers excellent T1 precision, although it is sensitive to magnetisation transfer (MT), T2, and heart rate effects. Additionally, the 17-heartbeat breath hold required for acquisition may be impractical for cardiac patients. Shorter MOLLI variants have thus been proposed to reduce breath hold duration and heart rate sensitivity.

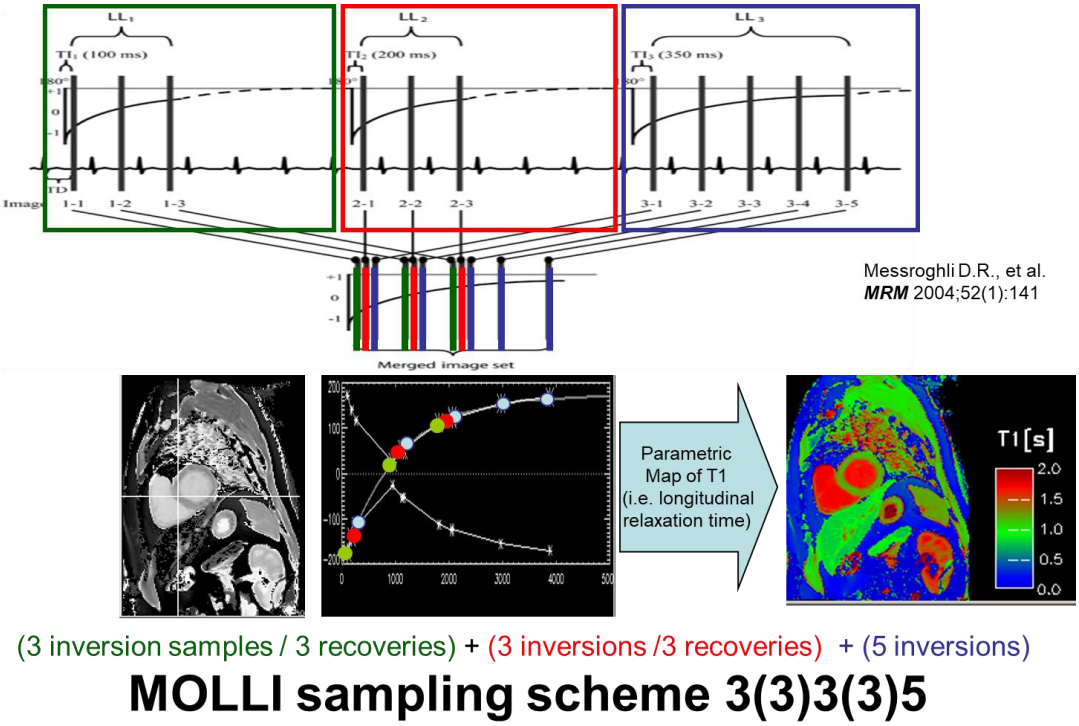


Figure 1.5: Example of the original MOLLI 3(3)3(3)5 sampling scheme. *There are three Look-Locker experiments with inversion recovery (IR)-weighted image acquisitions, acquiring samples along a T1 recovery curve. The samples are pooled together to allow the pixel-wise reconstruction of a parametric T1-map. Figure provided by Professor Stefan K Piechnik.*

1.4.2.2 ShMOLLI 5(1)1(1)1

The shortened MOLLI (ShMOLLI) sequence is a widely used T1-mapping method which allows reduced scan time and shorter breath holds compared to original MOLLI, for the price of a modest noise penalty, but with similar overall accuracy. ShMOLLI is acquired using a 9-heartbeat 5(1)1(1)1 sampling scheme with a front-loading approach, meaning that most samples are acquired at the beginning of the breath hold. This sampling scheme works perfectly for tissues with short T1 values (as shown on the simulated recovery

and signal plots for a short T1 of 500 ms in **Figure 1.6A**), but for tissues with long T1 the need for longer recovery periods is immediately apparent. The second and third inversion recovery experiments start from incompletely relaxed conditions, therefore introducing measurement error where the measured signal samples diverge from the ideal recovery curve, as shown in **Figure 1.6B**.

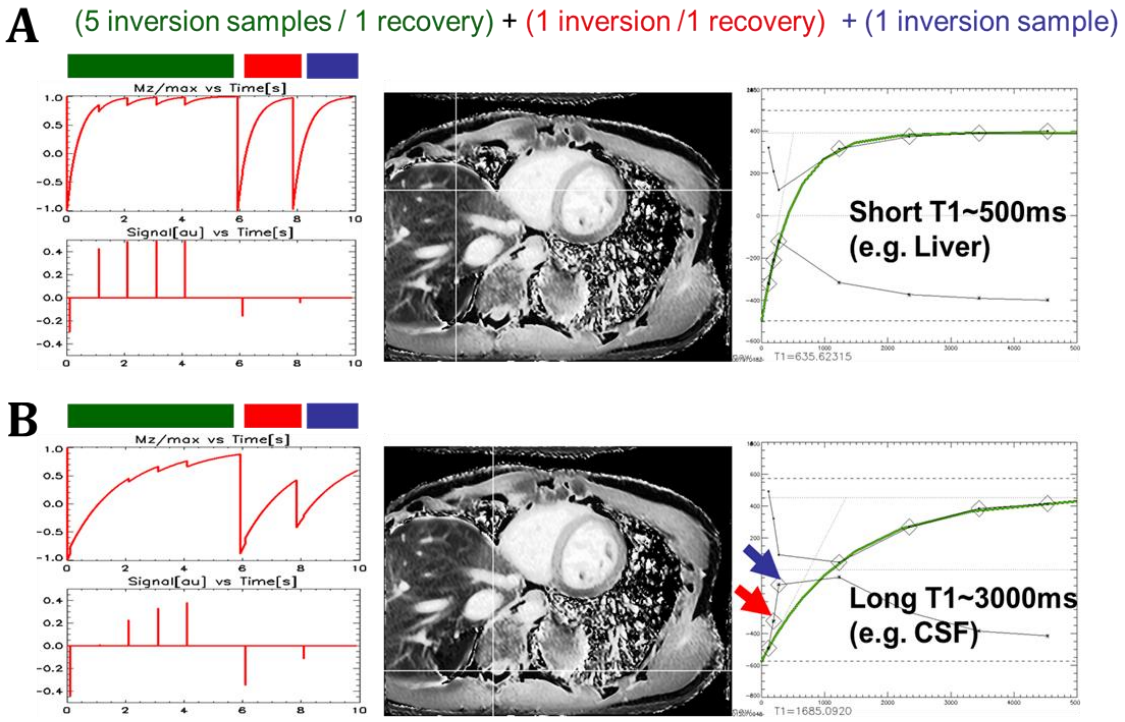


Figure 1.6: Simulated recovery and signal plots for tissues with short T1 and long T1. *Tissues with short T1 (A) fully recover Mz prior to the subsequent inversion recovery experiments, resulting in a well-fitting T1 recovery curve. Tissues with long T1 (B) such as cerebral spinal fluid (CSF) do not recover Mz completely prior to the second and third inversion recovery experiments, thus introducing error between the measured and ideal T1 recovery curves (arrows, bottom right panel B). Simulations performed at a heart rate of 60 bpm. Figure provided by Professor Stefan K Piechnik.*

To account for these potential errors, ShMOLLI uses an in-built conditional reconstruction algorithm that automatically selects the required number of samples for the best fit for long, intermediate, and short T1. The first five samples are always included as the five-heartbeat recovery period is sufficient for tissues with longer T1 to more-or-less achieve complete recovery of Mz. The sixth and seventh samples however are included only for estimated relaxation times that are shorter than the heartbeat recovery period (i.e., have sufficient time for Mz to recover before the next inversion pulse). Typically, this means that for tissues with short T1, all of the acquired data is used, while for longer T1 only data from the first inversion recovery experiment are used. It is possible to imagine the impact of elevated heart rate (**see 1.6.4**) on this process, where a faster heart rate results in less time for complete recovery of Mz and is therefore likely to introduce technical inaccuracies in T1 measurement.

Although the reconstruction algorithm makes ShMOLLI largely heart rate independent, it may be more sensitive to ECG mis-triggering due to the lack of data redundancy typically acquired from multiple longer Look-Locker cycles. Fortunately, parametric goodness-of-fit (R^2) maps are available in-line at time of acquisition, providing a means to allow critical assessment of T1-map quality almost immediately post-acquisition, and the opportunity to re-acquire maps of insufficient quality (**Figure 1.7**).



Figure 1.7: Example of an excellent quality parametric goodness-of-fit (R^2) map. *This was acquired from the same patient as in* ***Figure 1.4*** *above. The LV myocardium has a mostly white appearance, signifying near-excellent fit between the measurements and the ideal signal recovery model predictions, and thus high likelihood of a good quality acquisition.*

ShMOLLI demonstrates excellent reproducibility and consistent results in normal individuals, with the largest study to-date showing intra-individual, intra-scanner, and inter-scanner variability of <2% relative change from the average, well below the threshold effects of most forms of acute myocardial disease (97). The primary source of error is typically partial volume effects from over-inclusion of neighbouring tissue during image analysis, which may be compensated for by focusing analysis on the mid-wall of the myocardium, although this may sometimes be challenging with diastolic readouts given the

relative thinness of the myocardium during this phase of the cardiac cycle. Mid-wall analysis may also miss pathology in the endocardium (e.g., subendocardial infarctions) and epicardium (e.g., myocarditis).

One way of accounting for this is the use of systolic T1-mapping readouts, which allows easier placement of endocardial and epicardial contours due to functionally increased myocardial thickness. This technique was designed to overcome the risk of ECG mistriggering and inaccurate T1 estimation during periods of tachycardia or tachyarrhythmia (98). The shortest possible imaging (trigger delay (TD) = 0 ms) may be used for simplicity, minimising trigger time and therefore maximising the heart rate tolerated before mistriggering occurs. This technique has been shown to reduce T1 variability and provides clinically equivalent T1 values to conventional diastolic readouts while avoiding heart rate mistriggering and producing excellent quality T1-maps (99). There is clear potential of systolic T1-mapping for stress applications.

1.4.2.3 MOLLI 5(3)3

The MOLLI 5(3)3 variant (100) has emerged as another modification of the original MOLLI sequence to reduce scan time, also at the cost of a modest noise penalty but with little impact on overall practical performance (101). This is the currently most used T1-mapping sequence worldwide, due to its position as the Siemens product variant (MyoMaps). It may be acquired in 11 heartbeats and is similar to ShMOLLI in that it adopts a front-loading

approach, with most samples acquired at the beginning of the breath hold. While this goes some way to reduce heart rate sensitivity, it does not eliminate it as all data are used to fit a single T1 recovery curve, regardless of whether the recovery epochs are sufficiently long for restoration of Mz or not (95). This is in direct contrast to the ShMOLLI sequence, which uses a conditional reconstruction algorithm to reject data where there has been incomplete recovery of longitudinal magnetisation.

Furthermore, subvariants of the MOLLI 5(3)3 sequence exist on the Siemens platform, designed to address the time available to acquire the IR-weighted images and thus heart rate sensitivity. Siemens MyoMaps product MOLLI variants are divided into “Low HR” (256 matrix readout) and “High HR” (192 matrix readout) variants, where the latter is recommended for heart rates greater than 80 bpm to reduce cardiac motion blurring. Although it is important to minimise the heart rate limitations of the sequence, this is potentially cumbersome for the end-user who may be required to make on-the-fly adjustments to scanning protocols depending on patient heart rates.

A downside of the reduced number of inversion time samples in the MOLLI 5(3)3 scheme is it negatively impacts the estimation of short (e.g., post-contrast) T1 values. As MOLLI 5(3)3 is suboptimal for short T1 ranges, separate variants, such as MOLLI 4(1)3(1)2 (also the current Siemens product variant) have been designed for post-contrast acquisitions (100). This 11-

heartbeat front-loaded variant reduces inaccuracies in the quantification of short T1, but with potentially severe limitations if used to estimate long (i.e., native) T1. Again, to reduce heart rate dependency, Low HR and High HR subvariants exist. It is conceivable that for pre- and post-contrast T1-mapping clinical studies, multiple MOLLI subvariants may be required to fully assess native and post-contrast T1 values depending on an individual's heart rate and contrast status. The additional layer of complexity in MOLLI subvariant selection for both long and short T1 has potential for error and inaccuracies in T1 estimation, particularly when compared to the flexibility of the heart-rate independent one-for-all ShMOLLI technique (**Figure 1.8**).

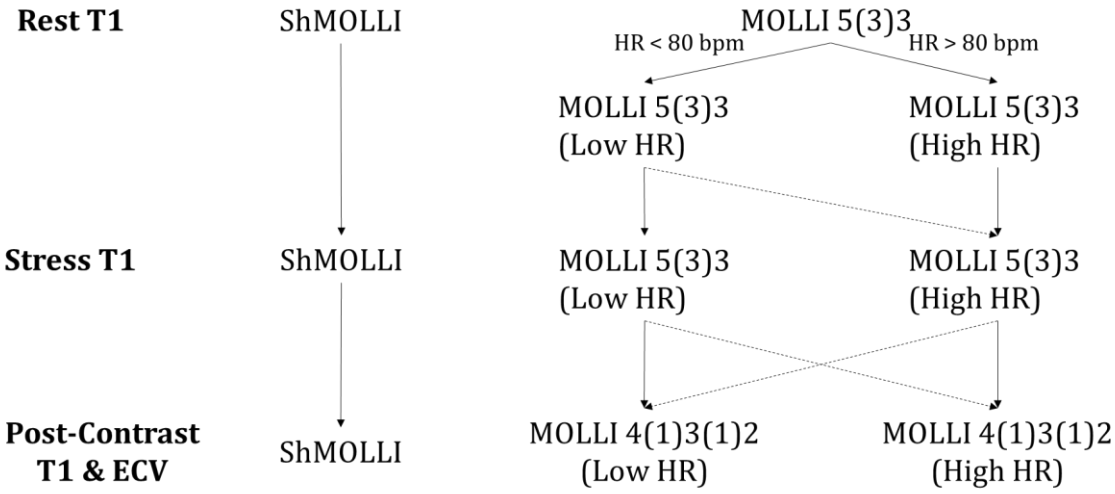


Figure 1.8: Schematic of the pitfalls of T1-mapping method using the MOLLI* a-priori *sequence selection for rest, stress, and post-contrast T1 applications. *Switching between MOLLI variants based on heart rate and contrast status risks incorrect sequence selection and subsequent error, compared to the one-for-all ShMOLLI sequence.*

1.4.2.4 MOLLI 5s(3s)3s

The most recent MOLLI variant uses a sampling scheme of 5s(3s)3s as a way of further reducing heart rate sensitivity (102). By using a minimum time requirement for each part of the acquisition this sequence theoretically mitigates heart rate dependency by standardising the time for Mz sampling and recovery during the acquisition epochs. However, this trade-off results in longer breath holds of ~12-15 seconds, which may be impractical for stress studies in clinical patients. Until now there are no reports of the effect of variable number of images acquired in each epoch on the specific absorption rate (SAR) or T2 and MT sensitivity. Further discussion of this is provided in section **1.5.4**.

1.5 Stress T1-mapping

1.5.1 Basic principles and the role of myocardial blood flow and myocardial blood volume

Stress T1-mapping is a novel T1-mapping application that may be used to assess the coronary vascular compartment and coronary vasodilatory reserve (95). It relies on the principle that coronary vasodilation increases myocardial blood flow (MBF) and myocardial blood volume (MBV). Satisfactory augmentation of MBF and MBV requires adequate coronary vasodilatory reserve, which may be interrogated by pharmacological vasodilatory stress. Myocardial blood volume accounts for approximately 10% of total myocardial

volume at rest and has been shown to increase by around two-fold during vasodilatory stress in healthy individuals with normal coronary vasodilatory reserve (26,103). This increase in MBV is theoretically detectable by stress T1-mapping, given that blood T1 is expected to increase the measured myocardial T1 via partial volume effects (95). Myocardial T1 has been shown to increase by ~6% with narrow normal ranges in healthy volunteers during adenosine vasodilator stress using ShMOLLI T1-mapping (6.2 ± 0.5% at 1.5T; 6.3 ± 1.1% at 3T) (104).

1.5.2 Clinical applications of stress T1-mapping

1.5.2.1 Patients with obstructive coronary artery disease

The assessment of coronary artery disease (CAD) and myocardial ischaemia is an obvious potential clinical application for stress T1-mapping. Although first-pass myocardial perfusion CMR using GBCAs directly assesses global and focal reductions in MBF at rest and during vasodilator stress and has high diagnostic accuracy in detecting significant obstructive CAD (20,105–107), MBF alone may not reflect all aspects of myocardial ischaemia (108).

Myocardial blood volume, which represents the total volume of capacitance vessels in both the coronary micro- and macro-circulations, may be a more comprehensive marker of global ischaemia, and has been shown to closely reflect the level of microvascular autoregulation (26,108–110). Indeed, MBV

is believed to better reflect changes in myocardial oxygen consumption, which is a more specific marker of cellular ischaemia (26,108,111).

As previously discussed (see section **1.2.2**), areas downstream of significant coronary stenosis have increased microvascular capillary recruitment, increased resting coronary vasodilatation, and impaired vasodilatory reserve. These compensatory changes result in increased MBV, which is expected to increase myocardial T1 values (as a surrogate for increased myocardial free water). Stress T1-mapping may thus detect microvascular and blood volume changes, with little reactivity expected in areas of myocardial ischaemia. Adenosine and exercise stress and rest T1-mapping has shown feasibility to distinguish between normal, infarcted, ischaemic, and remote myocardium without the need for GBCAs (104,112–115). Further work is required to validate stress T1-mapping against invasive haemodynamic assessments of coronary physiology as markers of ischaemia.

1.5.2.2 Patients without obstructive CAD

There is further clinical potential for stress T1-mapping to assess coronary vasodilatory reserve and microvascular dysfunction in patients without obstructive CAD. For example, in patients with severe aortic stenosis (AS), the natural physiological response to the increased demands of the hypertrophied and pressure-loaded ventricle is a compensatory increase in resting coronary blood flow, microvascular dilatation, and increased MBV (116,117). Native T1

values thus increase with worsening severity of aortic stenosis and symptom status, reflecting a degree of microvascular compensatory changes (73). Interrogation of these T1 signal changes using adenosine stress (in patients with severe AS but no obstructive CAD) showed a ceiling of stress T1 reactivity similar to healthy volunteers, but with a blunted overall delta T1 response (due to increased resting T1 values) (72). Normalisation of resting myocardial T1 and stress T1 reactivity after aortic valve replacement adds weight to the hypothesis that T1 abnormalities at rest and stress mainly reflect changes in the microvasculature (in the absence of obstructive epicardial CAD) and the intravascular compartment (rather than interstitial fibrosis) (72).

Furthermore, stress T1-mapping may also assess vasodilatory reserve and microvascular dysfunction in patients with systemic diseases such as type 2 diabetes mellitus (T2DM) and end-stage renal disease (ESRD). While these conditions are often associated with obstructive CAD, they may also be associated with microvascular dysfunction, which increases the risk of adverse cardiovascular events and overall mortality. One study in patients with T2DM has shown that impaired coronary vasodilatory reserve is associated with increased cardiovascular mortality, comparable to that of patients with obstructive CAD (118). Blunted myocardial stress T1 reactivity has been seen in patients with T2DM without obstructive CAD, suggesting that stress T1-mapping is indeed a promising technique to assess coronary vasodilatory reserve and microvascular dysfunction (119). These techniques have also

been applied in patients with ESRD (115,120), although whether the blunted stress T1 response in these patients is due to microvascular dysfunction, increased resting coronary vasodilatation, or myocardial fibrosis remains to be determined.

1.5.3 Pharmacological stress agents

Currently there are five pharmacological stress agents approved for use in CMR. These include the coronary vasodilators (adenosine and adenosine triphosphate, regadenoson, and dipyridamole) and one inotropic stress agent (dobutamine) (49).

1.5.3.1 Coronary vasodilators (adenosine, regadenoson, dipyridamole)

The vasodilator stress agents mediate coronary vasodilatation, increased MBF, and increased MBV via interactions with adenosine cell surface receptors on coronary vascular smooth muscle cells and endothelial cells (121). There are four adenosine receptor subtypes, namely A_1, A_{2A}, A_{2B}, and A_3, all of which are expressed in the coronary vasculature. A_{2A} receptor activation is largely responsible for coronary vasodilatation and regulation of MBF and MBV, although activation of the A_{2B} receptor may also play a role (122).

Adenosine is widely used in CMR units as a coronary vasodilator stress agent, typically administered via intravenous (IV) infusion over 3-4 minutes to

achieve maximal hyperaemia. It has a potentially increased adverse-effect profile due to non-selective activation of all four adenosine receptors and is contraindicated in patients with atrioventricular block or reactive airways disease. Dipyridamole is also administered via IV infusion and has a similar mechanism of action to adenosine, given its main mechanism of action is to inhibit the breakdown of adenosine. Regadenoson is a selective A_{2A}-receptor agonist, has similar efficacy as adenosine with a theoretically lower adverse-effect profile, and has advantages in clinical workflow given its ease of administration as a single IV bolus (123).

Recently, animal studies have assessed differences in the adenosine receptor subtypes that mediate myocardial perfusion and T1 reactivity (121). Results have shown that the increases in MBF secondary to vasodilatation of the main epicardial coronary arteries and arterioles is entirely A_{2A} receptor dependent. Adenosine stress T1 reactivity however is more likely to be affected by modulation of MBV (the majority of which is contained within the terminal arterioles and capillaries), with results indicating that this is mediated through both the A_{2A} and A_{2B} receptors (121). The A_{2A} receptor may mediate these effects on MBV by stimulating endothelial nitric oxide synthase (eNOS) activity either directly or indirectly (via flow-mediated dilatation), whereas increased capillary recruitment and MBV via A_{2B} receptor activity simply relates to direct receptor-mediated stimulation of microvascular smooth muscle cells. Conversely, changes in myocardial perfusion and MBF seem to occur

independently of eNOS activity (121). Ultimately, this highlights that stress T1 reactivity and regulation of MBV is a complex mechanism with many vascular mediators, but that this could be a potentially novel translational therapeutic target that can be monitored using CMR stress T1-mapping.

1.5.3.2 Inotropes (dobutamine)

Dobutamine is a commonly used pharmacological stress agent in both echocardiography and CMR for the assessment of obstructive CAD and myocardial viability. It is a synthetic sympathomimetic catecholamine with strong beta1-adrenergic receptor activity, and mild alpha1- and beta2-receptor activity. This results in marked inotropic effects at low doses (<10 μg/kg/min), with increased chronotropic effects alongside increased myocardial oxygen demand and myocardial work at higher doses (20-40 μg/kg/min) (124). Flow-limiting coronary stenosis means that increased myocardial oxygen demand cannot be met by an increase in MBF, resulting in supply-demand mismatch. This in turn results in myocardial ischaemia, with the development of regional wall motion abnormalities which may be detected by CMR cine imaging. Additionally, differences in contractile response to low, intermediate, and high dobutamine doses may help differentiate between areas of non-viable and viable myocardium, which typically demonstrates contractile reserve at lower doses. Dobutamine stress CMR provides important diagnostic and prognostic information for the assessment of patients with CAD (125).

Dobutamine is rapidly metabolised (half-life approximately two minutes) and has a short onset of action, making it suitable for stress testing (126). It is administered as an IV infusion, typically starting at 5 μg/kg/min (especially for viability assessment), followed by an increase to 10 μg/kg/min after 3 minutes and then in 10 μg/kg/min increments every 3 minutes thereafter to a maximum dose of 40 μg/kg/min. A typical endpoint is achievement of a target heart rate of 85% of maximal predicted heart rate, which has been shown to improve diagnostic accuracy for detecting significant obstructive CAD (127), with overall sensitivity and specificity of 83% and 86% respectively (128). While dobutamine CMR may be combined with first-pass perfusion imaging (at peak dobutamine stress) to increase diagnostic accuracy (129,130), it has not been explored for stress T1-mapping applications, which may offer a contrast-free alternative to improve ischaemia detection in combination with wall motion assessment.

A head-to-head comparison of the different pharmacological stress agents in terms of drug dose, half-life, mechanism of action, contraindications, and adverse effects is provided (**Table 1.1**).

Table 1.1: Pharmacological stress agents

	Dose	Half-life	Mechanism of Action & Contraindications	Adverse Effects
VASODILATORS				
Adenosine	140-200 µg/kg/min (for 3-4 min) Requires infusion pump with extension tubing and two separate IV cannulas (to prevent adenosine bolus post-Gd injection)	10 sec	Non-selective adenosine receptor agonist (indirect coronary vasodilation) A_1: ↓ atrioventricular (AV) conduction A_{2A}: coronary vasodilation A_{2B}: peripheral vasodilation, bronchospasm A_3: bronchospasm C/I: reactive airways disease; 2° or 3° AV block or symptomatic bradycardia; hypotension (<90 mmHg) or uncontrolled HTN (>200/110 mmHg); ACS; recent caffeine intake	Flushing & nausea Chest pain Dyspnoea Palpitations AV block Bronchospasm
Regadenoson	400 µg bolus injection (peak effect 30-60 sec) Reversal: aminophylline (25-100 mg)	2-4 min with up to 30 min intermediate phase	Selective A_{2A} agonist and direct coronary artery vasodilator C/I: 2° or 3° AV block or symptomatic bradycardia; hypotension (<90 mmHg) or uncontrolled HTN (>200/110 mmHg); ACS; recent caffeine intake	Dyspnoea Flushing & nausea Chest pain Palpitations
Dipyridamole	0.142 mg/kg/min (for 4 min) (0.56 mg/kg total) Reversal: aminophylline (25-100 mg)	30-45 min	Inhibits adenosine deaminase and ↓ intracellular reuptake of adenosine → similar mechanism of action as adenosine with indirect coronary vasodilation C/I: as for adenosine	Chest pain Headache Dizziness Flushing & nausea AV block
INOTROPES				
Dobutamine	Infusion protocol: • 5 µg/kg/min • 10 µg/kg/min • 20 µg/kg/min • 30 µg/kg/min • 40 µg/kg/min	2-3 min	Direct adrenergic β1 and β2 receptor stimulation (inotropic at low doses; ↑ HR and BP responses at higher doses) C/I: ACS; LVOT obstruction (e.g., HCM, AS); uncontrolled tachyarrhythmias or HTN (>200/110 mmHg); aortic dissection Reverse with IV beta blockers if necessary	Chest pain Palpitations Headache Flushing Dyspnoea Arrhythmias

1.5.4 Stress T1-mapping pitfalls and method selection

As previously discussed (see section **1.4.2**), there are multiple current T1-mapping techniques, all with different properties and norms. This is particularly relevant for stress T1-mapping applications, where methods that are less sensitive to heart rate effects are desirable. Current data suggests that the MOLLI 5(3)3 method may underestimate the stress T1 response, with ShMOLLI showing a >40% larger stress response in healthy controls (6.2 ± 0.5% at 1.5T (104) vs. 4.3 ± 2.8% at 1.5T (131)). These comparative differences in effect sizes may have real clinical implications and could lead to the misdiagnosis of significant cardiac pathology.

It is likely that this inter-method discrepancy in stress T1 response is due to heart rate sensitivity, with MOLLI 5(3)3 underestimating T1 values at higher heart rates. This is due to measurement error inherent within the MOLLI sequence from its inability to disregard data acquisitions where Mz has not sufficiently recovered, thus resulting in underestimation of stress T1 values and a smaller delta T1. ShMOLLI, which has eliminated heart rate dependency (via its conditional reconstruction algorithm), would thus seem far more suited to stress applications during dynamic heart rate changes. ShMOLLI also has the added benefits of short breath holds (~5 seconds per T1-map acquisition at a HR >100bpm) and greater flexibility and practicality in that it is an "all-in-one" technology that can reliably assess both long and short T1 times at a variety of heart rates without the need for additional subvariant

selection (95). Simulations and phantom experiments have shown the increased underestimation error with original MOLLI compared to ShMOLLI (**Figure 1.9A**), which may be extrapolated to include MOLLI 5(3)3 (**Figure 1.9B**).

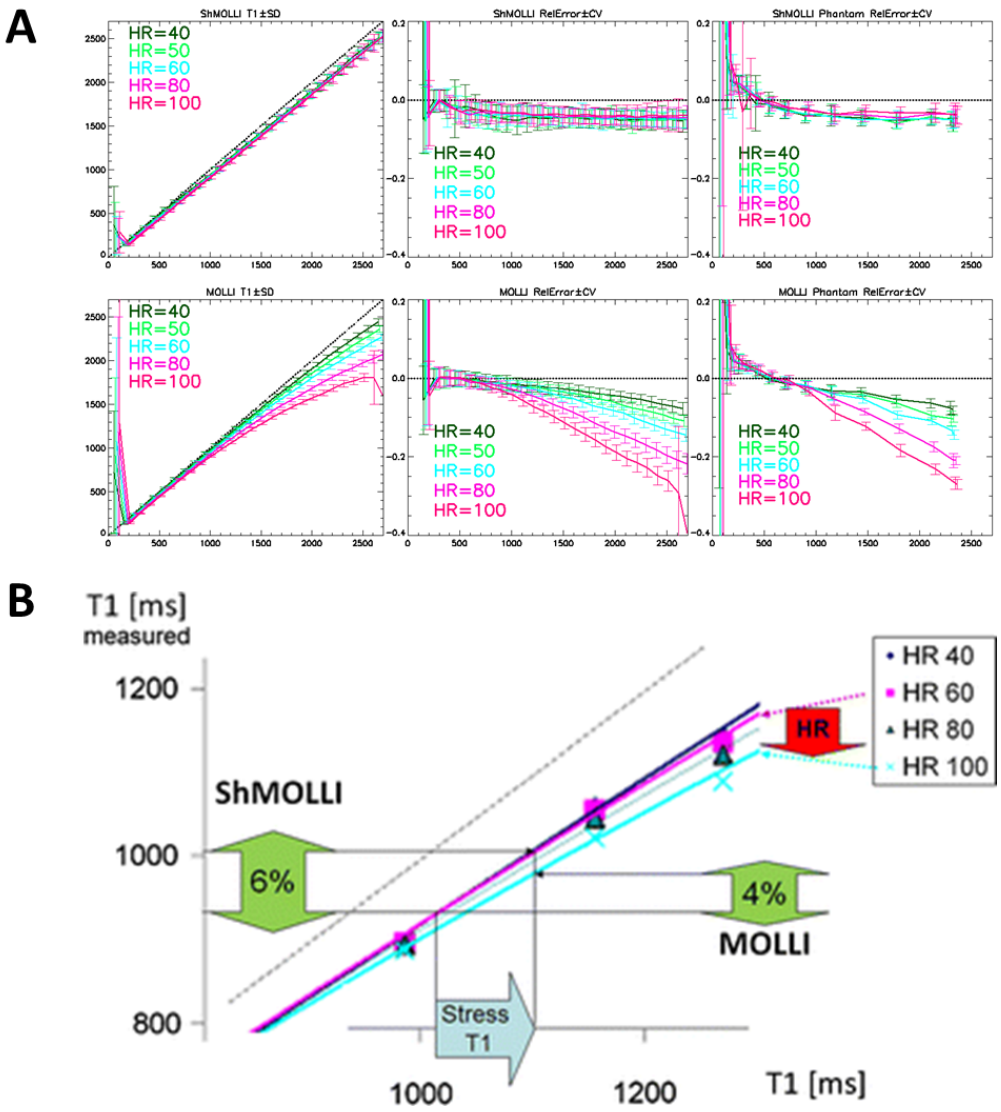


Figure 1.9: Heart rate sensitivity of T1-mapping methods. *Relationship between T1 measurements for ShMOLLI (top row) and original MOLLI (bottom row) across a range of T1 times and heart rates in both computer simulations and phantom experiments (A). The diagonal line represents the ideal identity line. The estimation error of ShMOLLI is consistently ~4%, while the error for original MOLLI depends both on T1 and particularly on heart rate. The mechanism for stress T1 underestimation using MOLLI 5(3)3 variant compared with ShMOLLI is also shown (B). ShMOLLI has no heart rate dependence and moves along a single linear relationship at different heart rates, preserving the relative size of the stress T1 response. In contrast, MOLLI switches between heart rate-dependent relationships, resulting in increased error and a lower (~4%) stress T1 response. Reproduced and adapted with permission from Piechnik et al. (92) (A) and Piechnik et al. + Lee et al. (95,132) (B).*

Similar to ShMOLLI, the MOLLI 5s(3s)3s research prototype may minimise heart rate sensitivity by the introduction of fixed seconds-based (rather than heartbeat-based) breath holds, thus giving greater time for Mz recovery during stress. MOLLI 5s(3s)3s has similar adenosine stress T1 reactivity to ShMOLLI at 1.5T of ~6.2% based on reported T1 values (133), but at the price of much longer breath holds (12-15 seconds per T1-map acquisition). These longer breath hold requirements are likely to worsen the substantial motion artefacts already reported from MOLLI 5(3)3 studies (131), thus introducing further T1 errors which can be only partly overcome by motion correction (MOCO) technology (95).

Furthermore, there are factors other than heart rate that may impact on stress T1-mapping, including T1 sensitivities to T2 and magnetisation transfer (MT) effects. The increased myocardial water content during stress (secondary to increased MBV) also directly affects T2 and MT to synergistically increase myocardial T1 (95). Magnetisation transfer effects in particular may be increased by T1-mapping methods that use seconds-based sampling schemes (e.g., MOLLI 5s(3s)3s), due to significant differences in MT sensitivity within the same variant during rest and stress. For example, MOLLI 5s(3s)3s would be expected to deploy as MOLLI 5(3)3 at heart rates of 60 bpm, but at 120 bpm (i.e., during stress) it would be closer to MOLLI 10(6)6, with twice as many image acquisitions per inversion recovery experiment and therefore more energy deposited into the invisible proton pools (95).

Although it is not possible to resolve all of these complex intrinsically linked factors, it highlights the importance of T1-mapping method selection, particularly for stress applications. There is a clear need for early method standardisation for stress T1-mapping to help advance the field forward.

1.6 Current knowledge gaps

It is clear from the evidence summarised in this introductory Chapter that stress T1-mapping holds potential as a novel contrast-free CMR technique that can assess multiple facets of cardiovascular disease including myocardial ischaemia and CAD, coronary vasodilatory reserve, and the state of the coronary microcirculation.

Despite these observations, the majority of the literature remains limited to original proof-of-principle studies using adenosine, even though there is widespread use of multiple other pharmacological stress agents in clinical CMR centres worldwide. There remains a need to systematically validate stress T1 reactivity against invasive markers of coronary ischaemia. Furthermore, there is ongoing uncertainty regarding the optimal T1-mapping method for stress applications given the distinct lack of head-to-head comparative studies. There is thus a clear need to prospectively validate, explore and standardise stress T1-mapping techniques against invasive physiology and across multiple pharmacological stress agents, and to directly

evaluate the most commonly used T1-mapping methods in their suitability for stress applications.

1.7 Overview of Thesis

This Thesis is based on a series of prospective studies that were designed to address several distinct scientific questions regarding stress T1-mapping in terms of validation, methodological development and standardisation, as well as clinical applications for the assessment of cardiovascular disease. A comprehensive and detailed description of methods used in these studies is contained in **Chapter 2**.

The clinical application of stress T1-mapping for the assessment of cardiovascular disease (particularly ischaemic heart disease) has thus far relied upon comparison with first-pass perfusion and LGE images (which may not be suitable in patients with ESRD) and requires more validation against invasive coronary angiography and physiology, which is needed to drive this field forward. The use of truly contrast-free adenosine stress T1-mapping as an up-front test for the evaluation of cardiovascular disease in patients with end-stage renal disease, validated against invasive coronary angiography and physiology (FFR, QFR, IMR, CFR) was examined. The results of these investigations are reported in **Chapter 3**.

One of the primary questions explored in this Thesis was whether stress T1-mapping could be carried out using regadenoson (a novel "coronary-selective" vasodilator often used when adenosine is contraindicated), evaluate whether the dynamic stress and post-contrast T1 (ECV) responses could be modelled over time, and explore the relationship between stress T1 and myocardial blood flow. The direct head-to-head performances of ShMOLLI versus MOLLI (the two most commonly used T1-mapping sequences worldwide) in terms of their effect size, variability, and measurement stability, were also examined to determine if there is an optimal stress T1-mapping method. The results of these investigations are described in **Chapter 4** and have been published as:

> **Burrage MK** et al. Cardiac stress T1-mapping response and extracellular volume stability of MOLLI-based T1-mapping methods. *Sci Rep.* 11, 13568 (2021). https://doi.org/10.1038/s41598-021-92923-4.

The methodological work performed in **Chapter 4** was essential groundwork allowing application of regadenoson stress T1-mapping to the investigation of ischaemic heart disease in patients with suspected or known CAD. Results of the clinical application of regadenoson stress T1-mapping and its ability to differentiate between normal, infarcted, ischaemic, and remote myocardium in patients with CAD, as determined by stress and rest perfusion and LGE images, are presented in **Chapter 5**. These findings have also been published as:

Burrage MK et al. Cardiovascular magnetic resonance stress and rest T1-mapping using regadenoson for detection of ischemic heart disease compared to healthy controls. *Int J Cardiol*. 2021 Jun 15;333:239-245. doi: 10.1016/j.ijcard.2021.03.010.

The groundwork laid in **Chapter 4** also provided the necessary experience in modelling stress T1 dynamic responses to allow further expansion of the technique to other commonly used pharmacological stress agents. The results of comprehensive stress T1 modelling during dobutamine and dipyridamole infusions in healthy volunteers, along with a comparison of stress T1 reactivity across the different pharmacological stress agents, are contained in **Chapters 6 and 7**.

Finally, the overall conclusions of this Thesis and future research directions are outlined in **Chapter 8**.

2 Methods

2.1 Ethical Considerations

Research procedures received a favourable opinion from the South Central – Oxford A Research Ethics Committee (REC reference: 13/SC/0376) of the National Research Ethics Service (NRES) representing the NRES Directorate within the National Patient Safety Agency and Research Ethics Committees in England. The study also received approval from the Health Research Authority and Oxford University Hospitals NHS Foundation Trust. All work was carried out in accordance with institutional procedures and the principles of the Declaration of Helsinki. All participants gave written informed consent for all study procedures. Data was recorded in an anonymised fashion and stored on a high-compliance server off-site. Written confidential data was kept in locked filing cabinets on-site.

2.2 Study Participants

Healthy Volunteers

Healthy volunteers were recruited from the community via local printed and electronic poster advertising. Interested individuals were provided with a

participant information leaflet and screened for eligibility. All participants gave written informed consent.

Patients with end-stage renal disease undergoing kidney transplant assessment

Patients with known end-stage renal disease (ESRD) referred to Oxford University Hospitals NHS Foundation Trust for kidney transplant work-up between September 2014 and March 2020 were screened for eligibility. Patients meeting inclusion criteria and without any exclusion criteria were provided with a patient information leaflet and invited to take part in the study. Patients who gave written informed consent were then enrolled into the study (see **Chapter 3**).

Patients with suspected obstructive coronary artery disease

Patients with known or suspected chronic CAD undergoing clinically indicated regadenoson stress perfusion CMR in Oxford University Hospitals NHS Foundation Trust were screened for eligibility. Data from patients meeting inclusion criteria and without any exclusion criteria and who had consented for their images to be used for research were prospectively included in the study (see **Chapter 5**).

2.2.1 Inclusion Criteria

All subjects

- Male or female, at least 18 years of age
- Able and willing to give informed consent for participation in the study and able to comply with all study requirements

Patients with ESRD undergoing kidney transplant assessment

- Referred to Oxford University Hospitals NHS Foundation Trust for assessment for kidney or simultaneous pancreas-kidney (SPK) transplantation with:
    - Abnormal myocardial perfusion imaging (SPECT) or abnormal dobutamine stress echocardiography requiring further clinically indicated evaluation with invasive coronary angiography +/- invasive coronary physiology
    - Satisfactory pre-transplant cardiac screening tests requiring no further cardiovascular assessment prior to transplant listing

Patients with suspected CAD

- Referred to University of Oxford Centre for Clinical Magnetic Resonance Research (OCMR) for clinically indicated regadenoson stress perfusion CMR:

- To assess ischaemic burden in patients with suspected or known anatomical CAD and symptomatic angina
- To guide revascularisation strategies following invasive coronary angiography

2.2.2 Exclusion Criteria

All subjects

- Age <18 years old
- Inability to give informed consent
- Significant valvular heart disease (particularly moderate or severe aortic stenosis)
- Severe outflow tract obstruction (hypertrophic cardiomyopathy)
- Uncontrolled arterial hypertension (persistently >180/100 mmHg)
- Uncontrolled arrhythmias
- Significant renal impairment (creatinine clearance <30 ml/min) will be excluded for CMR scans involving intravenous contrast agent administration (but can still safely undergo CMR scans which do not involve contrast administration)
- Contraindications to adenosine (asthma, 2nd or 3rd degree AV block) or regadenoson (2nd or 3rd degree AV block)
- Female who is pregnant, lactating, or planning pregnancy during the course of the study

- Inability to tolerate CMR scanning (claustrophobia, inability to lie flat)
- Contraindications to CMR scanning (implantable devices or other metallic implants, cardiac pacemaker, internal cardioverter-defibrillator, cranial aneurysm clips, metallic ocular foreign bodies, hypersensitivity to gadolinium or other study drugs)
- Any other significant disease or disorder which may put the participant at risk or affect the participant's ability to participate in the study, or may influence the reliability of the study results as determined by the Investigator

2.3 Clinical Assessment

On the day of scanning, all subjects underwent a focused clinical assessment. This included history for:

- Inclusion and exclusion criteria as above
- MRI safety screening questionnaire
- Drug history including allergies
- History of recent caffeine intake (subjects were required to have avoided caffeine for at least 24 hours before the scan)

The following study procedures were also performed:

- Height (cm) and weight (kg) using calibrated scales

- Blood pressure measurement
- 12-lead electrocardiogram (ECG)
- Intravenous cannulation and blood test for haematocrit

2.4 CMR Protocols

Subjects underwent CMR scanning which included the following assessments:

1) Left ventricular volumes and cardiac function
2) Native T1-mapping for tissue characterisation
3) Stress T1-mapping (adenosine, regadenoson, dobutamine, or dipyridamole) as a novel marker of ischaemia and coronary vasodilatory reserve
4) Stress/rest perfusion imaging (regadenoson or dipyridamole) to assess for perfusion defects and quantification of myocardial blood flow
5) Late gadolinium enhancement (LGE) to assess for focal areas of cellular necrosis/fibrosis
6) Post-contrast T1-mapping and extracellular volume (ECV) estimation

CMR examinations were performed using a 1.5-Tesla MRI scanner (MAGNETOM AvantoFit, Siemens Healthcare, Erlangen, Germany) unless otherwise specified (i.e., **Chapter 7**), using an 18-channel phased-array surface coil with the participant supine. Careful skin preparation included cleaning of the skin with a special abrasive skin prepping gel to enhance ECG

connections. Electrodes were positioned carefully to ensure good ECG quality and a large R-wave to T-wave ratio, to reduce the risk of mistriggering during acquisitions. Images were typically acquired during a breath hold at the end of normal expiration to minimise respiratory motion effects.

2.4.1 Cine imaging for cardiac volumes and function

After standard planning, cine images were acquired in three long axis views (horizontal long axis, HLA; vertical long axis, VLA; left ventricular outflow tract view, LVOT) and in short axis slices covering the whole left ventricle (LV) using balanced steady-state free precession cine imaging. Scan parameters were typically: TR/TE = 40.5/1.14 ms, flip angle = 55°, FOV = 380 x 380 mm, voxel size = 2.0 x 2.0 x 8.0 mm, slice thickness = 8.0 mm, GRAPPA = 3, reference lines = 24, segments = 15, measurements = 1, concatenations = 1, bandwidth = 930 Hz/Px. Cines were acquired using retrospective ECG gating for participants in sinus rhythm at the time of the scan. For patients in atrial fibrillation/flutter or with frequent ectopy and where acceptable images could not be obtained, prospectively-triggered cines were acquired instead.

Image analysis for biventricular indices was performed offline in accordance with Society for Cardiovascular Magnetic Resonance (SCMR) guidelines (134), using cvi42 post-processing software (version 5.10.1, Circle Cardiovascular Imaging Inc., Calgary, Canada). Epicardial and endocardial borders on LV short

axis images were manually contoured at end-diastole; endocardial contours were also placed at end-systole. End-systolic (ESV) and end-diastolic (EDV) volumes were used to calculate stroke volume (SV) as SV = EDV – ESV. Ejection fraction (EF) was calculated as EF = SV/EDV. Papillary muscles were included as part of the LV volume but excluded from LV mass. LV mass is calculated as the difference between the total epicardial volume (sum of epicardial cross-sectional areas multiplied by the sum of the slice thickness and interslice gap) minus the total endocardial volume, multiplied by the specific density of myocardium (1.05 g/ml).

2.4.2 Choice of short axis slice positions

Three short axis cine images (basal, mid-ventricular, and apical) were chosen for subsequent imaging sequences. The basal slice was carefully chosen to avoid the LV outflow tract in systole using the LVOT view; the mid-ventricular slice was chosen to include the papillary muscles; the apical slice was carefully selected to ensure that it contained sufficient myocardium to minimise partial volume effects (134). These short axis slice positions were subsequently copied and used for T1-mapping, perfusion imaging, and LGE imaging to allow cross-modality comparisons.

2.4.3 T1-mapping (native)

Myocardial T1-mapping was performed using the ShMOLLI 5(1)1(1)1 sequence as previously published (92). Typical scan parameters were: TR/TE = 378.98/1.07 ms, flip angle = 35°, FOV read = 360 mm, FOV phase = 75%, interpolated voxel size = 0.9 x 0.9 x 8.0 mm, slice thickness = 8.0 mm, trigger delay (TD) = 260 ms, TI 260 ms, measurements = 1, concatenations = 1, bandwidth = 898 Hz/Px. T1-maps were acquired either in a short axis stack covering the entire LV (matched to cine images) or in the basal, mid-ventricular, and apical slices as described above.

Specific modifications to the ShMOLLI sequence above were undertaken to permit application in the presence of tachycardia (i.e., during stress or in the presence of tachyarrhythmias) (99). Briefly, the trigger delay (TD) was reduced to permit readout in systole, thereby reducing the risk of mistriggering that is often encountered when applying the standard diastolic readout (TD = 260 ms) sequence in the presence of tachycardia. Typically, a TD of 0 ms was used to standardise measurements for stress applications.

Quality assessment of ShMOLLI T1-maps was performed using parametric goodness-of-fit (R^2) maps (**Figure 1.7)**, which were available in-line at time of acquisition (64,92). R^2 maps provide a means to allow critical assessment of the quality of T1-maps generated, identify areas of potentially compromised

T1 accuracy, and re-acquire maps of insufficient quality (64). No motion correction techniques were employed.

For inter-method comparisons, MOLLI 5(3)3 (MyoMaps, Siemens Healthcare, Erlangen, Germany) T1-maps were acquired from vendor-provided product protocols including "Low HR" (256 matrix) and "High HR" (192 matrix) variants. Typical scan parameters for MOLLI "Low HR" were: TR/TE = 279.84/1.13 ms, flip angle = 35°, FOV read = 360 mm, FOV phase = 85.2%, voxel size = 1.4 x 1.4 x 8.0 mm, slice thickness = 8.0 mm, resolution = 256, measurements = 1, concatenations = 1, bandwidth = 1085 Hz/Px. Typical scan parameters for MOLLI "High HR" were: TR/TE = 263.55/1.01 ms, flip angle = 35°, FOV read = 360 mm, FOV phase = 85.4%, voxel size = 1.9 x 1.9 x 8.0 mm, slice thickness = 8.0 mm, resolution = 192, measurements = 1, concatenations = 1, bandwidth = 1085 Hz/Px. MOLLI T1-maps were carefully matched to ShMOLLI slice positions and trigger delay to allow fair comparisons.

Offline post-processing of T1-maps was conducted using dedicated in-house software (MC-ROI) developed by Professor Stefan K Piechnik (Interactive Data Language v6.1, Exelis Visual Information Solutions, Boulder, Colorado, USA). Endocardial and epicardial contours were placed using dedicated automated software (135) and manually checked for errors and corrected in compliance with internal training standards (136). Care was taken to minimise

contamination of the myocardium by blood-pool and extra-myocardial structure partial volume effects (**Figure 2.1**).

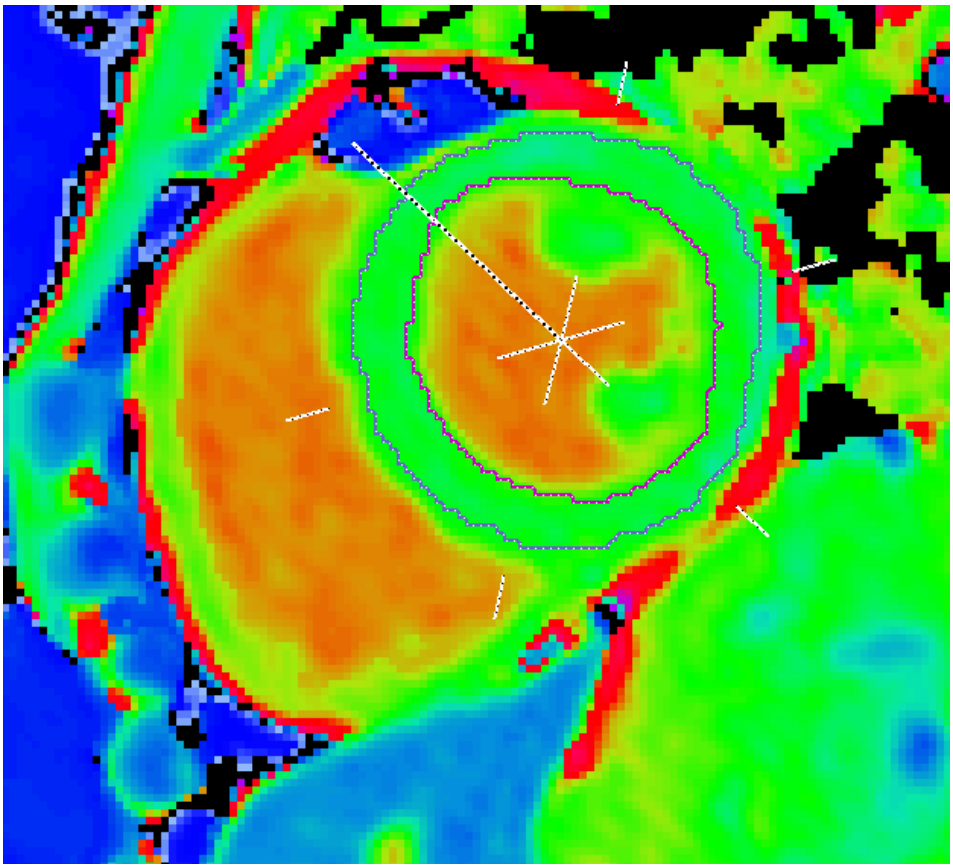


Figure 2.1: T1-map analysis from a mid-ventricular slice using MC-ROI software. *The anterior right ventricular insertion point is marked, while endocardial and epicardial contours are placed within the myocardium so as to avoid contamination from extra-myocardial tissues and partial volume effects.*

Each slice was divided into segments based on the American Heart Association (AHA) 17-segment model (137), using the anterior right-ventricular-left-ventricular insertion point as reference (**Figure 2.2**). Mean T1 values were extracted based on analysis of all voxels in each myocardial segment so as to

determine global and segmental T1 values. Manually drawn regions of interest were also placed in areas of focal myocardial abnormality (e.g., areas of infarction or hypoperfusion) and the LV blood pool, away from the papillary muscles if present, to obtain an estimate of the blood T1 value.

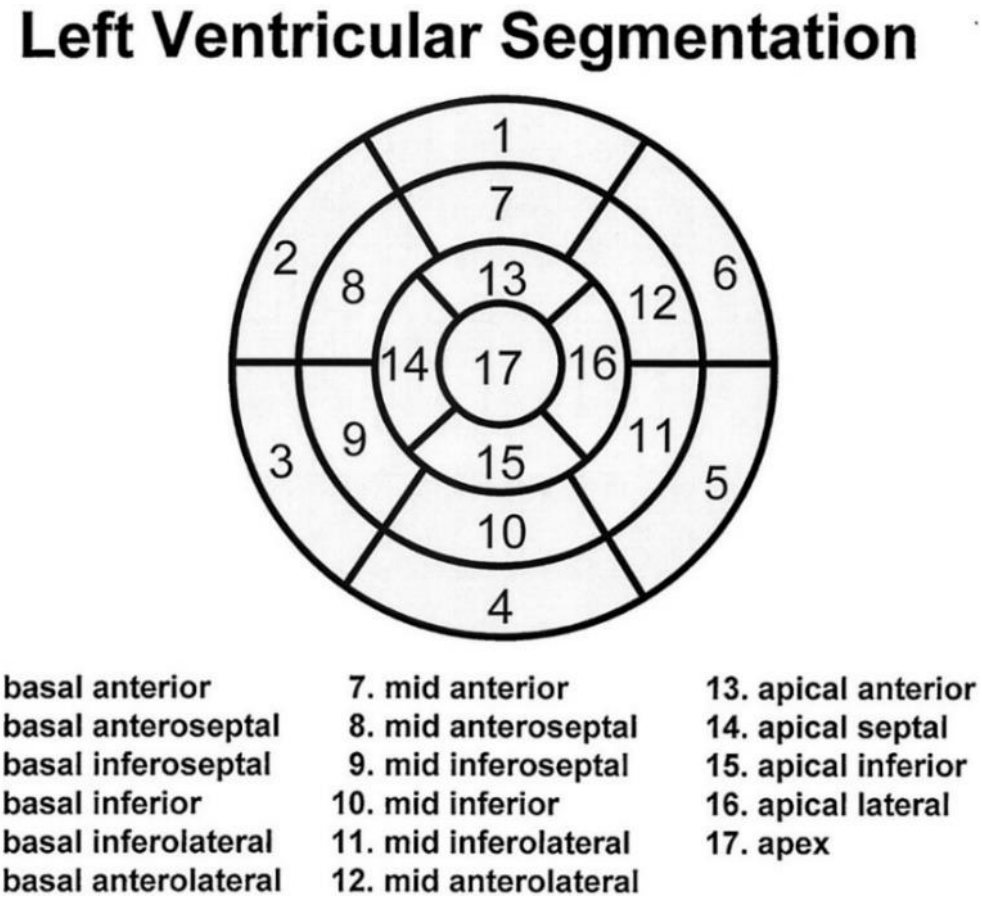


Figure 2.2: American Heart Association (AHA) 17 segment model of Left Ventricular Segmentation. *Reproduced with permission from: Cerqueira et al. Standardised myocardial segmentation and nomenclature for tomographic imaging of the heart. A statement for healthcare professionals from the Cardiac Imaging Committee of the Council on Clinical Cardiology of the American Heart Association. Circulation. 2002 Jan 29;105(4):539-42. (137)*

2.4.4 Stress T1-mapping

Stress T1-maps were acquired following administration of an intravenous stress agent (adenosine, regadenoson, dobutamine, or dipyridamole). Slice position and sequence parameters (with the exception of trigger delay) were identical to those for native T1-mapping. Offline post-processing of stress T1-maps was conducted using the same methods as outlined for native T1-maps (see **2.4.3**). The different pharmacological stress protocols are described in **2.4.5** and **6.3.2** (dobutamine).

Stress T1 reactivity was calculated as:

$$\text{Delta T1} = \frac{stress\ \text{T1} - rest\ \text{T1}}{rest\ \text{T1}} * 100\%$$

2.4.5 Stress and rest perfusion (regadenoson, dipyridamole, adenosine)

Participants were requested to abstain from caffeine and other adenosine antagonists for 24 hours prior to imaging. An intravenous cannula with a three-way tap was placed into the antecubital fossa to allow independent administration of both the pharmacological stress agent and a bolus of gadolinium-based contrast agent. For protocols where participants underwent stress T1-mapping immediately upon first injection of the stress

agent, or required use of an infusion pump, a long line of extension tubing was used so that the participant could remain in the magnet bore.

Regadenoson (Rapiscan, GE Healthcare AS, Oslo, Norway) was administered as an intravenous bolus injection (400 μg over 5-10 seconds) followed by a 10 ml 0.9% sodium chloride saline flush over 10 seconds. Dipyridamole (Persantine) was administered as an intravenous infusion at a standardised dose of 0.56 mg/kg over 4 minutes. Adenosine was administered as an intravenous infusion for at least 3 minutes, initially at 140 μg/kg/min but increased up to a maximum of 210 μg/kg/min depending on presence of a satisfactory haemodynamic response. This was defined as a heart rate increase of at least 10 beats per min from the baseline heart rate and/or a drop in systolic blood pressure drop of at least 10 mmHg from the baseline systolic blood pressure. Heart rate and blood pressure were measured at baseline and at regular intervals during and after pharmacological stress.

Perfusion imaging was performed every cardiac cycle (over 60 heart beats) during the first pass of an intravenous gadolinium-based contrast agent using a T1-weighted fast (spoiled) gradient echo sequence. A test scan was acquired first without contrast agent to allow any problems (e.g., mistriggering, artefacts) to be identified and addressed. Typical scan parameters were: TR/TE = 142/1.04 ms, flip angle = 50°, FOV read = 360 mm, FOV phase = 75%, voxel size = 1.9 x 1.9 x 8.0 mm, slice thickness = 8.0 mm, TI = 105 ms, GRAPPA

= 3, measurements = 60, segments = 37, phases = 1, concatenations = 1, bandwidth = 1085 Hz/Px.

For protocols where automatic inline pixel-wise perfusion mapping was performed, a dual sequence approach with separate pulse sequences for arterial input function (AIF) and myocardial tissue was utilised (138). The AIF is calculated using the LV blood pool signal, which is automatically segmented from optimised low-resolution images acquired in parallel with higher spatial resolution images used for estimating myocardial perfusion (138,139). First-pass perfusion imaging was performed on matching short axis slices (basal, mid-ventricular, apical) to the T1-maps after completion of the stress T1-mapping protocols. A 0.05 mmol/kg intravenous bolus injection of a gadolinium contrast agent (e.g., gadoterate meglumine, Dotarem; gadobutrol, Gadovist; or gadobenate dimeglumine, MultiHance, depending on local protocols) was given, immediately followed by a 15-20 ml saline flush, both administered at 4-6 ml/sec via a power injector. This injection was manually triggered after an interval of 8 heart beats from the initiation of image acquisition. Automated inline pixel-wise perfusion maps were immediately generated, which provide absolute quantification of MBF based on the AHA 16-segment model (137–139).

Stress was reversed (in cases where regadenoson or dipyridamole were used) with an intravenous reversal agent (aminophylline, 100 mg over 10 seconds)

followed immediately by a 10 ml saline flush also over 10 seconds). The adenosine infusion was discontinued after completion of the stress protocol. Rest perfusion imaging was performed in an identical fashion (but without stress agent administration) after a gap of at least 15 minutes following reversal of the pharmacological stress agent.

Offline perfusion analysis was performed using cvi42 post-processing software (version 5.10.1, Circle Cardiovascular Imaging Inc., Calgary, Canada). First-pass stress and rest perfusion images were carefully analysed for the presence of reversible perfusion defects. Quality assessment of the dual AIF sequence approach was performed based on correct positioning of the region of interest (ROI) within the LV blood pool, as well as heart rate mistriggering. Global and segmental quantitative myocardial blood flow measurements were derived from rest and stress pixel-wise perfusion maps (**Figure 2.3**).

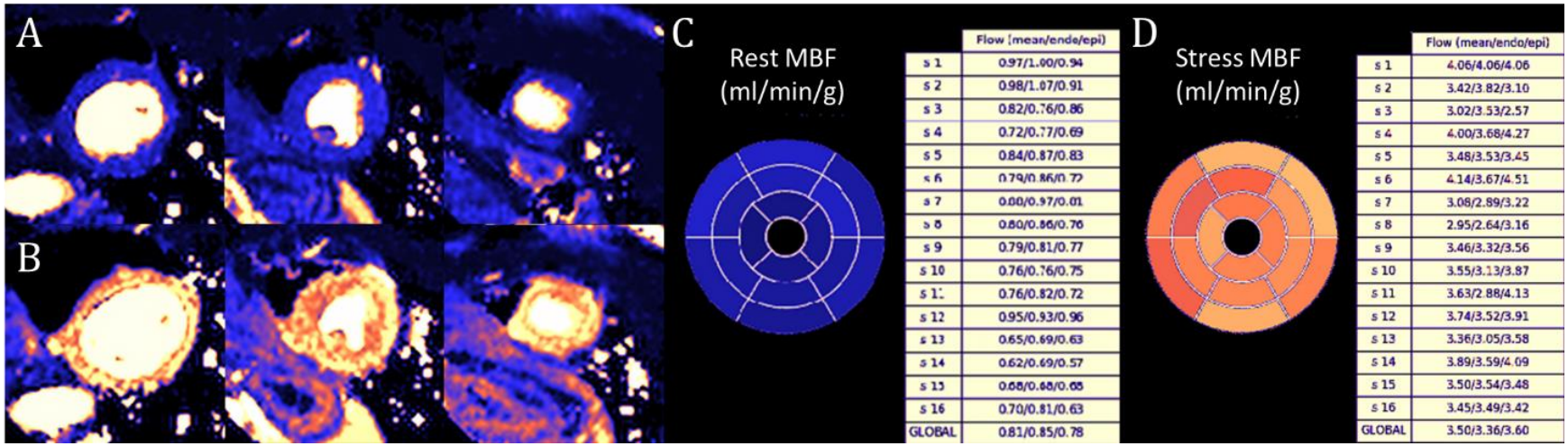


Figure 2.3: Pixel-wise perfusion maps for quantification of myocardial blood flow. *Examples of perfusion maps at rest (A) and stress (B), acquired in the basal, mid-ventricular, and apical slice positions. This visualises the quantitative estimates of myocardial blood flow (MBF) measurements for rest (C) and stress (D), with both segmental and global estimates.*

2.4.6 Late gadolinium enhancement imaging

Late gadolinium enhancement (LGE) images were acquired using a prospectively triggered T1-weighted phase-sensitive inversion recovery sequence approximately 8-10 minutes after administration of a top up of the same intravenous gadolinium-based contrast agent (0.1 mmol/kg; **see 2.4.5**). The inversion time (TI) was adjusted for optimal nulling of remote normal myocardium. LGE images were acquired in standard long and short axis slices covering the whole LV, as well as matched T1-maps and perfusion slices. Typical scan parameters were: TR/TE = 750/3.38 ms, flip angle = 25°, FOV read = 380 mm, FOV phase = 75%, voxel size = 1.5 x 1.5 x 8.0 mm, slice thickness = 8.0 mm, GRAPPA = 2, reference lines = 24, measurements = 1, segments = 25, phases = 1, concatenations = 1, bandwidth = 130 Hz/Px.

Images were evaluated qualitatively in cvi42 post-processing software (version 5.10.1, Circle Cardiovascular Imaging Inc., Calgary, Canada) for the presence or absence, pattern (subendocardial, mid-wall, subepicardial, transmural), and regional distribution of LGE areas. LGE suspected on short axis imaging was confirmed with additional imaging in long axis views or perpendicular to the lesion.

2.4.7 Post-contrast T1-mapping and ECV estimation

Post-contrast T1-maps were acquired following administration of an intravenous gadolinium-based contrast agent. Slice position and sequence parameters were essentially unchanged to those used for native T1-mapping (see **2.4.3**).

Offline post-processing of post-contrast T1-maps was conducted using the same methods as outline for native T1-maps (see **2.4.3**). R1 of blood and myocardium was calculated as R1 = 1/T1 for both native and post-contrast maps. Haematocrit was measured on a blood sample drawn on the same day, immediately prior to the CMR scan.

Extracellular volume (ECV) was calculated using the equation (140):

$$\text{ECV} = (1 - \text{haematocrit}) \times \left(\frac{\Delta R1_{myocardium}}{\Delta R1_{blood}}\right)$$

2.5 Coronary Angiography

Clinically indicated invasive coronary angiography was performed at Oxford University Hospitals NHS Foundation Trust. Participants gave written informed consent to have additional invasive physiology measurements performed if this was in addition to routine clinical care. These were obtained

during maximal hyperaemia, achieved by an intravenous infusion of adenosine, initially at 140 μg/kg/min but increased up to a maximum of 210 μg/kg/min depending on presence of a satisfactory haemodynamic response, for 3-4 minutes.

Measurements were obtained using a coronary PressureWire (Abbott, Santa Clara, California, USA). Aortic pressure (Pa) was recorded from the guiding catheter. Fractional flow reserve (FFR) was defined as the ratio of distal pressure (Pd) measured using the pressure wire and Pa during maximal hyperaemia. Coronary flow reserve (CFR) was defined as the hyperaemic coronary flow divided by resting flow. Index of microcirculatory resistance (IMR) was defined as the mean hyperaemic distal coronary pressure (Pd) multiplied by the mean hyperaemic transit time. Transit times were measured via thermistor-detected temperature changes, calculated as a mean from three injections of 3-5 ml room-temperature saline through the guiding catheter, recorded at baseline and hyperaemia.

To provide a haemodynamic assessment of all coronary vessels in cases where FFR was not possible, the quantitative flow ratio (QFR) was calculated. This novel angiography-based index is derived from the application of computational flow dynamics to three-dimensional modelling of the coronary artery based on two standard angiographic projections (**Figure 2.4**) (141,142). QFR has good correlation with invasive FFR and appears superior

to 2D quantitative coronary angiography for the assessment of intermediate coronary stenoses (143). QFR does not require the use of a coronary pressure wire and was measured offline using QAngio XA 3D software (Medis, Leiden, Netherlands).

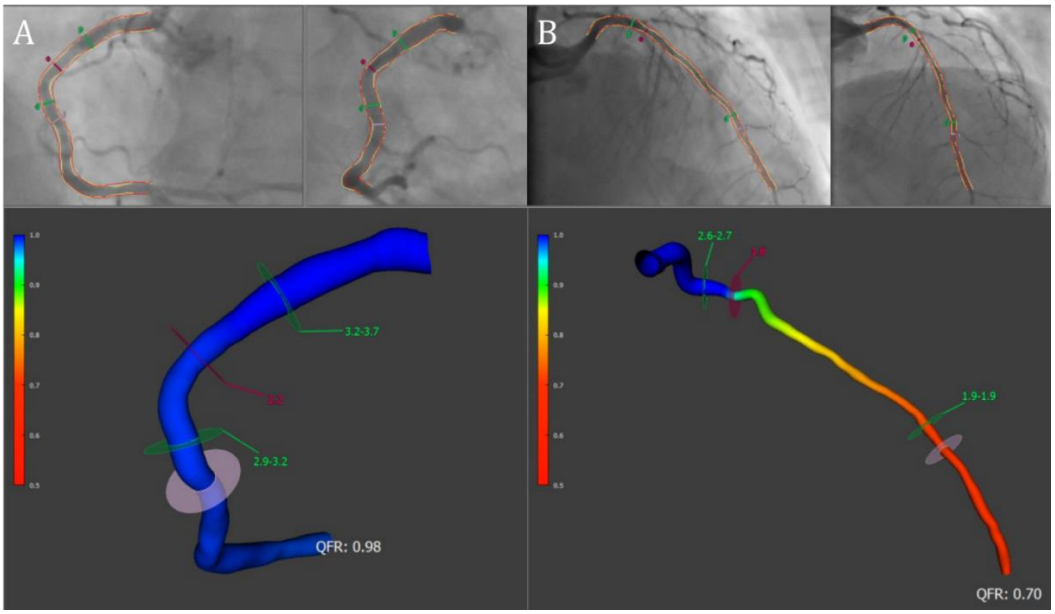


Figure 2.4: Quantitative flow reserve analysis. *QFR measurements are obtained for the right coronary artery (A) and left anterior descending artery (B).Two angiographic projections for each vessel (top) are outlined and used to create a haemodynamic assessment of the selected vessel (bottom). In this example case, there is normal flow reserve in the right coronary artery (QFR 0.98), whereas the left anterior descending artery is diffusely diseased and has evidence of flow limitation (QFR 0.70).*

2.6 Summary

The methods described above provide the backbone for the work conducted in this Thesis. Each individual Chapter will also provide further details and clarification of the specific techniques and methods used.

3 *Adenosine stress T1-mapping to assess cardiovascular disease in kidney transplant candidates*

3.1 Abstract

3.1.1 Background

Kidney transplant candidates are at high risk for adverse cardiovascular events given the increased burden of accelerated coronary artery disease (CAD) that often characterises end-stage renal disease (ESRD). Although guidelines recommend screening for CAD before kidney transplantation, the optimal strategy is not well-defined. Stress perfusion cardiovascular magnetic resonance (CMR) is well-validated in detecting and prognosticating obstructive CAD, but requires the use of gadolinium-based contrast agents (GBCAs). Adenosine stress T1-mapping is a novel contrast-free advanced CMR tissue characterisation technique that has been shown to differentiate between normal, infarcted, ischaemic, and remote myocardium in patients with CAD. This is of particular relevance in patients with ESRD and could act as a potential 'gate-keeper' to invasive coronary angiography. This study therefore aims to explore further clinical application of adenosine stress T1-

mapping in patients with ESRD referred for kidney transplant and provide additional validation of stress T1 reactivity against gold standard invasive measures of coronary ischaemia.

3.1.2 Methods

Patients with ESRD (n=35) referred for kidney or simultaneous pancreas-kidney (SPK) transplant were prospectively recruited and divided into two pre-specified groups based on the presence of normal (n=11) or abnormal (n=24) cardiac functional screening tests. Healthy controls (n=12) were also included. All participants underwent adenosine stress CMR at 1.5-Tesla for assessment of stress T1 reactivity (delta T1), which was calculated on a per-coronary artery territory basis. Patients with abnormal cardiac screening also underwent clinically indicated invasive coronary angiography, including measures of coronary physiology such as fractional flow reserve (FFR). In vessels where FFR was not undertaken, offline analysis to derive quantitative flow reserve (QFR) was performed.

3.1.3 Results

Healthy controls had normal resting native T1 values with normal stress reactivity (delta T1 6.8 ± 1.1%), while this was significantly blunted in patients with ESRD and normal cardiac functional testing (delta T1 3.0 ± 1.9%; $p<0.0001$) and patients with ESRD and abnormal functional testing but no

obstructive CAD (delta T1 2.4 ± 1.9%; p<0.0001). Stress T1 reactivity was abolished in areas of myocardial infarction (delta T1 0.1 ± 2.9%; p<0.0001) and in ischaemic territories (FFR or QFR <0.8) downstream of obstructive CAD (delta T1 1.0 ± 1.5%; p<0.0001). A stress delta T1 threshold of 1.8% showed good diagnostic performance for detecting obstructive epicardial CAD in ESRD on ROC analysis (AUC 0.71 ± 0.07; p=0.003), with a sensitivity of 77%, specificity of 65%, positive predictive value of 46%, and negative predictive value of 88%.

3.1.4 Conclusions

Adenosine CMR stress T1-mapping is able to detect and differentiate between obstructive and non-obstructive CAD in patients with ESRD, as validated against gold standard invasive coronary angiography and physiology, and perform advanced myocardial phenotyping, without the need for radiation or gadolinium-based contrast agents.

3.2 Introduction

Cardiovascular disease is highly prevalent and is the leading cause of morbidity and mortality in end-stage renal disease (ESRD), even after kidney transplantation (144,145). The increased burden of accelerated cardiovascular disease that characterises advanced chronic kidney disease (CKD) reflects a combination of typical risk factors (e.g., insulin resistance, diabetes mellitus, hypertension, hypercholesterolaemia) and CKD-related risk factors such as inflammation, oxidative stress, vascular calcification, and endothelial dysfunction (146). Comorbidities such as diabetes in particular, along with the effects of more advanced CKD (e.g., uraemia, anaemia, autonomic dysfunction), often renders these patients asymptomatic with regard to typical cardiac symptoms despite the presence of severe ischaemic heart disease (146).

Guidelines recommend screening for coronary artery disease (CAD) in ESRD patients before kidney transplantation (144) to determine the risk of an adverse cardiac event before and after transplant, thereby informing decisions on transplant candidacy and safety, and to guide pre-transplant management to maximise both patient and graft health and improve survival (147). A non-invasive strategy is preferred, given that kidney disease is associated with an increased risk of procedural complications from invasive coronary angiography (ICA) and revascularisation (148).

The optimal non-invasive screening strategy to risk stratify and guide management for patients pre- and post-transplant is not well-defined. Both exercise and pharmacological stress imaging tests in CKD and ESRD have higher rates of false-positive and false-negative tests compared to the normal population (149). Single-photon emission computed tomography (SPECT) imaging is commonly used and is predictive of mortality based on ischaemic burden (150). However, SPECT requires ionising radiation, which is an important consideration given the frequent serial evaluation performed whilst on the transplant waiting list, and is less accurate than dobutamine stress echocardiography for the detection of obstructive CAD (149). Computed tomography coronary angiography (CTCA) has a high negative predictive value and is non-invasive, but requires radiation and still presents a significant proportion of false-positive tests in ESRD due to a higher prevalence of vascular calcification (151). Additionally, the iodinated contrast agents used in both CTCA and ICA carry a risk of contrast-induced nephropathy and further decline in any residual renal function (152).

Stress perfusion cardiovascular magnetic resonance (CMR) is well-validated in detecting and prognosticating obstructive CAD with a high degree of accuracy (22,153–155). While CMR is an established superior tool for myocardial tissue characterisation, stress perfusion imaging and late gadolinium enhancement (LGE) imaging to distinguish ischaemic from non-ischaemic pathologies both require gadolinium-based contrast agents

(GBCAs), which are relatively contraindicated in ESRD due to the risk of nephrogenic systemic fibrosis (156). A non-invasive diagnostic test that detects myocardial disease and inducible ischaemia, without the need for contrast agents or radiation, would be of great value and could act as a 'gate-keeper' to invasive coronary angiography.

Native T1-mapping is a contrast-free advanced CMR tissue characterisation technique that is sensitive to detecting disease or a change in physiology in a wide range of myocardial and systemic diseases (including CKD), and may detect changes beyond conventional LGE imaging (157–164). T1-mapping is particularly sensitive to changes in myocardial free water and thus myocardial blood volume (MBV) via partial volume effects, which is of particular relevance in the assessment of myocardial ischaemia. Near-maximal compensatory vasodilatation in the coronary microcirculation in ischaemic myocardium downstream of a significant coronary artery stenosis results in an increased MBV, which is likely to demonstrate little further reactivity with vasodilator stress (165,166). These changes are detectable using CMR stress T1-mapping.

In a proof-of-concept study, adenosine stress T1-mapping has been shown to differentiate between normal, infarcted, ischaemic, and remote myocardium in patients with CAD without the need for GBCAs (167). Normal myocardium in controls demonstrates significantly increased stress T1 reactivity, which is near-abolished in ischaemic or infarcted myocardium (167). This contrast-

free approach for the assessment of myocardial ischaemia is of particular potential relevance in patients with ESRD and could act as a potential 'gate-keeper' to invasive coronary angiography by allowing advanced cardiac phenotyping for determining ischaemic and non-ischaemic myocardial pathologies. While adenosine stress T1-mapping has been shown to be safe and feasible in patients with ESRD (168,169), no studies have validated the performance of this technique against invasive gold standard coronary physiology measures for detection of ischaemia (such as fractional flow reserve, FFR and quantitative flow reserve, QFR).

This Chapter therefore aims to build on the existing stress T1-mapping development literature. It will provide further clinical validation of the novel adenosine stress T1-mapping technique by directly comparing stress T1 reactivity with gold standard invasive measures of coronary ischaemia (FFR, QFR), and apply this in a population of patients who would benefit most from this technology (i.e., those with ESRD who are kidney transplant candidates). I hypothesised that in kidney transplant candidates with ESRD, contrast-free CMR stress and rest T1-mapping can: 1) detect obstructive CAD (correlated to invasive coronary angiography and physiology); 2) provide reassurance of non-obstructive CAD if the stress T1 response is normal; and 3) detect non-ischaemic myocardial disease.

3.3 Methods

3.3.1 Study population

108 patients with known end-stage renal disease (ESRD) referred to Oxford University Hospitals NHS Foundation Trust for kidney or simultaneous pancreas-kidney (SPK) transplant work-up were screened for eligibility. Patients satisfying the inclusion and exclusion criteria (see **2.2**) were contacted either via telephone or during clinical consultation, provided with a patient information leaflet, and invited to take part in the study. Thirty-five (n=35) patients with ESRD were prospectively recruited and divided into two pre-specified groups based on their clinical characteristics.

Group 1 (n=11): Patients with cardiovascular risk factors (e.g., type 1 or type 2 diabetes mellitus, hypertension, hypercholesterolaemia, history of vascular disease, etc.) but normal pre-transplant cardiac functional screening tests requiring no further cardiovascular assessment prior to transplant listing.

Group 2 (n=24): Patients with abnormal myocardial perfusion imaging (SPECT/MPS) or abnormal dobutamine stress echocardiography requiring further clinically indicated evaluation with invasive coronary angiography.

Healthy controls (n=12) were included from our existing database to compare the normal ranges for rest and stress T1-mapping.

3.3.2 Data acquisition

3.3.2.1 CMR image acquisition

CMR imaging was performed using a 1.5-Tesla MRI scanner (AvantoFit, Siemens Healthcare, Erlangen, Germany), using an 18-channel phased-array coil with the participant supine. After standard planning, cine images were acquired in three long axis views (HLA, VLA, LVOT) and in short axis slices covering the whole left ventricle (LV) using retrospectively ECG-gated balanced steady-state free precession cine imaging (170,171). T1-maps were acquired in matching short-axis slices covering the whole heart based on the ShMOLLI sequence as previously described (172). T1-maps were acquired using both the default trigger delay of 260 ms (i.e., diastolic imaging) and a pre-specified trigger delay of 0 ms (i.e., systolic imaging) to minimise the risk of mistriggering during tachycardia (173). Quality assessment of ShMOLLI T1-maps was performed in-line at time of acquisition using parametric goodness-of-fit (R^2) maps (172).

Adenosine stress was administered as an intravenous infusion for at least 3 minutes prior to scanning so as to achieve maximal hyperaemia. The infusion was commenced initially at 140 μg/kg/min but increasing to a maximum of 210 μg/kg/min, depending on presence of a satisfactory haemodynamic response. This was defined as a heart rate increase of at least 10 beats per min from the baseline heart rate and/or a drop in systolic blood pressure drop of at least 10 mmHg from the baseline systolic blood pressure. Heart rate and

blood pressure were measured at baseline and at one-minute intervals during and after pharmacological stress. Stress T1-maps were acquired in a matching short axis stack covering the whole heart and paired to the rest images. There were typically 5 short axis T1-map slices per patient (median number of slices 5; IQR 5, 6). The trigger delay was adjusted based on the R-R interval to achieve a diastolic readout without mistriggering. A second set of systolic stress T1-maps were acquired (in identical slice positions) using a pre-specified trigger delay of 0 ms as described above. Gadolinium-based contrast agents were not administered.

3.3.2.2 Coronary angiography

Clinically indicated invasive coronary angiography was performed on the same day as CMR scanning at the John Radcliffe Hospital by expert operators blinded to the research CMR results. Site of access and catheter choices were at the discretion of the operator. Invasive coronary physiology measurements (including FFR, IMR, and CFR) were obtained as described in **Chapter 2.5**.

3.3.2.3 Data blinding for analysis

Blinded analysis was undertaken for all subjective analysis techniques (e.g., cine imaging, T1-mapping, coronary angiography QFR). The randomisation function in Microsoft Excel was used to generate anonymous codes for all scans. The order of the anonymised codes was therefore randomised with

respect to the different patient groups and kept separate from the operator in a password-protected spreadsheet. DICOMs were then batch anonymised in this randomised order using DICOM Anonymizer version 1.1.6.1 (Open Source software, copyright Shah He 2008). Anonymised DICOMs were then imported into cmr42 post-processing software (version 5.10.1, Circle Cardiovascular Imaging Inc., Calgary, Canada) and MC-ROI (dedicated inhouse T1-map analysis software developed by Professor Stefan K Piechnik in Interactive Data Language v6.1, Exelis Visual Information Solutions, Boulder, Colorado, USA).

3.3.3 Data analysis

3.3.3.1 CMR data analysis

Image analysis for cardiac indices was performed offline in accordance with SCMR guidelines (171), using cmr42 post-processing software by an operator who was blinded to patient clinical status. Endocardial and epicardial contouring of paired rest and stress T1-maps was performed manually offline using MC-ROI by a second blinded and independent operator who was not involved with data acquisition and was blinded to clinical status, whether T1-maps were rest or stress, and to the overall study design. T1-maps were segmented according to the American Heart Association (AHA) 17-segment model (174). T1-maps underwent rigorous quality control. Only segments with good to excellent image quality were included to ensure maximal accuracy, as previously described (158). Segments with artefacts or other confounders were excluded, resulting in rejection of 21% of myocardial

segments (n=432 out of 2028 total segments) across the combined rest and stress data sets. This is a higher rejection rate than reported elsewhere for rest-T1-mapping studies (158), partly due to the exclusion of segments in rest/stress pairs so as to allow meaningful comparisons.

Mean segmental myocardial T1 values were allocated to each coronary artery territory according to the AHA 16-segment model, accounting for coronary artery dominance (174). Segments were typically allocated as follows: left anterior descending (LAD) artery (segments 1, 2, 7, 8, 13, 14); right coronary artery (RCA) (segments 3, 4, 9, 10, 15); left circumflex (LCx) artery (segments 5, 6, 11, 12, 16), allowing for anatomical variation depending on coronary anatomy. Segmental T1 values were averaged to derive the mean rest and stress T1 values for each coronary artery territory (174), which were then compared to coronary physiology measurements (FFR, IMR, CFR, QFR) on a per-vessel basis after formal unblinding.

3.3.3.2 Coronary angiography data analysis

Coronary physiology measurements were obtained as previously described by expert operators blinded to the research CMR results. Significant obstructive coronary artery disease was defined by an FFR <0.8 (175). Coronary microvascular dysfunction was defined as downstream of vessels without significant obstructive coronary artery disease (FFR ≥0.8), and IMR ≥25 Units or CFR <2.0 (176,177). In vessels where FFR was not performed, offline

analysis to derive QFR was undertaken by two independent operators who were blinded to clinical status, research CMR results, and study design; consensus was achieved by a third independent blinded operator in one case where there were discrepant results. A QFR <0.8 was used to define significant coronary flow obstruction, given its excellent correlation with FFR (178).

3.3.4 Statistical analysis

Data are presented as mean ± SD for all parametric data, and median with interquartile ranges [IQR] for non-parametric data, based on Shapiro-Wilks tests for normality. Paired Student's t-tests were used to assess differences between rest and stress in the same individuals; unpaired t-tests were used otherwise. Between-group differences were assessed using one-way ANOVA with Tukey's post-hoc multiple comparisons. Categorical data was compared using Fisher's exact test. The diagnostic performance of CMR stress T1-mapping for detecting obstructive CAD and depletion of coronary vasodilatory reserve was assessed using receiver operating characteristic (ROC) curves and the associated area under the ROC curve (AUC). Coronary angiography measurements were treated independently for per-vessel analysis of their relationship with stress T1-mapping parameters. A two-tailed $p<0.05$ was considered statistically significant. Statistical analysis and data modelling were performed using R Studio (RStudio Team (2018). RStudio: Integrated Development for R. RStudio, Inc., Boston, MA).

3.4 Results

3.4.1 Study population

Two participants from Group 1 did not undergo research CMR scanning due to body size limitations and claustrophobia, respectively, and were excluded. Two participants from Group 2 underwent invasive coronary angiography but not adenosine stress CMR due to lack of intravenous access and were thus excluded, as was one participant who failed to achieve a haemodynamic response to intravenous adenosine. Two further participants from Group 2 with strongly abnormal cardiac functional testing results had previously undergone coronary angiography at a peripheral centre and did not undergo repeat invasive assessment following multi-disciplinary transplant team discussion; these patients still underwent a research CMR and were included in the analysis. One further participant from group 2 underwent a CTCA rather than invasive angiogram due to technical reasons, but also had a research CMR scan and was included in the analysis. All other participants completed the study protocol and tolerated the procedures without complications. Baseline characteristics of patients and control subjects are detailed in **Table 3.1.**

Table 3.2: Baseline characteristics of the study participants

	Controls (n=12)	Group 1 (ESRD with normal screening) (n=9)	Group 2 (ESRD with abnormal screening) (n=21)	p value *
Age (years)	38 ± 16	51 ± 10	53 ± 13	**0.006**
Male (%)	8 (75)	7 (78)	17 (81)	0.42
BMI (kg/m^2)	22 ± 2	25 ± 2	29 ± 6	**0.0002**
Risk factors				
T1DM	N/A	7 (78)	12 (57)	-
T2DM	N/A	1 (11)	7 (33)	-
Hypertension	N/A	8 (89)	16 (76)	-
Dyslipidaemia	N/A	4 (44)	7 (33)	-
Smoking history	N/A	2 (22)	6 (29)	-
History of IHD	N/A	2 (22)	7 (33)	-
Microvascular complications				
Retinopathy	N/A	7 (78)	7 (33)	-
Neuropathy	N/A	3 (33)	4 (19)	-
Dialysis status				
Pre-dialysis	N/A	4 (44)	9 (43)	-
Peritoneal dialysis	N/A	2 (22)	2 (9)	-
Haemodialysis	N/A	3 (33)	9 (43)	-

*Counts given as number (%); continuous variables as mean ± SD. * p values for between-group differences are based on one-way ANOVA or Fisher's exact test as appropriate.*

Tables 3.2 and 3.3 below summarise the CMR parameters and adenosine stress haemodynamic data, and coronary angiographic findings. During coronary angiography, 68% of patients had obstructive CAD (≥ 50% stenosis on visual assessment), with 50% of patients having multi-vessel (2 or 3-vessel) obstructive CAD, while 32% of patients had no significant angiographic disease (<50% stenosis on visual assessment). FFR was performed in 14/53 (26%) possible vessels; the remaining 39 coronary arteries were not assessed due to severe (n=6) or chronic total occlusions (n=4) or operator discretion (n=29, clearly non-obstructed vessels or were angiographically complex). QFR was performed in 44/53 (83%) of possible vessels; the remaining 9 coronary arteries could not be assessed due to inadequate angiographic views or frame rates. 8 patients subsequently underwent coronary revascularisation via either percutaneous coronary intervention (PCI, n=4) or coronary artery bypass grafting (CABG, n=5); 1 patient required urgent CABG following a failed attempt at PCI.

Table 3.3: CMR parameters and adenosine stress haemodynamic data

	Controls (n=12)	Group 1 (ESRD with normal screening) (n=9)	Group 2 (ESRD with abnormal screening) (n=21)	p value *
Age (years)	38 ± 16	51 ± 10	53 ± 13	**0.006**
Male (%)	8 (75)	7 (78)	19 (86)	0.42
CMR parameters				
LVEF (%)	62 ± 4	60 ± 8	58 ± 12	0.5
LVEDVi (ml/m^2)	75 ± 9	89 ± 16	88 ± 23	0.14
LVMi (g/m^2)	51 ± 13	70 ± 23	75 ± 17	**0.002**
Haemodynamic data				
Rest heart rate (bpm)	67 ± 12	76 ± 14	68 ± 11	0.2
Stress heart rate (bpm)	107 ± 19	93 ± 14	82 ± 13	**0.001**
Rest SBP (mmHg)	116 ± 13	160 ± 26	163 ± 33	**<0.0001**
Stress SBP (mmHg)	113 ± 16	143 ± 26	145 ± 20	**0.0005**

*Counts given as number (%); continuous variables as mean ± SD. * p values for between-group differences are based on one-way ANOVA or Fisher's exact test as appropriate.*

Table 3.4: Invasive coronary angiography findings

	Group 1 (ESRD with normal screening) (n=9)	Group 2 (ESRD with abnormal screening) (n=21)
Coronary angiography		
1-vessel CAD (≥ 50% stenosis)	-	4 (19)
2-vessel CAD	-	9 (43)
3-vessel CAD	-	2 (10)
3-vessel NOCAD (<50% stenosis)	-	7 (33)
Chronic total occlusions (CTOs)	-	4 (19)
Intra-coronary measurements (FFR)		
Number of vessels assessed out of 53 available (excluding CTOs)	-	14 (26)
Vessels with FFR <0.8	-	4 (29)
Vessels with FFR ≥ 0.8	-	10 (71)
Number of vessels revascularized		13 (25)
PCI	-	4 (31)
CABG	-	10 (77)
Offline coronary measurements (QFR)		
Number of vessels assessed out of 53 available (excluding CTOs)	-	44 (83)
Vessels with QFR <0.8	-	12 (27)
Vessels with QFR ≥ 0.8	-	32 (73)

Counts given as number (%). NOCAD refers to "no obstructive CAD".

3.4.2 Myocardial stress T1-mapping

3.4.2.1 Myocardial stress T1 in normal controls and patients with ESRD with normal cardiac functional testing

Healthy controls had normal resting native T1 values (rest T1 953 ± 23 ms) with normal stress T1 reactivity (stress T1 1018 ± 23 ms; delta T1 6.8 ± 1.1%). Patients with end-stage renal disease and cardiac risk factors but normal cardiac functional testing (Group 1) had numerically higher resting native T1 values (rest T1 971 ± 26 ms; p=0.82) but significantly blunted stress T1 reactivity (stress T1 1000 ± 23 ms; delta T1 3.0 ± 1.9%; p<0.0001) compared to healthy controls.

3.4.2.2 Myocardial stress T1 to distinguish between obstructive and non-obstructive coronary arteries

Patients with end-stage renal disease and abnormal cardiac functional testing requiring invasive coronary angiography (Group 2) were further divided based on resting myocardial tissue or invasive angiographic characteristics (**Table 3.4**). Myocardial infarction was defined based on the presence of myocardial thinning, akinesia, and/or a corresponding fixed perfusion defect on non-CMR stress imaging. Obstructive CAD referred to territories downstream of a significant epicardial coronary artery stenosis based on a physiological assessment of ischaemia (FFR or QFR <0.8). Rest and stress T1 values and T1 reactivity for patients with ESRD compared to healthy controls are presented in **Figure 3.1** and **3.2**.

Infarcted segments (n=19 segments in 5 patients) had significantly elevated resting myocardial T1 values (1112 ± 88 ms; $p<0.0001$) compared to healthy controls, with abolished stress T1 reactivity (delta T1 0.1 ± 2.9%; $p<0.0001$). After infarcted segments were excluded, there were no significant differences in resting tissue characteristics across the different groups (all $p>0.05$), although patients with ESRD tended to have numerically higher resting myocardial T1 values.

Myocardium downstream of obstructive CAD had a significantly lower delta T1 compared to downstream of non-obstructive vessels (delta T1 1.0 ± 1.5% vs. 2.4 ± 1.9%; $p=0.04$) and to Group 1 patients with normal cardiac functional testing (delta T1 3.0 ± 1.9%; $p<0.01$). This ischaemic myocardium had similarly impaired stress T1 reactivity compared to areas of myocardial infarction (delta T1 1.0 ± 1.5% vs. 0.1 ± 2.9%; $p=0.77$). All patients with ESRD had significantly blunted stress T1 reactivity compared to healthy controls ($p<0.0001$ for all comparisons). The effect size for using CMR stress T1-mapping (based on delta T1 reactivity) to distinguish between myocardium downstream of obstructive coronary arteries and either myocardium downstream of non-obstructive coronary arteries or ESRD with normal functional testing was large (Cohen's d 0.82 and 1.17 respectively).

Table 3.5: Myocardial T1 tissue characteristics

	Controls	**ESRD with normal functional testing (Group 1)**	**ESRD with abnormal functional testing (Group 2)**			**All**	
	Normal myocardium	**Normal screening**	**No obstructive CAD (FFR ≥0.8 or QFR ≥0.8)**	**Obstructive CAD (FFR <0.8 or QFR <0.8)**	**Myocardial Infarction**	**LV blood pool**	**ANOVA p-value**
Rest T1 (ms)	953 ± 23	971 ± 26	976 ± 39	980 ± 44	1112 ± 80 *†‡§	1614 ± 93	<0.0001
Stress T1 (ms)	1018 ± 23	1000 ± 23	998 ± 33	990 ± 41	1113 ± 82 *†‡§	1565 ± 94	<0.0001
Delta T1 (%)	6.8 ± 1.1	3.0 ± 1.9 *§	2.4 ± 1.9 *§	1.0 ± 1.5 *†‡	0.1 ± 2.9 *†‡	-3.0 ± 3.2	<0.0001

*Delta T1 is calculated as previously described. Data are given as mean ± SD. All statistical analyses were performed using one-way ANOVA with Tukey's post-hoc multiple comparisons. * p<0.05 compared to controls; † p<0.05 compared to patients with ESRD with normal functional testing (group 1); ‡ p<0.05 compared to patients with ESRD without angiographic obstructive CAD (group 2); § p<0.05 compared to patients with ESRD and ischaemic myocardium (group 2) downstream of obstructive CAD (FFR or QFR <0.8).*

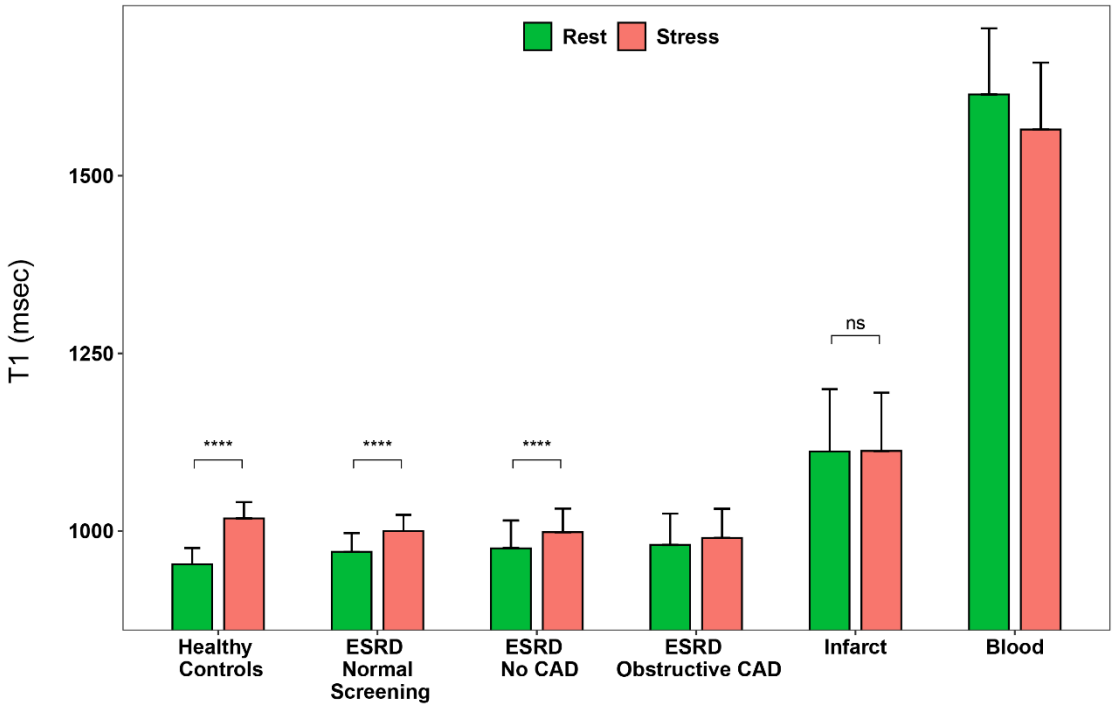


Figure 3.1: Myocardial T1 tissue profiles at rest and during adenosine stress in healthy controls and patients with ESRD referred for kidney transplantation. *T1 values at rest were similar in all groups. Infarcted segments had the highest myocardial T1 values of all groups and tissue classes but remained lower than the reference LV blood pool. During adenosine stress there was a significant rise in myocardial T1 from baseline, which was relatively unchanged in territories supplied by obstructive CAD and in areas of infarction. **** p<0.0001; ns = not significant.*

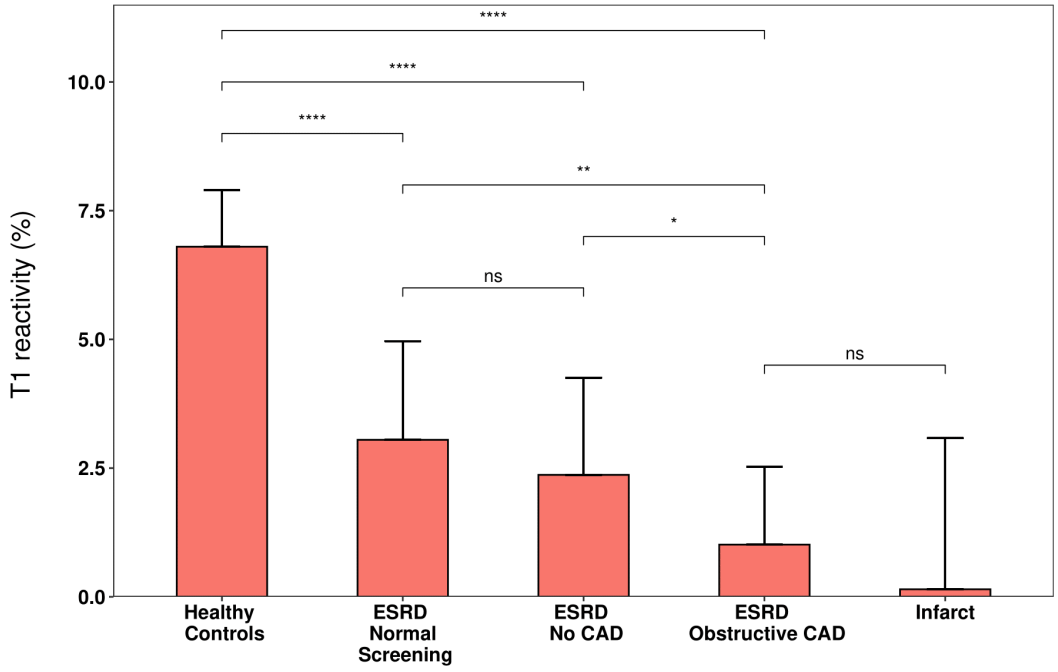


Figure 3.2: Myocardial stress T1 reactivity in healthy controls and patients with ESRD referred for kidney transplantation. *T1 reactivity is defined as the relative change in T1 with stress compared to rest (i.e., delta T1). Patients with ESRD had significantly blunted T1 reactivity compared to healthy controls. There was little to no reactivity in those territories with evidence of myocardial ischaemia (i.e., ESRD obstructive CAD) or infarction. * p<0.05; ** p<0.01; *** p<0.001; **** p<0.0001; ns = not significant.*

3.4.2.3 Diagnostic performance of stress T1-mapping to detect obstructive CAD

A stress delta T1 threshold of 1.8% (using Youden's optimal cut-off method) showed good diagnostic performance for detecting obstructive epicardial CAD (FFR or QFR <0.8) in ESRD on ROC analysis (AUC 0.71 ± 0.07; p=0.003; **Figure 3.3**), with a sensitivity of 77% (95% CI: 50-93%), specificity of 65% (95% CI: 49-79%), positive predictive value (PPV) of 46% (95% CI: 31-79%), and

negative predictive value (NPV) of 88% (95% CI: 68-93%). A stress delta T1 threshold of 3.2% showed good performance for excluding obstructive CAD with a sensitivity of 100% (95% CI: 81-100%), specificity of 26% (95% CI: 14-41%), and NPV of 100% (95% CI: 73-100%).

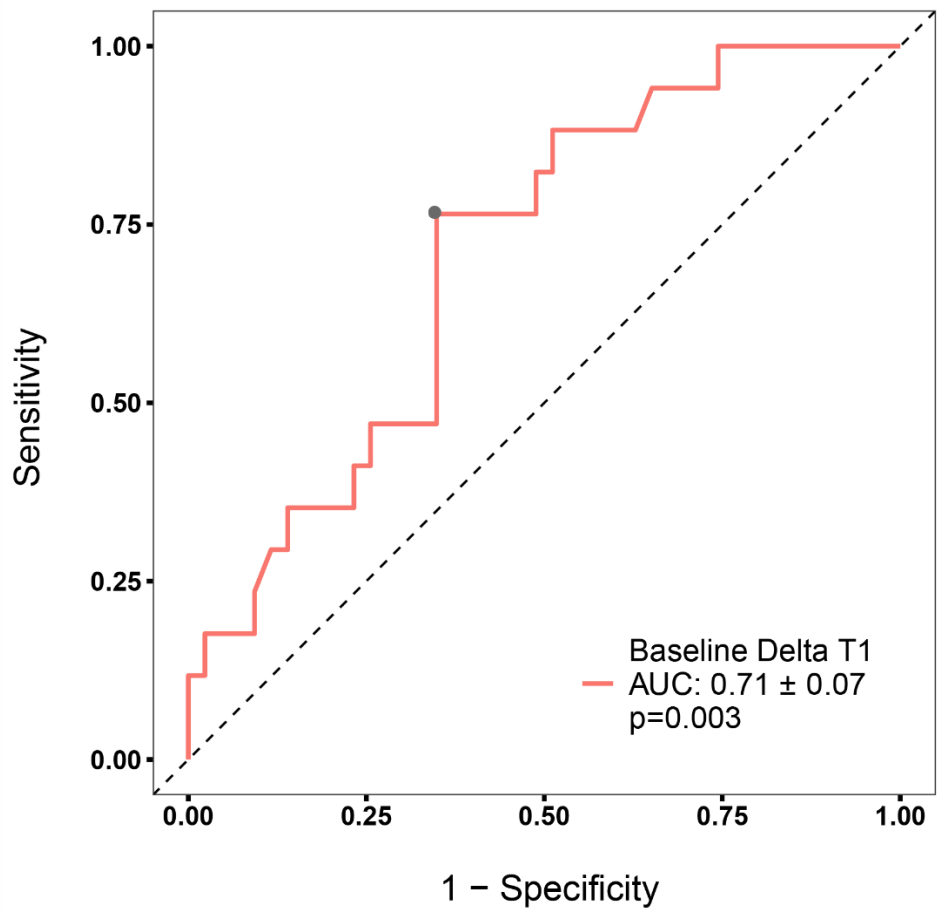


Figure 3.3: Diagnostic performance of CMR stress T1-mapping for detecting obstructive coronary artery disease in patients with end-stage renal disease referred for kidney transplantation. *True positive: myocardial segments downstream of obstructive coronary arteries (FFR or QFR <0.8); true negative: myocardial segments downstream of non-obstructive coronary arteries (FFR or QFR ≥0.8). Stress T1-mapping (AUC 0.71 ± 0.07, p=0.003) had good diagnostic performance for detecting obstructive CAD. The grey dot represents the optimal cut-off point with sensitivity 77% and specificity 65%. Data are based on 60 coronary artery territories in 21 patients.*

The relationship between stress myocardial delta T1 and invasive FFR and QFR is presented in **Figure 3.4 and 3.5**. The established delta T1 threshold of 1.8% was optimal for distinguishing myocardial territories downstream of coronary arteries with FFR and QFR <0.8 and FFR and QFR ≥0.8, with few false negative cases.

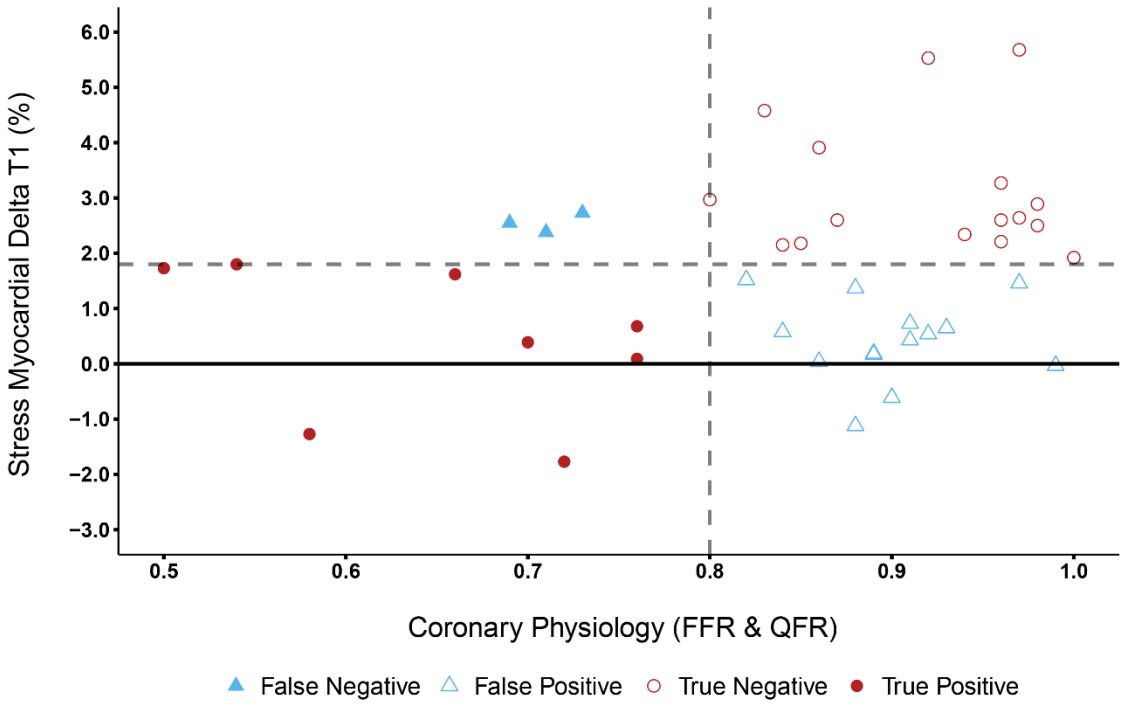


Figure 3.4: Relationship between stress myocardial T1 reactivity and coronary physiology assessed by invasive fractional flow reserve (FFR) and quantitative flow reserve (QFR). *The grey dashed lines represent the established delta T1 threshold of 1.8% (horizontal) and the FFR and QFR cut-off of 0.8 (vertical) suggesting obstructive coronary physiology. Data presented are from 41 vessels in 18 patients. False negatives: 3 vessels in 3 out of 18 patients; false positives: 14 vessels in 8 out of 18 patients; true positives: 8 vessels in 6 out of 18 patients; true negatives 16 vessels in 11 out of 18 patients.*

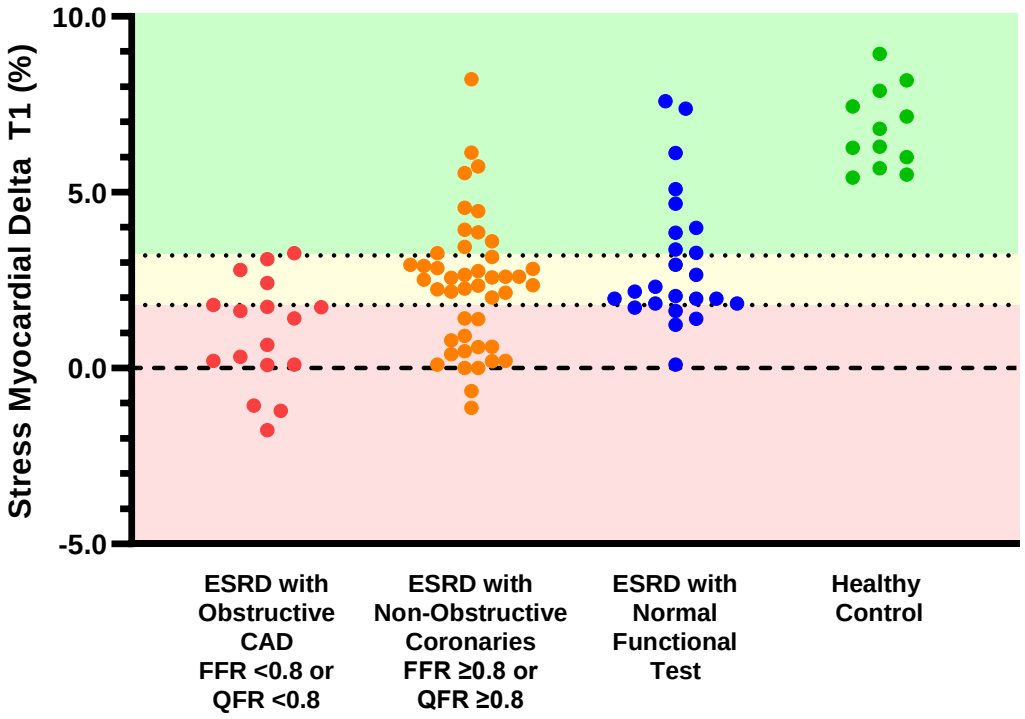


Figure 3.5: Stress T1-mapping as an up-front test to assess for obstructive coronary artery disease in patients with end-stage renal disease referred for renal transplant assessment. *The red, orange, and blue dots represent non-infarcted coronary artery territories. The green dots represent healthy controls. The red shaded area represents a stress delta T1 <1.8% (sensitivity 77%, specificity 65%, PPV 46%) suggesting obstructive CAD. The green shaded area represents a stress delta T1 >3.2% (sensitivity 100%, specificity 26%, NPV 100%), suggesting no obstructive CAD.*

3.4.2.4 Stress T1 polar maps for up-front assessment of cardiovascular disease

Anonymised polar maps showing the gradient of stress T1 reactivity changes from base to apex were created, based on the AHA 16-segment model (**Figure 3.6**). An experienced cardiologist with 13 years of CMR and T1-mapping experience reviewed these polar maps on a case-by-case basis and was blinded

to all other clinical information except for CMR cine imaging. The blinded observer correctly identified the presence or absence of myocardial infarction in 95% (20/21) of cases. They correctly identified the presence or absence of obstructive CAD in 67% (14/21) of individual cases. The use of polar maps identified the three false negative cases (**Figure 3.4** above; solid blue triangles) and correctly re-classified them as having obstructive CAD. This was due to the obstructive coronary lesion being located in the mid vessel; the preserved stress T1 reactivity was driven by a high delta T1 in the basal segments (i.e., proximal to the lesion), but significantly blunted or near abolished downstream of the stenosis (**Figure 3.6**).

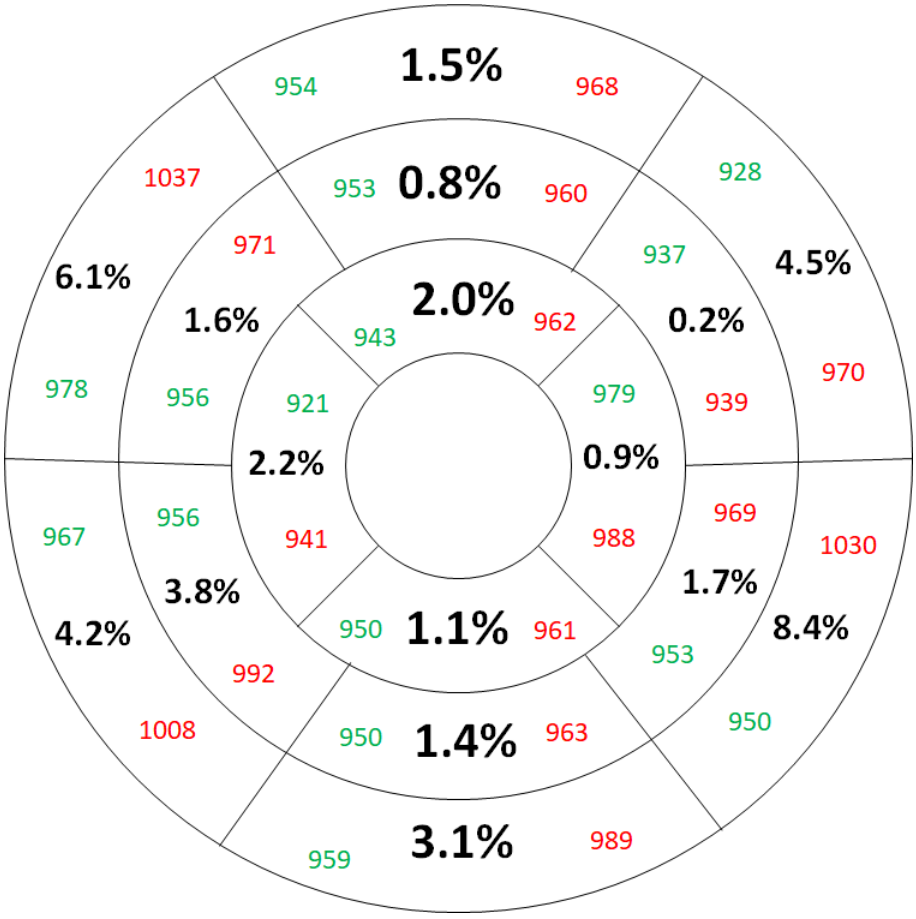


Figure 3.6: Representative polar map example based on segmental stress T1 analysis. *The LAD territory in this case had an overall stress T1 reactivity of 2.4% (i.e., >1.8% ischaemic threshold) when averaged across all segments. Blinded analysis correctly identified that this was driven by normal stress T1 reactivity in the basal anterior septum (6.1%), which was upstream of the haemodynamically significant angiographic stenosis; downstream segments in the mid anteroseptal, anterior, and anterolateral walls had blunted stress T1 reactivity suspicious for ischaemia. The green numbers represent rest T1 and the red numbers represent stress T1.*

These cases were re-classified based on the stress T1 reactivity downstream of the presumed coronary stenosis from the polar map analysis. The same optimal stress delta T1 threshold of 1.8% showed near trend-level significance for improved diagnostic performance (p=0.09 comparing the two models) of

stress T1 for detecting obstructive epicardial CAD (AUC 0.75±0.06, p<0.0001) with a sensitivity of 94% (95% CI: 71-99%), specificity of 65% (95% CI: 49-79%), PPV of 52% (95% CI: 36-98%), and NPV of 97% (95% CI: 81-98%) (**Figure 3.7**).

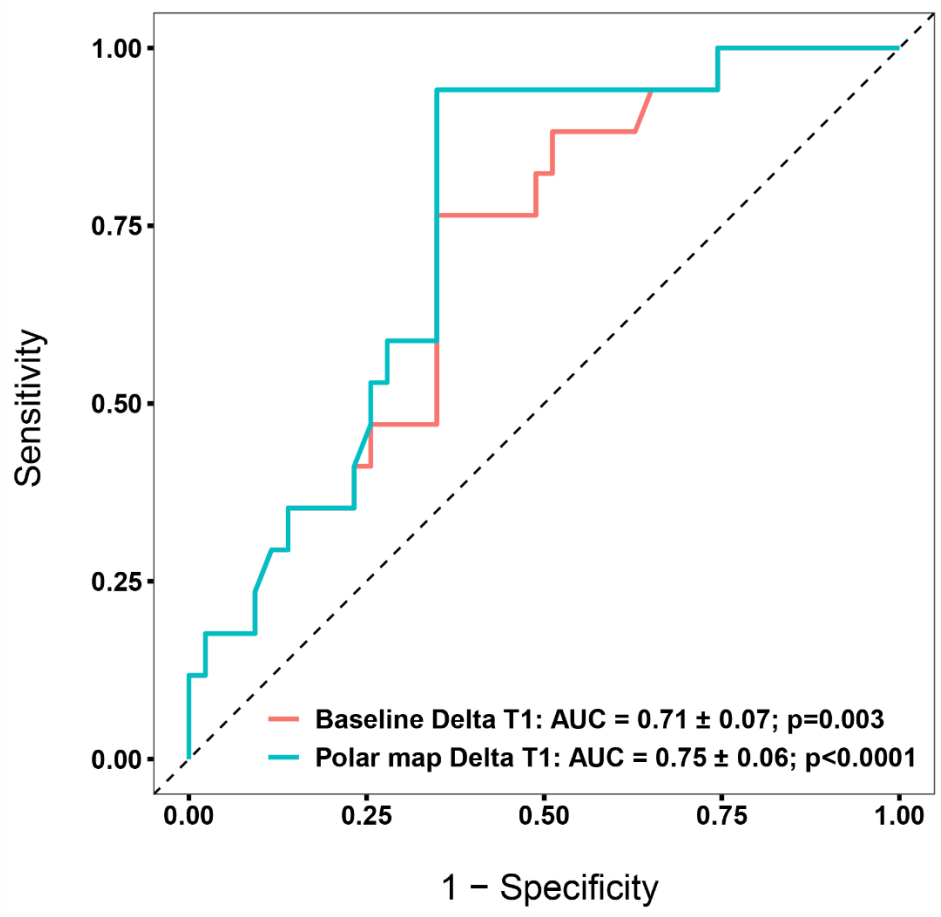


Figure 3.7: Diagnostic performance of CMR stress T1-mapping for detecting obstructive coronary artery disease in patients with end-stage renal disease referred for kidney transplantation following polar map analysis. *The red curve (Baseline Delta T1) refers to the original up-front use of stress T1-mapping without the use of polar maps; the blue curve (Polar map Delta T1) follows blinded polar map analysis and re-classification of three false negative cases. The diagnostic performance of stress T1-mapping for detective obstructive CAD has improved (AUC 0.71 ± 0.07 to 0.75 ± 0.06).*

3.5 Discussion

This is the first study to systematically evaluate the diagnostic performance of CMR adenosine stress T1-mapping for detecting obstructive epicardial CAD, as defined by invasive coronary angiography and invasive physiological measurements, in patients with ESRD referred for kidney transplant assessment. Stress T1-mapping showed good diagnostic performance for detecting obstructive CAD (as defined by an FFR or QFR <0.8) from territories with non-obstructive CAD.

3.5.1 Stress T1-mapping to differentiate myocardial tissue profiles in patients with ESRD

Adenosine stress and rest T1-mapping was able to determine different myocardial tissue profiles in patients with ESRD. Healthy controls had normal resting myocardial T1 values with significant coronary vasoreactivity, while ischaemic and infarcted myocardium in patients had significantly blunted or abolished stress T1 reactivity. Infarcted myocardium had significantly elevated resting T1 values, which clearly differentiated it from other myocardial tissue classes. These results are broadly consistent with other adenosine stress T1-mapping studies, which similarly differentiated between myocardial tissue profiles (167,168,179). Compensatory microcirculatory vasodilatation occurs to maintain adequate myocardial perfusion downstream of a significant coronary artery stenosis, with little change in resting

myocardial blood flow (180). The abolished stress T1 response seen in ischaemic myocardium likely reflects this depletion of coronary vasodilatory reserve, with near-maximal coronary vasodilatation and increased resting myocardial blood volume which is unable to augment further during vasodilatory stress (181). Infarcted tissue, which has significantly elevated T1 values at rest due to the presence of fibrosis and myocardial scar, displays no T1 reactivity.

3.5.1.1 Blunted stress T1 reactivity in patients with ESRD

Patients with ESRD and normal cardiac screening tests had significantly blunted stress T1 reactivity compared to healthy controls (delta T1 3.0 ± 1.9% vs. 6.8 ± 1.1%; $p<0.0001$). This was even more pronounced in patients with ESRD and abnormal cardiac screening tests but no obstructive CAD (delta T1 2.4 ± 1.9% vs. 6.8 ± 1.1%; $p<0.0001$). The magnitude of the blunted stress T1 response was more profound than previously reported for remote myocardium in patients with CAD (ShMOLLI delta T1 3.9 ± 0.6%) (167) or CKD (ShMOLLI delta T1 4.0 ± 4.8%) (168), but similar to that of a population of ESRD patients requiring haemodialysis (MOLLI 3(3)3(3)5 delta T1 2.9 ± 2.5%) (169). There are several interlinked mechanisms which could explain this phenomenon.

CKD is independently associated with a graded reduction in coronary microvascular function, even in the absence of obstructive CAD (182–186).

Coronary microvascular dysfunction (CMD) is also highly prevalent in patients with diabetes, which was a common comorbidity in the current study (187). The severity of CMD, typically assessed as a reduction in stress myocardial blood flow or coronary vasodilatory reserve, is an independent predictor of adverse cardiovascular outcomes and prognosis in patients with ESRD (188,189). CMD may be due to structural abnormalities in the coronary microvasculature such as arteriolar remodelling (with increased media thickness and marked calcification) (190) and microvascular rarefaction (191), defined as a loss of perfused microvessels resulting in a significant decrease in microvascular capillary density, all of which are common findings in biopsy, autopsy, and imaging studies in patients with CKD and ESRD (192). These changes, combined with functional abnormalities such as endothelial dysfunction, all contribute to reduced coronary flow reserve, reduced myocardial perfusion and tissue hypoxia. This sets the stage for the development of myocardial fibrosis, which is another frequent finding in patients with ESRD (162–164). Coronary microvascular dysfunction, near-maximal compensatory resting vasodilatation, depleted coronary vasodilatory reserve, and myocardial fibrosis, are all plausible explanations for the significantly blunted stress T1 response shown here in patients with ESRD (see **3.5.2.2)**.

3.5.2 Diagnostic performance of stress T1-mapping to detect obstructive coronary artery disease in patients with ESRD

3.5.2.1 Comparison of stress T1-mapping with other non-invasive imaging strategies

Stress T1-mapping showed good diagnostic performance for detecting obstructive epicardial CAD, as validated against invasive haemodynamic assessment, with a stress delta T1 threshold of 1.8% yielding a sensitivity of 77% and specificity of 65%. This is comparable to the diagnostic performance of contemporary non-invasive screening strategies such as dobutamine stress echocardiography (sensitivity 76%; specificity of 88%) and SPECT myocardial perfusion imaging (sensitivity 67%; specificity 77%) in similar populations of renal transplant candidates (149). Importantly, the performance of stress T1-mapping was able to be further improved by incorporating polar maps and cine imaging (sensitivity 94%; specificity 65%), which re-classified a number of false negative cases (see **3.5.2.2**). CMR also has added advantages being a radiation-free and imaging gold standard for cardiac structure and function, with excellent reproducibility of these measures, and thus holds promise to become a "one-stop shop" comprehensive imaging option for assessing renal transplant candidates.

Perhaps the greatest strength of stress T1-mapping is the high sensitivity and negative predictive value for excluding significant obstructive CAD. A stress delta T1 threshold of 3.2%, comparable to the delta T1 seen in patients with

ESRD with normal cardiac functional testing or non-obstructive CAD, was highly effective for excluding significant CAD (NPV 100%). Evidence of preserved coronary vasoreactivity may be reassuring for clinicians to proceed with kidney transplant without the need for invasive coronary angiography in these patients, although larger, multi-centre studies are required to further test this and any impact it may have on clinical outcomes.

3.5.2.2 Microvascular dysfunction and myocardial fibrosis may explain blunted stress T1-reactivity in the absence of obstructive CAD

As previously discussed, three false negative cases (stress delta T1 >1.8% with obstructive CAD) were correctly re-classified as having obstructive CAD following polar map analysis, which allowed a more realistic assessment of the gradient of stress delta T1 changes across the myocardium from base to apex, as would be expected based on coronary anatomy and the site of coronary stenosis. In addition to these false negative cases, there were a number of false positive cases (n=14 vessels in 8 patients with a delta T1 ≤1.8% but no obstructive CAD, based on an FFR or QFR ≥0.8), which are worthy of more detailed discussion below.

Full invasive assessment of microvascular function was performed in 3 patients, including derivation of IMR (index of microcirculatory resistance) and CFR (coronary flow reserve). Two of these patients (n=6 vessels) had evidence of severe microvascular dysfunction with global CFRs of 1.1 (normal

>2.0-2.5) but with normal FFR and QFR. Four of these vessels had significantly impaired stress T1 reactivity (i.e., delta T1 ≤1.8%) as shown in bold in **Table 3.5**. This highlights that microvascular dysfunction and loss of coronary vasodilatory reserve may be associated with significantly blunted stress T1 reactivity and can explain several of these false positive cases.

Table 3.6: Coronary microvascular dysfunction and stress T1 reactivity

Patient ID	Vessel	FFR	CFR	Delta T1 (%)
SPK021	LAD	0.89	1.1	**0.2**
SPK021	RCA	0.97	1.1	**1.5**
SPK021	LCx	0.96	1.1	3.3
SPK022	LAD	0.88	1.1	**1.4**
SPK022	RCA	0.86	1.1	**0.1**
SPK022	LCx	0.85	1.1	2.2

Evidence of severe coronary microvascular dysfunction based on invasive coronary physiology in two patients with ESRD with abnormal cardiac functional testing and the relationship with stress T1 reactivity (delta T1).

Furthermore, two other patient cases (contributing n=5 vessels) with abnormal cardiac functional testing were found to have no obstructive CAD on invasive angiography but severely impaired stress T1 reactivity (delta T1 -1.1% to 0.7%; the 6th vessel had relatively preserved (although still blunted) T1 reactivity with a delta T1 of 2.2%). Resting global and segmental T1 was

significantly elevated in these two cases, ranging from 1012 to 1097 ms, suggesting a concomitant underlying pathological process such as diffuse myocardial fibrosis or inflammation (**Figure 3.8**).

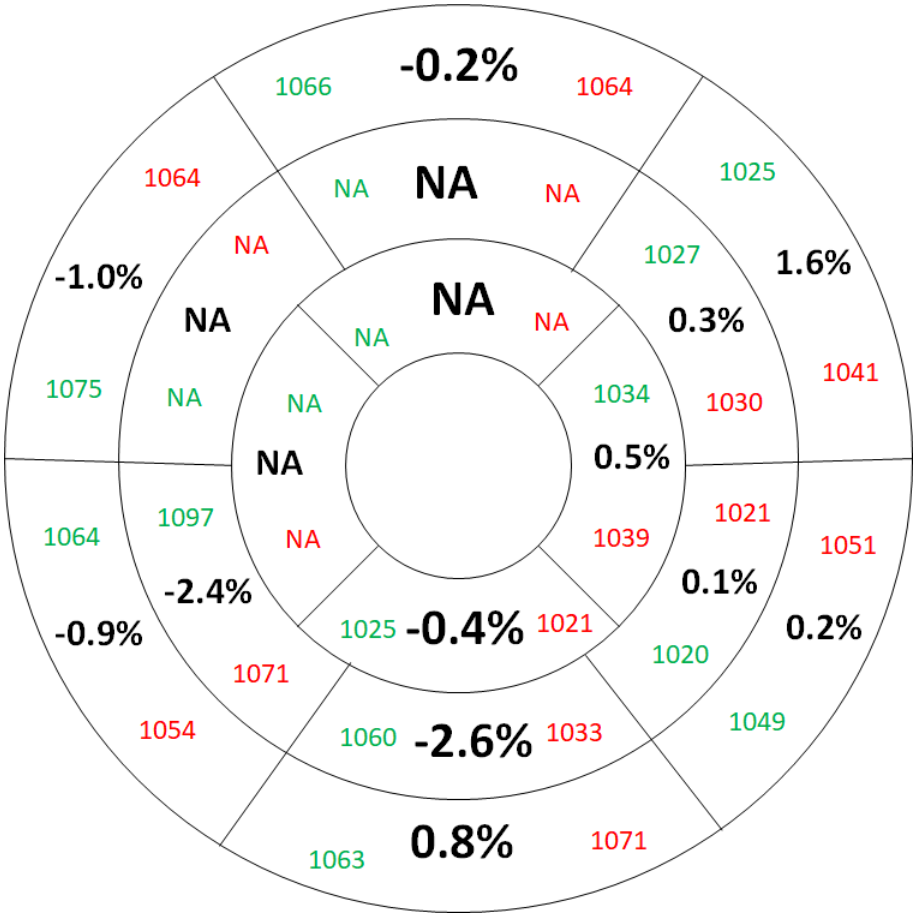


Figure 3.8: Polar map example of a patient with significantly elevated myocardial T1 values and abolished stress T1 reactivity. *T1 values ranged from 1020-1097 ms in this case. This may be related to a diffuse inflammatory or fibrotic process. Four segments in the mid-apical anterior and septal walls in this case (marked NA) were excluded due to artefact. The green numbers represent rest T1, and the red numbers represent stress T1.*

Non-ischaemic myocardial fibrosis, which is frequently seen in ESRD (162–164), may indeed be an important cause of elevated native myocardial T1 values and blunted stress T1 reactivity. Indeed, a post-mortem study of patients with CKD and without significant CAD showed that >90% have myocardial fibrosis (193). A non-invasive method to detect fibrosis in patients with ESRD is highly relevant, given histopathology studies have shown that the extent of fibrosis is a strong predictor of cardiac death (194). Significantly higher myocardial T1 values have been seen in patients with ESRD on haemodialysis compared to controls and may represent subclinical myocardial fibrosis (163), although further histological validation to determine the association of elevated myocardial T1 with fibrosis in this population is required. The blunted stress T1 reactivity seen in this study in the absence of obstructive CAD could certainly be explained by diffuse non-ischaemic myocardial fibrosis, which is expected to demonstrate minimal change in T1 with vasodilator stress.

Interestingly, when presented with these cases on polar map analysis, the blinded independent observer highlighted that the blunted stress T1 reactivity in these cases was likely attributable to a diffuse inflammatory or fibrotic process rather than widespread chronic ischaemia or infarction, particularly given the presence of normal wall motion and systolic function. Increased resting vasodilatation and myocardial blood volume could also explain a high T1 with minimal stress reactivity, which may also be relevant in patients with

ESRD, who typically have a high circulating blood volume and may develop adaptive physiological changes to maintain coronary perfusion during haemodialysis (195).

3.5.3 Limitations and future directions

This study was performed in a small cohort of patients with ESRD, who were subdivided into smaller pre-specified groups based on the results of screening cardiac investigations and clinical risk factors. The small numbers present in this study may limit the interpretation of the findings. Additionally, the healthy controls were not well age-matched to the patient groups (38 ± 16 years vs 51 ± 10 years in patients with ESRD and normal screening vs 53 ± 13 years in patients with ESRD and abnormal cardiac screening). This may have implications for the results, particularly when looking at changes in T1 during stress, given that native myocardial T1 may reduce slightly with age (on average by 8-11 ms/decade (196). Gender also influences native myocardial T1 (with females tending to have a higher native T1 (196,197)), although the majority of the participants in this study were males, which lessens the impact of sex differences on the findings.

This study provides invasive haemodynamic validation of adenosine stress T1-mapping as a contrast-free non-invasive imaging technique to assess for obstructive CAD in patients with ESRD. However, invasive FFR was not able to

be performed on all vessels or in all patients. To maximise power for haemodynamic stenosis evaluation, offline QFR was measured and combined with FFR results. QFR has good correlation with invasive FFR ($r = 0.88$; $p<0.001$) with excellent agreement between the assessments (mean difference: 0.002 ± 0.06) (178). QFR also has excellent per-vessel diagnostic accuracy of 92.7% (95% CI: 89.3-95.3%) for providing concordant results with FFR based on the pre-specified reference standard FFR cut-off of 0.8 (178). Nonetheless, this still could have influenced results, particularly for vessels with a QFR near the 0.8 threshold, which could potentially have been mis-classified. Only one vessel in this study had a discordant FFR/QFR result; this case was adjudicated upon prior to analysis by an experienced interventional cardiologist who was blinded to all clinical and CMR information.

Invasive assessment of coronary microvascular dysfunction (i.e., IMR and CFR) was only performed in n=3 patients (n=9 vessels); further work is required to evaluate the utility of stress T1-mapping for the assessment of microvascular dysfunction. Chronic total occlusions were excluded from analysis in this study (n=4), given the unknown effect of collateralisation on stress T1 reactivity and the inability to classify ischaemia based on a measured FFR or QFR. Gadolinium contrast was not administered in the patients with ESRD, and thus an accurate estimate of myocardial scar could not be made; infarcted segments were instead defined using surrogates of wall thinning and akinesia in combination with fixed perfusion defects on non-CMR stress imaging. Further

work is required to evaluate the utility of stress T1-mapping for the detection of ischaemia in more complex CAD such as chronic total occlusion or after coronary artery bypass grafting, and for assessing potential viability.

The T1-map analysis method in this study was based on individual myocardial segments, which differs from that previously described where a region of interest was placed in an area co-localised to a visible hypoperfusion defect using CMR stress perfusion and LGE imaging as reference (167). The greater volume of myocardium assessed may actually lose sensitivity, as hypoperfusion due to myocardial ischaemia typically affects the subendocardial region of the myocardium first, meaning that impaired stress T1 reactivity may be 'diluted' by the presence of otherwise normal or well-perfused myocardium. Further work and validation are required to develop a 'subendocardial' assessment method, whereby T1-map analysis is programmed to provide results only from the subendocardial third of the myocardium for a given segment, theoretically maximising yield for detecting myocardial ischaemia. Pixel-wise stress T1 reactivity maps, that display a gradient of stress T1 changes from the epicardial to endocardial border similar to current pixel-wise perfusion maps (198,199), is the subject of further work. Finally, this study paves the way for a future program of work and larger multi-centre studies to determine the wider diagnostic value of CMR with stress and rest T1-mapping as an upfront, "one-stop shop" non-invasive, contrast- and radiation-free screening strategy in patients with ESRD referred for renal

transplant, and to evaluate this approach in guiding clinical decision making and predicting long-term prognosis.

3.6 Conclusions

Adenosine CMR stress T1-mapping is able to detect and differentiate between obstructive and non-obstructive CAD in patients with ESRD, and perform advanced myocardial phenotyping, without the need for radiation or gadolinium-based contrast agents. It is a viable non-invasive screening strategy in patients referred for renal transplantation that allows safe serial testing and can act as a gatekeeper to invasive coronary angiography pending further clinical validation.

4 Regadenoson stress T1-mapping and extracellular volume stability of MOLLI-based T1-mapping methods

---

The work presented in this Chapter has been published in Nature: Scientific Reports as:

Burrage MK, Shanmuganathan M, Zhang Q, Hann E, Popescu IA, Soundarajan R, Chow K, Neubauer S, Ferreira VM, Piechnik SK. Cardiac stress T1-mapping response and extracellular volume stability of MOLLI-based T1-mapping methods. *Sci Rep.* 11, 13568 (2021). https://doi.org/10.1038/s41598-021-92923-4

4.1 Abstract

4.1.1 Background

Stress and rest T1-mapping may assess for myocardial ischemia and extracellular volume (ECV). However, the stress T1 response is method-dependent, and underestimation may lead to misdiagnosis. Further, ECV quantification may be affected by time, as well as the number and dosage of gadolinium (Gd) contrast administered. This study compared two commonly available T1-mapping approaches (ShMOLLI and MOLLI) in their stress T1 response and ECV measurement stability.

4.1.2 Methods

Healthy subjects (n=10, 50% female, 35 ± 8 years) underwent regadenoson stress CMR (1.5-Tesla) on two separate days. Prototype ShMOLLI 5(1)1(1)1 sequence was used to acquire consecutive mid-ventricular T1-maps at rest, stress and post-Gd contrast to track the T1 time evolution. For comparison, standard MOLLI sequences were used: MOLLI 5(3)3 Low (256 matrix) & High (192 matrix) Heart Rate (HR) to acquire rest and stress T1-maps, and MOLLI 4(1)3(1)2 Low & High HR for post-contrast T1-maps. Stress and rest myocardial blood flow (MBF) maps were acquired after IV Gd contrast (0.05 mmol/kg each). Stress T1 reactivity (delta T1) was defined as the relative percentage increase in native T1 between rest and stress. Myocardial T1

values for delta T1 and ECV were calculated. Residuals from the identified time dependencies were used to assess intra-method variability.

4.1.3 Results

ShMOLLI achieved a greater stress T1 response compared to MOLLI Low and High HR (peak delta T1 6.4 ± 1.7% vs. 4.8 ± 1.3% vs. 3.8 ± 1.0%, respectively; both $p<0.0001$). ShMOLLI delta T1 correlated strongly with stress MBF ($r = 0.77$, $p<0.001$), compared to MOLLI Low HR ($r = 0.65$, $p<0.01$) and MOLLI High HR ($r = 0.43$, $p=0.07$). ShMOLLI ECV was more stable to gadolinium dose with less time drift (0.006-0.04% per minute) than MOLLI variants. Overall, ShMOLLI demonstrated less intra-individual variability than MOLLI variants for stress T1 and ECV quantification. Power calculations indicate up to a 4-fold (stress T1) and 7.5-fold (ECV) advantage in sample-size reduction using ShMOLLI.

4.1.4 Conclusions

These results indicate that ShMOLLI correlates strongly with increased MBF during regadenoson stress and achieves a significantly higher stress T1 response, greater effect size, and greater ECV measurement stability compared with the MOLLI variants tested.

4.2 Introduction

Quantitative T1-mapping allows in-vivo myocardial tissue characterisation in detecting a variety of cardiovascular diseases (35,63,65,82,84,200,201). Native (pre-contrast) T1 values are prolonged by increased tissue free water content, and are dependent on blood T1 and myocardial blood volume (MBV) via partial volume effects (54). Changes in MBV from coronary vasodilatation during stress may thus be detectable by cardiovascular magnetic resonance (CMR) T1-mapping (95). Several studies have used the change in myocardial T1 during stress (T1 reactivity) to differentiate ischaemic, infarcted, remote, and normal myocardium in patients with obstructive coronary artery disease (CAD) (104,112,113,115,202,203), and impaired vasodilatory reserve in diseases with non-obstructive CAD (72,119). Stress T1-mapping holds potential for translation into clinical applications as a non-invasive method for assessing coronary vasoreactivity.

Several approaches for measuring myocardial T1 have been described (54). Despite excellent T1 precision, the original modified Look-Locker inversion recovery (MOLLI) 3(3)3(3)5 sequence (91) required a 17-heartbeat breath hold for acquisition and was limited by heart rate sensitivity. Newer sequences, such as ShMOLLI 5(1)1(1)1 (92) and MOLLI 5(3)3 (102), allow shorter breath holds and are widely used in clinical practice. ShMOLLI uses a 9 heartbeat breath hold for acquisition, is largely heart rate independent due to its in-built conditional reconstruction algorithm, and is potentially a “one-

stop-shop" T1-mapping sequence for native, stress and post-contrast T1-mapping (92,97). More recent front-loaded MOLLI 5(3)3 improves on but does not eliminate earlier recognised heart rate sensitivity, which may explain lower stress T1 responses (95). As MOLLI 5(3)3 is suboptimal for short T1 ranges, separate variants, such as MOLLI 2(2)2(2)4 or MOLLI 4(1)3(1)2, have been designed for post-contrast acquisitions (102,204). Independently of the chosen T1-mapping method, drifts in post-contrast T1 and, to a lesser degree, in extracellular volume (ECV) over time have been reported (205–207).

Underestimation of stress T1 reactivity due to method-dependent heart rate sensitivity, along with related impacts on measuring post-contrast T1 and ECV after vasodilator stress, has potentially important clinical implications. There have been no head-to-head studies to determine the optimal stress T1-mapping method. The current study therefore sought to determine the relationship between different T1-mapping methods in normal physiology and has two main aims: 1) to directly compare the relationship between ShMOLLI and MOLLI in terms of their stress T1 response, variability, and effect size; and 2) compare their response with regards to ECV measurement stability over time.

4.3 Methods

4.3.1 Study population

Eleven healthy volunteers with no use of cardiovascular medication, no history of cardiovascular or systemic disease, no cardiovascular risk factors, and no previous history of cardiovascular symptoms were prospectively recruited. All subjects abstained from caffeine for 24 hours before undergoing CMR examination. Blood haematocrit testing was performed immediately before each CMR study.

4.3.2 Image acquisition

CMR imaging was performed using a 1.5-Tesla MRI scanner (AvantoFit, software version VE11C, Siemens Healthcare, Erlangen, Germany) using an 18-channel phased-array coil with the participant supine. The timeline of the CMR scanning protocol is provided in **Figure 4.1**. Cine imaging was performed in three long axis views and in short axis slices covering the entire left ventricle (LV), using retrospectively ECG-gated balanced steady state free precession (bSSFP) (49,134). T1-maps were acquired based on the ShMOLLI sequence as previously published (92), prototype version WIP1048. Quality assessment of ShMOLLI T1-maps using parametric goodness-of-fit (R^2) maps were available in-line at time of acquisition (64,92), based on open source reconstruction (208). MOLLI (MyoMaps, Siemens Healthcare, Erlangen, Germany) T1-maps were acquired from vendor-provided product protocols: “Long T1” MOLLI

5(3)3 was used for rest and stress native T1-mapping and "Short T1" MOLLI 4(1)3(1)2 was used for post-contrast T1-mapping. Both sampling scheme protocols had "Low HR" (256 matrix) and "High HR" (192 matrix) variants, where the latter is recommended for heart rates greater than 80bpm to reduce cardiac motion blurring.

The main study protocol (**Figure 4.1**) included ninety-two T1-maps (60 ShMOLLI, 32 MOLLI) per participant from a single mid-ventricular slice. Systolic imaging (trigger delay (TD) of zero (0) ms) was used for T1-mapping sequences to standardise measurements and reduce the risk of mistriggering during tachycardia (99). With exception of the initial rapid transition periods, stress and post-contrast T1-maps were acquired using repeated "blocks" alternating five T1-mapping sequences to allow interpolation of T1 measurements for direct comparison between the T1-mapping techniques under dynamic conditions.

Stress T1-maps were acquired consecutively, commencing immediately upon intravenous (IV) injection of regadenoson (Rapiscan, GE Healthcare AS, Oslo, Norway; 400 μg over 5-10 seconds followed by a 10 ml 0.9% sodium chloride saline flush over 10 seconds). Heart rate and blood pressure were recorded throughout. First-pass perfusion imaging was performed after completion of the stress T1-mapping protocol (~15 minutes after injection of regadenoson) with an IV bolus injection of gadolinium (Gd) contrast (0.05 mmol/kg,

gadoterate meglumine, Dotarem, Guerbet SA, Paris, France) followed by a 15-20 ml saline flush, both administered at 4-6 ml/sec. Pixel-wise perfusion maps were generated automatically using inline perfusion mapping software as previously described, to allow quantitative assessment of myocardial blood flow (MBF) (138).

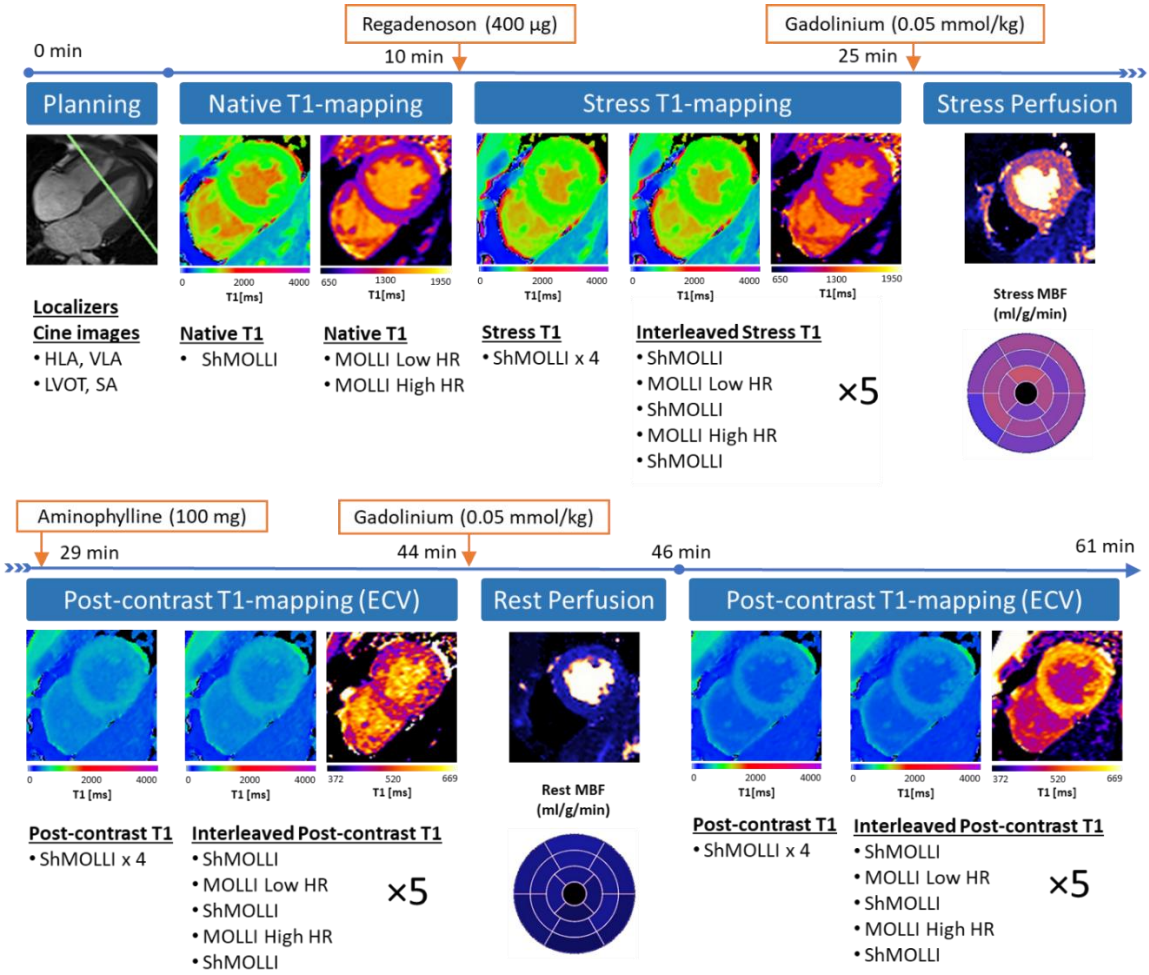


Figure 4.1: CMR scanning protocol for assessing T1 time dependencies. *After planning, native T1-mapping is performed at rest using ShMOLLI, MOLLI Low HR, and MOLLI High HR. Stress T1-mapping is performed following administration of regadenoson (IV 400 µg). This consists of four ShMOLLI measurements to cover the initial transition period and peak stress, followed by blocks of interleaved ShMOLLI and MOLLI variants. First-pass perfusion imaging is performed after gadolinium injection (0.05 mmol/kg). Allowing 4 minutes for the reconstruction of MBF data, stress is reversed with aminophylline (IV 100 mg) followed immediately by the same pattern of ShMOLLI and MOLLI acquisitions. Rest perfusion is performed after a second dose of gadolinium (0.05 mmol/kg), followed immediately by T1-mapping.*

After a four-minute delay (to allow for online reconstruction of pixel-wise perfusion maps), pharmacological stress was reversed (aminophylline 100 mg IV over 5-10 seconds followed by a 10 ml saline flush). Post-contrast T1-mapping was then performed with the same alternating T1-mapping sequence blocks (**Figure 4.1**) immediately after injection of aminophylline. Rest first-pass perfusion imaging was then performed as described above. The post-contrast T1-mapping protocol was then repeated to allow assessment of the prolonged effects of time and a second dose of gadolinium on post-contrast T1 values. For simplicity, the time epochs following the first dose of gadolinium are referred to as "half-dose Gd" (i.e., 0.05 mmol/kg) while those after the second dose are referred to as "whole-dose Gd" (i.e., 0.1 mmol/kg).

All participants underwent a second (**Figure 4.2**) regadenoson stress CMR (median interval 7 days), which provided additional stress T1 and MBF values (analysis performed only for mid-ventricular slices) for comparison at a time point closer to peak stress (within 1.5-4 minutes of regadenoson administration). Late gadolinium enhancement (LGE) imaging was performed in long and short axis views to exclude myocardial infarction or other types of scarring, as per SCMR guidelines (49,134).

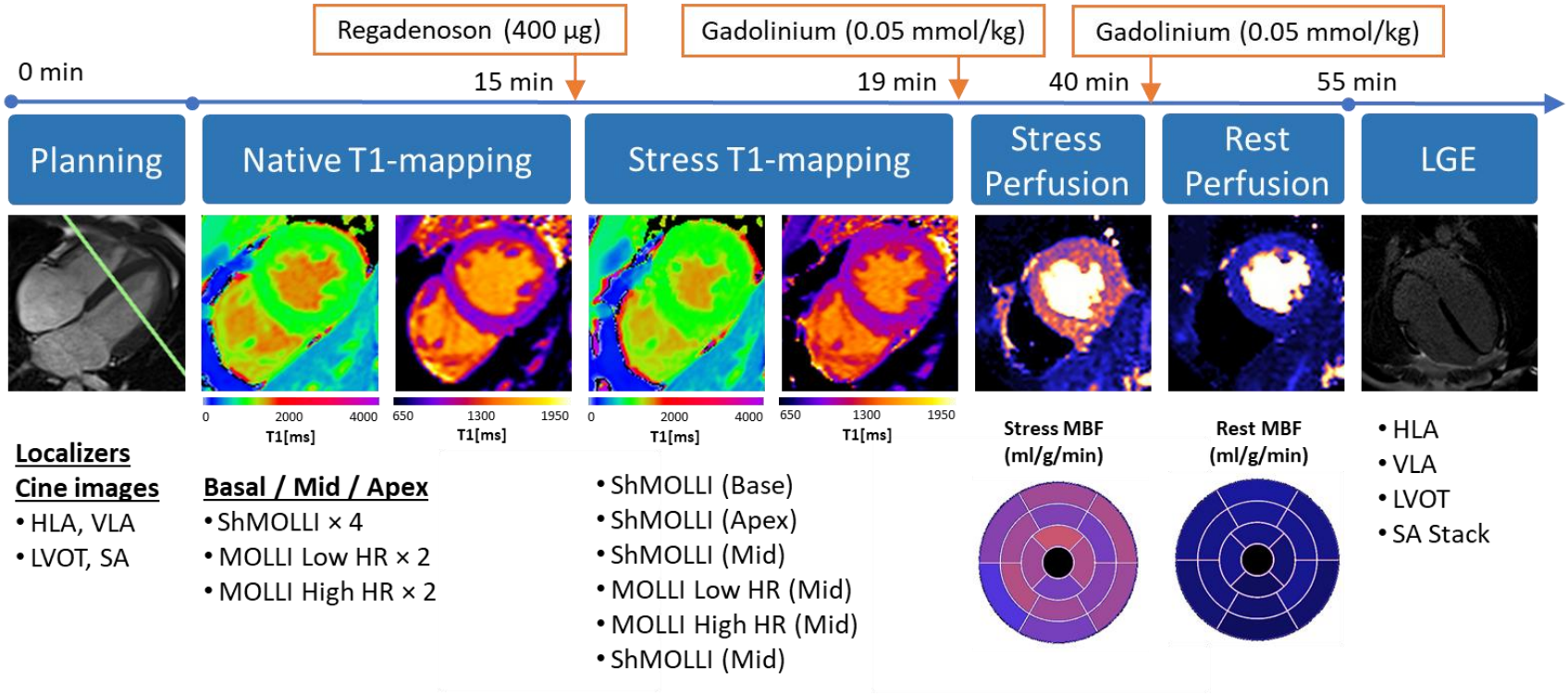


Figure 4.2: Modified second CMR scanning protocol for assessing stress T1 and MBF. *Native T1-mapping is performed at rest using ShMOLLI, MOLLI Low HR, and MOLLI High HR in basal, mid-ventricular, and apical slice positions. Stress T1-mapping is performed following administration of regadenoson (IV 400 µg) in the basal, apical, and mid-ventricular slices as illustrated. Stress is reversed with aminophylline (IV 100 mg) at ~25 minutes. Rest perfusion and late gadolinium enhancement images are acquired.*

4.3.3 Image analysis

Image analysis for biventricular indices was performed offline in accordance with SCMR guidelines (49), using cmr42 post-processing software (version 5.10.1, Circle Cardiovascular Imaging Inc., Calgary, Canada). Offline post-processing of T1-maps involved endocardial and epicardial contouring using MC-ROI. Automated contours were placed (135,209) and manually checked for errors and corrected in compliance with internal training standards (136). T1-mapping results were based on quantitative analysis of all T1-maps, with global slice average T1 values of all myocardial segments per slice. The ECV fraction was calculated as previously described (134). Stress and rest MBF were recorded as the mid-ventricular slice average for the respective perfusion sequences, acquired from inline perfusion mapping software (138).

4.3.4 Data modelling and statistical analysis

To enable direct comparison of the different T1-mapping sequences for the dynamic stress response, ShMOLLI T1 values were linearly interpolated for each MOLLI time point. Relative stress responses were calculated for heart rate, MBF, and T1, as shown for stress T1 reactivity (delta T1) on per-slice basis below:

$$\text{Delta T1} = \frac{stress\ \text{T1} - rest\ \text{T1}}{rest\ \text{T1}} * 100\%$$

The relationships between ShMOLLI and MOLLI variants for stress T1, delta T1, post-contrast T1, and ECV were assessed with Pearson's linear correlation coefficient (r), as well as the slope and intercept of the regression lines. A mono-exponential decay model was fitted to all subjects combined, starting after 1.5 minutes post-regadenoson stress for ShMOLLI delta T1, being the method of choice with most samples acquired. Given the dynamic nature of this stress study, datapoints were grouped in 1-minute intervals so as to better present the effects of time on T1 evolution. Independent fitting of MOLLI data was found suboptimal due to narrower dynamic range, and thus only the scale was fitted to match, in keeping with the presumption that ShMOLLI and MOLLI follow the same decay pattern. Data modelling was performed offline after image analysis.

Residual errors from linear and non-linear modelling were calculated from regression equations as the difference between the predicted values and individual means. To correct for inter-subject variability, individual linear (ECV) and non-linear (delta T1) models were fitted. Residual errors were pooled and analysed, based on the standard deviation of the residuals (root mean square error; RMSE), to assess intra-individual measurement variance between T1-mapping methods. Intergroup differences were assessed using ANOVA with post-hoc testing as appropriate. Given non-normal distribution of residuals, statistical differences in variability between T1-mapping methods were assessed using Levene's test. Paired tests were used whenever possible.

A two-tailed $p<0.05$ is considered statistically significant. Statistical analysis and data modelling were performed using R Studio (RStudio Team (2018). RStudio: Integrated Development for R. RStudio, Inc., Boston, MA).

4.4 Results

4.4.1 Study population

All participants completed the study protocol and tolerated regadenoson without complications. One participant was excluded after CMR detection of a large, incidental myocardial infarction on LGE imaging, leaving a total of ten healthy participants (50% female, mean age 35 ± 8 years) included in the study. All 10 participants had structurally normal hearts, with normal resting cardiac volumes (LVEDVi 79 ± 15 ml/m^2) and systolic function (LVEF 60 ± 3%) and no LGE. One participant did not undergo first-pass perfusion and MBF quantification due to a sequence malfunction on the day of the study visit.

4.4.2 Effect of regadenoson stress on heart rate and MBF

Clear physiological effects of regadenoson were seen on all variables of interest. Heart rate increased from baseline 66 ± 13 bpm to 107 ± 12 bpm ($p<0.0001$) recorded first after 1 minute post-regadenoson injection (**Figure 4.3A**). MBF was significantly elevated when measured at 4 minutes (stress MBF 2.43 ± 0.92 ml/g/min compared to rest MBF 0.83 ± 0.22 ml/g/min; $p<0.0001$) and at 15 minutes (stress MBF 1.48 ± 0.76 ml/g/min; rest MBF 0.69

± 0.22 ml/g/min; p<0.01) post-regadenoson (**Figure 4.3B**). Stress MBF at 4 minutes was significantly greater than stress MBF at 15 minutes (p<0.0001).

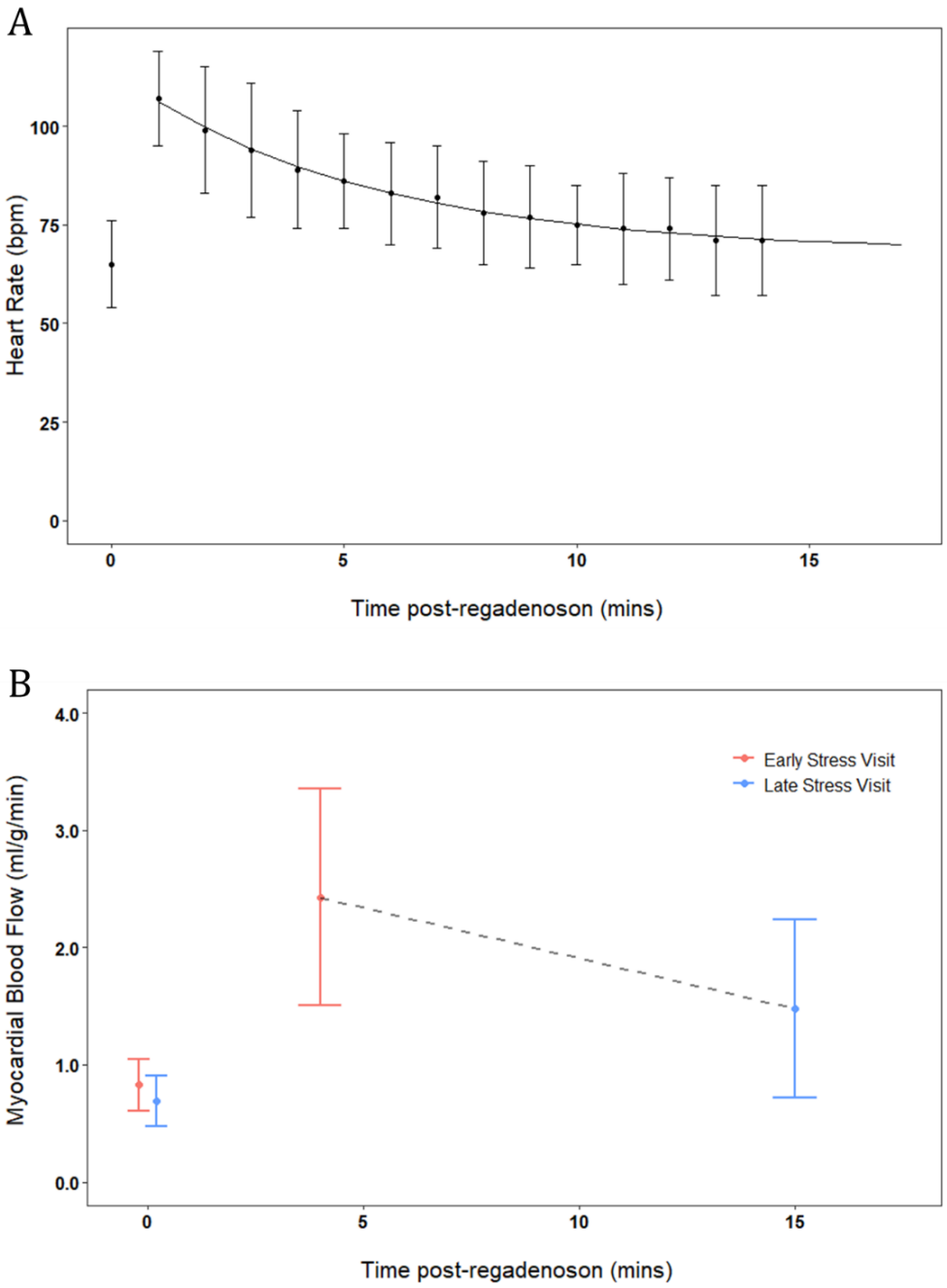


Figure 4.3: Physiological effects of regadenoson stress. *There are clear physiological effects on HR (A), and MBF (B) with regadenoson. In panel (B), time point 0 corresponds to the baseline conditions and is included to illustrate MBF at rest.*

4.4.3 Regadenoson stress T1 response between ShMOLLI and MOLLI variants

After regadenoson injection, ShMOLLI peak delta T1 rose an average of 6.4 ± 1.7% within 30-120 seconds (response amplitude derived from averages of sample points 2-5; see **Figure 4.4**). This was significantly higher than extrapolated peak delta T1 values for MOLLI Low HR (4.8 ± 1.3%; p<0.0001) and MOLLI High HR (3.8 ± 1.0%; p<0.0001).

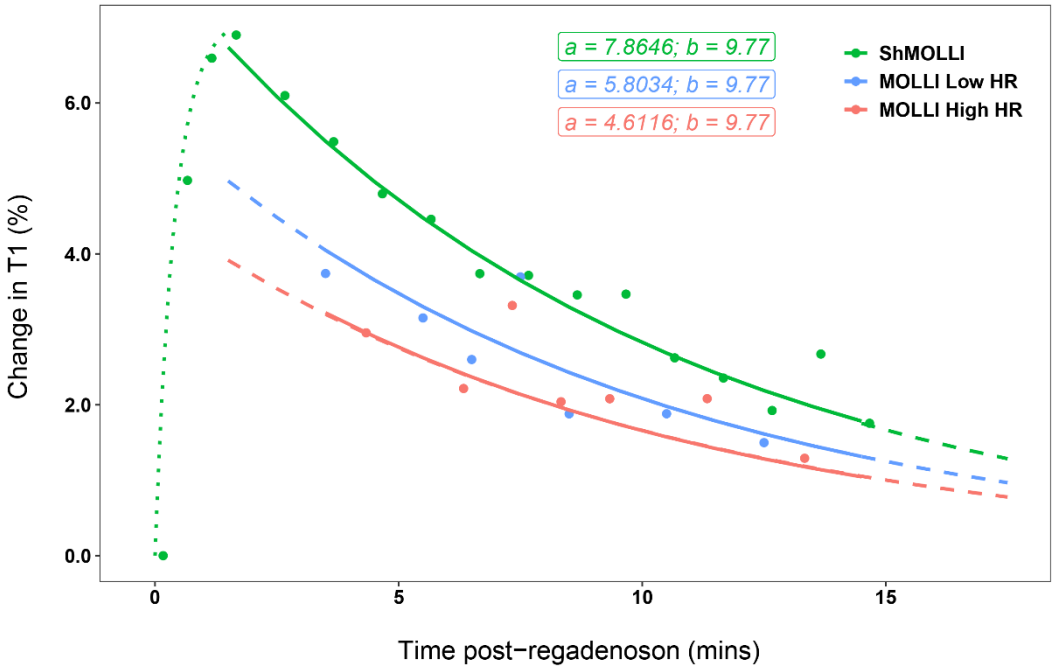


Figure 4.4: Regadenoson stress effects on delta T1 with overlaid mono-exponential decay models. *The mono-exponential decay model is: y = a*exp(-x/b).The decay time* b *has been established for ShMOLLI only, and only amplitudes scaled to best fit other MOLLI variants. The dashed lines mark the extrapolation of the MOLLI models beyond the respective data ranges. The rising part of the T1 response to stress (dotted green line), HR and MBF responses (fitted to relative changes and transposed) are to guide the eye only.*

ShMOLLI delta T1 also demonstrated the greatest slope and a strong linear correlation with stress MBF (**Figure 4.5**) for equivalent time points (r = 0.77, p<0.001) compared to MOLLI Low HR (r = 0.65, p<0.01) and MOLLI High HR (r = 0.43, p=0.07).

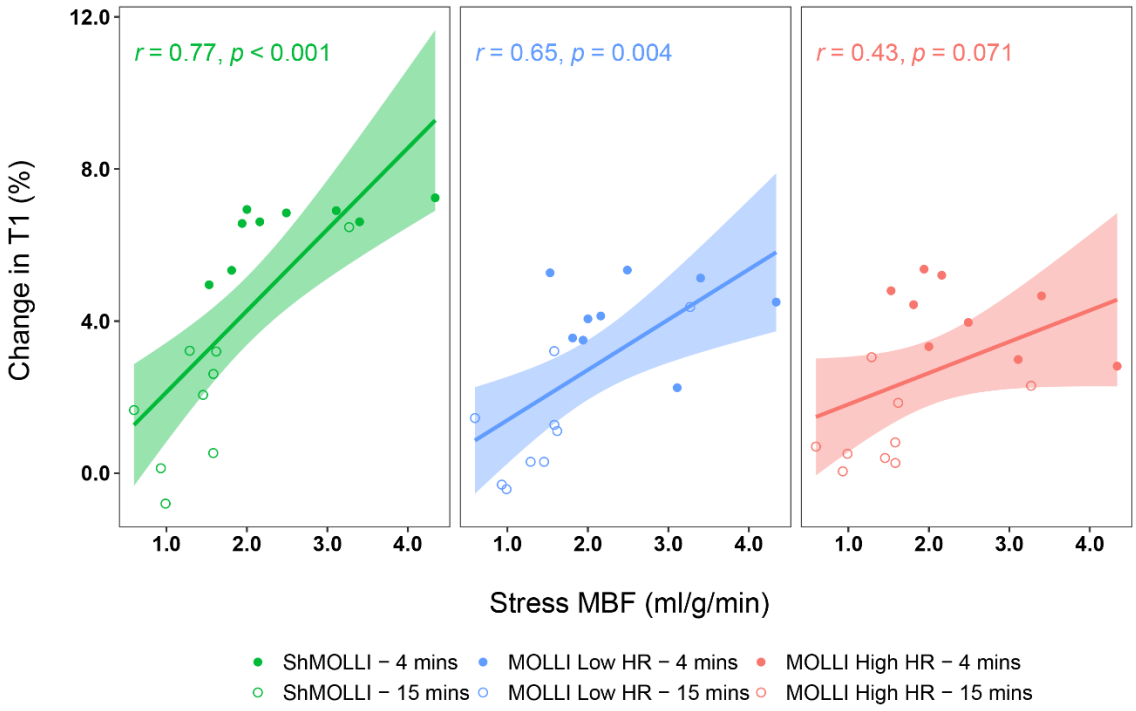


Figure 4.5: Correlation between stress MBF and delta T1 during regadenoson stress. *Stress MBF measured at ~4 (early stress) and ~15 minutes (late stress) after regadenoson in the same individuals on two separate days. Comparisons between delta T1 and stress MBF are made for measured delta T1 at the time point closest to MBF (all stress T1 data points measured within 90 seconds prior to MBF acquisition). Confidence intervals for the linear regressions are included (shaded ranges).*

Rest and stress native T1 values, along with post-contrast T1 values, are presented in **Table 4.1**.

Table 4.1: Differences between methods for rest, stress, and post-contrast T1

Variant	Rest T1 (ms)	Peak Stress T1 (ms)	Half-Dose Gd T1 (ms)	Whole-Dose Gd T1 (ms)
ShMOLLI	921 ± 19	979 ± 28	678 ± 41	556 ± 48
MOLLI Low HR	1001 ± 23 *	1049 ± 23 * $	723 ± 42 *	602 ± 53 *
MOLLI High HR	990 ± 23 * †	1027 ± 24 * ‡ $	724 ± 39 * †	611 ± 48 * †

*Data are presented as mean ± SD. * = P < 0.001 compared with ShMOLLI. † = P > 0.05 compared with MOLLI Low HR. ‡ = P < 0.001 compared with MOLLI Low HR. $ Stress T1 data for MOLLI Low and High HR from extrapolated model-predicted delta T1. Post-contrast T1 reflects the average T1 across each epoch, with statistical comparisons performed at n=44 samples (based on the maximum number of MOLLI samples per epoch) to assure fair inter-method comparison.*

4.4.4 ECV measurement stability after dual gadolinium dose administration

Following the first "half-dose" Gd-contrast injection (0.05 mmol/kg), ShMOLLI ECV rapidly achieved a steady-state equilibrium and remained stable over ~20 minutes, while MOLLI measurements showed clear positive trends in ECV over time, particularly for the Low HR variant (**Figure 4.6**). Over the first Gd-contrast epoch, ShMOLLI ECV demonstrated little change with time (ECV trend = 0.006% per minute) and was significantly more stable over time than ECV measured with both MOLLI Low HR (0.17% per minute; p<0.0001) and MOLLI High HR (0.07% per minute; p<0.001). Over the second "whole-dose" Gd-

contrast epoch (another 0.05 mmol/kg), the ShMOLLI ECV trend was again significantly more stable than MOLLI Low HR (0.04% per minute vs 0.12% per minute; $p<0.001$) but was not different compared with MOLLI High HR (0.04% per minute vs 0.03% per minute; $p=0.18$).

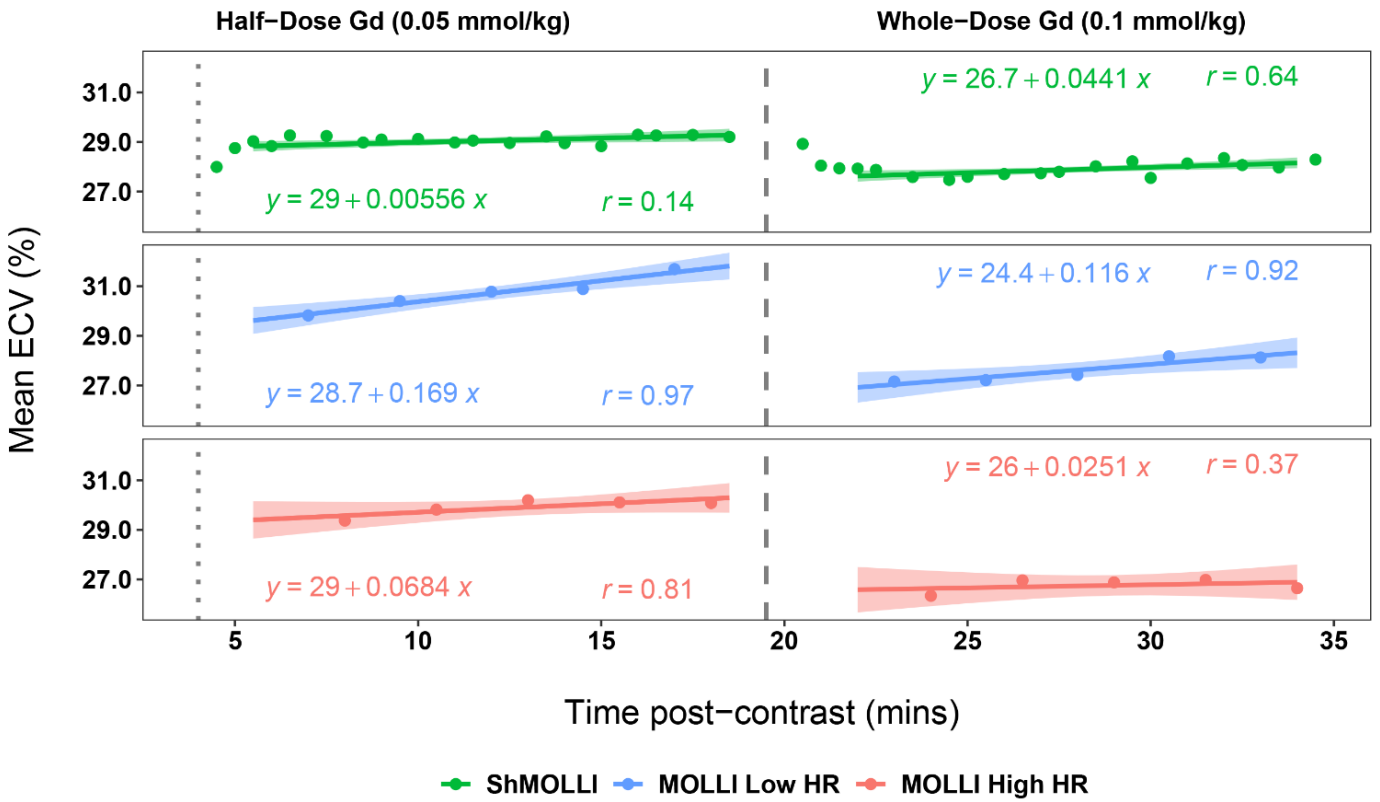


Figure 4.6: Effect of time and gadolinium dose on ECV. *Linear regressions are shown for half-dose and whole-dose Gd epochs. Stress was reversed at 4 minutes (dotted vertical line); Gd was given at 0 minutes and a second dose at 19 minutes (dashed vertical line). The early rapid variation in ECV estimates after Gd seen in the ShMOLLI panel (data points outside the ranges marked by regression models) were excluded from analysis to allow fair inter-method comparisons. ShMOLLI ECV demonstrates little change in ECV with time, whereas MOLLI ECV (particularly MOLLI Low HR) is subject to linear time drift. Confidence intervals for the linear regressions are included (shaded ranges).*

Furthermore, there were significant gadolinium dose dependencies for MOLLI ECV, with both Low HR and High HR variants yielding ECV 3.01-3.11% lower with whole-dose compared to half-dose Gd-contrast ($p<0.001$; **Table 4.2**). ShMOLLI ECV was less sensitive to the second Gd dose, with a drop in ECV of ~1.2% at trend level significance ($p=0.06$).

Table 4.2: Effect of gadolinium dose on ECV

Variant	**Half-Dose Gd ECV (%)**	**Whole-Dose Gd ECV (%)**	**p value §**
ShMOLLI	29.10 ± 2.96	27.93 ± 2.79	0.06
MOLLI Low HR	30.84 ± 3.12 *	27.83 ± 2.72 †	<0.001
MOLLI High HR	30.00 ± 3.34 † ‡	26.89 ± 2.93 † ‡	<0.001

*Data are presented as mean ± SD. * = p < 0.05 compared with ShMOLLI. † = p > 0.05 compared with ShMOLLI. ‡ = p > 0.05 compared with MOLLI Low HR. § = all p values reported at n=44 samples (based on the maximum number of MOLLI samples per epoch) to assure fair inter-method comparison. ECV calculated as the cohort average per epoch.*

4.4.5 Relationship between T1 measured by ShMOLLI and MOLLI variants

There were very strong linear relationships between ShMOLLI and both MOLLI Low HR and MOLLI High HR (both $r > 0.99$, $p<0.00001$), across native (pre-contrast) stress and post-contrast T1 values (**Figure 4.7A**). However, analysis of differences (**Figure 4.7B**) showed obvious departures from a single

linear relationship depending on the T1 range (particularly for the long T1 range during stress) between the methods.

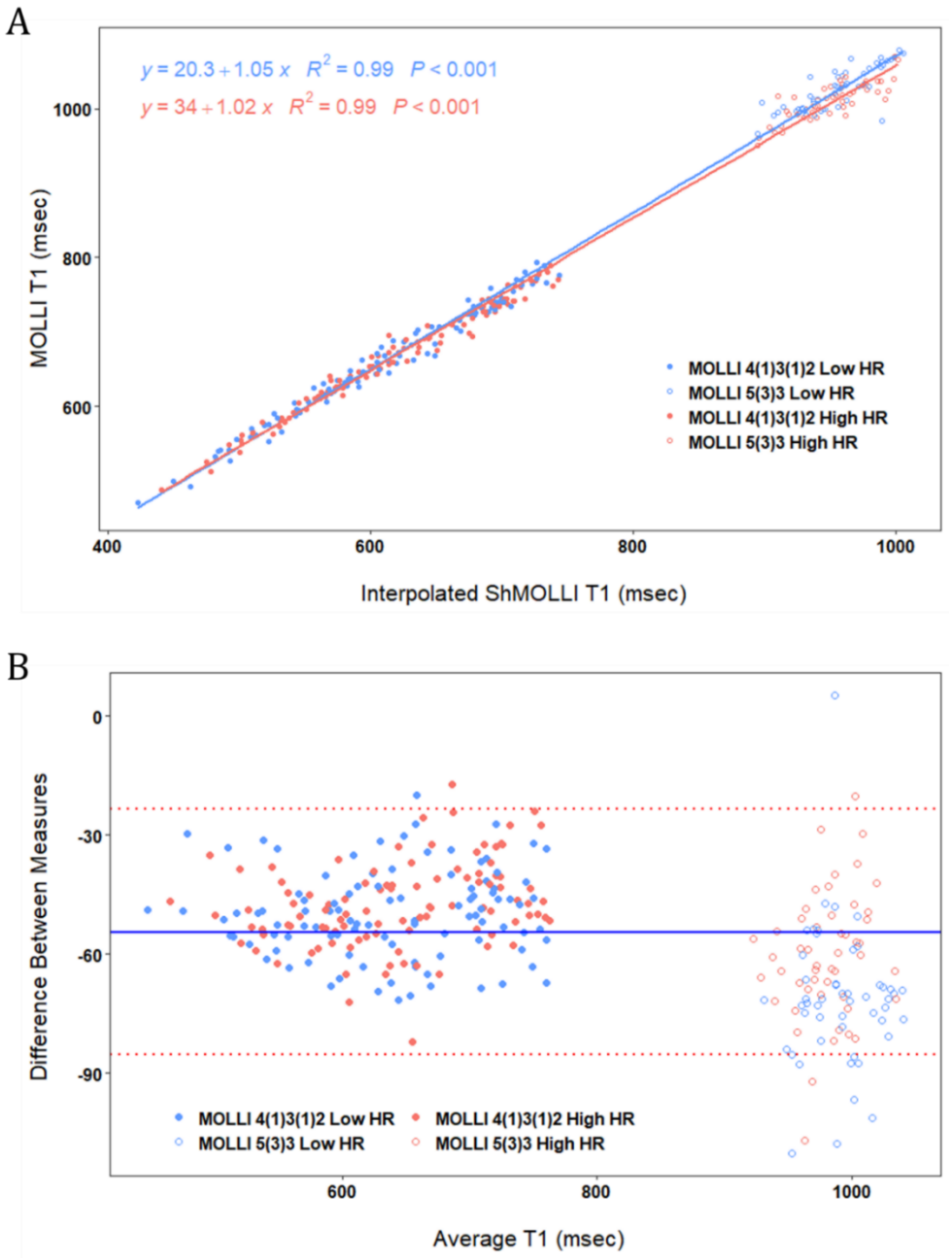


Figure 4.7: Relationship between T1-mapping variants. *Linear fit for T1-mapping variants on native rest, stress, and post-contrast T1 (A) and analysis of differences plot comparing the results from MOLLI variants against all interpolated ShMOLLI values (B). The blue solid line (B) indicates the mean difference between ShMOLLI and MOLLI. The red dotted lines (B) indicate the 95% limit of agreement for all pooled MOLLI compared to ShMOLLI. Post-contrast T1 values are measured using the MOLLI 4(1)3(1)2 sequence with Low and High HR sub-variants; stress T1 values are measured using the MOLLI 5(3)3 sequence and Low and High HR sub-variants.*

Stress responses (delta T1) for MOLLI Low HR and MOLLI High HR were modestly correlated with those measured by ShMOLLI (r = 0.5-0.58, **Figure 4.8A**). Relationships for ECV between the T1 methods were stronger (r = 0.8-0.81), with nearly identical slopes for MOLLI Low HR and MOLLI High HR, but intercepts were offset by 1.5% between the variants (**Figure 4.8B**). Similar trends were observed for ECV stratified by half-dose (0.05 mmol/kg) and whole-dose (0.1 mmol/kg) gadolinium concentrations (**Figure 4.8B**), regression lines not shown for clarity).

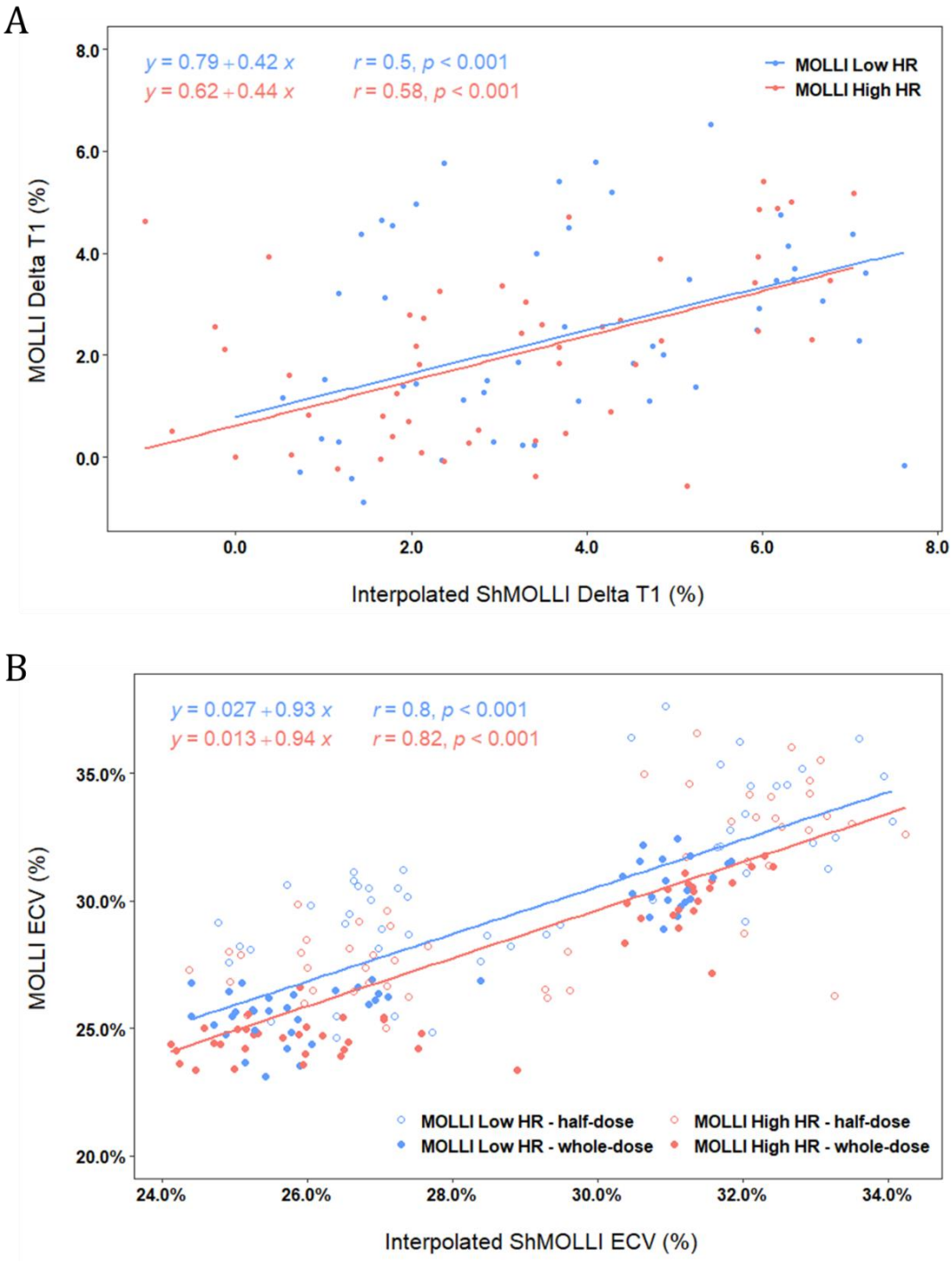


Figure 4.8: Impacts of MOLLI choice on estimation of stress delta T1 and ECV. *Only modest correlations between methods are seen for MOLLI Low HR (r = 0.5) and MOLLI High HR (r = 0.58) respectively for delta T1 (A). Relationships are stronger for ECV for MOLLI Low HR (r = 0.8) and MOLLI High HR (r = 0.81) with distributions also shown for half-dose and whole-dose gadolinium (B). MOLLI variants correspond to time equivalent interpolated ShMOLLI.*

4.4.6 Intra-individual and intra-method variability between T1-mapping variants

For stress T1-mapping, ShMOLLI showed significantly less intra-individual variability than MOLLI Low HR ($p<0.0001$), with a lower coefficient of variance than MOLLI High HR, although not statistically significant ($p=0.24$) at the numbers available (**Table 4.3**). For ECV estimation at half-dose Gd concentration, ShMOLLI ECV was significantly less variable than MOLLI Low HR ($p<0.0001$). ShMOLLI ECV also showed significantly less intra-individual variability than both MOLLI Low HR ($p<0.0001$) and MOLLI High HR ($p<0.05$) at the whole-dose Gd concentration. There was significantly less variability within individuals at the whole-dose Gd concentration compared to half-dose ($p<0.01$) for all T1-mapping variants (**Table 4.3**).

Table 4.3: Measures of intra-individual variability across different T1-mapping variants

Variability	**Delta T1** RMSE [CV]	**ECV – depending on Gd Dose** RMSE [CV]		
		Half-Dose	**Whole-Dose**	**p value**
ShMOLLI	1.30 [0.37]	0.35 [0.012]	0.22 [0.008]	<0.001
MOLLI Low HR	1.92 [0.74] *	0.79 [0.026] *	0.61 [0.022] *	<0.001
MOLLI High HR	1.44 [0.65] †	0.46 [0.016] † ‡	0.34 [0.013] * ‡	<0.01

*Intra-individual variability is assessed using RMSE and CV. * = p < 0.05 compared with ShMOLLI. † = p > 0.05 compared with ShMOLLI. ‡ = p < 0.05 compared with MOLLI Low HR. RMSE = Root Mean Square Error and refers to the standard deviation of the residuals. CV = Coefficient of Variance (RMSE/mean). The p value column is for comparision between half-dose and whole-dose Gd.*

4.5 Discussion

This is the first systematic study to characterise regadenoson stress T1 dynamics over time, and to directly compare the relationship and variability between MOLLI variants for stress and post-contrast T1-mapping. This study demonstrates that: 1) the regadenoson effect can be measured by stress T1-mapping, paving the way to clinical applications similar to those demonstrated previously with adenosine (104,114,115,131); 2) ShMOLLI stress T1-mapping correlates strongly with MBF and achieves a greater overall stress T1 response compared to the MOLLI variants tested; and 3) ShMOLLI ECV can be robustly

estimated at lower Gd doses and a wide range of times, and quickly achieves a post-Gd steady-state equilibrium with greater measurement stability over time and less variability compared with MOLLI variants.

4.5.1 Dynamic response of T1-mapping during regadenoson stress

This study demonstrated a stress T1 dynamic profile consistent with known regadenoson pharmacokinetics, with peak effects typically seen within 30-120 seconds followed by a long terminal elimination phase. This is similar to results from Lieu et al., with invasive coronary blood flow velocity measurements increasing by >2.5- (3.1 ± 0.52) fold at regadenoson IV 400 μg) for a sustained duration of 2.3 minutes (comparable to the response induced by gold-standard intracoronary adenosine), and accompanied by a rise in heart rate (210).

In contrast, an abolished stress T1 response may be seen in areas of pathology. **Chapter 5** will show that the normal regadenoson stress T1 response can be characterised across separate myocardial slices and individual myocardial segments (compared to the global T1 values reported in the current study), with sufficient signal-to-noise ratio to differentiate between infarcted, ischaemic, normal and remote myocardium in clinical patients, as validated by

regions of interest co-localised to first-pass perfusion abnormalities and LGE images and corroborated against invasive coronary angiography (203).

Stress T1 estimation is a crucial progress and has potential implications for contrast-free assessments of MBF and MBV. Nickander et al. recently demonstrated that increases in native myocardial T1 during vasodilatory stress correlate strongly with increases in MBV and MBF (133). Although it is likely that change in MBV is more directly related to the underlying mechanism of T1 reactivity than change in MBF, this study similarly observed strong linear correlations between ShMOLLI delta T1 and MBF measured across two separate stress time points (~4 minutes and ~15 minutes), with a greater r than seen with the MOLLI variants. However, higher stress MBF results in healthy controls have been reported elsewhere (139). This likely reflects the timings of the first-pass perfusion acquisitions, which were not performed at peak stress in this study (i.e., acquired at 4 minutes and 15 minutes vs. typically 1-2 minutes in clinical practice) rather than the choice of vasodilator agent, given recent animal studies have shown no significant differences in MBF when comparing adenosine and regadenoson (121). Data from this study supports that there are clear differences in stress T1 reactivity between the methods tested, with ShMOLLI demonstrating a significantly greater stress T1 response and effect size.

4.5.1.1 Dose-response relationships between T1-mapping and MBF

While a strong linear relationship between ShMOLLI delta T1 and MBF has been observed, scrutiny of the data suggests that a nonlinear or dose-response curve may better information the relationship. A nonlinear logarithmic relationship was first explored (**Figure 4.9**) given the hypothesis that the flattening of the delta T1 response with increasing MBF may partly relate to the expectation that delta T1 is mostly driven by MBV rather than MBF.

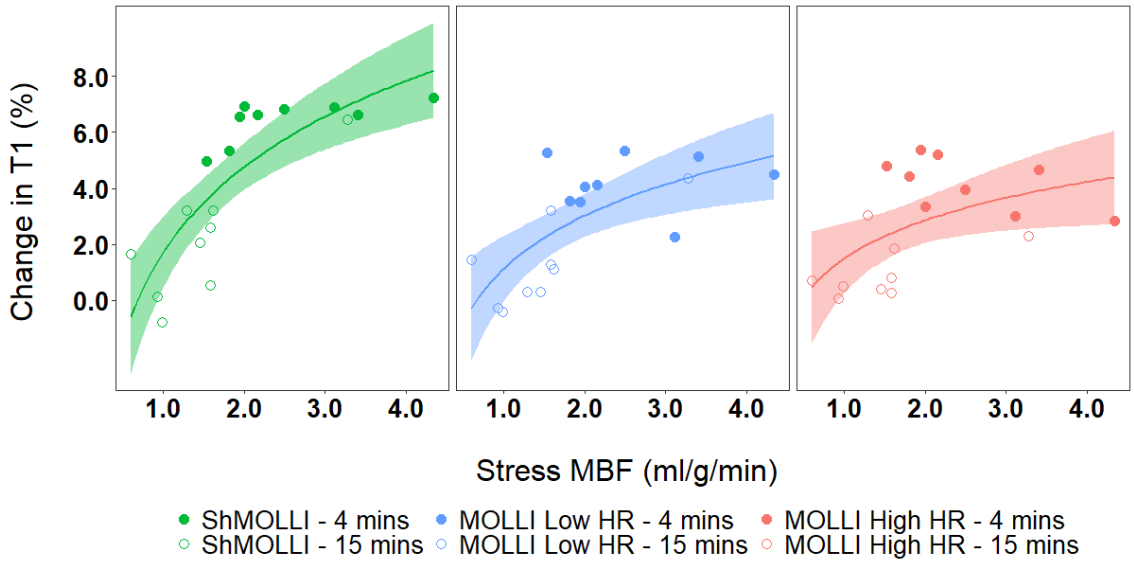


Figure 4.9: Nonlinear logarithmic relationship between stress MBF and delta T1 during regadenoson stress. *Stress MBF measured at ~4 (early stress) and ~15 minutes (late stress) after regadenoson in the same individuals on two separate days. Comparisons between delta T1 and stress MBF are made for measured delta T1 at the time point closest to MBF (all stress T1 data points measured within 90 seconds prior to MBF acquisition). Confidence intervals for the regressions are included (shaded ranges). Correlation coefficients (r) for ShMOLLI, MOLLI Low HR, and MOLLI High HR are 0.81, 0.69, and 0.53 respectively.*

The curve fits for this nonlinear relationship are slightly better than that seen with the linear correlations. This may be explained by the fact that there is an established nonlinear relationship between changes in cerebral blood flow (CBF) and volume (CBV) on blood oxygenation level dependent (BOLD) contrast imaging ($CBV = 0.80 * CBF^{0.38}$) (211,212). Although only validated in cerebral imaging, it is plausible that a nonlinear relationship should also be expected for changes in MBF and MBV, with delta T1 expected to follow more closely with MBV.

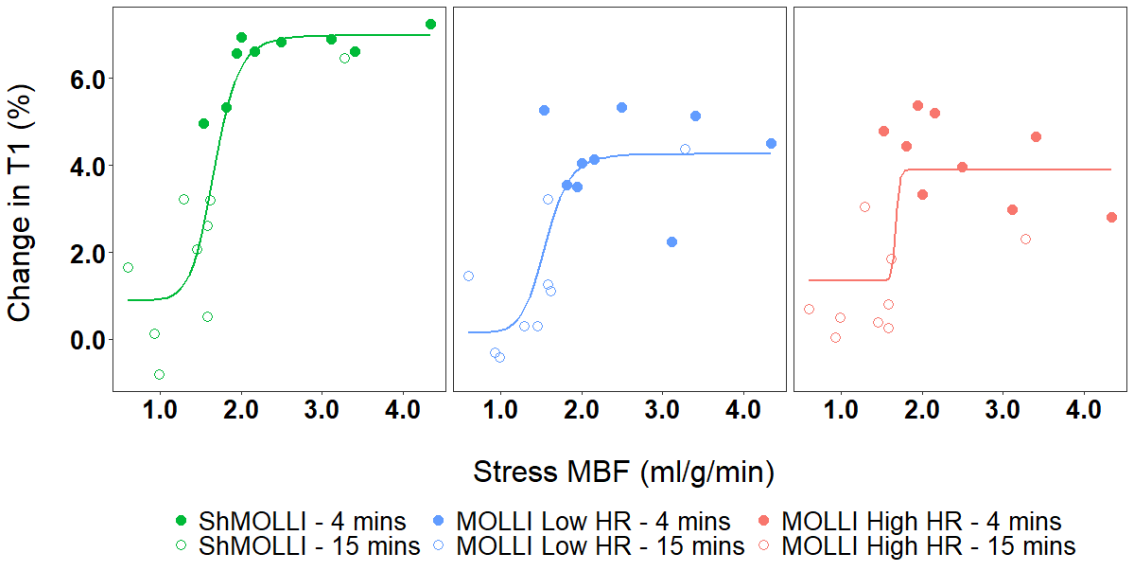


Figure 4.10: Dose-response relationship between stress MBF and delta T1 during regadenoson stress. *Stress MBF measured at ~4 (early stress) and ~15 minutes (late stress) after regadenoson in the same individuals on two separate days. Comparisons between delta T1 and stress MBF are made for measured delta T1 at the time point closest to MBF (all stress T1 data points measured within 90 seconds prior to MBF acquisition). Correlation coefficients (r) for ShMOLLI, MOLLI Low HR, and MOLLI High HR are 0.91, 0.79, and 0.7 respectively.*

A dose-response curve was also explored (**Figure 4.10**). This again showed a significantly improved fit, particularly for ShMOLLI delta T1 (r = 0.91). Although this provides the best fit, it should be noted that delta T1 is another measure of an effect rather than the actual stressor or drug and caution should therefore be applied when interpreting this finding in case of over-fitting, given the few data samples available. It is interesting that the relationship flattens, with delta T1 becoming saturated while MBF continues to rise. This again may relate to the fact that CBV (and thus MBV, which delta T1 is thought to better approximate) flattens with greater increases in CBF as discussed above, further demonstrating that this relationship is indeed nonlinear. It is possible that MBV (and thus the delta T1 surrogate) becomes maximal at a certain increase in MBF, with little response beyond this point. Further work and larger datasets are required to better define the relationship between delta T1 and changes in MBF and MBF, particularly given the known complexities and relationships between these parameters.

4.5.1.2 Heart rate sensitivities between stress T1-mapping variants

ShMOLLI and MOLLI variants may demonstrate different sensitivities to heart rate (102), which may result in differences in delta T1 values during stress T1-mapping protocols. The head-to-head comparisons performed in this study are broadly consistent with prior observations of lower stress delta T1 responses seen with MOLLI 5(3)3 (4.3 ± 2.8% (131); 4.79 ± 3.14% (114); 5.4 ± 2.4% (213)) compared with results achieved using ShMOLLI (6.2 ± 0.5%

(104); 7.1 ± 3.8% (115); 6.4 ± 1.7% in the current study). The MOLLI 5s(3s)3s research prototype scheme with the guaranteed minimum duration of acquisition epochs using a sampling scheme measured in seconds (rather than in heartbeats) (102) was previously shown to have similar adenosine reactivity as ShMOLLI (~6.2%, based on reported T1 values in (133)). However, the MOLLI 5s(3s)3s variant was not tested here due to its minimum breath holds of ~12-15 seconds, i.e., 2-3 times longer than any tested MOLLI variant in this study, which required ~5 seconds at an observed peak HR >100 bpm. The use of sequences with short breath hold requirements (as used in this study) is more practical for implementation of stress T1-mapping in the clinical setting and is likely to result in less cardiac motion artefacts compared with those dependent on longer patient breath holds (95,131). Kuijpers et al. (131) had reported substantial motion artefacts using MOLLI 5(3)3 for stress T1-mapping, and these are likely to worsen using MOLLI 5s(3s)3s due to even longer breath hold requirements.

4.5.2 ECV quantification depends on gadolinium dosage, post-contrast time and T1 method

Post-contrast estimation of ECV relies on a steady-state Gd-equilibrium between the intravascular and interstitial compartments. This study demonstrated that ShMOLLI ECV achieved a time-independent equilibrium early (within 7-10 minutes) following Gd administration, whereas MOLLI 4(1)3(1)2 variants (particularly MOLLI Low HR) yielded ECV that continued

to increase over time. Schelbert et al. (0.6% rise in ECV over 30 minutes) and Kawel et al. (3% rise in ECV over ~40 minutes) also reported linear increases in ECV over time using MOLLI 3(3)5 (205,206). Weingartner et al. similarly demonstrated method dependencies in ECV estimation at 3T, showing an absolute ~1.5% rise in MOLLI 4(1)3(1)2 ECV over a 10-minute period (between 15-25 minutes after Gd), compared to much smaller changes using saturation recovery techniques (SAPPHIRE ~0.8%; SASHA ~0.6%) (207). Further, this study demonstrated ECV dependencies on Gd dosage, with ShMOLLI ECV nearly threefold less affected than MOLLI ECV (1.2% vs. 3.01-3.11%). Caballeros et al., who recorded ECV 15 minutes after a first (0.1 mmol/kg) and then second (0.1 mmol/kg) dose of Gd, similarly showed that MOLLI 4(1)3(1)2 ECV dropped by 2.3 ± 1.1% with a second Gd-dose (214).

Given that post-contrast T1 values in this study were generally >600ms during the half-dose Gd epoch, this may affect MOLLI 4(1)3(1)2 T1, being subject to increased underestimation error outside the validated application ranges (102). However, as no gold standard T1 or ECV measurements were available, the underlying reason for the differences between ShMOLLI and MOLLI T1 changes over time cannot be concluded from this study alone. Larger case numbers, lower Gd-dosage and extended post-contrast observation times may be required to clarify the mechanism of the observed differences. Further research may be warranted, given that the ability to measure ECV at earlier

time points and with lower Gd doses has potential benefits in reducing scanner time and costs.

4.5.3 Pre-contrast, stress and post-contrast T1-mapping using different MOLLI variants

Despite strong correlations between ShMOLLI and MOLLI T1-mapping variants, the overall relationship is not strictly linear, with between-method differences and residuals showing trends which differ between MOLLI variants and for pre- and post-contrast and stress conditions. Given different biases between the different protocols (as evidenced by different rest T1 values), they should not be used interchangeably or combined at all. This adds a layer of further complexity above the known wide range of T1 offsets within the MOLLI family (215–217).

4.5.4 Intra-individual and intra-method variability between T1-mapping variants and their impact on power calculations for clinical studies

Noise and relative effect sizes are a critical factor in sample size estimation for clinical studies. Repeat variability, normalised to observed effects, is an adequate measure to compare power calculations between methods. For stress T1-mapping, this study observed 1.75 to 2-fold greater relative

differences in effect sizes for ShMOLLI compared to MOLLI. Assuming that severe pathology (e.g. ischaemia due to obstructive CAD) leads to a near-abolished or nullified stress T1 response (104,131,203), this would translate to an estimated reduction in case numbers of at least 3 to 4-fold for the same study power when using ShMOLLI. This study also demonstrated important differences in intra-method consistency across T1-mapping variants for ECV estimation. The study showed greater relative differences in effect sizes of 1.3 to 2.2-fold (half-dose Gd epoch) and 1.6 to 2.75-fold (whole-dose Gd epoch) for ShMOLLI compared to MOLLI. Assuming the scale of pathological ECV effects to be in order of its absolute value, similar reasoning would lead to an expected 1.8 to 7.5-fold reduction in case numbers to achieve the same study power when using ShMOLLI.

4.5.5 Limitations

This study was conducted in a small cohort of 10 healthy controls and excluded one silent major myocardial infarction case, highlighting that small groups can suffer from significant sampling bias. One female participant in the study cohort demonstrated a sustained stress response, with delta T1 persisting near peak over the entire stress period. Although the study did not specifically analyse sex differences, this may have contributed, with Nickander et al. recently showing higher stress MBV in females compared with males (218). Bodyweight may also be a consideration (62kg; BMI 23.9 in this case), given the one-size-fits-all regadenoson dosing protocol. Although stress T1-mapping

typically has a relatively small effect size, and the effect in all healthy subjects within the cohort was able to be reliably measured, larger studies are needed to confirm the reliability of this technique in future.

Given the limited sampling period to about 2 measurements per minute, the findings are limited to a single mid-ventricular short axis slice, which is sufficient for an initial proof of concept study on T1 time evolution. Due to different number of preparations and matrix-size, the choice of TD = 0 ms, led to slightly different cardiac phases, i.e., trigger time (272.5 ms for ShMOLLI, 185 ms for MOLLI), depending on the variant. While there were no visual differences in image quality, this may need further investigation. As it is impossible to acquire different T1-mapping methods simultaneously, we relied on ShMOLLI to enable comparisons and establish relationships between methods. This was based on shorter breath holds (lesser burden to subjects) and the excellent intra-individual, intra-scanner, and inter-scanner variability of ShMOLLI (<2%) (97). Repeating the experiments using MOLLI as the baseline modelling technique would not be a practical use of resources given the demonstrated noise ratios and power calculations. Given the vast cost and complexity of the protocols, the benefit of increasing subject numbers in further studies, preferably multi-site and multivendor, must be carefully weighed against consistency of evidence in published literature. Whilst multiple T1-mapping variants exist, this study elected to compare ShMOLLI with Siemens product MOLLI 5(3)3 variants, based on similarly short breath

holds for stress applications, more widespread sequence availability, and thus greater generalisability.

Further work is required to characterise the underlying mechanism for the observed differences in stress T1 response between the sequences tested. ShMOLLI and MOLLI are both known to be sensitive to a number of factors such as heart rate, T2, motion, inflow and magnetisation transfer (MT) effects in a complex manner, which are difficult to control in an in-vivo study. For example, heart rate and motion are both increased during stress and differing sensitivities to these between ShMOLLI and MOLLI may contribute to differences in their stress T1 response. Additionally, the MOLLI family of pulse sequences have a strong T2 dependence (219), which may also influence the change in T1 with stress, particularly in the presence of an already elevated T2 as may be seen in some pathologies. However, as these confounders are intrinsic to the physiological stress response, their effects cannot be easily separated. Phantom experiments that can to some degree control for T1 and T2 effects may provide some insight into these mechanisms but are not expected to be able to fully simulate the complex interrelations between heart rate and stress-induced changes in T1, T2, T2*, and vascular volumes. Further study with comparison to a T1-mapping sequence insensitive to these factors such as SASHA may also help to clarify the contribution of these confounders to the ShMOLLI and MOLLI stress T1 response.

4.6 Conclusions

Like adenosine, regadenoson stress causes significant dynamically changing responses in myocardial T1 relaxation time measured using CMR. While myocardial T1 measurements by different techniques correlate strongly with each other, ECV and the stress T1 response show significant differences depending on the T1-mapping method, even within the related family of inversion recovery based bSSFP MOLLI variants. These results indicate that ShMOLLI correlates strongly with increased MBF during regadenoson stress and achieves a significantly higher stress T1 response, greater effect size, and greater ECV measurement stability over time compared with the MOLLI variants tested, with critical differences in intra-individual variability and effect sizes suggesting potential significant impact on power calculations depending on the T1 method used.

5 Regadenoson stress and rest T1-mapping for the assessment of coronary artery disease

---

The work presented in this Chapter has been published in the International Journal of Cardiology as:

Burrage MK, Shanmuganathan M, Masi A, Hann E, Zhang Q, Popescu IA, Soundarajan R, Leal Pelado J, Chow K, Neubauer S, Piechnik SK, Ferreira VM. Cardiovascular magnetic resonance stress and rest T1-mapping using regadenoson for detection of ischemic heart disease compared to healthy controls. *Int J Cardiol*. 2021 Jun 15;333:239-245. doi: 10.1016/j.ijcard.2021.03.010.

5.1 Abstract

5.1.1 Background

Adenosine stress T1-mapping on cardiovascular magnetic resonance (CMR) can differentiate between normal, ischaemic, infarcted, and remote myocardial tissue classes without the need for contrast agents. Regadenoson, a selective coronary vasodilator, is often used in stress perfusion imaging when adenosine is contra-indicated, and has advantages in ease of administration, safety profile, and clinical workflow. This study aimed to characterise the regadenoson stress T1-mapping response in healthy individuals, and to investigate its ability to differentiate between myocardial tissue classes in patients with coronary artery disease (CAD).

5.1.2 Methods

Eleven healthy controls and 25 patients with CAD underwent regadenoson stress perfusion CMR, as well as rest and stress ShMOLLI T1-mapping. Native T1 values and stress T1 reactivity were derived for normal myocardium in healthy controls and for different myocardial tissue classes in patients with CAD.

5.1.3 Results

Healthy controls had normal myocardial native T1 values at rest (931 ± 22 ms) with significant global regadenoson stress T1 reactivity (delta T1 8.2 ± 0.8% relative to baseline; p<0.0001). Infarcted myocardium had significantly higher resting T1 (1215 ± 115 ms) than ischaemic, remote, and normal myocardium (all p<0.0001) with an abolished stress T1 response (delta T1 -0.8% [IQR: -1.9-0.5]). Ischaemic myocardium had elevated resting T1 compared to normal (964 ± 57 ms; p<0.01) with an abolished stress T1 response (delta T1 0.5 ± 1.6%). Remote myocardium in patients had comparable resting T1 to normal (949 ms [IQR: 915-973]; p=0.06) with blunted stress reactivity (delta T1 4.3% [IQR: 3.1-6.3]; p<0.0001).

5.1.4 Conclusions

Healthy controls demonstrate significant stress T1 reactivity during regadenoson stress. Regadenoson stress and rest T1-mapping is a viable alternative to adenosine and exercise for the assessment of CAD and can distinguish between normal, ischaemic, infarcted, and remote myocardium.

5.2 Introduction

Cardiovascular magnetic resonance (CMR) has demonstrable utility in the assessment of suspected coronary artery disease (CAD) and the selection of patients for invasive coronary catheterisation. First-pass myocardial perfusion CMR using gadolinium contrast directly assesses global and focal reductions in myocardial blood flow (MBF) at rest and during vasodilator stress, and has high diagnostic accuracy in detecting significant coronary disease (20,105–107). However, myocardial blood volume (MBV), which represents both coronary macro- and microcirculations, may constitute a more comprehensive global marker of ischaemia than MBF (108,220). Satisfactory augmentation of MBF and MBV requires adequate coronary vasodilatory reserve, which may be interrogated by pharmacological vasodilatory stress (49,221).

Application of this principle for the assessment of CAD is based on the fact that myocardial territories downstream of a significant coronary stenosis have increased resting coronary vasodilation and capillary recruitment (104) and thus increased MBV with significantly impaired stress coronary vasoreactivity. These changes in MBV may be interrogated by stress T1-mapping, based on the principle that native T1 values are sensitive to tissue free water content and may thus detect changes in MBV during vasodilatory stress (95). Previous studies and Chapters have shown that adenosine stress T1-mapping on CMR can distinguish between normal, ischaemic, infarcted, and remote

myocardium, without the need for gadolinium-based contrast agents (GBCAs) (104,112,114,115).

However, although adenosine is widely used in CMR units as a coronary vasodilator stress agent, it has a potentially increased side-effect profile due to non-selective activation of all adenosine receptors (A_1, A_{2A}, A_{2B}, and A_3) and requires an intravenous (IV) infusion (3-4 minutes) before images may be acquired. Regadenoson, a selective A_{2A}-receptor agonist coronary vasodilator, has similar cardiac efficacy as adenosine whilst minimising adverse effects, is often used in stress perfusion imaging when adenosine is contra-indicated, and has advantages in ease of administration (IV bolus), safety profile, and clinical workflow (123). The normal stress T1-mapping response to regadenoson vasodilatory stress has not been previously studied for its potential clinical applicability. This study aimed to characterise the normal stress T1-mapping response to regadenoson in healthy controls, and to then investigate the ability of regadenoson stress T1-mapping to differentiate between normal, ischaemic, infarcted, and remote myocardium as an additional method for contrast-free assessments of CAD in the future.

5.3 Methods

5.3.1 Study Population

Eleven healthy controls with no history of cardiovascular disease or cardiac symptoms, and twenty-five patients with known chronic CAD undergoing clinically indicated regadenoson stress perfusion CMR, were prospectively included. Participants with contraindications (see **2.2**) to stress perfusion CMR scanning or other significant comorbidities or pregnancy were excluded. All participants were advised to avoid caffeine for ≥24 hours before the scan.

5.3.2 Image acquisition

CMR imaging was performed using a 1.5-Tesla MRI scanner (MAGNETOM AvantoFit, Siemens Healthcare, Erlangen, Germany) using an 18-channel phased-array coil. After standard planning, cine images were acquired in three long axis views (HLA, VLA, LVOT) and in short axis slices covering the whole left ventricle (LV) using balanced steady-state free precession cine imaging (49,134). T1-mapping was performed using the Shortened Modified Look-Locker Inversion recovery (ShMOLLI) prototype sequence as previously described (92). In-line quality assessment of ShMOLLI T1-maps was performed using parametric goodness-of-fit (R^2) maps at time of acquisition (64,92,136,222). In healthy controls, native T1-maps were acquired at rest and during peak (first acquisition within 30 seconds) vasodilator stress (regadenoson 400 µg IV bolus injection over 10 seconds followed by a 10 ml

0.9% sodium chloride saline flush over 10 seconds) in 3 short axis slices (basal, mid-ventricular, and apical).

CAD patients underwent rest and regadenoson stress T1-mapping as described above. Stress first-pass perfusion imaging was performed on matching short axis slices to the T1-maps during peak stress, with a bolus of gadolinium (0.05 mmol/kg IV, gadoterate meglumine, Dotarem, Guerbet SA, Paris, France) followed by a 15-20 ml saline flush, both administered at 4-6 ml/sec (104). Regadenoson stress was reversed using aminophylline (100 mg IV over 10 seconds followed by a 10 ml saline flush also over 10 seconds). Rest first-pass perfusion imaging was then performed as described above, typically at least 5-10 minutes after aminophylline reversal. Late gadolinium enhancement (LGE) imaging was performed ~8 to 10 minutes after an additional bolus of gadolinium (0.1 mmol/kg) in long and short axis slices covering the LV, as well as matched to the T1-maps and perfusion slices.

5.3.3 Image analysis

Image analysis for biventricular indices was performed offline in accordance with SCMR guidelines (49), using cmr42 post-processing software (version 5.10.1, Circle Cardiovascular Imaging Inc., Calgary, Canada). First-pass myocardial perfusion and LGE images were analysed as previously described (72,104). Offline post-processing of ShMOLLI T1-maps was performed using

MC-ROI. Endocardial and epicardial contours were placed using dedicated automated software and manually checked for errors. Quality assessment of parametric goodness-of-fit (R^2) maps resulted in exclusion of 6.6% of myocardial segments. For healthy controls, mean myocardial T1 values were derived from rest and stress T1-maps on a per-slice and per-segment basis according to the AHA 17-segment model (63). Stress T1 reactivity was calculated as previously described (see section **2.4.4** and **4.3.4**).

In CAD patients, mean T1 values were derived from regions of interest (ROIs) carefully placed within ischaemic, infarcted, and remote myocardium, and LV blood pool for reference, based on first-pass perfusion and LGE findings as previously described (**Figure 5.1**) (104). Briefly, ischaemic myocardium was defined as an area corresponding to a reversible perfusion defect on first-pass stress perfusion imaging in the absence of LGE. Infarcted myocardium was defined as an area of infarction on LGE images; infarct ROIs were placed in the core of the infarcts to avoid partial volume contamination from the LV blood pool, carefully referenced against corresponding cine images (104). Remote myocardium was defined as areas contralateral to ischaemic myocardium and without evidence of first-pass perfusion defects, regional wall motion abnormalities, or LGE. ROIs were carefully matched between rest and stress images.

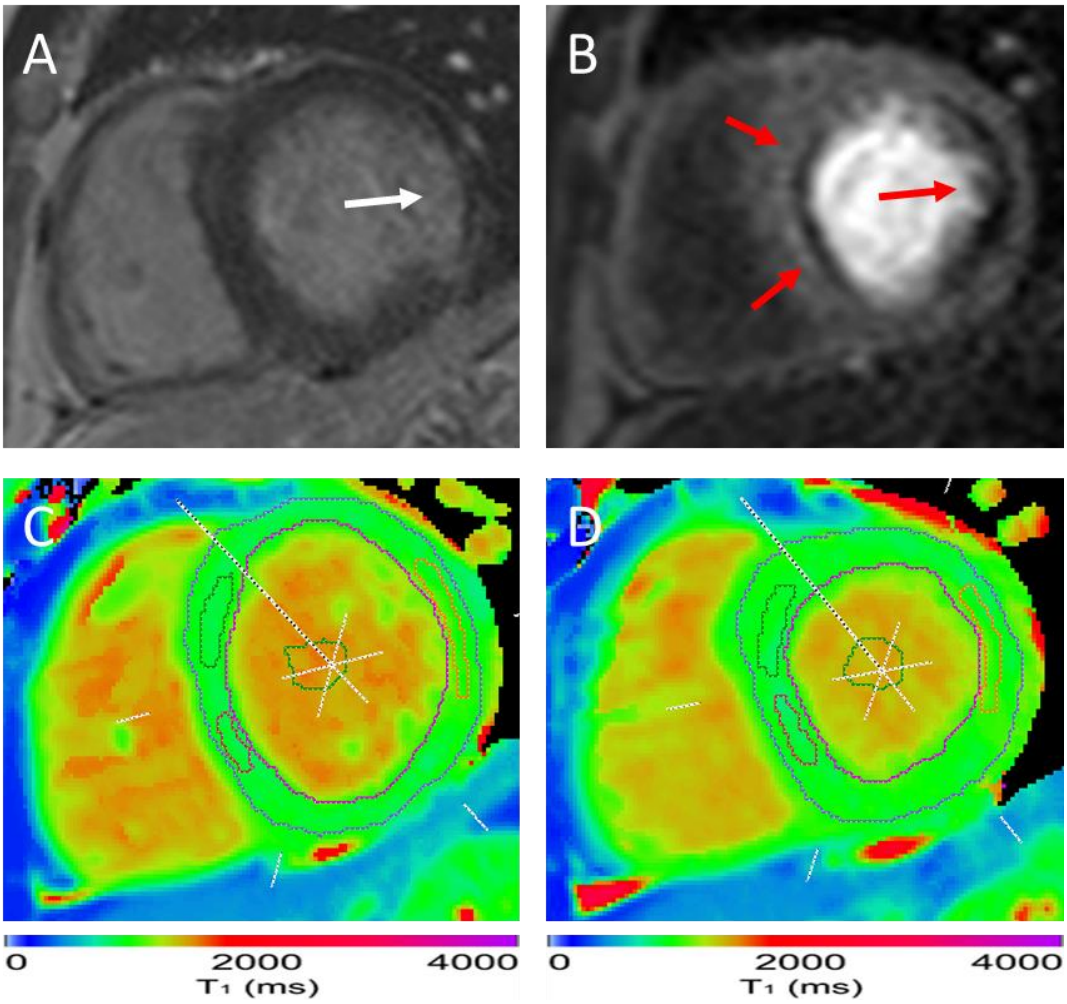


Figure 5.1: Example image analysis of a patient with coronary artery disease. *Late gadolinium enhancement image (A) shows evidence of a lateral myocardial infarction (white arrow). On first-pass stress perfusion (B) there is a fixed hypoperfusion defect in the lateral wall corresponding to the area of infarction, as well as inducible hypoperfusion in the septum (red arrows). Regions of interest are placed in the areas of ischaemia and infarction and LV blood pool on T1-maps at rest (C) and stress (D). Delta T1 was significantly abolished in the anterior septum (1.3%), inferior septum (-0.8%), and in the lateral infarction (-0.4%). For comparison, the remote myocardium in this case had a delta T1 of 3.7%. This participant had severe left anterior descending artery disease on invasive angiography, as well as a chronic total occlusion of the left circumflex artery.*

5.3.4 Statistical analysis

Data are presented as mean ± SD for all parametric data, and median with interquartile ranges (IQR) for non-parametric data, based on Shapiro-Wilks tests for normality. For parametric data, paired t-tests are used whenever possible to assess differences between rest and stress in the same individuals; unpaired t-tests are used to assess differences between groups for selected myocardial tissue types. For non-parametric data, Wilcoxon signed rank test and Mann Whitney U test are used. Repeated measures within subjects were accounted for using a linear mixed effects model. A two-tailed $p<0.05$ is considered statistically significant. Statistical analysis and data modelling were performed using R Studio (RStudio Team (2018). RStudio: Integrated Development for R. RStudio, Inc., Boston, MA).

5.4 Results

5.4.1 Myocardial stress T1 reactivity to regadenoson in healthy controls

Baseline characteristics are presented in **Table 5.1**. All controls completed the CMR protocol without complications. One participant was excluded after incidental detection of a large myocardial infarction on LGE imaging, leaving a total of ten healthy controls (50% male, median age 32 [IQR: 29-37] years). All remaining healthy controls had structurally normal hearts with normal resting cardiac volumes (LVEDVi 79 [IQR: 67-88] ml/m^2) and systolic function (LVEF

59% [IQR: 57-63%]), no inducible perfusion defects, and no LGE (**Table 5.2**). All participants had a significant heart rate response to regadenoson (healthy controls 67 ± 12 to 114 ± 12 bpm; CAD patients 65 ± 11 to 93 ± 17 bpm; all $p<0.0001$).

Table 5.1: Baseline characteristics of the study participants.

	Healthy controls (n = 10)	CAD patients (n = 25)
Male	5 (50)	23 (92)
Age (years)	32 [29-37]	69 [55-74]
Body mass index (kg/m^2)	25 [24-26]	27 [24-29]
Clinical risk factors		
Smoking history	–	7 (28)
Hypertension	–	11 (44)
Hypercholesterolemia	–	4 (16)
Diabetes mellitus	–	14 (56)

Counts given as number (%); continuous variables as median [interquartile range].

Table 5.2: CMR parameters and angiographic data

	Healthy controls (n=10)	CAD patients (n=25)
CMR clinical indices (all)		
LVEF (%)	59 [57-63]	52 [43-64]
LVEDVi (ml/m^2)	79 [67-88]	86 [78-108]
Remote myocardial segments (no ischaemia or infarction)	0 (0)	54 (13)
Ischaemic myocardial segments (on first-pass perfusion)	0 (0)	58 (15)
Infarcted myocardial segments (on LGE)	0 (0)	56 (14)
Angiographic data (n=10)		
≥1 lesion (>50% visual diameter stenosis)	–	10 (100)
LAD	–	10
LCx	–	6
RCA	–	8

Counts given as number (%); continuous variables as median [interquartile range].

Healthy controls had normal global myocardial native T1 values at rest (**Table 5.3**) in accordance with previously published normal ranges (97). Compared to rest, there was a significant rise in myocardial T1 values with regadenoson stress ($p<0.0001$).

Table 5.3: Rest and regadenoson stress native T1-mapping myocardial tissue profiles

	Healthy Controls (n = 10)	**CAD Patients** (n = 25)			
	Normal	**Remote**	**Ischaemic**	**Infarct**	**LV Blood Pool**
Rest T1 (ms)	931 ± 22	949 [915-973]	964 ± 57	1214 ± 115	1506 ± 78
Stress T1 (ms)	1008 ± 24	988 [955-1013]	969 ± 55	1213 ± 108	1503 ± 75
Delta T1 (%)	8.2 ± 0.8	4.3 [3.1-6.3]	0.5 ± 1.6	-0.8 [-1.9-0.5]	-0.01 ± 1.1

Data are presented as mean ± SD or median [interquartile range].

On per slice analysis, there was a significant rise in myocardial T1 values with regadenoson for the basal (rest 924 ± 18 ms; stress 1014 ± 25 ms; delta T1 9.7 ± 1.6%), mid-ventricular (rest 926 ± 24 ms; stress 999 ± 24 ms; delta T1 7.7 ± 1.2%), and apical (rest 943 ± 29 ms; stress 1008 ± 33 ms; delta T1 7.1 ± 1.4%) slices ($p<0.0001$ for all comparisons; **Figure 5.2A**), as well as for individual myocardial segments (**Figure 5.2B**). There were no significant differences in stress T1 reactivity between the basal, mid-ventricular, and apical slices (all $p>0.05$).

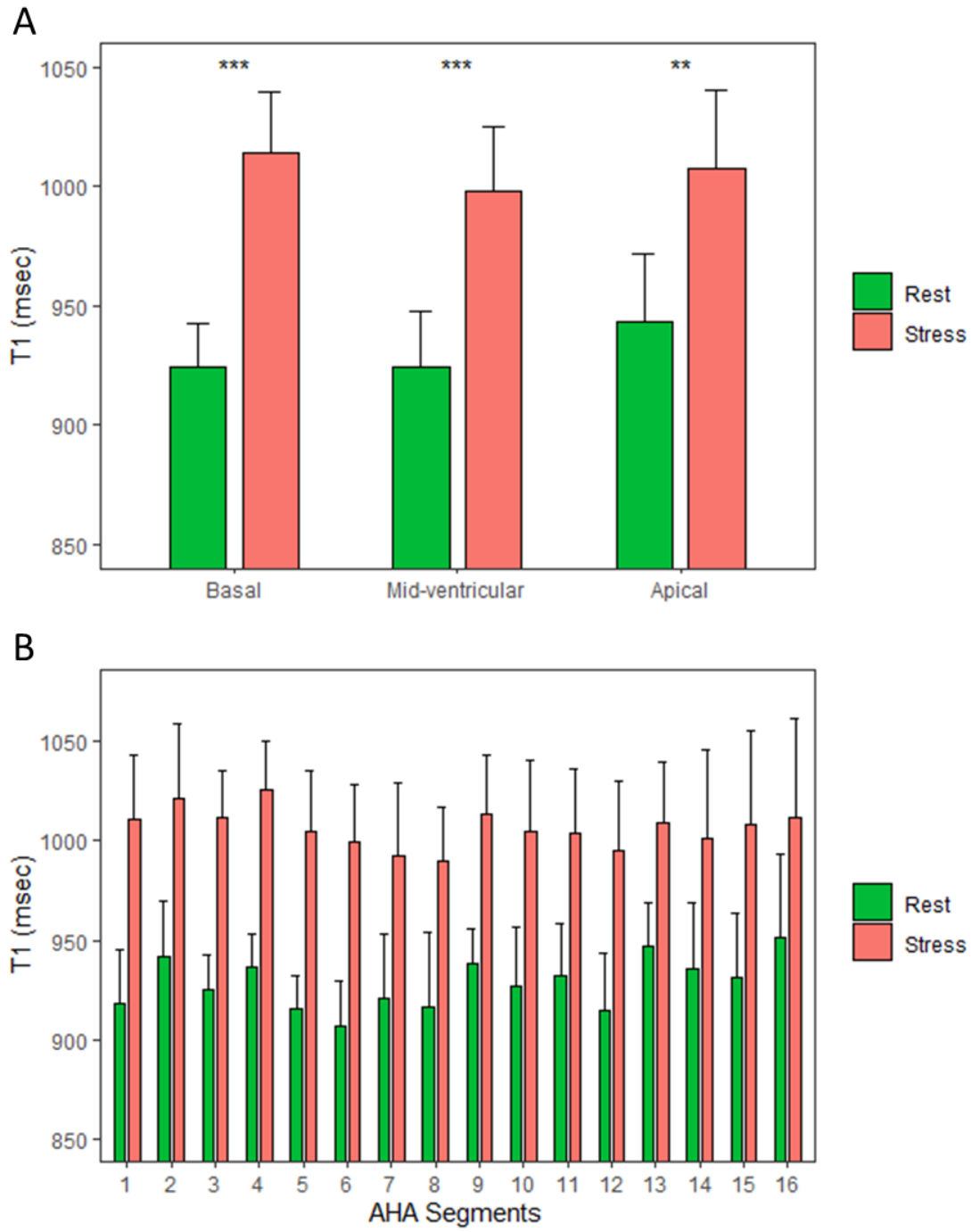


Figure 5.2: Normal regadenoson stress T1 responses in healthy controls. *Comparison of native myocardial T1 values at rest and during regadenoson stress in healthy controls in standard short-axis slice positions (A) and in the AHA 16-segments (B). There are significant increases in T1 values during stress for all slices and myocardial segments. Data presented as mean and standard deviation (error bars). **p<0.01; ***p<0.001; ****p<0.0001; ns=not significant*

5.4.2 Myocardial stress T1 reactivity to regadenoson in patients with CAD

Twenty-five patients (92% male, median age 69 [IQR: 55-74] years) with known CAD underwent clinically indicated stress perfusion CMR at 1.5-Tesla, including LV function, regadenoson stress/rest T1-mapping, first-pass perfusion, and LGE. Patients with CAD had normal LV volumes (LVEDVi 86 [IQR: 78-108] ml/m^2) with mildly reduced systolic function (LVEF 52% [IQR: 43-64%]) (**Table 5.2** above). All patients had evidence of myocardial ischaemia on first-pass perfusion imaging (referenced to ≥1 angiographically significant coronary stenosis in n=10 patients) or infarction on LGE with n=13 (52%) having imaging evidence of both ischaemia and infarction. No patients with acute myocardial infarction were included in the study.

Rest and stress T1 values and stress reactivity (delta T1) for patients with CAD are presented in **Table 5.3** above. At rest, remote myocardial T1 in CAD patients was similar to healthy controls (p=0.06). Ischaemic myocardial T1 was significantly higher than normal myocardium (p<0.01), but not remote myocardium (p=0.15). Infarcted myocardium had significantly higher resting T1 than ischaemic, remote, and normal myocardium (all p<0.0001) (**Figure 5.3A**) but shorter than that of LV blood pool (p<0.0001). There were no significant correlations between infarcted myocardial T1 and ischaemic (r = 0.18, p=0.19) or remote (r = 0.1, p=0.46) myocardium or with LV blood pool (r = 0.01, p=0.94).

Ischaemic and infarcted myocardium both had an abolished stress T1 response compared with normal controls (both $p<0.0001$). Remote myocardial stress T1 reactivity was significantly blunted compared to normal controls ($p<0.0001$), although still significantly greater than ischaemic and infarcted myocardium (both $p<0.0001$) (**Figure 5.3B**). For comparison, LV blood pool had little stress T1 reactivity.

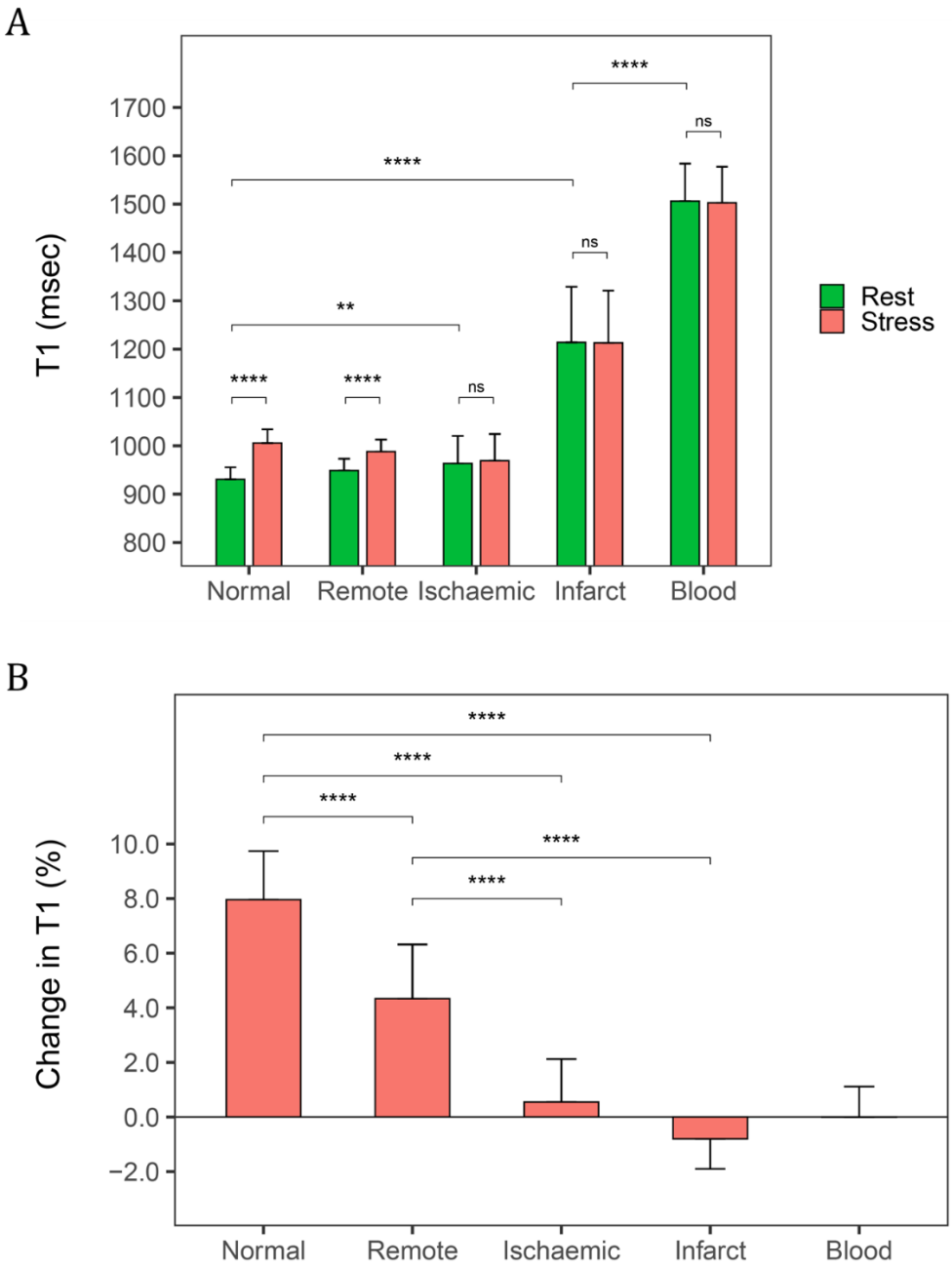


Figure 5.3: Regadenoson stress T1-mapping distinguishes between different myocardial tissue classes. *Myocardial tissue T1 profiles in healthy controls and CAD patients are based on absolute T1 values (A) and stress delta T1, i.e., the percentage change in T1 between rest and stress (B). Normal and remote myocardium demonstrate significant stress T1 reactivity, whereas areas of myocardial ischemia and infarction have a near-abolished stress delta T1 response. Data presented as mean and standard deviation (error bars) or median and IQR (error bars). **p<0.01; ***p<0.001; ****p<0.0001; ns=not significant.*

5.5 Discussion

This is the first study to demonstrate the normal regadenoson stress T1-mapping response, and its ability to distinguish between normal, ischaemic, infarcted and remote myocardium, further supporting the findings that regadenoson is a viable alternative to adenosine stress T1-mapping in the assessment of CAD (202).

5.5.1 Regadenoson stress T1 reactivity in healthy controls

In healthy controls there was an overall global regadenoson stress delta T1 response of 8.2 ± 0.8%, with delta T1 reactivities of 9.7 ± 1.6%, 7.7 ± 1.2%, and 7.1 ± 1.4% for the basal, mid-ventricular, and apical slices respectively. Although not statistically significant, there seemed to be a numerically greater stress T1 response in the basal slice, which is worthy of discussion.

Regadenoson is a more potent in vitro vasodilator than adenosine, with greater selectivity for the coronary circulation in animals (223). Interestingly, this has been seen to translate to significantly higher stress MBF (ml/min/g) and myocardial perfusion reserve (MPR) with regadenoson compared with adenosine and dipyridamole (224). However, these effects on MBF and MPR seemed to be driven by the higher heart rate responses achieved with regadenoson rather than by more potent vasodilation (224). It is possible that the acquisition timings for the basal slice in this study (acquired early within

30 seconds of regadenoson administration) could have coincided with peak heart rate effects of the drug. This could have contributed to a numerically higher stress T1 response, especially given the known physiological myocardial changes that occur during elevated heart rates and their additional biological effects on myocardial T1 values in vivo (6 ms increase in ShMOLLI T1 for every 10 bpm rise in heart rate) (97). Other possible confounds may be due to partial-volume effects during stress, as the basal slice may be subject to changes in the extent of longitudinal atrioventricular plane descent with regadenoson through heart rate and ventricular filling. Further work is required to fully ascertain the true relationship of these effects over time, particularly given the known rapid rise and slow decay pharmacokinetic profile of regadenoson (210), as opposed to the more steady-state adenosine infusion.

5.5.2 Regadenoson stress T1 reactivity for the assessment of CAD

These findings are consistent with previous adenosine and exercise stress T1-mapping studies in patients with CAD (104,112–115). The results in this study are similar to Bohnen et al. (202), who also used regadenoson stress T1-mapping to assess for the presence of inducible ischaemia, although notably their study did not include healthy controls for reference nor investigated the normal regadenoson stress T1 response in healthy individuals. The lack of stress reactivity seen in ischaemic myocardium may reflect depletion of

coronary vasodilatory reserve and suggests that myocardial blood volume at rest may already be maximally elevated in areas of significant coronary artery stenosis. This is further supported by the observed elevation in native T1 values at rest in these segments. Areas of infarction, which have significantly elevated T1 values at rest due to the presence of fibrosis and myocardial scar, are not expected to display much T1 reactivity, as observed previously (104,112–115).

This study also confirmed significantly blunted stress T1 reactivity in remote myocardium compared to healthy controls, in line with similar findings from other studies (104,115,202). This may suggest a degree of microvascular dysfunction, possibly in combination with compensatory resting vasodilation or other pathophysiological factors in chronic CAD not yet elucidated. The numerically increased rest native myocardial T1 values in remote myocardium in those with obstructive CAD compared to healthy controls may indeed reflect an element of compensatory resting vasodilation, although the rest T1 values in controls seen in this study (931 ± 22 ms; Table 5.3) were lower than that reported previously both in the literature (962 ± 25 ms; (197)) and this Thesis (953 ± 23 ms; **Chapter 3**). Despite this, there remains a clear difference in stress T1 reactivity between normal myocardium in controls and remote myocardium in patients with CAD which is worthy of further discussion.

Type 2 diabetes mellitus is a traditional risk factor for cardiovascular disease and has been shown to directly affect the structure and function of the myocardium, leading to adverse outcomes (119). Blunted stress T1 reactivity has been seen in patients with type 2 diabetes in the absence of obstructive CAD, possibly reflecting coronary microvascular dysfunction (119). There was a high prevalence of type 2 diabetes in the cohort of patients with CAD in this study (56%), which may therefore explain the blunted stress T1 reactivity seen in the remote myocardium. Indeed, the degree of stress T1 reactivity seen in the remote myocardium in this study (delta T1 4.3% [3.1-6.3%]) was similar to that seen in a cohort of patients with type 2 diabetes and no obstructive CAD (delta T1 4.1 ± 2.9%) (119). The presence of other cardiovascular risk factors such as hypertension, which may also affect native T1 values, is another important consideration when evaluating the remote myocardium in patients with CAD (225). Other CMR methods have shown similar blunted responses in absolute myocardial perfusion and stress/rest blood oxygen level dependence in remote myocardium, also postulating whether this may be due to microvascular dysfunction (226). Further work is required to determine the underlying mechanism behind these blunted physiological responses in remote myocardium and in other cardiovascular pathologies.

5.5.3 Limitations

This is a proof-of-principle study for regadenoson stress T1-mapping in healthy controls and in patients with CAD referred for a clinical CMR. Having a

larger cohort of healthy controls would provide greater confidence in the regadenoson stress T1 response and the standard deviation, as smaller sample sizes may be subject to sampling bias. The healthy controls in this study were not age-matched to patients with CAD, which is a possible confounder given the known reductions in hyperaemic flow and myocardial perfusion reserve with increasing age (227). Additionally, there may be potential sex bias given the majority (92%) of the CAD cohort in this study were male, compared with the controls (50%). This is potentially relevant given higher quantitative perfusion and MBV in female healthy volunteers during adenosine stress (218), although no significant sex differences in the diagnostic performance of CMR have been reported (21). Further work with larger cohorts is required to study the effects of sex on stress T1 reactivity.

This study used stress-perfusion CMR as the non-invasive reference for inducible myocardial ischaemia, which is known to have high sensitivity and specificity for CAD (20). Although not all patients underwent invasive coronary angiography, the fact that stress T1-mapping is able to detect CMR signal changes on perfusion and LGE imaging supports the validity of this technique, as shown in previous studies (104,112–115), including the use of SPECT as a reference (113). However, although this demonstrates the utility of stress T1-mapping to differentiate myocardial tissue classes, areas of ischaemia or infarction were identified from myocardial first-pass perfusion and LGE images as reference. Further work is required to develop a completely

gadolinium-free approach for identification of pathology in patients with cardiovascular disease based solely on stress T1-mapping.

5.6 Conclusions

Healthy controls demonstrate significant stress T1 reactivity during regadenoson stress. Regadenoson stress and rest T1-mapping is a viable alternative to adenosine and exercise for the assessment of CAD and can distinguish between normal, ischaemic, infarcted, and remote myocardium.

6 *Cardiac stress T1-mapping response to dobutamine*

6.1 Abstract

6.1.1 Background

Pharmacological stress cardiovascular magnetic resonance (CMR) is well-validated for the assessment of myocardial ischaemia and may be performed using either vasodilator (e.g., adenosine, regadenoson, dipyridamole) or inotropic (e.g., dobutamine) agents. Adenosine and regadenoson stress T1-mapping on CMR can assess for ischaemic heart disease without the need for intravenous contrast agents, based on the sensitivity of native T1 to changes in myocardial free water content and therefore changes in myocardial blood flow (MBF) and volume (MBV) during stress. The stress T1-mapping response to dobutamine (which may be used when vasodilators are contraindicated) has not previously been characterised. This study aimed to characterise the stress T1 time and dose-related response to dobutamine and explore its suitability for future clinical applications.

6.1.2 Methods

Healthy volunteers (n=10, 50% female, 42 ± 11 years) underwent dobutamine stress CMR at 1.5-Tesla. ShMOLLI T1-maps were acquired from a single mid-ventricular slice at rest and consecutively at increasing doses of dobutamine (commencing at 5 μg/kg/min and increasing in a stepwise fashion to a maximum of 40 μg/kg/min). Heart rate and blood pressure were recorded at 1- to 2-minute intervals to track the physiological response and estimate the rate pressure product. Stress T1 reactivity (delta T1) was defined as the relative increase in native T1 between rest and stress.

6.1.3 Results

There was a progressive increase in myocardial T1 and delta T1 over time during the dobutamine infusion, with peak effects seen at the 40 μg/kg/min dose (rest T1 921 ± 22 ms; peak stress T1 1019 ± 54 ms; delta T1 10.6 ± 3.7%; $p<0.0001$). The rise in T1 was strongly correlated with markers of the physiological response such as the relative change in heart rate and rate pressure product ($r = 0.98$, $p<0.0001$ for both), although there were clear inter-individual differences in the regression slopes for these parameters.

6.1.4 Conclusions

Dobutamine stress causes significant dynamic responses in myocardial T1 over time in healthy individuals as measured using CMR. Dobutamine is a

viable pharmacological stress agent that may be suitable for future stress T1-mapping clinical applications in the assessment of cardiovascular disease.

6.2 Introduction

Pharmacological stress cardiovascular magnetic resonance (CMR) is highly useful for the assessment of myocardial ischaemia and may be performed using either vasodilator or inotropic agents. Vasodilator agents (e.g., adenosine, regadenoson, dipyridamole) demonstrate areas of reduced myocardial blood flow and hypoperfusion downstream of significant coronary artery stenoses on first-pass perfusion imaging, while dobutamine (the only approved inotropic agent) promotes ischaemia by inducing myocardial oxygen demand mismatch (228). The safety and feasibility of vasodilator and dobutamine stress CMR has been demonstrated in large multi-centre registry studies (229).

Studies and prior Chapters have shown that adenosine and regadenoson stress T1-mapping on CMR can assess for ischaemic heart disease without the need for intravenous contrast agents (167,179,203,230,231). This relies on the principle that native T1 values are sensitive to myocardial free water content and therefore changes in myocardial blood flow (MBF) and volume (MBV) during vasodilator stress, which may be reduced in cases of obstructive coronary artery disease (CAD) or microvascular dysfunction. Given the potential contrast-free applications of stress T1-mapping, there is clear interest to expand and standardise the technique across a wide range of clinically available pharmacological stress agents.

The stress T1-mapping response to dobutamine (which may be used when vasodilators are contraindicated) has not previously been characterised. This may be of particular interest, given that first-pass perfusion is often combined with wall motion assessment during dobutamine stress CMR to improve sensitivity for the diagnosis of significant obstructive CAD (232,233). Stress T1-mapping may therefore confer a similar benefit but without the need for contrast agents and additional intravenous (IV) access.

This study therefore aimed to characterise the stress T1 time and dose-related response to dobutamine and the suitability of this method for future clinical applications.

6.3 Methods

6.3.1 Study population

Ten healthy volunteers with no history of cardiovascular disease or cardiac symptoms were prospectively recruited from Oxford University Hospitals NHS Foundation Trust.

6.3.2 Image acquisition

CMR imaging was performed using a 1.5-Tesla MRI scanner (AvantoFit, software version VE11C, Siemens Healthcare, Erlangen, Germany) using an 18-

channel phased-array coil with the participant supine. After standard planning, cine images were acquired in three long-axis views (HLA, VLA, LVOT) and in short axis slices covering the whole left ventricle (LV) using retrospectively ECG-gated bSSFP cine imaging (170,171). T1-maps were acquired in matching short axis slices based on the ShMOLLI sequence as previously described (172), prototype version C2P. Quality assessment of ShMOLLI T1-maps was performed in-line at time of acquisition using parametric goodness-of-fit (R^2) maps (172).

The main dobutamine CMR scanning protocol is provided in **Figure 6.1** and consisted of repeated ShMOLLI T1-maps (n=62 T1-maps per participant) and cine images from a single mid-ventricular slice, at rest and at increasing doses of dobutamine. Systolic imaging (TD = 0 ms) was used for T1-mapping sequences as previously described (**Chapter 4**). Stress T1-maps were acquired consecutively, commencing immediately upon starting the IV infusion of dobutamine. The dobutamine protocol commenced at 5 μg/kg/min for 5 minutes and increased in a stepwise fashion to 10 μg/kg/min for 5 minutes, 20 μg/kg/min for 5 minutes, 30 μg/kg/min for 4 minutes, and 40 μg/kg/min for 4 minutes (**Table 6.1**). The final T1 measurement before each dose increment was taken as the maximum T1 response for each corresponding epoch.

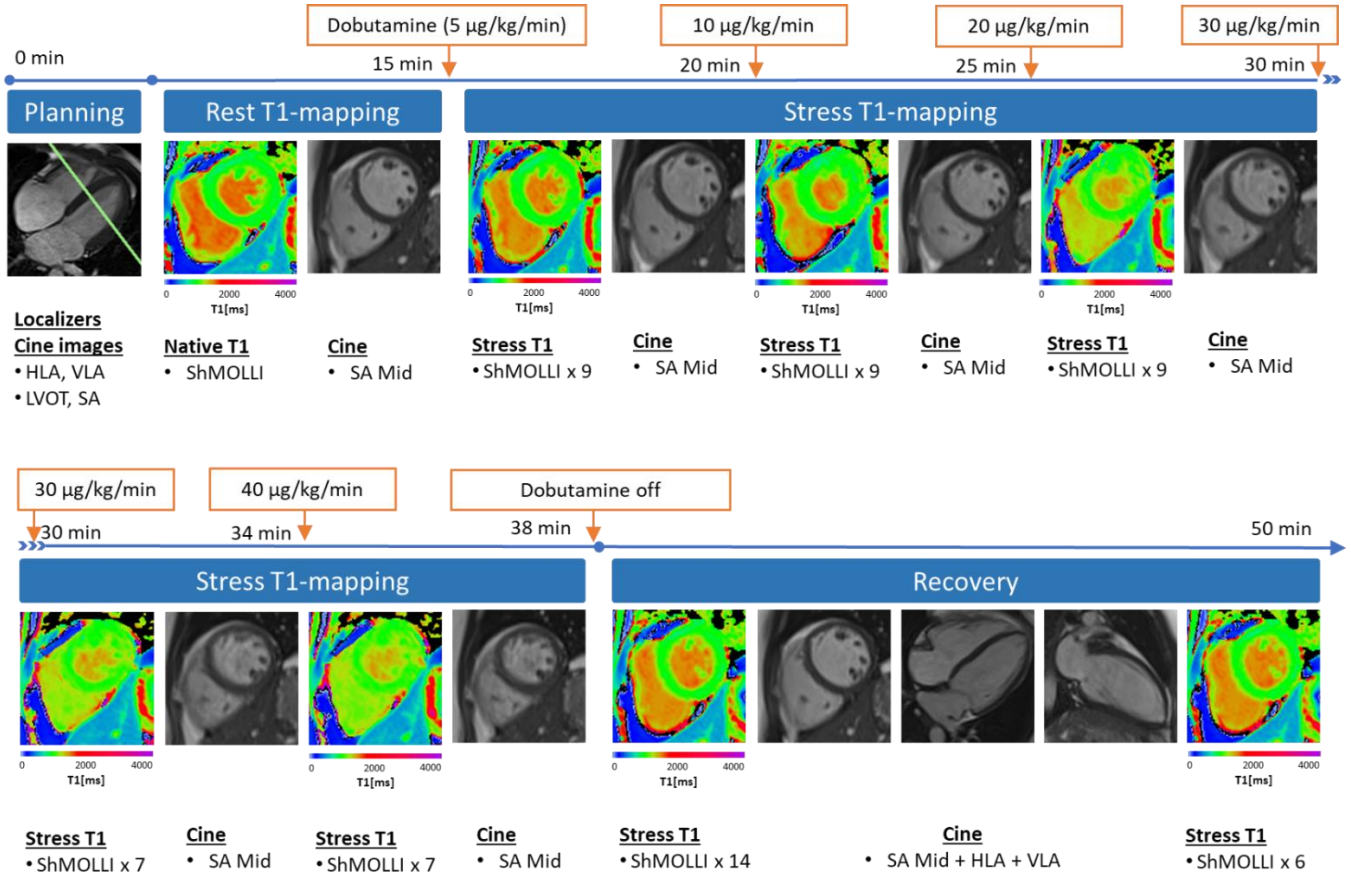


Figure 6.1: Dobutamine stress T1-mapping protocol for assessing time dependencies. *After planning, native ShMOLLI T1-mapping is performed using a trigger delay of 0 ms in a mid-ventricular short axis slice. A cine image in a matching slice position is also acquired to assess changes in contractility. The sequence of 7-9 ShMOLLI stress T1-maps and one short axis stress cine image is repeated at increasing doses of dobutamine for fixed time points, as well as a prolonged recovery phase of 20 ShMOLLI T1-maps.*

Table 6.1: Dobutamine dosing protocol and time intervals

Dobutamine dose	Cumulative Time (mins)	Length of epoch (mins)
Baseline	0	N/A
5 μg/kg/min	0-5	5
10 μg/kg/min	5-10	5
20 μg/kg/min	10-15	5
30 μg/kg/min	15-19	4
40 μg/kg/min	19-23	4
Recovery	23-35	12

Cumulative time refers to time elapsed since commencing the dobutamine infusion. Length of epoch refers to the length of time for each dosing interval.

Imaging continued for a further 12 minutes after cessation of the dobutamine infusion, to allow the offset effect to be estimated. A single mid-ventricular short axis cine image was also performed penultimately at the end of each stage of the dobutamine infusion protocol to assess changes in myocardial contractility. Heart rate and blood pressure were recorded throughout at one and two-minute intervals respectively.

6.3.3 Image analysis

Image analysis for cardiac indices was performed offline in accordance with SCMR guidelines (171), using cmr42 post-processing software (version 5.10.1,

Circle Cardiovascular Imaging Inc., Calgary, Canada). Endocardial and epicardial contouring of T1-maps was performed manually offline using MC-ROI. T1-maps underwent rigorous quality control and segments with artefacts or other confounders were excluded. A total of 5.3% of myocardial segments were excluded (mainly due to sequence mistriggering (n=138 segments) or increased motion-blurring artefact (n=58 segments) at peak dobutamine). This is similar to that reported with regadenoson in clinical patients (see **Chapter 4**). T1-mapping results were based on quantitative analysis of all T1-maps, with global slice average T1 values of all included myocardial segments per slice.

6.3.4 Data modelling and statistical analysis

Relative stress responses were calculated for heart rate, myocardial contractility, and delta T1, as previously described (see section **2.4.4** and **4.3.4**). The relationships between T1-mapping variants for stress T1 and delta T1 were assessed with linear regression models and Pearson's correlation coefficient (r). The relationships between T1-mapping derivatives and markers of physiological stress (i.e., heart rate, relative change in heart rate, and cardiac workload as estimated by the rate pressure product [systolic blood pressure x heart rate]) were assessed. Given the dynamic nature of the pharmacological stress agents, datapoints were grouped in 30-second intervals (according to the protocol) so as to improve data sampling and better display the dynamic effects of time on T1 evolution, based on prior experience

from **Chapter 4**. Data are presented as mean ± SD. A two-tailed $p<0.05$ is considered statistically significant. Statistical analysis and data modelling were performed using R Studio (RStudio Team (2018). RStudio: Integrated Development for R. RStudio, Inc., Boston, MA).

6.4 Results

6.4.1 Study population

All 10 participants (50% female, mean age 42 ± 11 years, BMI 25 ± 3 kg/m^2) completed the study protocol and tolerated dobutamine without complications. Participants had structurally normal hearts with normal resting cardiac volumes (LVEDVi 71 ± 9 ml/m^2), mass (LVMi 54 ± 9 g/m^2) and systolic function (LVEF 64 ± 4%).

6.4.2 Physiological effect of pharmacological stress

Clear physiological effects of dobutamine were seen on all variables of interest. Heart rate significantly increased over the course of the dobutamine infusion from 68 ± 10 bpm at baseline to a maximum of 129 ± 16 bpm ($p<0.0001$). Peak heart rate (i.e., the fastest recorded heart rate) was achieved at the highest dose of dobutamine (40 μg/kg/min) for all individuals (**Figure 6.2**). Nine participants achieved at least 65% of maximal predicted heart rate (MPHR) by age; however only one participant achieved the conventional stress testing target of 85% MPHR (15).

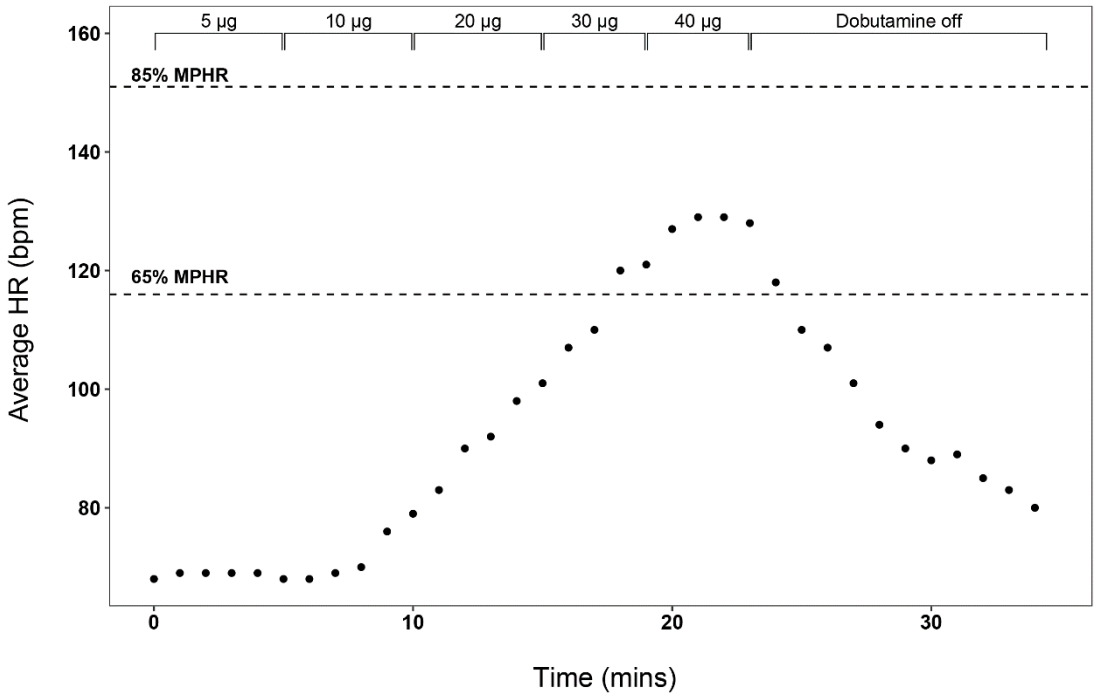


Figure 6.2: Effect of time and dobutamine dose on heart rate. *There is a clear rise in heart rate with increasing doses of dobutamine over time, averaged across the participants. The dashed lines represent the average 65% and 85% maximal predicted heart rate (MPHR) by age.*

There was a significant rise in systolic blood pressure (122 ± 15 mmHg to 146 ± 23 mmHg; p=0.01) and mean arterial pressure (91 ± 11 mmHg to 103 ± 19 mmHg; p=0.02) during dobutamine infusion. There was an associated rise in rate pressure product (HR x systolic blood pressure), rising from 8258 ± 1804 to 18408 ± 3248 mmHg*bpm (p<0.0001), with the greatest cardiac workload recorded at 40 µg/kg/min of IV dobutamine as expected. Myocardial contractility also increased in a stepwise fashion with increasing doses of dobutamine, based on single mid-ventricular short axis cine images acquired

as the penultimate measurement for each dose epoch. There was a 3 ± 3% (p=0.01) relative increase in contractility (as normalised to baseline) at 5 μg/kg/min, increasing to 14 ± 8%, 22 ± 9%, 26 ± 10%, and 28 ± 11% for 10, 20, 30, and 40 μg/kg/min of IV dobutamine respectively (all p<0.0001 compared with baseline). Myocardial contractility remained relatively increased compared to baseline towards the end of the recovery period ~9 minutes after stopping dobutamine (8 ± 4%; p<0.001).

6.4.3 Dobutamine stress T1 response and relationship to the physiological response

6.4.3.1 Dobutamine stress T1 response

During dobutamine infusion, there was a progressive increase in LV myocardial T1 and delta T1, with peak effects seen at the 40 μg/kg/min dobutamine dose. T1 rose from 921 ± 22 ms to a peak of 1019 ± 54 ms (p<0.0001; **Figure 6.3A**) and delta T1 of 10.6 ± 3.7% (**Figure 6.3B)**.

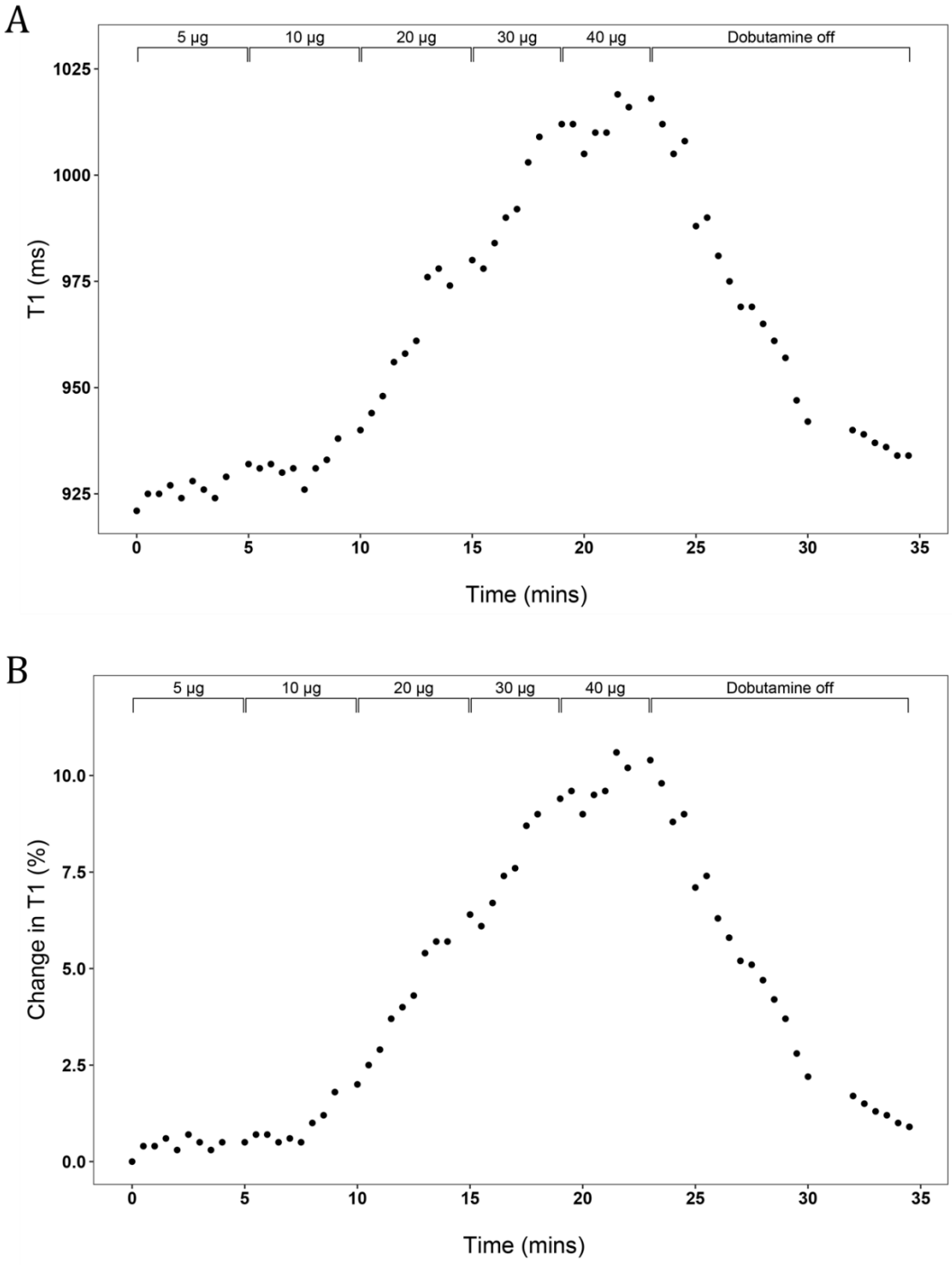


Figure 6.3: Change in LV myocardial T1 values with time and increasing dobutamine doses. *The rise in actual myocardial T1 (A) and the relative change in T1 (i.e., delta T1) as normalised to baseline (B) are shown.*

There was a small but significant change in T1 from baseline, based on myocardial T1 measured within the final 30 seconds of the 5 μg/kg/min dobutamine epoch (T1 932 ± 21 ms; delta T1 0.5 ± 0.5%; p=0.03), which increased further by the end of the 10 μg/kg/min stage (T1 940 ± 33 ms; delta T1 2.0 ± 1.7%; p=0.004). The rise in T1 was much more accelerated for the 20 μg/kg/min (T1 980 ± 56 ms; delta T1 6.4 ± 4.1%; p=0.001) and 30 μg/kg/min (T1 1012 ± 50 ms; delta T1 9.4 ± 3.6%; p<0.0001) epochs. The peak stress T1 response was achieved at 40 μg/kg/min of dobutamine (T1 1019 ± 54 ms; delta T1 10.6 ± 3.7%; p<0.0001). There was a clear trend for T1 to return to near baseline (934 ± 22 ms; delta T1 0.9 ± 1.5%; p=0.08) by the end of the recovery period (**Table 6.2**). There were significantly different decay time constants at different stages of the T1 recovery curve ($e^{-0.173x}$ vs $e^{-0.256x}$ i.e., ~4 vs 5.8 minutes; p<0.001) and non-linear regression slopes for the change in T1 over time once the dobutamine infusion had been ceased, although these varied depending on the time into recovery.

Table 6.2: Myocardial T1 and relative change (delta T1) recorded at the end of each dobutamine dose epoch

Dobutamine dose	Time (mins)	T1 (ms)	Delta T1 (%)	p value
Baseline	0	921 ± 22	0 (reference)	N/A
5 μg/kg/min	5	932 ± 21	0.5 ± 0.5	**0.03**
10 μg/kg/min	10	940 ± 33	2.0 ± 1.7	**0.004**
20 μg/kg/min	15	980 ± 56	6.4 ± 4.1	**0.001**
30 μg/kg/min	19	1012 ± 50	9.4 ± 3.6	**<0.0001**
40 μg/kg/min	23	1019 ± 54	10.6 ± 3.7	**<0.0001**
Recovery	34.5	934 ± 22	0.9 ± 1.5	0.08

Data are presented as mean ± SD. P values reported are paired t-tests compared to baseline.

6.4.3.2 Dobutamine stress T1 response and its association with physiological variables

There was a clear relationship between the rise in T1 and physiological variables, indicating a pharmacological stress response. At the group level, there were significant near-linear correlations between: mean HR and mean T1, mean relative change in HR and delta T1, and mean rate pressure product and both T1 and delta T1 ($r = 0.98$, $p<0.0001$ for all).

When assessed at the individual level, there were again strongly significant correlations between relative change in HR and delta T1 ($r = 0.82$-0.96; all

$p<0.0001$; average regression slope 0.92 ± 0.04 %bpm/%delta T1) (**Figure 6.4A**) and between rate pressure product and delta T1 ($r = 0.77$-0.99; all $p<0.0001$; average regression slope 0.92 ± 0.07 bpm.mmHg/%delta T1) (**Figure 6.4B**). Despite these linear trends, there were clear inter-individual differences in the regression slopes. There were no apparent associations of the individual regression slopes to conventional parameters such as BMI, weight, LV mass, or LV mass index.

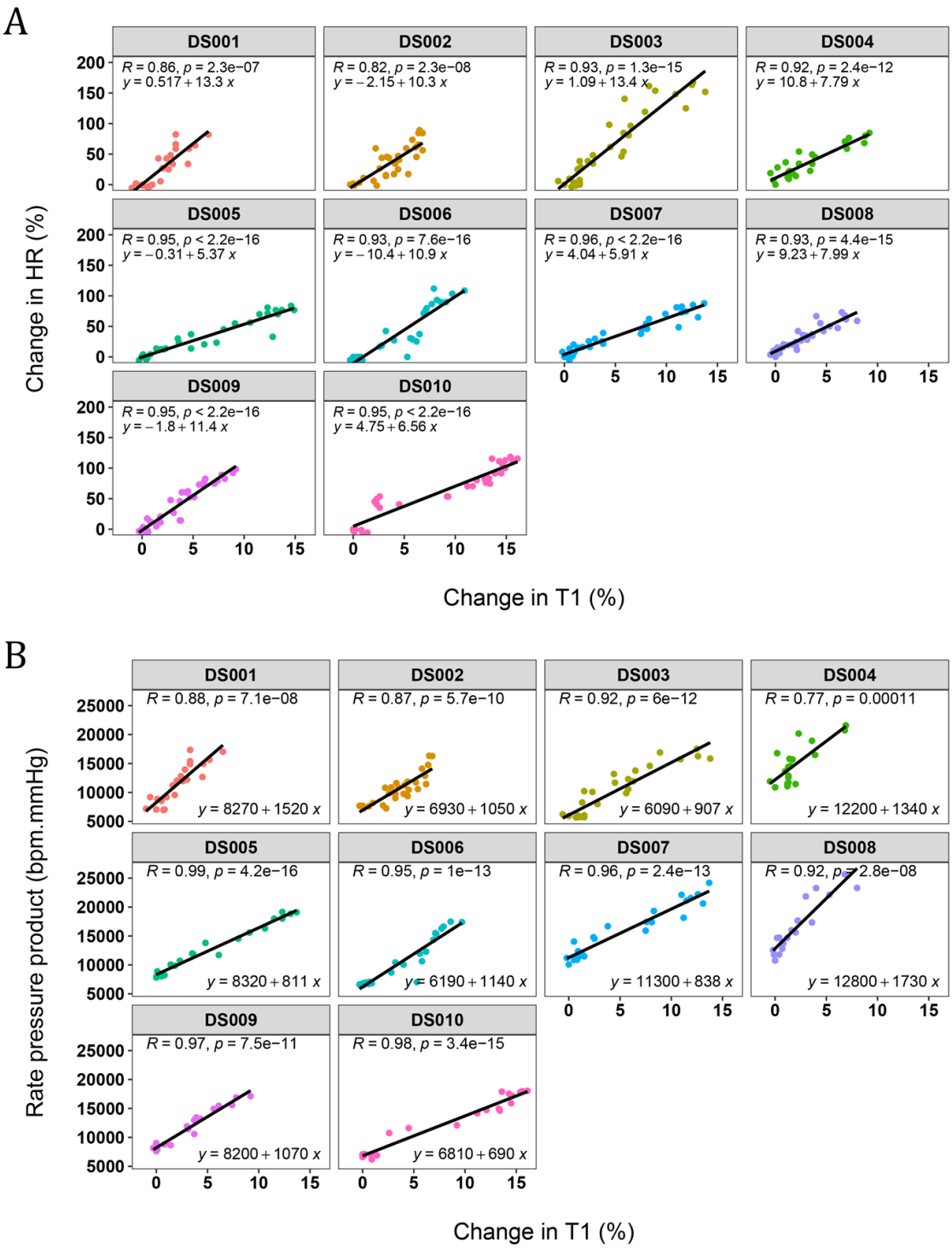


Figure 6.4: Inter-individual variability for physiological and stress T1 responses with IV dobutamine in healthy controls. *Individual correlations for relative change in heart rate versus delta T1 (A) and rate pressure product versus delta T1 (B). The observed variability in the slopes was not associated with typical individual characteristics such as body mass index, weight, or left ventricular mass.*

6.5 Discussion

This is the first systematic study to characterise dobutamine stress T1 dynamics over time. The study demonstrates that: 1) the effects of dobutamine may be reliably measured using stress T1-mapping, suggesting similar clinical utility to that previously demonstrated with adenosine and regadenoson (167,179,203,230,231); and 2) the stress T1 response closely mirrors markers of physiological stress and cardiac workload, although these vary on an individual basis.

6.5.1 Dynamic response of T1-mapping during dobutamine stress

The current study showed a significant progressive stepwise increase in myocardial stress T1 reactivity with increasing doses of dobutamine, although the dosing protocol used in clinical practice was unsuitable to fully estimate dose responses and response times, given that a steady-state was not achieved for each dose epoch. Interestingly, the peak delta T1 achieved was much higher than seen with vasodilator stress agents. The mechanism by which dobutamine may result in increased myocardial blood flow and volume is worthy of extended discussion below in this section. Although the mechanism of action differs from that of primary directly acting vasodilators (such as adenosine, regadenoson, dipyridamole), in both cases, there is a presumed maximal reduction of myocardial resistance.

6.5.1.1 Effect of dobutamine on myocardial blood flow

Dobutamine increases myocardial blood flow via several different mechanisms. Increases in cardiac workload result in a metabolic-mediated increase in coronary flow to meet the myocardium's increased oxygen and substrate needs (234,235), while high-dose dobutamine results in a dose-dependent dilation of normal coronary arteries via direct stimulation of alpha1-, beta 1-, and beta2- adrenergic receptors in the coronary vascular wall (236,237). The slope of dose-dependent dilatation (**Figure 6.5**) seen follows a similar response pattern to that shown in this experiment with the dose-dependent rise in T1 and delta T1 (**Figure 6.3** in results above).

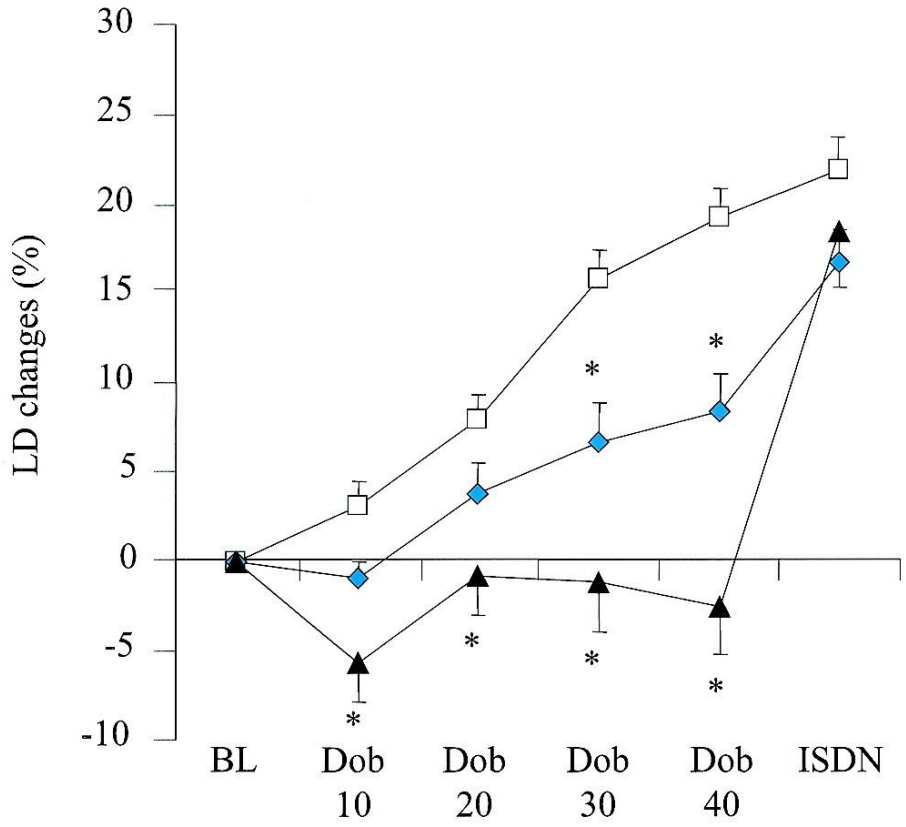


Figure 6.5: Effect of dobutamine on coronary artery luminal diameter. *There is a dose-dependent progressive increase in luminal diameter (LD) in those with normal coronary arteries (white squares), mildly atherosclerotic coronary arteries (blue diamonds), and stenotic coronary arteries (black triangles). There is significantly less coronary vasodilation ($p<0.05$) in those with coronary artery disease compared to normal coronary arteries. The increase in luminal diameter with increasing doses of dobutamine or isosorbide dinitrate (ISDN) follows a similar pattern to that seen with change in T1 from this experiment. Reproduced with permission from Barbato E, Bartunek J, Wyffels E, Wijns W, Heyndrickx G, De Bruyne B. Effect of intravenous dobutamine on coronary vasomotion in humans. JACC. 2003;42(9):1596-1601. (236).*

The distribution of these adrenergic receptors may be heterogeneous, however, as beta1-receptors are crucial in the regulation of coronary vasomotion in epicardial coronary arteries, while beta2-receptors may play more of a role in the regulation of the resistance vessels (236,238).

Additionally, increased myocardial contractility and oxygen consumption results in the release of endogenous vasodilatory mediators, such as adenosine, which further dilates the coronary vasculature. Increases in heart rate also induces flow-mediated vasodilation (239).

It is clear that the dobutamine-stimulated increase in myocardial work alone (as estimated by the rate pressure product) does not fully explain the entire myocardial blood flow response. Quantitative estimates of myocardial blood flow on positron emission tomography (PET) have shown reasonable correlations with rate pressure product (240) during dobutamine infusion, while invasive coronary studies have shown some disparity (241). Studies have shown that the modest rate pressure product increase during dobutamine infusion is much lower than that reported during exercise (242), despite greater increases in contractility (243). This suggests a dissociation between increases in myocardial mechanical work and myocardial blood flow.

Invasive haemodynamic studies have shown that while a dose of 20 μg/kg/min may be sufficient to achieve maximal coronary flow reserve depletion downstream of coronary stenoses (with little further benefit of increasing the dobutamine dose to 30-40 μg/kg/min) (241), this is not the case for normal coronary arteries, which continue to demonstrate increases in coronary flow with higher dobutamine doses (see **Figure 6.5**) (236,244). Interestingly, the addition of an intracoronary adenosine bolus showed no

change in myocardial blood flow in stenotic coronary arteries, while normal coronary arteries demonstrated a further significant hyperaemic response (244). Additionally, isosorbide dinitrate was able to increase coronary luminal diameter when dobutamine failed to do so in stenotic coronary arteries (236), suggesting that there are other receptors and mechanisms that contribute to and can achieve further coronary vasodilation in diseased vessels. This highlights that the hyperaemic response to dobutamine may be in excess of that predicted by cardiac workload and the rate pressure product alone. There are likely additional effects on the coronary vasculature, resistance vessels, and myocardial blood volume, which may potentially be assessed using stress T1-mapping.

6.5.1.2 Effect of dobutamine on myocardial T1

It is interesting to consider the stress T1 response to dobutamine in light of the above underlying physiology. The current experiment showed peak ShMOLLI stress T1 reactivity of 10.6 ± 3.7% at 40 μg/kg/min of dobutamine. This is much higher than the delta T1 responses previously reported with other coronary vasodilators (see **Chapter 4** and **Chapter 7**). Interestingly, the delta T1 response at 20 μg/kg/min (6.4 ± 4.1%) in this study is much more comparable to the vasodilator reactivity reported with adenosine and dipyridamole. Since normal vessels are expected to further increase coronary flow with higher doses of dobutamine (244), this may support other data suggesting that the "maximal" hyperaemia reported with adenosine at 140

μg/kg/min is in fact submaximal, given the further increases seen in MBF when the adenosine dose is increased to 210 μg/kg/min (245). The concept of 'maximal hyperaemia' may be more dynamic than first thought.

Additionally, the increased T1 response at higher dobutamine doses may be mediated by tachycardia, given the tachycardia induced by high-dose dobutamine was much higher than seen with adenosine, regadenoson, or dipyridamole. This is an important consideration as the previously reported 6 ms increase in T1 for every 10 bpm increase in heart rate (197) could translate to an additional ~2-3% increase in delta T1 (when comparing with reported peak heart rate responses for adenosine and dipyridamole). This is plausible and would seem to be an extension of the established relationship between T1 and heart rate changes (see also **6.5.1.3**), perhaps reflecting a greater physiological stress. The effects of increased myocardial contractility may also play a role. Certainly, there was noticeably increased motion blurring at higher dobutamine doses and heart rates (despite high-quality R^2 maps), which may have affected the accuracy of T1 measurements via increased partial volume effects, although every effort was made to focus the analysis on the mid-wall myocardium as much as possible to avoid this. Nonetheless, it is reassuring that myocardial stress T1 reactivity can be measured robustly across a range of dobutamine doses.

Presuming that the dobutamine stress T1 response to significant pathology (e.g., obstructive CAD, microvascular dysfunction) is nulled (and does not augment at high doses), this could pave the way to a more accelerated stress imaging protocol. For example, evidence of a significant stress T1 response (e.g., delta T1 5-6%) at 20 μg/kg/min of dobutamine (in combination with heart rate and blood pressure evidence of a physiological response) may be sufficient to rule out severe pathology without needing to escalate to higher doses, which may be poorly tolerated. This will be discussed further in **Chapter 8 (General conclusions and future directions)**. Further clinical validation studies (including determining the pattern of response in areas of presumed hibernating myocardium) is required.

The rate of rise of myocardial T1 during dobutamine stress is also of interest. It is hard to ascertain if the response is truly non-linear or rather exhibits non-linear lag. The onset of action of dobutamine is reported as within 1-2 minutes, but up to 10 minutes may be required to obtain the peak effect (234). Despite what were deemed prolonged dose epochs (i.e., 5 minutes at lower doses of dobutamine compared to the usual 3 minutes used in most clinical stress protocols) in the study design, the T1 responses did not show clear evidence of reaching the steady-state for any epoch. This makes it challenging to separate when the effect of the increased infusion truly occurs or whether there is lag from the preceding doses. Based on the decay time constant (tau) of ~5 minutes established above, it can be calculated that the response at the

end of each epoch would be roughly 30% below the steady-state. Usually, recovery epochs as long as 3 * tau (i.e., 15 minutes) are required to bring this response error to within an acceptable ~5% level. Extending each dose epoch out to 10-15 minutes in future experiments may be necessary to properly assess the dose response, although might be impractical both from a patient comfort point of view, as well as significantly increased scan time.

6.5.1.3 Effect of physiological response on myocardial T1 with dobutamine

This experiment showed strong linear relationships between physiological response variables (i.e., heart rate, rate pressure product) and the myocardial stress T1 response with dobutamine. The 2.2-fold increase in rate pressure product seen in this study falls within the range of increases reported previously (246,247). A similar relationship between rate pressure product and myocardial blood flow with dobutamine has been reported, with a 2.7-fold increase in rate pressure product matched by a 2.9-fold increase in myocardial blood flow when assessed with a C-11 acetate PET tracer, suggesting that the increase in cardiac demand with dobutamine is highly correlated with an increase in supply and oxidative metabolism (240).

It is not surprising that the myocardial T1 would also increase in association with these physiological variables, given they signify the pharmacological stress effects as hyperaemia is induced. However, this current experiment showed significant variability in the slopes between physiological variables

and T1 responses for each individual healthy volunteer, which could not be standardised using simple metrics such as body mass index or cardiac mass. This reflects the heterogeneity of pharmacological stress responses within even healthy individuals and suggests that, in clinical practice, stress T1-mapping (and even stress CMR in general) studies may need to be tailored to each individual's response.

Finally, it is important to remember that, although the stress T1 response has been discussed in the context of MBF (which is easier to quantify both invasively and non-invasively), the stress T1 response itself is more likely to reflect changes in MBV. Although MBF and MBV tend to correlate well with each other, the relationship is not strictly linear (248), with MBV tending to be more closely associated with increases in cardiac oxygen demand, which may be of greater relevance in the setting of coronary stenosis (181). Thus, there may be additional effects of MBV on top of the reported changes in MBF, primarily through increases in MBV mediated by the small capacitance vessels within the microcirculation. This may also explain differences in the T1 response between vasodilator stress and dobutamine stress. In other words, the stress T1 response to dobutamine may initially reflect changes in MBF due to increased myocardial demand and workload, with later effects of MBV seen at higher doses when there are further hyperaemic effects (as shown invasively when intracoronary adenosine is given on top of peak dobutamine (244)), in combination with the effects of tachycardia and dose-dependent

adrenergic receptor-mediated coronary vasodilation as discussed previously. The change in T1 during vasodilator stress has been shown to relate to both changes in quantitative myocardial perfusion on CMR (MBF) as well as MBV and extracellular volume (ECV), but the exact contributions of each, not to mention the impacts of T2 and magnetisation transfer (MT) effects, remains unclear (249).

6.5.1.4 Clinical applications of dobutamine stress T1-mapping

Similar to that demonstrated with adenosine and regadenoson, dobutamine stress T1-mapping may have clinical utility in the assessment of patients with CAD. Dobutamine stress CMR often includes first-pass perfusion imaging at peak stress in clinical practice, which increases diagnostic accuracy for the detection of significant obstructive coronary stenosis (232,233). Stress T1-mapping, which co-localises pathology well to inducible hypoperfusion defects on first-pass perfusion (see **Chapter 5**) (167,203), may therefore be a useful contrast-free adjunct for this application. Further clinical validation studies are required to determine the relative sensitivity and specificity of dobutamine stress T1-mapping for this indication, either in isolation or in combination with wall motion scoring. The utility of stress T1-mapping for the assessment of viability or functional recovery in hibernating myocardium or areas of abnormal resting wall motion is another novel application that will be the subject of future work.

6.5.2 Limitations

This study was conducted in a small cohort of healthy controls, which may be subject to sampling bias. Body size is likely to be less of a concern, given the dobutamine is dosed according to body weight. Steady-state T1 responses were not achieved for the different dobutamine dose epochs, which hinders the ability to separate the effect of different doses on stress T1; however, prolonged dobutamine dose epochs to test this would be impractical, given the likely requirement of extended 10-15-minute scanning epochs based on established time constants. Inter-individual heterogeneity in the physiological and stress T1 responses to dobutamine stress needs further investigation, but may hamper dose-based attempts to standardise the technique, pointing instead towards an individualised approach on a case-by-case basis. Further clinical validation work is required to assess the potential applications of dobutamine stress T1-mapping in the assessment of cardiovascular disease.

6.6 Conclusions

Dobutamine stress causes significant dynamic responses in myocardial T1 over time in healthy individuals as measured using CMR. Although the magnitude of the observed responses is related to dose, there are likely additional intrinsic effects on the coronary vasculature, resistance vessels, and MBV through individual physiological responses and changes in cardiac workload that also contribute to the stress T1 response. Dobutamine is a viable

pharmacological stress agent that may be suitable for future stress T1-mapping clinical applications in the assessment of cardiovascular disease.

7 Cardiac stress T1-mapping response to dipyridamole

7.1 Abstract

7.1.1 Background

There is clear interest to investigate and expand cardiovascular magnetic resonance (CMR) stress T1-mapping across a wide range of clinically available pharmacological stress agents as a novel contrast-free assessment for cardiovascular disease. The stress T1-mapping response to dipyridamole has not previously been characterised but is of clear clinical interest, given the frequent use of dipyridamole for stress imaging in CMR centres worldwide. The slower onset of dipyridamole (compared to regadenoson) theoretically allows better estimation and comparison of the acute rise in T1 between different T1-mapping methods, given the known method-sensitivities to changes in T1 during stress (such as seen between ShMOLLI and MOLLI). This study therefore aimed to characterise the dipyridamole stress T1 response over time and its suitability for future clinical applications, directly compare the relationship between ShMOLLI and MOLLI in terms of the acute rise in stress T1 and overall effect size, and compare stress T1-mapping relationships between different pharmacological stress agents.

7.1.2 Methods

Healthy volunteers (n=13, 55% female, 49 ± 16 years) were prospectively recruited from Mackay Memorial Hospital (Taipei, Taiwan) by our collaborators and underwent dipyridamole stress CMR at 1.5-Tesla. Scanning supervision was provided by remote video link until the local team had gained familiarity and independence with the research protocol. Consecutive ShMOLLI T1-maps were acquired from the mid-ventricular slice at rest and during stress to track the T1 time evolution. Interleaved standard MOLLI product sequences (MOLLI 5(3)3 Low and High Heart Rate) were used to compare and assess method-dependencies in the stress T1 response. Data from existing studies was pooled to compare the stress T1 relationships across multiple pharmacological stress agents.

7.1.3 Results

There was a progressive increase in myocardial T1 and delta T1 during the dipyridamole infusion, with a peak but plateaued response seen 6-8 minutes after the start of the infusion. ShMOLLI had a greater effect size and significantly higher peak delta T1 response (6.3 ± 1.6%) compared with MOLLI Low HR (4.6 ± 1.5%; p=0.02) and MOLLI High HR (3.9 ± 1.3%; p=0.001) for the equivalent time period. Dipyridamole delta T1 had the steepest slope of relationship with physiological markers of response (such as heart rate and rate pressure product) compared to dobutamine and regadenoson.

7.1.4 Conclusions

Dipyridamole vasodilator stress causes significant dynamic responses in myocardial T1 over time in healthy individuals, as measured using CMR, and achieves stress T1 results consistent with literature values for adenosine and regadenoson. ShMOLLI dipyridamole stress T1-mapping had a significantly higher stress T1 response and greater effect size at peak stress compared with the MOLLI variants tested. Dipyridamole is a viable and cheaper alternative vasodilator stress agent to adenosine and regadenoson and is suitable for future stress T1-mapping clinical applications.

7.2 Introduction

As discussed in **Chapter 6**, there is clear interest to investigate and expand the stress T1-mapping technique across a wide range of clinically available pharmacological stress agents including coronary vasodilators and inotropes.

The stress T1-mapping response to dipyridamole has not previously been characterised but is of clear clinical interest, given the frequent use of dipyridamole in CMR centres around the world (particularly in Asia and Europe (229)) for stress imaging. Dipyridamole, a non-selective coronary vasodilator which acts by inhibiting breakdown of adenosine, is given as a slow IV infusion over 4-6 minutes and has a slower onset of action than regadenoson. This theoretically allows better estimation and comparison of the acute rise in T1 between different T1-mapping methods (250), given the method-sensitivities to changes in T1 during stress that I have shown in **Chapter 4**.

This chapter therefore aimed to: 1) characterise the dipyridamole stress T1 response over time and its suitability for future clinical applications; 2) directly compare the relationship between ShMOLLI and MOLLI in terms of the acute rise in stress T1 and overall effect size with dipyridamole; and 3) compare the stress T1-mapping relationships between different pharmacological stress agents.

7.3 Methods

7.3.1 Study population

Thirteen healthy volunteers with no history of cardiovascular disease or cardiac symptoms were prospectively recruited from Mackay Memorial Hospital in Taipei, Taiwan by our collaborators. All subjects abstained from caffeine for 24 hours before undergoing CMR examination. Participation was voluntary and all participants provided written informed consent. The study received ethical approval from the local Research Ethics Review Committee and Institutional Review Board and was performed in accordance with relevant local guidelines and regulations.

7.3.2 Method translation to an international centre

The data acquisition was undertaken in collaboration with Mackay Memorial Hospital in Taipei, Taiwan as dipyridamole is not in use within Oxford University Hospitals. Investigation of dipyridamole in this work has been made possible by our collaborator Dr. Leo Yun, who had expressed interest in developing a stress T1-mapping research program. The study and CMR scanning protocols were designed in Oxford (closely mirrored on **Chapter 4**) using the Siemens scanner console and then transferred to and installed on the Mackay Hospital scanner with the on-site help of local Siemens scientists. I had personally organised and attended, with my supervisors, several two to three-hour-long scanning training sessions that were held remotely using a video

link connected directly to the external-site scanner console, so as to provide remote support for the scanning team to master the research protocol. Once the local radiographer and clinical team had gained familiarity and independence, supervision was provided on an ad hoc basis. Three study participant scans were supervised to completion remotely via video link, while the remaining ten scans were done independently by the Taiwan team. Quality was assessed every three scans via remote DICOM transfer to scrutinise slice positioning and image quality and ensure that study data had been acquired to the correct standard.

7.3.3 Image acquisition

CMR imaging was performed using a 1.5-Tesla MRI scanner (MAGNETOM Aera, Siemens Healthcare, Erlangen, Germany) with the participant supine. The CMR scanning protocol is provided in **Figure 7.1**. Cine imaging was performed in three long axis views and in short axis slices covering the whole left ventricle (LV), using retrospectively ECG-gated bSSFP imaging (170,171). T1-maps were acquired based on the ShMOLLI sequence as previously published (172), prototype version C2P. Quality assessment of ShMOLLI T1-maps using parametric goodness-of-fit (R^2) maps were available in-line at time of acquisition (64,172), based on open source reconstruction (208). MOLLI (MyoMaps, Siemens Healthcare, Erlangen, Germany) T1-maps were acquired from vendor-provided product protocols: “Long T1” MOLLI 5(3)3 was used for rest and stress native T1-mapping. The sampling scheme protocols had “Low

HR" (256 matrix) and "High HR" (192 matrix) variants, where the latter is recommended for heart rates greater than 80bpm to reduce cardiac motion blurring. Rest and stress T1-maps (ShMOLLI and MOLLI) were acquired from a single mid-ventricular slice using systolic imaging (TD = 0 ms) to standardise measurements and reduce the risk of mistriggering during tachycardia (173), as previously described in **Chapter 4**.

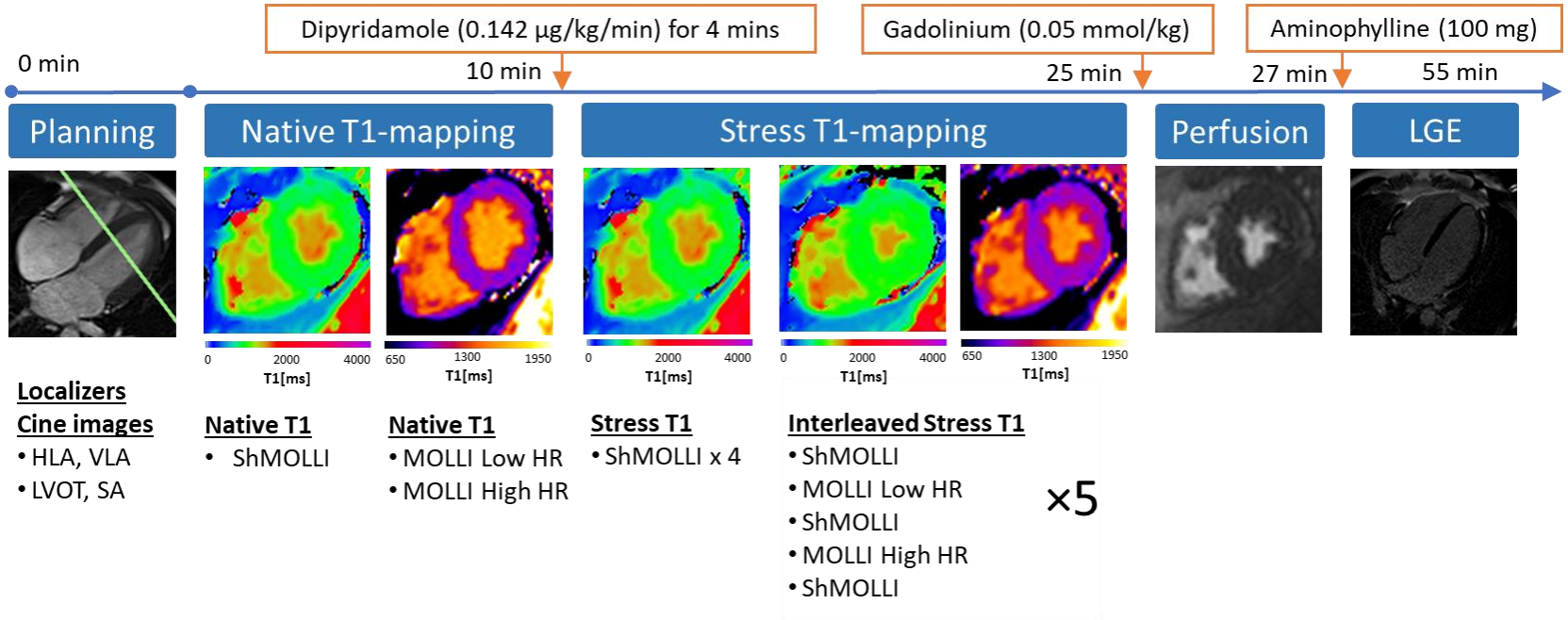


Figure 7.1: Dipyridamole stress CMR protocol for assessing T1 time dependencies. *After planning, native T1-mapping is performed at rest using ShMOLLI, MOLLI Low HR, and MOLLI High HR in a single mid-ventricular short axis slice (TD = 0 ms). Stress T1-mapping is performed immediately following commencement of an intravenous dipyridamole infusion (0.142 mg/kg/min for 4 minutes). This consists of four ShMOLLI measurements to assess the initial transition period, followed by blocks of interleaved ShMOLLI and MOLLI variants. First-pass perfusion imaging is performed after gadolinium injection (0.05 mmol/kg), before stress is reversed with aminophylline (IV 100 mg). Rest perfusion and late gadolinium enhancement images are also acquired.*

Stress T1-maps were acquired consecutively, commencing immediately upon initiation of an IV infusion of dipyridamole (Persantine), given at 0.142 mg/kg/min over 4 minutes (0.56 mg/kg total). Heart rate and blood pressure were recorded throughout. Pharmacological stress was reversed using aminophylline (100 mg IV over 5-10 seconds followed by a 10 ml saline flush) following completion of the stress T1-mapping protocol (after ~15 minutes). Stress and rest first-pass perfusion imaging was performed with an IV bolus injection of gadolinium (Gd) contrast (0.05 mmol/kg, gadobenate dimeglumine, MultiHance) followed by a 15-20 ml saline flush, both administered at 4-6 ml/sec. Late gadolinium enhancement (LGE) imaging was performed in long and short-axis views to exclude myocardial infarction or other types of scarring by the on-site team in Taiwan, as per SCMR guidelines (170,171).

7.3.3 Image analysis

Image analysis for cardiac indices was performed offline in accordance with SCMR guidelines (171), using IntelliSpace Portal (ISP) MR cardiac software (version 9.0, Philips Medical Systems, Netherlands) by the Taiwan team and checked for accuracy by myself using cmr42 post-processing software. Anonymised DICOMs were securely transferred to Oxford for T1-map analysis. Endocardial and epicardial contouring of T1-maps was performed manually offline using MC-ROI software. T1-maps underwent rigorous quality control

and segments with artefacts or other confounders were excluded. Quality was excellent with <1% (n=12) segments excluded due to mistriggering.

7.3.4 Data modelling and statistical analysis

Relative stress responses were calculated for heart rate and T1, as previously described (see section **2.4.4** and **4.3.4**). The relationships between T1-mapping variants for stress T1 and delta T1 over time were assessed, as well as relative to markers of physiological stress (i.e., heart rate, relative change in heart rate). Pearson's linear correlation coefficient (r) was used, as well as the slope and intercept of the regression lines. Given the dynamic nature of the pharmacological stress agents, datapoints were grouped in 30-second intervals according to the protocol so as to improve data sampling and better display the dynamic effects of time on T1 evolution, based on prior experience from **Chapter 4**. To compare the stress T1 relationships across multiple pharmacological stress agents, data was also pooled from **Chapter 4** (regadenoson) and **Chapter 6** (dobutamine). Data are presented as mean ± SD. A two-tailed $p<0.05$ is considered statistically significant. Statistical analysis and data modelling were performed using R Studio (RStudio Team (2018). RStudio: Integrated Development for R. RStudio, Inc., Boston, MA).

7.4 Results

7.4.1 Study population

All participants completed the study protocol and tolerated dipyridamole without complications. Two participants were excluded. One participant was excluded due to failure to begin the CMR scanning protocol at the correct time of commencement of the dipyridamole infusion (i.e., scanning was not commenced until completion of the dipyridamole infusion, approximately 5 minutes late). This was the first research CMR scan performed at the collaborating institution and related to a problem with the stress perfusion hardware setup, which was corrected for all subsequent scans. A second participant was excluded due to apparent movement within the scanner during the experiment, which resulted in inconsistencies between slice positions, namely a significant shift of the stress T1-maps into the LVOT precluding meaningful calculation of myocardial T1 throughout the experiment. This left a total of 11 healthy participants (55% female, mean age 49 ± 16 years, BMI 24 ± 3 kg/m^2) included in the study. All 11 participants were validated by the local team to have structurally normal hearts with normal resting cardiac volumes (LVEDVi 65 +/- 7 ml/m^2) and systolic function (LVEF 63 +/- 4%) and no pathological LGE.

7.4.2 Physiological effect of pharmacological stress

There was a significant rise in heart rate with the dipyridamole infusion, rising from 64 ± 9 bpm at baseline to a maximum of 86 ± 13 bpm ($p<0.0001$). Maximum heart rate (defined as the highest recorded heart rate) was achieved ~6 minutes following the start of the dipyridamole infusion (**Figure 7.2**). There was a non-significant reduction in both systolic and diastolic blood pressure at these same corresponding time points (118/74 ± 16/6 mmHg at baseline → 114/69 ± 14/9 mmHg at peak stress; $p>0.05$). All participants achieved a good overall haemodynamic response to the dipyridamole infusion (based on an increase in baseline heart rate of >10 bpm).

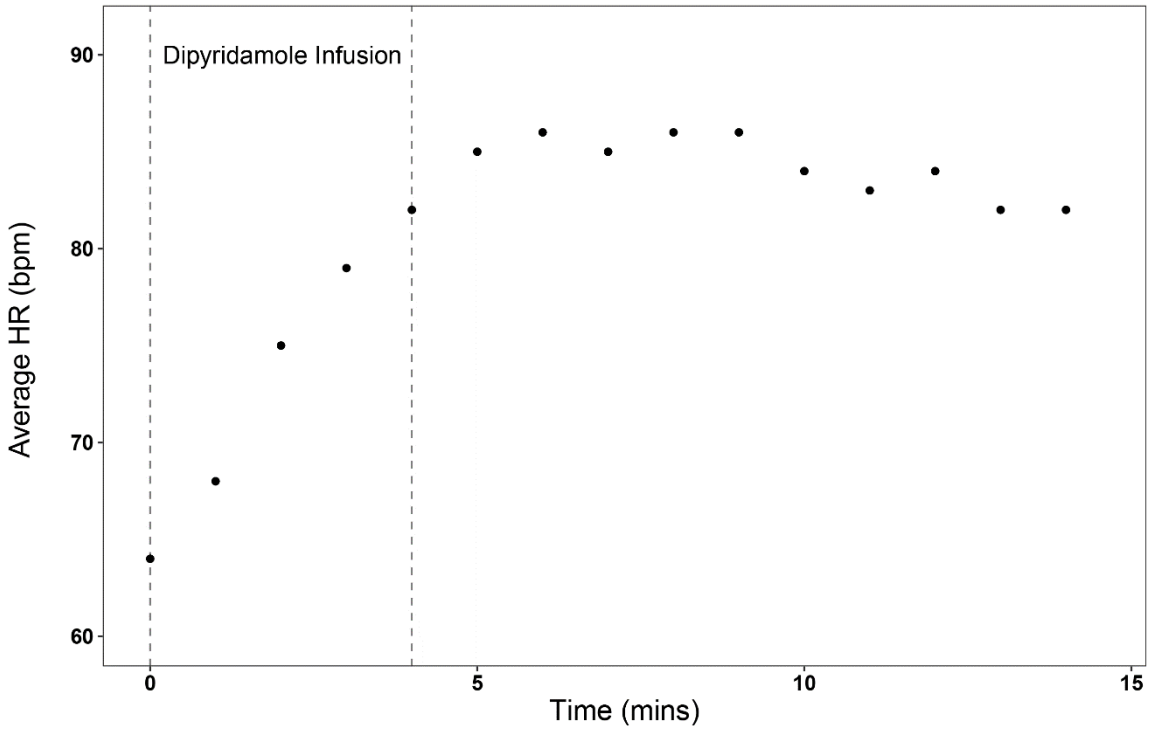


Figure 7.2: Average heart rate response to intravenous dipyridamole infusion over time. *The intravenous dipyridamole infusion (0.142 mg/kg/min) runs from 0 to 4 minutes (dashed lines).*

7.4.3 Dipyridamole stress T1 response between ShMOLLI and MOLLI variants

There was a progressive increase in myocardial T1 and delta T1 during the dipyridamole infusion, with a plateau response seen 6-8 minutes after the start of the infusion. ShMOLLI T1 rose from 948 ± 32 ms to 1006 ± 48 ms (delta T1 6.1 ± 2.0%) at 6 minutes and 1008 ± 43 ms (delta T1 6.3 ± 1.6%) at 8 minutes ($p<0.0001$ for both). This was significantly higher than the corresponding peak delta T1 responses for MOLLI Low HR (4.6 ± 1.5%; $p=0.02$) and MOLLI High HR (3.9 ± 1.3%; $p=0.001$) for the same time periods. ShMOLLI had a lower

coefficient of variation (i.e., SD/mean) at peak stress (CV = 0.25), while the coefficients of variation for the MOLLI variants were similar (both CV = 0.33). The effect size for ShMOLLI compared to MOLLI, as estimated by the ratio of coefficients of variation, was 1.3. The rest and stress native T1 values and delta T1 for the different variants are presented in **Table 7.1**.

Table 7.1: Differences in myocardial T1 measurements between methods for rest and dipyridamole stress T1

Variant	Rest T1 (ms)	Peak Stress T1 (ms)	Delta T1 (%)
ShMOLLI	948 ± 32	1008 ± 43	6.3 ± 1.6
MOLLI Low HR	1026 ± 35	1072 ± 42	4.6 ± 1.5
MOLLI High HR	1023 ± 38	1063 ± 42	3.9 ± 1.3%

Data are presented as mean ± SD.

The change in delta T1 over time for each of the variants is displayed in **Figure 7.3**. ShMOLLI achieves a greater peak delta T1 (measured 8 minutes after starting the dipyridamole infusion) compared to the MOLLI variants, despite the stress T1 response plateauing at a similar time point for each variant. For the acute rising period (i.e., from baseline to peak stress effects), ShMOLLI had significantly steeper linear regression slopes for both T1 and delta T1 than MOLLI High HR (p=0.006 and p=0.007 respectively) but not MOLLI Low HR

(p=0.14 and p=0.07 respectively). This likely reflects the fact that ShMOLLI had a larger amplitude of the response, rather than true differences in time constants. There were no differences in regression slopes between MOLLI Low HR and MOLLI High HR for the acute rise in T1 and delta T1 (p=0.39 and p=0.65).

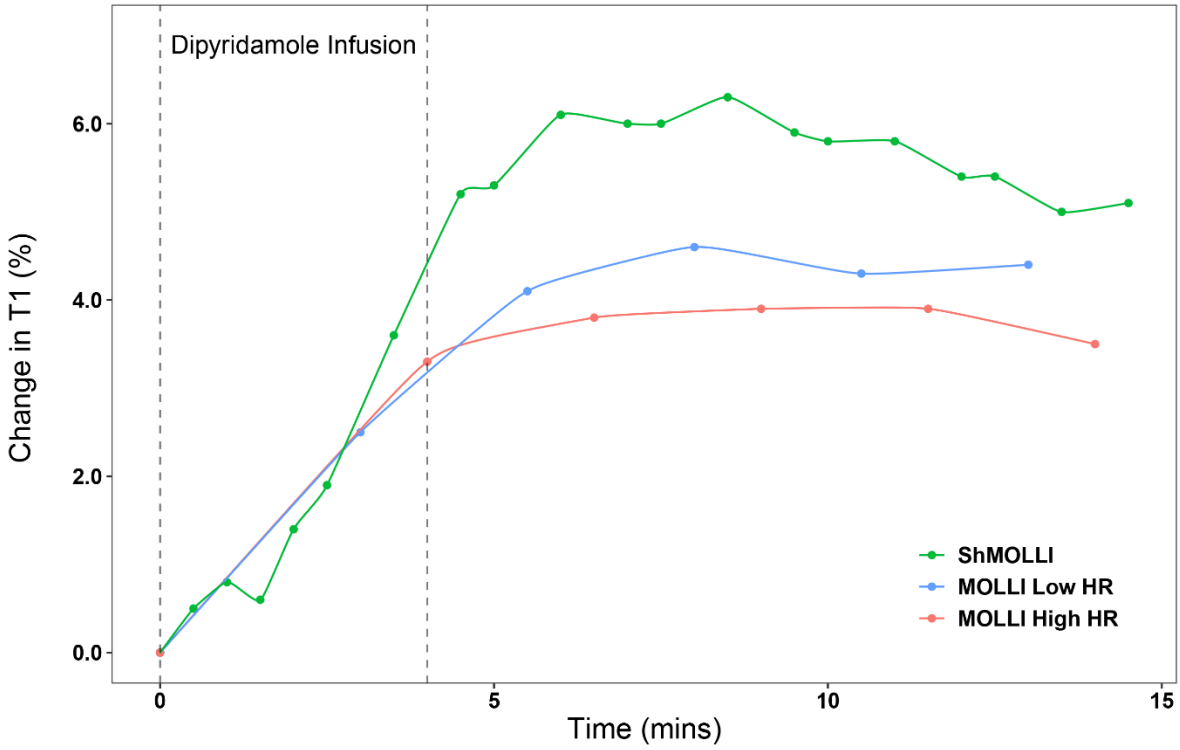


Figure 7.3: Effects of dipyridamole on delta T1 over time. *Results for the ShMOLLI (green), MOLLI Low HR (blue), and MOLLI High HR (red) T1-mapping variants are shown. Lines are spline interpolated between points to guide the eye. Peak delta T1 effects were seen ~6-8 minutes after commencement of the dipyridamole infusion.*

7.5 Discussion

This is the first systematic study to characterise dipyridamole stress T1 dynamics over time. The study demonstrates that: 1) the effects of dipyridamole may be reliably measured using stress T1-mapping, suggesting similar clinical utility to that previously demonstrated with adenosine and regadenoson (167,179,203,230,231); 2) ShMOLLI stress T1-mapping using dipyridamole achieves a greater overall stress T1 response and effect size compared to the MOLLI variants tested, further reinforcing the results shown in **Chapter 4**. Although there are different stress T1 responses across different drugs, dobutamine and dipyridamole may prove to be viable and cost-effective options for stress T1-mapping clinical and research applications in future.

7.5.1 Dynamic response of T1-mapping during dipyridamole stress

Invasive haemodynamic studies have shown that a 4-minute intravenous infusion of dipyridamole (0.56 mg/kg) induces hyperaemia and increases coronary blood flow velocities by 3.8- to 7-fold, despite heterogeneous time- and dose-response characteristics (251). Peak coronary flow velocity is seen at an average of 6.5 minutes (range 2.5 to 8.7 minutes), with average mean flow velocity at the end of the 4-minute infusion only reaching 67% of the eventual peak (251). The hyperaemic effect of dipyridamole may last for more than 50 minutes with a reported half-life of 30-45 minutes (234). A tri-

exponential decay pattern has been shown in pharmacokinetic studies with a terminal half-life of 11.6 ± 2.2 hours (252).

The invasive and pharmacokinetic modelling studies above are broadly consistent with the stress T1 dynamic profile seen in this study following the 4-minute (0.56 mg/kg) dipyridamole infusion. The stress T1 response plateaued at 6-8 minutes and remained elevated (i.e., delta T1 of ~6%) until the end of the stress study protocol, with minimal decay and a long elimination phase. This is consistent with the long half-life and slow tri-exponential decay pattern reported with dipyridamole. The decay pattern was not fully observed (it would be impractical to keep participants in a stressed state within the scanner for a sufficiently long time to measure this given the reported half-life of 30-45 minutes) and therefore not able to be analysed for time coefficients, unlike the other agents.

7.5.1.1 Dipyridamole stress T1 response for different T1-mapping sequences

The dipyridamole peak stress T1 response with ShMOLLI was significantly higher than that using the MOLLI 5(3)3 sequences, with ShMOLLI also demonstrating a greater effect size. ShMOLLI achieved a peak stress delta T1 response with dipyridamole (6.3 ± 1.6%) which is consistent with previous adenosine stress T1 studies using the heart rate-independent ShMOLLI (6.2 ± 0.5% (167); 7.1 ± 3.8% (168)) and MOLLI 5s(3s)3s methods (6.2% (249)).

Similarly, the dipyridamole MOLLI 5(3)3 stress T1 response observed in this study (MOLLI Low HR 4.6 ± 1.5%; MOLLI High HR 3.9 ± 1.3%) was similar to that previously reported with adenosine (4.3 ± 2.8% (253); 4.79 ± 3.14% (179)). It is plausible that dipyridamole would result in similar stress T1 reactivity as adenosine, given the mechanism of action of dipyridamole is to act as an adenosine agonist by inhibiting the degradation of cyclic adenosine monophosphate (cAMP) and blocking the cellular reuptake of endogenous adenosine (234).

One benefit of the slower onset of action of dipyridamole (given via slow IV infusion) compared to regadenoson (see **Chapter 4**) is that the peak stress T1 effects for ShMOLLI and MOLLI variants could be directly compared at the time of peak pharmacological stress without the need for extrapolations from pharmacokinetic stress T1 modelling. This provides further evidence to support that ShMOLLI has a larger stress T1 response and greater effect size than the standard vendor-provided product MOLLI sequences, which likely reflects greater heart rate sensitivity and T1 underestimation during stress for the MOLLI sequence (**Chapter 4**). Switching between heart rate-dependent relationships as myocardial T1 increases during vasodilatory stress, with subsequent underestimation of T1, results in lower stress T1 responses when MOLLI 5(3)3 variants are used (254).

7.5.2 Differences in stress T1-mapping response across different pharmacological stress agents

Healthy control data from the regadenoson (**Chapter 4**) and dobutamine (**Chapter 6**) experiments were pooled with the current dipyridamole results to compare the relationships between ShMOLLI stress T1 and physiological stress parameters for the different pharmacological stress agents (**Figure 7.4A**). Dipyridamole had the steepest slope of relationship between mean delta T1 and heart rate when compared to dobutamine and regadenoson (both $p<0.001$) There were no significant differences between the slopes for dobutamine and regadenoson ($p=0.35$). This was also seen when comparing mean delta T1 and mean rate pressure product. Dipyridamole again had the steepest slope (**Figure 7.4B**) compared to dobutamine and regadenoson ($p<0.001$ for both), while there was no difference between dobutamine and regadenoson ($p=0.89$).

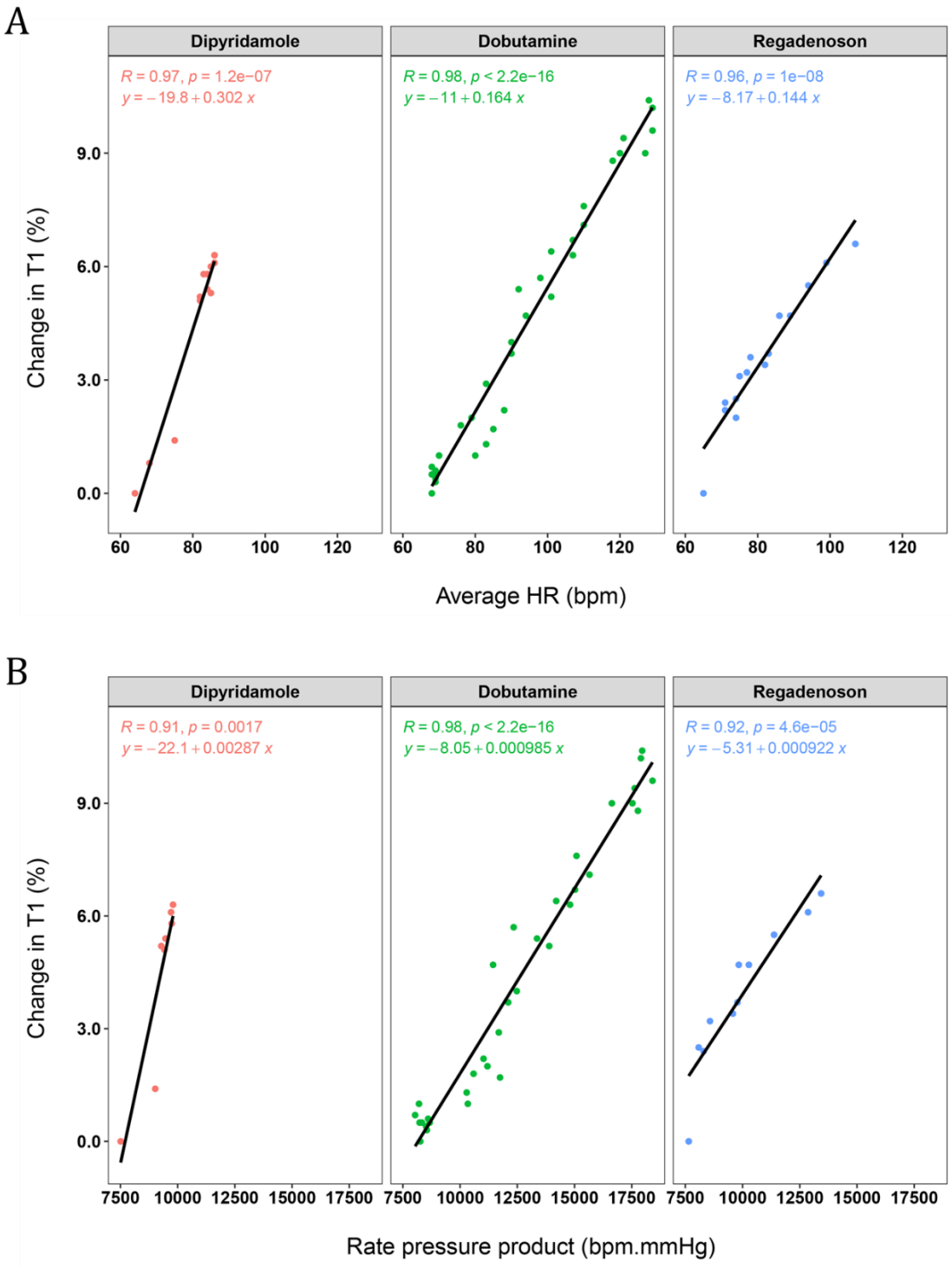


Figure 7.4: Physiological and myocardial stress T1 responses for different pharmacological stress agents. *Differences in terms of the response relationship between the three different pharmacological stress agents for delta T1 and heart rate (A) and delta T1 and rate pressure product (B). Statistical comparisons were performed based on ANOVA for the slope coefficient only.*

The observed differences from the pooled meta-data analyses of stress responses across different pharmacological stress agents and physiological and myocardial T1 responses is the subject of extended discussion below.

7.5.2.1 Myocardial blood flow and volume changes with dipyridamole compared to regadenoson

Quantitative perfusion CMR has shown that regadenoson produces higher stress MBF than both dipyridamole and adenosine, but that this response seems to be driven by the additional increase in heart rate seen with regadenoson (255). Interestingly, the steepness of the slope for dipyridamole (when comparing quantitative CMR perfusion MBF with heart rate) was greater than that for adenosine or regadenoson (as also shown in this Chapter), despite the greater stress MBF with regadenoson (255). Conflictingly, a PET-based study of quantitative MBF directly comparing regadenoson with dipyridamole showed that regadenoson only achieved at most 90% of the hyperaemic blood flow achieved with dipyridamole (256). The above study recommended perfusion imaging after a 50-60 second delay from the time of regadenoson administration (counter to the recommended timing from the regadenoson package insert of 10-20 seconds) to maximise hyperaemia, which is consistent with the timing of the peak stress T1 effect shown in **Chapter 4**.

7.5.2.2 Myocardial blood flow and volume changes with dipyridamole compared to dobutamine

PET and nuclear imaging studies have shown that dobutamine, either alone (247) or when co-administered with atropine (257), results in a greater MBF than dipyridamole, yet others have shown that adenosine (at a standard 140 μg/kg/min dose) may produce greater increases in MBF than dobutamine (246,258). One canine study that assessed both MBV and MBF changes showed that there is a significantly greater blood volume change and increased capillary recruitment for an equivalent change in MBF during dobutamine stress than during dipyridamole vasodilation, which may be related to the increased global oxygen demand and cardiac workload with dobutamine on top of coronary vasodilatation (181).

It would be good to investigate deeper whether these discrepancies in myocardial blood flow relate to methodological differences across the studies or intrinsic patient selection bias rather than differences in the achieved hyperaemia itself, given the stress agents used (regadenoson, dobutamine, dipyridamole) are all reported to induce maximal hyperaemia with standard clinical dosing protocols (259). However, whether this is truly maximal hyperaemia remains unclear (as also discussed in **Chapter 6**), given the additional increases in MBF seen when adenosine is increased to a high-dose protocol (245).

7.5.2.3 Myocardial stress T1-mapping and PET myocardial blood flow

It is important to understand the relationship between myocardial stress T1-mapping and PET MBF, so as to make better sense of these inter-drug comparisons. One recent study investigated the relationship between CMR stress T1-mapping and PET measurements of myocardial perfusion, showing a moderate correlation between stress T1 and MBF, but only a weak association for delta T1 and MBF (260). This diverges from the results in **Chapter 4**, which showed strong correlations between stress T1 reactivity and quantitative MBF on CMR. One likely explanation for this was that imaging in the PET study was commenced after only 2 minutes of intravenous adenosine at 140 μg/kg/min (i.e., before maximal hyperaemia), compared to the typical 3-6 minutes required to achieve maximal hyperaemia in other studies and guideline recommendations. This may explain the lower stress T1 responses in the PET study (ShMOLLI T1 909 ± 26 ms at rest; 940 ± 25 ms at stress; delta T1 3.8 ± 2.2%) and thus weaker statistical measures of association between the measurement modalities. In **Chapter 4**, the scanning protocol comparing regadenoson stress T1-mapping and MBF dictated that quantitative MBF was acquired later into the stress period, which makes comparison between these studies with different timings difficult. Other studies have shown that adenosine stress T1-mapping correlates strongly with indices of myocardial perfusion (i.e., myocardial blood flow) and myocardial blood volume on CMR, although the novel quantitative MBV maps used in that particular study require further validation using independent reference standards (249).

7.5.2.4 Cost effectiveness for different pharmacological stress agents

Chapter 6 and **Chapter 7** have shown that dobutamine and dipyridamole are viable stress agents to characterise the stress T1 response, which may be of clinical use as a contrast-free application for the assessment of cardiovascular disease. This is of particular interest, given the average costs of pharmacological stress agents for imaging studies. For a typical patient with a body weight of 75 kg, the cost of dipyridamole (0.56 mg/kg) or dobutamine (250mg IV bag) for stress imaging is $6.30 or $6.59 per patient respectively, while this rises to $64.55 for adenosine (based on a standard 140 μg/kg/min infusion for 6 minutes), and $213.26 for regadenoson (400 μg vial) (234). Demonstration of the viability of these cheaper agents for stress T1-mapping is crucial as it provides a validated and cheap alternative for future stress T1-mapping studies compared to other agents. Further work is required to assess cost-benefit analysis of using various stress agents and diagnostic performance measures for T1-mapping and MBF approaches in clinical patients.

7.5.3 Limitations

The dipyridamole experiment was performed in a separate international centre using a different MR scanner to that used in the previous Chapters. Although close supervision and guidance was provided remotely via video link during the data acquisitions, consistency between the study sites in terms of MR scanner performance is not guaranteed. This is minimised as much as

possible by the use of quality control standardisation phantoms, which are designed to standardise T1-mapping measurements across different MR scanners and sites. The full provision of up-to-date ShMOLLI T1-mapping sequences, as well as a custom-designed scanning protocol, also helps to ensure that the experiment and all subsequent data analysis was standardised across sites. Importantly, the rest T1 data for these healthy volunteers falls within the reported normal range for ShMOLLI T1 at 1.5T (197), which also suggests a high level of consistency between the sites. The relative difference between rest and stress (i.e., delta T1) may also help to mitigate inter-scanner differences. Sampling bias may influence the results given the population differences between the sites, although participants were similar in terms of age and BMI. Body size is also less relevant for infusion-based stress studies where the pharmacological stress agent is dosed according to body weight. The fact that dipyridamole generated stress T1 responses consistent with the previous literature is reassuring. Given the long half-life of dipyridamole, the tri-exponential decay curve could not be adequately modelled, although the slower onset of action allowed successful comparison between T1-mapping methods for the peak stress response.

7.6 Conclusions

Dipyridamole vasodilator stress causes significant dynamic responses in myocardial T1 over time as measured using CMR and achieves stress T1 results consistent with literature values for adenosine and regadenoson.

ShMOLLI dipyridamole stress T1-mapping demonstrates a significantly higher stress T1 response and greater effect size at peak stress compared with the MOLLI variants tested. Dipyridamole is a viable and cheaper alternative stress agent to adenosine and regadenoson and is suitable for future stress T1-mapping clinical applications in the assessment of cardiovascular disease.

8 General conclusions and future directions

In conclusion, this Thesis has provided novel insights into stress T1-mapping as a promising technique for the assessment of cardiovascular disease, including important validation work against invasive coronary physiology and demonstrating its utility across a variety of pharmacological stress agents and T1-mapping methods. The main findings of this Thesis are:

1. Adenosine stress T1-mapping has good diagnostic performance for the detection of obstructive coronary artery disease in patients with end-stage renal disease, as validated against invasive coronary physiology. This diagnostic performance may be improved upon with the up-front use of stress T1 polar maps, which give an indication of the gradient of potential myocardial ischaemia from base to apex. Stress T1-mapping may also give an indication of depletion of coronary vasodilatory reserve, coronary microvascular dysfunction, or suggest alternative pathological processes such as diffuse myocardial inflammation or fibrosis. It has similar diagnostic performance to other commonly used cardiac functional tests in routine clinical practice worldwide, such as dobutamine stress echocardiography and SPECT myocardial perfusion imaging in this population, but with the added benefit of being contrast-

and radiation-free, whilst providing additional advanced myocardial tissue characterisation.

2. Regadenoson is a viable alternative pharmacological stress T1-mapping agent and, similarly to adenosine, can be used to differentiate between normal, remote, ischaemic, and infarcted myocardium in patients with ischaemic heart disease.
3. ShMOLLI stress T1-mapping correlates strongly with increased myocardial blood flow during regadenoson stress and achieves a significantly higher stress T1 response, greater effect size, and greater ECV measurement stability compared with MOLLI product variants. This translates to significant reductions in sample size when using ShMOLLI. This work highlights that ShMOLLI may be the stress T1-mapping method of choice for future studies and in clinical practice, where a certain level of confidence is required in whether a blunted stress T1 response is due to pathology or method-dependency.
4. This is reinforced by the results from dipyridamole stress T1-mapping, where ShMOLLI was again shown to achieve a greater stress T1 response and had a greater effect size compared with the MOLLI variants tested.
5. Dobutamine stress causes significant dynamic responses in myocardial T1 over time in healthy individuals. The magnitude of observed responses is closely related to dose and individual physiological responses, although there are likely additional intrinsic effects on the

coronary vasculature, resistance vessels, and changes in myocardial blood volume that all contribute to the individual stress T1 response.

6. Dipyridamole and dobutamine are both viable pharmacological stress agents for stress T1-mapping and may represent a cheaper and more cost-effective option for future clinical studies.

There are a number of research directions for future stress T1-mapping method development and clinical studies based on this work, given that this is a novel and rapidly expanding field. The following concepts may be of greatest interest:

1. The complex interrelated biophysical properties of T1, T2, T2*, changes in vascular volumes, blood oxygenation level dependent (BOLD) effects, heart rate, and myocardial contraction are all intrinsic to the physiological stress response. Determining the exact contribution of each to the stress T1 response requires future work, which may help to improve the accuracy and precision of stress T1-mapping for the quantitation of specific myocardial pathology.
2. Myocardial ischaemia manifests as a gradient from the vulnerable subendocardium through to the less vulnerable subepicardium. Current segmental analysis techniques include the entire myocardium, which may therefore diminish the sensitivity of stress T1-mapping to detect ischaemic changes. Development and validation of techniques focusing on the subendocardial myocardium may improve the ability of

stress T1-mapping to detect this pathology. Further extension of this would be the development of stress T1 reactivity maps, with pixel-wise differences between rest and stress T1-mapping displayed as a polar map, similar to pixel-wise perfusion maps used in clinical practice. The stress T1 datasets used in this Thesis are being actively applied to this topic using a combination of machine learning and segmental co-registration techniques, with the aim to develop an inline stress T1 reactivity polar map for inline implementation that may be suitable for clinical use. Future work would include validation of this against quantitative myocardial perfusion and invasive coronary measurements.

3. Coronary microvascular dysfunction is increasingly recognised as an important contributor to cardiovascular morbidity and mortality. This Thesis has shown that stress T1-mapping may have utility in the detection of microvascular dysfunction and depletion of coronary vasodilatory reserve. Further comparison with invasive coronary physiology is required to explore the suitability of stress T1-mapping as a contrast-free technique for the assessment of microvascular dysfunction.
4. One of the potential limitations of dobutamine stress imaging is the risk of side effects at the higher doses of conventional dosing protocols, which may be poorly tolerated by patients. This Thesis has shown that there is a significant stress T1 response at lower doses of dobutamine (i.e., 20 μg/kg/min) that is similar to the maximal response seen with

vasodilatory stress agents. Evidence of normal stress T1 reactivity at lower doses of dobutamine may be sufficient to rule out severe pathology in patients being assessed for significant obstructive CAD without need to escalate to higher doses of the dobutamine protocol. This would be expected to be better tolerated by patients and minimise the risk of adverse events such as tachyarrhythmias. Further work in patients with CAD is required to establish a "rapid rule-out" dobutamine stress T1 protocol at lower doses of dobutamine, as well as exploring the utility of dobutamine stress T1-mapping to assess for myocardial viability in areas of presumed hibernating myocardium in combination with conventional wall motion assessment.

5. Further stress T1-mapping technical advances are required to reduce segment rejection due to artefacts, given that uncorrected and unrecognised motion artefacts may cause errors in T1 estimation and lead to incorrect diagnosis. Motion correction (MOCO) on multiple acquired T1-weighted images is able to improve the robustness and clinical utility of mapping techniques by aligning the raw images before construction. This process may be further enhanced by the use of deep learning and convolutional neural networks. This is an area of active research within our group with the recent technical development of MOCOnet, a convolutional neural network solution that has been shown in preliminary data to rapidly and successfully suppress a wide range of motion artefacts with significantly greater performance compared to a traditional image registration approach. This will be

applied to the stress T1 datasets used in this Thesis to further develop a stress T1 MOCO technology that can rapidly suppress motion artefacts and improve the utilisation of acquired stress datasets with minimal segment rejection.

6. Finally, this Thesis has highlighted the utility of stress T1-mapping for assessment of coronary vasoreactivity across a range of pharmacological stress agents. Further work is required to assess cost-benefit analysis of various stress agents and diagnostic performance measures for T1-mapping and MBF approaches in clinical patients. Further investigation of coronary vasoreactivity as a viable non-invasive imaging biomarker that can be used for individual prognostication requires larger scale clinical studies that correlate with cardiovascular outcomes.

This Thesis has provided important insights into novel contrast-free stress T1-mapping applications for the assessment of cardiovascular disease and sets the scene for future mechanistic, developmental, and outcome-based work towards translation of this technique into more widespread clinical practice.

Bibliography

1. WHO. Cardio-Vascular Diseases. [Internet]. 2017 [cited 2019 Oct 22]. p. 1–6. Available from: https://www.who.int/en/news-room/fact-sheets/detail/cardiovascular-diseases-(cvds)

2. Heart statistics - Heart and Circulatory Diseases in the UK | BHF [Internet]. [cited 2021 Mar 13]. Available from: https://www.bhf.org.uk/what-we-do/our-research/heart-statistics

3. Dweck MR, Williams MC, Moss AJ, Newby DE, Fayad ZA. Computed Tomography and Cardiac Magnetic Resonance in Ischemic Heart Disease. Vol. 68, Journal of the American College of Cardiology. Elsevier USA; 2016. p. 2201–16.

4. Dweck MR, Doris MK, Motwani M, Adamson PD, Slomka P, Dey D, et al. Imaging of coronary atherosclerosis — evolution towards new treatment strategies. Nat Rev Cardiol. 2016 Sep;13(9):533–48.

5. Emond M, Mock MB, Davis KB, Fisher LD, Holmes DR, Chaitman BR, et al. Long-term survival of medically treated patients in the Coronary Artery Surgery Study (CASS) Registry. Circulation. 1994 Dec;90(6):2645–57.

6. Tonino PAL, De Bruyne B, Pijls NHJ, Siebert U, Ikeno F, van' t Veer M, et al. Fractional flow reserve versus angiography for guiding percutaneous coronary intervention. N Engl J Med. 2009 Jan 15;360(3):213–24.

7. Vanhoenacker PK, Heijenbrok-Kal MH, Van Heste R, Decramer I, Van Hoe LR, Wijns W, et al. Diagnostic Performance of Multidetector CT Angiography for Assessment of Coronary Artery Disease: Meta-analysis. Radiology. 2007 Aug 1;244(2):419–28.

8. Douglas PS, Hoffmann U, Patel MR, Mark DB, Al-Khalidi HR, Cavanaugh B, et al. Outcomes of anatomical versus functional testing for coronary artery disease. N Engl J Med. 2015 Apr 2;372(14):1291–300.

9. CT coronary angiography in patients with suspected angina due to coronary heart disease (SCOT-HEART): an open-label, parallel-group, multicentre trial. The Lancet. 2015 Jun 13;385(9985):2383–91.

10. Oikonomou EK, Marwan M, Desai MY, Mancio J, Alashi A, Hutt Centeno E, et al. Non-invasive detection of coronary inflammation using computed tomography and prediction of residual cardiovascular risk (the CRISP CT study): a post-hoc analysis of prospective outcome data. The Lancet. 2018;392(10151):929–39.

11. Oikonomou EK, Williams MC, Kotanidis CP, Desai MY, Marwan M, Antonopoulos AS, et al. A novel machine learning-derived radiotranscriptomic signature of perivascular fat improves cardiac risk prediction using coronary CTangiography. European Heart Journal. 2019 Nov;40(43):3529–43.

12. Lin A, Kolossváry M, Yuvaraj J, Cadet S, McElhinney PA, Jiang C, et al. Myocardial Infarction Associates With a Distinct Pericoronary Adipose Tissue Radiomic Phenotype: A Prospective Case-Control Study. JACC Cardiovasc Imaging. 2020 Nov;13(11):2371–83.

13. Hachamovitch R, Berman DS, Shaw LJ, Kiat H, Cohen I, Cabico JA, et al. Incremental prognostic value of myocardial perfusion single photon emission computed tomography for the prediction of cardiac death: differential stratification for risk of cardiac death and myocardial infarction. Circulation. 1998 Feb 17;97(6):535–43.

14. Hachamovitch R, Hayes SW, Friedman JD, Cohen I, Berman DS. Comparison of the short-term survival benefit associated with revascularization compared with medical therapy in patients with no prior coronary artery disease undergoing stress myocardial perfusion single photon emission computed tomography. Circulation. 2003 Jun 17;107(23):2900–7.

15. Pellikka PA, Arruda-Olson A, Chaudhry FA, Chen MH, Marshall JE, Porter TR, et al. Guidelines for Performance, Interpretation, and Application of Stress Echocardiography in Ischemic Heart Disease: From the American Society of Echocardiography. J Am Soc Echocardiogr. 2020 Jan;33(1):1-41.e8.

16. Marwick TH, Case C, Vasey C, Allen S, Short L, Thomas JD. Prediction of Mortality by Exercise Echocardiography. Circulation. 2001 May 29;103(21):2566–71.

17. Marwick TH, Case C, Sawada S, Rimmerman C, Brenneman P, Kovacs R, et al. Prediction of mortality using dobutamine echocardiography. Journal of the American College of Cardiology. 2001 Mar 1;37(3):754–60.

18. Woodward W, Dockerill C, McCourt A, Upton R, O'Driscoll J, Balkhausen K, et al. Real-world performance and accuracy of stress

echocardiography: the EVAREST observational multi-centre study. Eur Heart J Cardiovasc Imaging. 2021 Jun 20;jeab092.

19. Alsharqi M, Woodward WJ, Mumith JA, Markham DC, Upton R, Leeson P. Artificial intelligence and echocardiography. Echo Res Pract. 2018 Oct 29;5(4):R115–25.

20. Greenwood JP, Maredia N, Younger JF, Brown JM, Nixon J, Everett CC, et al. Cardiovascular magnetic resonance and single-photon emission computed tomography for diagnosis of coronary heart disease (CE-MARC): A prospective trial. The Lancet. 2012 Feb 4;379(9814):453–60.

21. Greenwood JP, Motwani M, Maredia N, Brown JM, Everett CC, Nixon J, et al. Comparison of cardiovascular magnetic resonance and single-photon emission computed tomography in women with suspected coronary artery disease from the clinical evaluation of magnetic resonance imaging in coronary heart disease (CE-MARC) trial. Circulation. 2014 Mar 11;129(10):1129–38.

22. Nagel E, Greenwood JP, McCann GP, Bettencourt N, Shah AM, Hussain ST, et al. Magnetic resonance perfusion or fractional flow reserve in coronary disease. New England Journal of Medicine. 2019 Jun;380(25):2418–28.

23. Walker S, Girardin F, McKenna C, Ball SG, Nixon J, Plein S, et al. Cost-effectiveness of cardiovascular magnetic resonance in the diagnosis of coronary heart disease: an economic evaluation using data from the CE-MARC study. Heart. 2013 Jun 15;99(12):873–81.

24. Kim RJ, Wu E, Rafael A, Chen E-L, Parker MA, Simonetti O, et al. The Use of Contrast-Enhanced Magnetic Resonance Imaging to Identify Reversible Myocardial Dysfunction. New England Journal of Medicine. 2000 Nov 16;343(20):1445–53.

25. Sörensson P, Ekenbäck C, Lundin M, Agewall S, Bacsovics Brolin E, Caidahl K, et al. Early Comprehensive Cardiovascular Magnetic Resonance Imaging in Patients With Myocardial Infarction With Nonobstructive Coronary Arteries. JACC: Cardiovascular Imaging. 2021 Sep 1;14(9):1774–83.

26. McCommis KS, Zhang H, Goldstein TA, Misselwitz B, Abendschein DR, Gropler RJ, et al. Myocardial Blood Volume Is Associated With Myocardial Oxygen Consumption. An Experimental Study With Cardiac Magnetic Resonance in a Canine Model. Vol. 2, JACC: Cardiovascular Imaging. JACC Cardiovasc Imaging; 2009. p. 1313–20.

27. Crea F, Lanza GA, Camici PG. Coronary microvascular dysfunction. Coronary Microvascular Dysfunction. 2013 Feb 22;356(8):1–257.

28. Mathew RC, Bourque JM, Salerno M, Kramer CM. Cardiovascular Imaging Techniques to Assess Microvascular Dysfunction. Vol. 13, JACC: Cardiovascular Imaging. Elsevier Inc.; 2020. p. 1577–90.

29. Schelbert HR. Anatomy and physiology of coronary blood flow. Vol. 17, Journal of Nuclear Cardiology. Springer; 2010. p. 545–54.

30. Kassab GS, Lin DH, Fung YCB. Morphometry of pig coronary venous system. American Journal of Physiology - Heart and Circulatory Physiology. 1994;267(6 36-6).

31. Nijjer SS, Dewaard GA, Sen S, Van De Hoef TP, Petraco R, Echavarría-Pinto M, et al. Coronary pressure and flow relationships in humans: Phasic analysis of normal and pathological vessels and the implications for stenosis assessment: A report from the Iberian-Dutch-English (IDEAL) collaborators. European Heart Journal. 2016 Jul 7;37(26):2069–80.

32. Lee JM, Hwang D, Park J, Zhang J, Tong Y, Kim CH, et al. Exploring coronary circulatory response to stenosis and its association with invasive physiologic indexes using absolute myocardial blood flow and coronary pressure. Circulation. 2017;136(19):1798–808.

33. de Waard GA, Cook CM, van Royen N, Davies JE. Coronary autoregulation and assessment of stenosis severity without pharmacological vasodilation. European Heart Journal. 2018 Dec 7;39(46):4062–71.

34. Ford TJ, Ong P, Sechtem U, Beltrame J, Camici PG, Crea F, et al. Assessment of Vascular Dysfunction in Patients Without Obstructive Coronary Artery Disease: Why, How, and When. JACC: Cardiovascular Interventions. 2020 Aug 24;13(16):1847–64.

35. Karamitsos TD, Arvanitaki A, Karvounis H, Neubauer S, Ferreira VM. Myocardial Tissue Characterization and Fibrosis by Imaging. Vol. 13, JACC: Cardiovascular Imaging. Elsevier; 2020. p. 1221–34.

36. Dongaonkar RM, Stewart RH, Geissler HJ, Laine GA. Myocardial microvascular permeability, interstitial oedema, and compromised cardiac function. Cardiovascular Research. 2010 Jul 15;87(2):331–9.

37. Ambale-Venkatesh B, Lima JAC. Cardiac MRI: A central prognostic tool in myocardial fibrosis. Nature Reviews Cardiology. 2015 Jan 28;12(1):18–29.

38. López B, Querejeta R, González A, Sánchez E, Larman M, Díez J. Effects of loop diuretics on myocardial fibrosis and collagen type I turnover in chronic heart failure. Journal of the American College of Cardiology. 2004 Jun 2;43(11):2028–35.

39. Weber KT, Brilla CG. Pathological hypertrophy and cardiac interstitium: Fibrosis and renin-angiotensin-aldosterone system. Circulation. 1991 Jun;83(6):1849–65.

40. Halliday BP, Prasad SK. The Interstitium in the Hypertrophied Heart. JACC: Cardiovascular Imaging. 2019 Sep 18;

41. Gulati A, Jabbour A, Ismail TF, Guha K, Khwaja J, Raza S, et al. Association of fibrosis with mortality and sudden cardiac death in patients with nonischemic dilated cardiomyopathy. JAMA - Journal of the American Medical Association. 2013 Mar 6;309(9):896–908.

42. Neglia D, Michelassi C, Giovanna Trivieri M, Sambuceti G, Giorgetti A, Pratali L, et al. Prognostic role of myocardial blood flow impairment in idiopathic left ventricular dysfunction. Circulation. 2002 Jan 15;105(2):186–93.

43. Taqueti VR, Solomon SD, Shah AM, Desai AS, Groarke JD, Osborne MT, et al. Coronary microvascular dysfunction and future risk of heart failure with preserved ejection fraction. European Heart Journal. 2018;39(10):840–9.

44. Zhou W, Lee JCY, Leung ST, Lai A, Lee TF, Chiang JB, et al. Long-Term Prognosis of Patients With Coronary Microvascular Disease Using Stress Perfusion Cardiac Magnetic Resonance. JACC: Cardiovascular Imaging. 2021 Mar 1;14(3):602–11.

45. Gdowski MA, Murthy VL, Doering M, Monroy-Gonzalez AG, Slart R, Brown DL. Association of Isolated Coronary Microvascular Dysfunction With Mortality and Major Adverse Cardiac Events: A Systematic Review and Meta-Analysis of Aggregate Data. Journal of the American Heart Association. 2020 May 5;9(9):e014954.

46. Schroder J, Michelsen MM, Mygind ND, Suhrs HE, Bove KB, Bechsgaard DF, et al. Coronary flow velocity reserve predicts adverse prognosis in women with angina and no obstructive coronary artery disease: results from the iPOWER study. European Heart Journal. 2021 Jan 20;42(3):228–39.

47. Grothues F, Smith GC, Moon JCC, Bellenger NG, Collins P, Klein HU, et al. Comparison of interstudy reproducibility of cardiovascular magnetic resonance with two-dimensional echocardiography in normal subjects and in patients with heart failure or left ventricular hypertrophy. American Journal of Cardiology. 2002 Jul 1;90(1):29–34.

48. Pennell DJ. Cardiovascular magnetic resonance: Twenty-first century solutions in cardiology. In: Clinical Medicine. Royal College of Physicians; 2003. p. 273–8.

49. Kramer CM, Barkhausen J, Bucciarelli-Ducci C, Flamm SD, Kim RJ, Nagel E. Standardized cardiovascular magnetic resonance imaging (CMR) protocols: 2020 update. Journal of Cardiovascular Magnetic Resonance. 2020 Feb 24;22(1):17.

50. Mahrholdt H, Wagner A, Judd RM, Sechtem U, Kim RJ. Delayed enhancement cardiovascular magnetic resonance assessment of non-ischaemic cardiomyopathies. European Heart Journal. 2005 Aug 1;26(15):1461–74.

51. Burrage MK, Ferreira VM. Cardiovascular Magnetic Resonance for the Differentiation of Left Ventricular Hypertrophy. Vol. 17, Current Heart Failure Reports. Springer; 2020. p. 192–204.

52. Gulani V, Calamante F, Shellock FG, Kanal E, Reeder SB. Gadolinium deposition in the brain: summary of evidence and recommendations. Vol. 16, The Lancet Neurology. Lancet Publishing Group; 2017. p. 564–70.

53. Ferreira VM, Piechnik SK. CMR Parametric Mapping as a Tool for Myocardial Tissue Characterization. Korean Circ J. 2020;50:e88.

54. Messroghli DR, Moon JC, Ferreira VM, Grosse-Wortmann L, He T, Kellman P, et al. Clinical recommendations for cardiovascular magnetic resonance mapping of T1, T2, T2* and extracellular volume: A consensus statement by the Society for Cardiovascular Magnetic Resonance (SCMR) endorsed by the European Association for Cardiovascular Imagi. J Cardiovasc Magn Reson. 2017;19(1):75.

55. Ferreira VM, Holloway CJ, Piechnik SK, Karamitsos TD, Neubauer S. Is it really fat? Ask a T1-map. European Heart Journal Cardiovascular Imaging. 2013 Nov 1;14(11):1060.

56. Sado DM, Maestrini V, Piechnik SK, Banypersad SM, White SK, Flett AS, et al. Noncontrast myocardial T1 mapping using cardiovascular magnetic resonance for iron overload. Journal of Magnetic Resonance Imaging. 2015 Jun 1;41(6):1505–11.

57. Sado DM, White SK, Piechnik SK, Banypersad SM, Treibel T, Captur G, et al. Identification and assessment of anderson-fabry disease by cardiovascular magnetic resonance noncontrast myocardial T1 mapping. Circulation: Cardiovascular Imaging. 2013 May;6(3):392–8.

58. Messroghli DR, Niendorf T, Schulz-Menger J, Dietz R, Friedrich MG. T1 mapping in patients with acute myocardial infarction. Journal of cardiovascular magnetic resonance : official journal of the Society for Cardiovascular Magnetic Resonance. 2003;5(2):353–9.

59. Messroghli DR, Walters K, Plein S, Sparrow P, Friedrich MG, Ridgway JP, et al. MyocardialT1 mapping: Application to patients with acute and chronic myocardial infarction. Magnetic Resonance in Medicine. 2007 Jul;58(1):34–40.

60. Iles L, Pfluger H, Phrommintikul A, Cherayath J, Aksit P, Gupta SN, et al. Evaluation of Diffuse Myocardial Fibrosis in Heart Failure With Cardiac Magnetic Resonance Contrast-Enhanced T1 Mapping. Journal of the American College of Cardiology. 2008 Nov 4;52(19):1574–80.

61. Lee H, Park J-B, Yoon YE, Park E-A, Kim H-K, Lee W, et al. Noncontrast Myocardial T1 Mapping by Cardiac Magnetic Resonance Predicts Outcome in Patients With Aortic Stenosis. JACC: Cardiovascular Imaging. 2018 Jul;11(7):974–83.

62. Ferreira VM, Piechnik SK, Dall'Armellina E, Karamitsos TD, Francis JM, Ntusi N, et al. T1 Mapping for the Diagnosis of Acute Myocarditis Using CMR: Comparison to T2-Weighted and Late Gadolinium Enhanced Imaging. JACC: Cardiovascular Imaging. 2013;6(10):1048–58.

63. Ferreira VM, Piechnik SK, Dall'Armellina E, Karamitsos TD, Francis JM, Ntusi N, et al. Native T1-mapping detects the location, extent and patterns of acute myocarditis without the need for gadolinium contrast agents. Journal of Cardiovascular Magnetic Resonance. 2014;16(1):36.

64. Ferreira VM, Piechnik SK, Dall'Armellina E, Karamitsos TD, Francis JM, Choudhury RP, et al. Non-contrast T1-mapping detects acute myocardial edema with high diagnostic accuracy: a comparison to T2-weighted cardiovascular magnetic resonance. Journal of Cardiovascular Magnetic Resonance. 2012 Jun 21;14(1):42.

65. Ferreira VM, Schulz-Menger J, Holmvang G, Kramer CM, Carbone I, Sechtem U, et al. Cardiovascular Magnetic Resonance in Nonischemic Myocardial Inflammation: Expert Recommendations. Journal of the American College of Cardiology. 2018 Dec 18;72(24):3158–76.

66. Ugander M, Bagi PS, Oki AJ, Chen B, Hsu LY, Aletras AH, et al. Myocardial edema as detected by pre-contrast T1 and T2 CMR delineates area at risk associated with acute myocardial infarction. JACC: Cardiovascular Imaging. 2012 Jun 1;5(6):596–603.

67. Liu D, Borlotti A, Viliani D, Jerosch-Herold M, Alkhalil M, De Maria GL, et al. CMR Native T1 Mapping Allows Differentiation of Reversible Versus Irreversible Myocardial Damage in ST-Segment-Elevation Myocardial Infarction: An OxAMI Study (Oxford Acute Myocardial Infarction). Circulation Cardiovascular imaging. 2017 Aug 1;10(8).

68. Dass S, Suttie JJ, Piechnik SK, Ferreira VM, Holloway CJ, Banerjee R, et al. Myocardial tissue characterization using magnetic resonance

noncontrast T1 mapping in hypertrophic and dilated cardiomyopathy. Circulation: Cardiovascular Imaging. 2012 Nov;5(6):726–33.

69. Hinojar R, Varma N, Child N, Goodman B, Jabbour A, Yu CY, et al. T1 Mapping in Discrimination of Hypertrophic Phenotypes: Hypertensive Heart Disease and Hypertrophic Cardiomyopathy: Findings from the International T1 Multicenter Cardiovascular Magnetic Resonance Study. Circulation: Cardiovascular Imaging. 2015 Dec 1;8(12).

70. Puntmann VO, Carr-White G, Jabbour A, Yu CY, Gebker R, Kelle S, et al. T1-Mapping and Outcome in Nonischemic Cardiomyopathy All-Cause Mortality and Heart Failure. JACC: Cardiovascular Imaging. 2016 Jan 1;9(1):40–50.

71. Everett RJ, Treibel TA, Fukui M, Lee H, Rigolli M, Singh A, et al. Extracellular Myocardial Volume in Patients With Aortic Stenosis. Journal of the American College of Cardiology. 2020 Jan 28;75(3):304–16.

72. Mahmod M, Piechnik SK, Levelt E, Ferreira VM, Francis JM, Lewis A, et al. Adenosine stress native T1 mapping in severe aortic stenosis: evidence for a role of the intravascular compartment on myocardial T1 values. Journal of Cardiovascular Magnetic Resonance. 2014;16(1):92.

73. Bull S, White SK, Piechnik SK, Flett AS, Ferreira VM, Loudon M, et al. Human non-contrast T1 values and correlation with histology in diffuse fibrosis. Heart. 2013 Jul;99(13):932–7.

74. Karamitsos TD, Piechnik SK, Banypersad SM, Fontana M, Ntusi NB, Ferreira VM, et al. Noncontrast T1 Mapping for the Diagnosis of Cardiac Amyloidosis. JACC: Cardiovascular Imaging. 2013 Apr 1;6(4):488–97.

75. Fontana M, Banypersad SM, Treibel TA, Maestrini V, Sado DM, White SK, et al. Native T1 mapping in transthyretin amyloidosis. JACC: Cardiovascular Imaging. 2014 Feb 1;7(2):157–65.

76. Banypersad SM, Fontana M, Maestrini V, Sado DM, Captur G, Petrie A, et al. T1 mapping and survival in systemic light-chain amyloidosis. European Heart Journal. 2015 Jan 21;36(4):244–51.

77. Martinez-Naharro A, Abdel-Gadir A, Treibel TA, Zumbo G, Knight DS, Rosmini S, et al. CMR-Verified Regression of Cardiac AL Amyloid After Chemotherapy. Vol. 11, JACC: Cardiovascular Imaging. 2018. p. 152–4.

78. Hur DJ, Dicks DL, Huber S, Mojibian HR, Meadows JL, Seropian SE, et al. Serial Native T1 Mapping to Monitor Cardiac Response to Treatment in Light-Chain Amyloidosis. Circ Cardiovasc Imaging. 2016 Oct;9(10).

79. Thompson RB, Chow K, Khan A, Chan A, Shanks M, Paterson I, et al. T1 mapping with cardiovascular MRI is highly sensitive for fabry disease independent of hypertrophy and sex. Circulation: Cardiovascular Imaging. 2013 Sep;6(5):637–45.

80. Nordin S, Kozor R, Bulluck H, Castelletti S, Rosmini S, Abdel-Gadir A, et al. Cardiac Fabry Disease With Late Gadolinium Enhancement Is a Chronic Inflammatory Cardiomyopathy. Journal of the American College of Cardiology. 2016 Oct 11;68(15):1707–8.

81. Mathur S, Dreisbach JG, Karur GR, Iwanochko RM, Morel CF, Wasim S, et al. Loss of base-to-apex circumferential strain gradient assessed by cardiovascular magnetic resonance in Fabry disease: Relationship to T1 mapping, late gadolinium enhancement and hypertrophy. Journal of Cardiovascular Magnetic Resonance. 2019 Aug 1;21(1):45.

82. Ntusi NAB, Piechnik SK, Francis JM, Ferreira VM, Rai ABS, Matthews PM, et al. Subclinical myocardial inflammation and diffuse fibrosis are common in systemic sclerosis – a clinical study using myocardial T1-mapping and extracellular volume quantification. Journal of Cardiovascular Magnetic Resonance. 2014;16(1):21.

83. Cutter C. Rahimi, K. McGale, P. Ferreira, V. Darby, S. DT, Skyttä T, Tuohinen S, Boman E, Virtanen V, Raatikainen P, et al. Morbidity of ischemic heart disease in early breast cancer 15–20 years after adjuvant radiotherapy. Yeh E and, editor. International Journal of Radiation Oncology*Biology*Physics. 04/24 ed. 2014 Nov 21;11(1):53–8.

84. Ferreira VM, Marcelino M, Piechnik SK, Marini C, Karamitsos TD, Ntusi NAB, et al. Pheochromocytoma is characterized by catecholamine-mediated myocarditis, focal and diffuse myocardial fibrosis, and myocardial dysfunction. Journal of the American College of Cardiology. 2016 May 24;67(20):2364–74.

85. Moon JC, Messroghli DR, Kellman P, Piechnik SK, Robson MD, Ugander M, et al. Myocardial T1 mapping and extracellular volume quantification: a Society for Cardiovascular Magnetic Resonance (SCMR) and CMR Working Group of the European Society of Cardiology consensus statement. Journal of Cardiovascular Magnetic Resonance. 2013;15(1):92.

86. aus dem Siepen F, Buss SJ, Messroghli D, Andre F, Lossnitzer D, Seitz S, et al. T1 mapping in dilated cardiomyopathy with cardiac magnetic resonance: quantification of diffuse myocardial fibrosis and comparison with endomyocardial biopsy. European Heart Journal - Cardiovascular Imaging. 2015 Feb 1;16(2):210–6.

87. Kidambi A, Motwani M, Uddin A, Ripley DP, McDiarmid AK, Swoboda PP, et al. Myocardial Extracellular Volume Estimation by CMR Predicts Functional Recovery Following Acute MI. JACC: Cardiovascular Imaging. 2017 Sep 1;10(9):989–99.

88. Treibel TA, Fridman Y, Bering P, Sayeed A, Maanja M, Frojdh F, et al. Extracellular Volume Associates With Outcomes More Strongly Than Native or Post-Contrast Myocardial T1. JACC: Cardiovascular Imaging. 2019 May 15;13(1):44–54.

89. Popescu IA, Werys K, Zhang Q, Puchta H, Hann E, Lukaschuk E, et al. Standardization of T1-mapping in cardiovascular magnetic resonance using clustered structuring for benchmarking normal ranges. International Journal of Cardiology. 2021 Mar 1;326:220–5.

90. Taylor AJ, Salerno M, Dharmakumar R, Jerosch-Herold M. T1 Mapping Basic Techniques and Clinical Applications. Vol. 9, JACC: Cardiovascular Imaging. Elsevier Inc.; 2016. p. 67–81.

91. Messroghli DR, Radjenovic A, Kozerke S, Higgins DM, Sivananthan MU, Ridgway JP. Modified look-locker inversion recovery (MOLLI) for high-resolution T 1 mapping of the heart. Magnetic Resonance in Medicine. 2004 Jul 1;52(1):141–6.

92. Piechnik SK, Ferreira VM, Dall'Armellina E, Cochlin LE, Greiser A, Neubauer S, et al. Shortened Modified Look-Locker Inversion recovery (ShMOLLI) for clinical myocardial T1-mapping at 1.5 and 3 T within a 9 heartbeat breathhold. J Cardiovasc Magn Reson. 2010;12:69.

93. Chow K, Flewitt JA, Green JD, Pagano JJ, Friedrich MG, Thompson RB. Saturation recovery single-shot acquisition (SASHA) for myocardial T 1 mapping. Magnetic Resonance in Medicine. 2014;71(6):2082–95.

94. Weingärtner S, Akçakaya M, Basha T, Kissinger K V., Goddu B, Berg S, et al. Combined saturation/inversion recovery sequences for improved evaluation of scar and diffuse fibrosis in patients with arrhythmia or heart rate variability. Magnetic Resonance in Medicine. 2014;71(3):1024–34.

95. Piechnik SK, Neubauer S, Ferreira VM. State-of-the-art review: stress T1 mapping—technical considerations, pitfalls and emerging clinical applications. Vol. 31, Magnetic Resonance Materials in Physics, Biology and Medicine. Springer Berlin Heidelberg; 2018. p. 131–41.

96. Look DC, Locker DR. Time saving in measurement of NMR and EPR relaxation times. Review of Scientific Instruments. 1970 Feb 11;41(2):250–1.

97. Piechnik SK, Ferreira VM, Lewandowski AJ, Ntusi NA, Banerjee R, Holloway C, et al. Normal variation of magnetic resonance T1 relaxation times in the human population at 1.5 T using ShMOLLI. Journal of Cardiovascular Magnetic Resonance. 2013 Dec 20;15(1):13.

98. Tessa C, Diciotti S, Landini N, Lilli A, Del Meglio J, Salvatori L, et al. Myocardial T1 and T2 mapping in diastolic and systolic phase. International Journal of Cardiovascular Imaging. 2015 Jun 29;31(5):1001–10.

99. Ferreira VM, Wijesurendra RS, Liu A, Greiser A, Casadei B, Robson MD, et al. Systolic ShMOLLI myocardial T1-mapping for improved robustness to partial-volume effects and applications in tachyarrhythmias. Journal of Cardiovascular Magnetic Resonance. 2015 Dec 28;17(1):77.

100. Kellman P, Wilson JR, Xue H, Ugander M, Arai AE. Extracellular volume fraction mapping in the myocardium, part 1: evaluation of an automated method. Journal of Cardiovascular Magnetic Resonance. 2012 Dec 10;14(1):63.

101. Roujol S, Weingärtner S, Foppa M, Chow K, Kawaji K, Ngo LH, et al. Accuracy, precision, and reproducibility of four T1 mapping sequences: A headto-head comparison of MOLLI, ShMOLLI, SASHA, and SAPPHIRE. Radiology. 2014 Apr 4;272(3):683–9.

102. Kellman P, Hansen MS. T1-mapping in the heart: Accuracy and precision. Journal of Cardiovascular Magnetic Resonance. 2014 Jan 4;16(1).

103. Judd RM, Levy BI. Effects of barium-induced cardiac contraction on large- and small-vessel intramyocardial blood volume. Circulation Research. 1991;68(1):217–25.

104. Liu A, Wijesurendra RS, Francis JM, Robson MD, Neubauer S, Piechnik SK, et al. Adenosine Stress and Rest T1 Mapping Can Differentiate Between Ischemic, Infarcted, Remote, and Normal Myocardium Without the Need for Gadolinium Contrast Agents. JACC: Cardiovascular Imaging. 2016;9(1):27–36.

105. Rieber J, Huber A, Erhard I, Mueller S, Schweyer M, Koenig A, et al. Cardiac magnetic resonance perfusion imaging for the functional assessment of coronary artery disease: a comparison with coronary angiography and fractional flow reserve. European Heart Journal. 2006 May 23;27(12):1465–71.

106. Nagel E, Greenwood JP, McCann GP, Bettencourt N, Shah AM, Hussain ST, et al. Magnetic resonance perfusion or fractional flow reserve in

coronary disease. New England Journal of Medicine. 2019 Jun 20;380(25):2418–28.

107. Kwong RY, Ge Y, Steel K, Bingham S, Abdullah S, Fujikura K, et al. Cardiac Magnetic Resonance Stress Perfusion Imaging for Evaluation of Patients With Chest Pain. Journal of the American College of Cardiology. 2019 Oct 8;74(14):1741–55.

108. McCommis KS, Goldstein TA, Abendschein DR, Misselwitz B, Pilgram T, Gropler RJ, et al. Roles of myocardial blood volume and flow in coronary artery disease: An experimental MRI study at rest and during hyperemia. European Radiology. 2010 Aug 24;20(8):2005–12.

109. McCommis KS, Goldstein TA, Zhang H, Misselwitz B, Gropler RJ, Zheng J. Quantification of myocardial blood volume during dipyridamole and doubtamine stress: A perfusion CMR study. Journal of Cardiovascular Magnetic Resonance. 2007 Sep;9(5):785–92.

110. Le DE, Jayaweera AR, Wei K, Coggins MP, Lindner JR, Kaul S. Changes in myocardial blood volume over a wide range of coronary driving pressures: role of capillaries beyond the autoregulatory range. Heart. 2004;90:1199–205.

111. Arnold JR, Karamitsos TD, Bhamra-Ariza P, Francis JM, Searle N, Robson MD, et al. Myocardial oxygenation in coronary artery disease: Insights from blood oxygen level-dependent magnetic resonance imaging at 3 Tesla. Journal of the American College of Cardiology. 2012 May 29;59(22):1954–64.

112. van Assen M, van Dijk R, Kuijpers D, Vliegenthart R, Oudkerk M. T1 reactivity as an imaging biomarker in myocardial tissue characterization discriminating normal, ischemic and infarcted myocardium. International Journal of Cardiovascular Imaging. 2019 Jul 1;35(7):1319–25.

113. Nakamori S, Fahmy A, Jang J, El-Rewaidy H, Neisius U, Berg S, et al. Changes in Myocardial Native T1 and T2 After Exercise Stress: A Noncontrast CMR Pilot Study. JACC: Cardiovascular Imaging. 2020 Mar 1;13(3):667–80.

114. Yimcharoen S, Zhang S, Kaolawanich Y, Tanapibunpon P, Krittayaphong R. Clinical assessment of adenosine stress and rest cardiac magnetic resonance T1 mapping for detecting ischemic and infarcted myocardium. Scientific Reports. 2020 Dec 1;10(1):14727.

115. Shah R, Sree Raman K, Walls A, Woodman RJ, Faull R, Gleadle JM, et al. Gadolinium-Free Cardiovascular Magnetic Resonance Stress T1 Mapping in Patients With Chronic Kidney Disease. JACC: Cardiovascular Imaging. 2019 Oct;12(10):2083–5.

116. Rajappan K, Rimoldi OE, Dutka DP, Ariff B, Pennell DJ, Sheridan DJ, et al. Mechanisms of Coronary Microcirculatory Dysfunction in Patients With Aortic Stenosis and Angiographically Normal Coronary Arteries. Circulation. 2002 Jan 29;105(4):470–6.

117. Marcus ML, Doty DB, Hiratzka LF, Wright CB, Eastham CL. Decreased Coronary Reserve. New England Journal of Medicine. 1982 Nov 25;307(22):1362–6.

118. Murthy VL, Naya M, Foster CR, Gaber M, Hainer J, Klein J, et al. Association between coronary vascular dysfunction and cardiac mortality in patients with and without diabetes mellitus. Circulation. 2012 Oct 9;126(15):1858–68.

119. Levelt E, Piechnik SK, Liu A, Wijesurendra RS, Mahmod M, Ariga R, et al. Adenosine stress CMR T1-mapping detects early microvascular dysfunction in patients with type 2 diabetes mellitus without obstructive coronary artery disease. Journal of Cardiovascular Magnetic Resonance. 2017;19(1).

120. Poli FE, Gulsin GS, March DS, Abdelaty AM, Parke KS, Wormleighton J V, et al. The reliability and feasibility of non-contrast adenosine stress cardiovascular magnetic resonance T1 mapping in patients on haemodialysis. Journal of Cardiovascular Magnetic Resonance. 2020 Dec 8;22(1):43.

121. Shah SA, Reagan CE, French BA, Epstein FH. Molecular Mechanisms of Adenosine Stress T1 Mapping. Circulation Cardiovascular imaging. 2021 Mar;14(3):e011774.

122. Morrison RR, Talukder MAH, Ledent C, Mustafa SJ. Cardiac effects of adenosine in A_{2A} receptor knockout hearts: uncovering A_{2B} receptors. American Journal of Physiology-Heart and Circulatory Physiology. 2002 Feb 1;282(2):H437–44.

123. Nguyen KL, Bandettini WP, Shanbhag S, Leung SW, Wilson JR, Arai AE. Safety and tolerability of regadenoson CMR. European Heart Journal Cardiovascular Imaging. 2014 Jul;15(7):753–60.

124. Zareba KM, Raman S V. Exercise and Dobutamine Stress CMR. In: Contemporary Cardiology. Springer, New York, NY; 2019. p. 175–84.

125. Kelle S, Chiribiri A, Vierecke J, Egnell C, Hamdan A, Jahnke C, et al. Long-term prognostic value of dobutamine stress CMR. JACC: Cardiovascular Imaging. 2011 Feb 1;4(2):161–72.

126. Ruffolo RR. Review: The pharmacology of dobutamine. American Journal of the Medical Sciences. 1987;294(4):244–8.

127. McNeill AJ, Fioretti PM, El-Said ESM, Salustri A, Forster T, Roelandt JRTC. Enhanced sensitivity for detection of coronary artery disease by addition of atropine to dobutamine stress echocardiography. The American Journal of Cardiology. 1992 Jul 1;70(1):41–6.

128. Nandalur KR, Dwamena BA, Choudhri AF, Nandalur MR, Carlos RC. Diagnostic Performance of Stress Cardiac Magnetic Resonance Imaging in the Detection of Coronary Artery Disease. A Meta-Analysis. Journal of the American College of Cardiology. 2007 Oct 1;50(14):1343–53.

129. Gebker R, Jahnke C, Manka R, Hamdan A, Schnackenburg B, Fleck E, et al. Additional value of myocardial perfusion imaging during dobutamine stress magnetic resonance for the assessment of coronary artery disease. Circulation Cardiovascular imaging. 2008;1(2):122–30.

130. Lubbers DD, Janssen CHC, Kuijpers D, van Dijkman PRM, Overbosch J, Willems TP, et al. The additional value of first pass myocardial perfusion imaging during peak dose of dobutamine stress cardiac MRI for the detection of myocardial ischemia. International Journal of Cardiovascular Imaging. 2008 Jan;24(1):69–76.

131. Kuijpers D, Prakken NH, Vliegenthart R, van Dijkman PRM, van der Harst P, Oudkerk M. Caffeine intake inverts the effect of adenosine on myocardial perfusion during stress as measured by T1 mapping. International Journal of Cardiovascular Imaging. 2016 Oct 1;32(10):1545–53.

132. Lee JJ, Liu S, Nacif MS, Ugander M, Han J, Kawel N, et al. Myocardial T1 and extracellular volume fraction mapping at 3 tesla. Journal of Cardiovascular Magnetic Resonance. 2011 Nov 28;13(1):75.

133. Nickander J, Themudo R, Thalén S, Sigfridsson A, Xue H, Kellman P, et al. The relative contributions of myocardial perfusion, blood volume and extracellular volume to native T1 and native T2 at rest and during adenosine stress in normal physiology. Journal of Cardiovascular Magnetic Resonance. 2019 Nov 25;21(1):73.

134. Schulz-Menger J, Bluemke DA, Bremerich J, Flamm SD, Fogel MA, Friedrich MG, et al. Standardized image interpretation and post-processing in cardiovascular magnetic resonance - 2020 update : Society for Cardiovascular Magnetic Resonance (SCMR): Board of Trustees Task Force on Standardized Post-Processing. Journal of cardiovascular magnetic resonance : official journal of the Society for Cardiovascular Magnetic Resonance. 2020 Mar 12;22(1):19.

135. Zhang Q, Hann E, Werys K, Wu C, Popescu I, Lukaschuk E, et al. Deep learning with attention supervision for automated motion artefact

detection in quality control of cardiac T1-mapping. Artificial Intelligence in Medicine. 2020 Nov 1;110:101955.

136. Carapella V, Puchta H, Lukaschuk E, Marini C, Werys K, Neubauer S, et al. Standardized image post-processing of cardiovascular magnetic resonance T1-mapping reduces variability and improves accuracy and consistency in myocardial tissue characterization. International Journal of Cardiology. 2020 Jan 1;298:128–34.

137. Cerqueira MD, Weissman NJ, Dilsizian V, Jacobs AK, Kaul S, Laskey WK, et al. Standardized Myocardial Segmentation and Nomenclature for Tomographic Imaging of the Heart. Circulation. 2002 Jan 29;105(4):539–42.

138. Kellman P, Hansen MS, Nielles-Vallespin S, Nickander J, Themudo R, Ugander M, et al. Myocardial perfusion cardiovascular magnetic resonance: optimized dual sequence and reconstruction for quantification. Journal of Cardiovascular Magnetic Resonance. 2017;19(1):43.

139. Kotecha T, Martinez-Naharro A, Boldrini M, Knight D, Hawkins P, Kalra S, et al. Automated Pixel-Wise Quantitative Myocardial Perfusion Mapping by CMR to Detect Obstructive Coronary Artery Disease and Coronary Microvascular Dysfunction: Validation Against Invasive Coronary Physiology. JACC Cardiovascular imaging. 2019 Oct 13;12(10):1958–69.

140. White SK, Sado DM, Fontana M, Banypersad SM, Maestrini V, Flett AS, et al. T1 Mapping for Myocardial Extracellular Volume Measurement by CMR. JACC: Cardiovascular Imaging. 2013;6(9):955–62.

141. Tu S, Westra J, Yang J, von Birgelen C, Ferrara A, Pellicano M, et al. Diagnostic Accuracy of Fast Computational Approaches to Derive Fractional Flow Reserve From Diagnostic Coronary Angiography: The International Multicenter FAVOR Pilot Study. JACC: Cardiovascular Interventions. 2016 Oct 10;9(19):2024–35.

142. De Maria GL, Scarsini R, Shanmuganathan M, Kotronias RA, Terentes-Printzios D, Borlotti A, et al. Angiography-derived index of microcirculatory resistance as a novel, pressure-wire-free tool to assess coronary microcirculation in ST elevation myocardial infarction. International Journal of Cardiovascular Imaging. 2020 Aug 1;36(8):1395–406.

143. Westra J, Andersen BK, Campo G, Matsuo H, Koltowski L, Eftekhari A, et al. Diagnostic performance of in-procedure angiography-derived quantitative flow reserve compared to pressure-derived fractional flow

reserve: The FAVOR II Europe-Japan study. Journal of the American Heart Association. 2018 Jul 1;7(14).

144. Lentine KL, Costa SP, Weir MR, Robb JF, Fleisher LA, Kasiske BL, et al. Cardiac Disease Evaluation and Management Among Kidney and Liver Transplantation Candidates: A Scientific Statement From the American Heart Association and the American College of Cardiology Foundation. Journal of the American College of Cardiology. 2012 Jul;60(5):434–80.

145. Go AS, Chertow GM, Fan D, McCulloch CE, Hsu C. Chronic Kidney Disease and the Risks of Death, Cardiovascular Events, and Hospitalization. New England Journal of Medicine. 2004 Sep 23;351(13):1296–305.

146. Dilsizian V, Gewirtz H, Marwick TH, Kwong RY, Raggi P, Al-Mallah MH, et al. Cardiac Imaging for Coronary Heart Disease Risk Stratification in Chronic Kidney Disease. JACC: Cardiovascular Imaging. 2021 Mar 1;14(3):669–82.

147. Palepu S, Prasad GVR. Screening for cardiovascular disease before kidney transplantation. World J Transplant. 2015 Dec 24;5(4):276–86.

148. Bangalore S, Maron DJ, O'Brien SM, Fleg JL, Kretov EI, Briguori C, et al. Management of Coronary Disease in Patients with Advanced Kidney Disease. New England Journal of Medicine. 2020 Apr 23;382(17):1608–18.

149. Wang LW, Fahim MA, Hayen A, Mitchell RL, Baines L, Lord S, et al. Cardiac testing for coronary artery disease in potential kidney transplant recipients. Cochrane Database of Systematic Reviews. 2011 Dec;(12):CD008691–CD008691.

150. Al-Mallah MH, Hachamovitch R, Dorbala S, Di Carli MF. Incremental prognostic value of myocardial perfusion imaging in patients referred to stress single-photon emission computed tomography with renal dysfunction. Circulation: Cardiovascular Imaging. 2009;2(6):429–36.

151. Winther S, Svensson M, Jørgensen HS, Bouchelouche K, Gormsen LC, Pedersen BB, et al. Diagnostic Performance of Coronary CT Angiography and Myocardial Perfusion Imaging in Kidney Transplantation Candidates. JACC: Cardiovascular Imaging. 2015 May 1;8(5):553–62.

152. Leung KCW, Tonelli M, James MT. Chronic kidney disease following acute kidney injury-risk and outcomes. Nat Rev Nephrol. 2013 Feb;9(2):77–85.

153. Greenwood JP, Maredia N, Younger JF, Brown JM, Nixon J, Everett CC, et al. Cardiovascular magnetic resonance and single-photon emission

computed tomography for diagnosis of coronary heart disease (CE-MARC): A prospective trial. The Lancet. 2012 Feb;379(9814):453–60.

154. Schwitter J, Wacker CM, Wilke N, Al-Saadi N, Sauer E, Huettle K, et al. MR-IMPACT II: Magnetic resonance imaging for myocardial perfusion assessment in coronary artery disease trial: Perfusion-cardiac magnetic resonance vs. single-photon emission computed tomography for the detection of coronary artery disease: A comparative. European Heart Journal. 2013 Mar;34(10):775–81.

155. Kwong RY, Ge Y, Steel K, Bingham S, Abdullah S, Fujikura K, et al. Cardiac Magnetic Resonance Stress Perfusion Imaging for Evaluation of Patients With Chest Pain. Journal of the American College of Cardiology. 2019 Oct;74(14):1741–55.

156. Beam AS, Moore KG, Gillis SN, Ford KF, Gray T, Steinwinder AH, et al. GBCAs and Risk for Nephrogenic Systemic Fibrosis: A Literature Review. Radiol Technol. 2017 Jan 7;88(6):583–9.

157. Messroghli DR, Walters K, Plein S, Sparrow P, Friedrich MG, Ridgway JP, et al. Myocardial T1 mapping: Application to patients with acute and chronic myocardial infarction. Magnetic Resonance in Medicine. 2007 Jul;58(1):34–40.

158. Ferreira VM, Piechnik SK, Dall'Armellina E, Karamitsos TD, Francis JM, Choudhury RP, et al. Non-contrast T1-mapping detects acute myocardial edema with high diagnostic accuracy: a comparison to T2-weighted cardiovascular magnetic resonance. Journal of Cardiovascular Magnetic Resonance. 2012 Jun;14(1):42–42.

159. Ferreira VM, Piechnik SK, Dall'Armellina E, Karamitsos TD, Francis JM, Ntusi N, et al. T1 Mapping for the Diagnosis of Acute Myocarditis Using CMR: Comparison to T2-Weighted and Late Gadolinium Enhanced Imaging. JACC: Cardiovascular Imaging. 2013;6(10):1048–58.

160. Ferreira VM, Piechnik SK, Dall'Armellina E, Karamitsos TD, Francis JM, Ntusi N, et al. Native T1-mapping detects the location, extent and patterns of acute myocarditis without the need for gadolinium contrast agents. Journal of Cardiovascular Magnetic Resonance. 2014;16(1):36–36.

161. Ferreira VM, Marcelino M, Piechnik SK, Marini C, Karamitsos TD, Ntusi NAB, et al. Pheochromocytoma is characterized by catecholamine-mediated myocarditis, focal and diffuse myocardial fibrosis, and myocardial dysfunction. Journal of the American College of Cardiology. 2016 May;67(20):2364–74.

162. Graham-Brown MPM, March DS, Churchward DR, Stensel DJ, Singh A, Arnold R, et al. Novel cardiac nuclear magnetic resonance method for

noninvasive assessment of myocardial fibrosis in hemodialysis patients. Kidney Int. 2016 Oct;90(4):835–44.

163. Rutherford E, Talle MA, Mangion K, Bell E, Rauhalammi SM, Roditi G, et al. Defining myocardial tissue abnormalities in end-stage renal failure with cardiac magnetic resonance imaging using native T1 mapping. Kidney Int. 2016 Oct;90(4):845–52.

164. Edwards NC, Moody WE, Yuan M, Hayer MK, Ferro CJ, Townend JN, et al. Diffuse interstitial fibrosis and myocardial dysfunction in early chronic kidney disease. Am J Cardiol. 2015 May 1;115(9):1311–7.

165. Lindner JR, Skyba DM, Goodman NC, Jayaweera AR, Kaul S. Changes in myocardial blood volume with graded coronary stenosis. American Journal of Physiology - Heart and Circulatory Physiology. 1997;272(1 41-1).

166. Le DE, Jayaweera AR, Wei K, Coggins MP, Lindner JR, Kaul S. Changes in myocardial blood volume over a wide range of coronary driving pressures: role of capillaries beyond the autoregulatory range. Heart. 2004;90:1199–205.

167. Liu A, Wijesurendra RS, Francis JM, Robson MD, Neubauer S, Piechnik SK, et al. Adenosine Stress and Rest T1 Mapping Can Differentiate Between Ischemic, Infarcted, Remote, and Normal Myocardium Without the Need for Gadolinium Contrast Agents. JACC: Cardiovascular Imaging. 2016;9(1):27–36.

168. Shah R, Sree Raman K, Walls A, Woodman RJ, Faull R, Gleadle JM, et al. Gadolinium-Free Cardiovascular Magnetic Resonance Stress T1 Mapping in Patients With Chronic Kidney Disease. JACC: Cardiovascular Imaging. 2019 Oct;12(10):2083–5.

169. Poli FE, Gulsin GS, March DS, Abdelaty AM, Parke KS, Wormleighton JV, et al. The reliability and feasibility of non-contrast adenosine stress cardiovascular magnetic resonance T1 mapping in patients on haemodialysis. Journal of Cardiovascular Magnetic Resonance. 2020 Dec;22(1):43–43.

170. Kramer CM, Barkhausen J, Bucciarelli-Ducci C, Flamm SD, Kim RJ, Nagel E. Standardized cardiovascular magnetic resonance imaging (CMR) protocols: 2020 update. Journal of Cardiovascular Magnetic Resonance. 2020 Feb;22(1):17–17.

171. Schulz-Menger J, Bluemke DA, Bremerich J, Flamm SD, Fogel MA, Friedrich MG, et al. Standardized image interpretation and post-processing in cardiovascular magnetic resonance - 2020 update : Society for Cardiovascular Magnetic Resonance (SCMR): Board of Trustees Task Force on Standardized Post-Processing. Journal of

cardiovascular magnetic resonance : official journal of the Society for Cardiovascular Magnetic Resonance. 2020 Mar;22(1):19–19.

172. Piechnik SK, Ferreira VM, Dall'Armellina E, Cochlin LE, Greiser A, Neubauer S, et al. Shortened Modified Look-Locker Inversion recovery (ShMOLLI) for clinical myocardial T1-mapping at 1.5 and 3 T within a 9 heartbeat breathhold. J Cardiovasc Magn Reson. 2010;12:69–69.

173. Ferreira VM, Wijesurendra RS, Liu A, Greiser A, Casadei B, Robson MD, et al. Systolic ShMOLLI myocardial T1-mapping for improved robustness to partial-volume effects and applications in tachyarrhythmias. Journal of Cardiovascular Magnetic Resonance. 2015 Dec;17(1):77–77.

174. Cerqueira MD, Weissman NJ, Dilsizian V, Jacobs AK, Kaul S, Laskey WK, et al. Standardized Myocardial Segmentation and Nomenclature for Tomographic Imaging of the Heart. Circulation. 2002 Jan;105(4):539–42.

175. De Bruyne B, Fearon WF, Pijls NHJ, Barbato E, Tonino P, Piroth Z, et al. Fractional flow reserve-guided PCI for stable coronary artery disease. N Engl J Med. 2014 Sep 25;371(13):1208–17.

176. Lee B-K, Lim H-S, Fearon WF, Yong AS, Yamada R, Tanaka S, et al. Invasive evaluation of patients with angina in the absence of obstructive coronary artery disease. Circulation. 2015 Mar 24;131(12):1054–60.

177. Fearon WF, Balsam LB, Farouque HMO, Caffarelli AD, Robbins RC, Fitzgerald PJ, et al. Novel index for invasively assessing the coronary microcirculation. Circulation. 2003 Jul 1;107(25):3129–32.

178. Xu B, Tu S, Qiao S, Qu X, Chen Y, Yang J, et al. Diagnostic Accuracy of Angiography-Based Quantitative Flow Ratio Measurements for Online Assessment of Coronary Stenosis. Journal of the American College of Cardiology. 2017 Dec 26;70(25):3077–87.

179. Yimcharoen S, Zhang S, Kaolawanich Y, Tanapibunpon P, Krittayaphong R. Clinical assessment of adenosine stress and rest cardiac magnetic resonance T1 mapping for detecting ischemic and infarcted myocardium. Scientific Reports. 2020 Dec;10(1):14727–14727.

180. Lee JM, Hwang D, Park J, Zhang J, Tong Y, Kim CH, et al. Exploring coronary circulatory response to stenosis and its association with invasive physiologic indexes using absolute myocardial blood flow and coronary pressure. Circulation. 2017;136(19):1798–808.

181. McCommis KS, Goldstein TA, Abendschein DR, Misselwitz B, Pilgram T, Gropler RJ, et al. Roles of myocardial blood volume and flow in

coronary artery disease: An experimental MRI study at rest and during hyperemia. European Radiology. 2010 Aug;20(8):2005–12.

182. Charytan DM, Shelbert HR, Di Carli MF. Coronary Microvascular Function in Early Chronic Kidney Disease. Circulation: Cardiovascular Imaging. 2010 Nov 1;3(6):663–71.

183. Ragosta M, Samady H, Isaacs RB, Gimple LW, Sarembock IJ, Powers ER. Coronary flow reserve abnormalities in patients with diabetes mellitus who have end-stage renal disease and normal epicardial coronary arteries. American Heart Journal. 2004 Jun 1;147(6):1017–23.

184. Caliskan Y, Oflaz H, Demirturk M, Yazici H, Turkmen A, Çimen A, et al. Coronary flow reserve dysfunction in hemodialysis and kidney transplant patients. Clinical Transplantation. 2008;22(6):785–93.

185. Bozbas H, Pirat B, Demirtas S, Simşek V, Yildirir A, Sade E, et al. Evaluation of coronary microvascular function in patients with end-stage renal disease, and renal allograft recipients. Atherosclerosis. 2009 Feb 1;202(2):498–504.

186. Bajaj NS, Singh A, Zhou W, Gupta A, Fujikura K, Byrne C, et al. Coronary Microvascular Dysfunction, Left Ventricular Remodeling, and Clinical Outcomes in Patients With Chronic Kidney Impairment. Circulation. 2020 Jan 7;141(1):21–33.

187. Levelt E, Piechnik SK, Liu A, Wijesurendra RS, Mahmod M, Ariga R, et al. Adenosine stress CMR T1-mapping detects early microvascular dysfunction in patients with type 2 diabetes mellitus without obstructive coronary artery disease. Journal of Cardiovascular Magnetic Resonance [Internet]. 2017;19(1). Available from: http://dx.doi.org/10.1186/s12968-017-0397-8

188. Murthy VL, Naya M, Foster CR, Hainer J, Gaber M, Dorbala S, et al. Coronary Vascular Dysfunction and Prognosis in Patients With Chronic Kidney Disease. JACC: Cardiovascular Imaging. 2012 Oct 1;5(10):1025–34.

189. Shah NR, Charytan DM, Murthy VL, Skali Lami H, Veeranna V, Cheezum MK, et al. Prognostic Value of Coronary Flow Reserve in Patients with Dialysis-Dependent ESRD. J Am Soc Nephrol. 2016 Jun;27(6):1823–9.

190. Schwarz U, Buzello M, Ritz E, Stein G, Raabe G, Wiest G, et al. Morphology of coronary atherosclerotic lesions in patients with end-stage renal failure. Nephrology Dialysis Transplantation. 2000 Feb 1;15(2):218–23.

191. Amann K, Breitbach M, Ritz E, Mall G. Myocyte/capillary mismatch in the heart of uremic patients. JASN. 1998 Jun 1;9(6):1018–22.

192. Querfeld U, Mak RH, Pries AR. Microvascular disease in chronic kidney disease: the base of the iceberg in cardiovascular comorbidity. Clinical Science. 2020 Jun 16;134(12):1333–56.

193. Mall G, Huther W, Schneider J, Lundin P, Ritz E. Diffuse intermyocardiocytic fibrosis in uraemic patients. Nephrol Dial Transplant. 1990;5(1):39–44.

194. Aoki J, Ikari Y, Nakajima H, Mori M, Sugimoto T, Hatori M, et al. Clinical and pathologic characteristics of dilated cardiomyopathy in hemodialysis patients. Kidney International. 2005 Jan 1;67(1):333–40.

195. Dasselaar JJ, Slart RHJA, Knip M, Pruim J, Tio RA, McIntyre CW, et al. Haemodialysis is associated with a pronounced fall in myocardial perfusion. Nephrology Dialysis Transplantation. 2009 Feb 1;24(2):604–10.

196. Rosmini S, Bulluck H, Captur G, Treibel TA, Abdel-Gadir A, Bhuva AN, et al. Myocardial native T1 and extracellular volume with healthy ageing and gender. Eur Heart J Cardiovasc Imaging. 2018 Jun;19(6):615–21.

197. Piechnik SK, Ferreira VM, Lewandowski AJ, Ntusi NA, Banerjee R, Holloway C, et al. Normal variation of magnetic resonance T1 relaxation times in the human population at 1.5 T using ShMOLLI. Journal of Cardiovascular Magnetic Resonance. 2013 Dec;15(1):13–13.

198. Kellman P, Hansen MS, Nielles-Vallespin S, Nickander J, Themudo R, Ugander M, et al. Myocardial perfusion cardiovascular magnetic resonance: optimized dual sequence and reconstruction for quantification. Journal of Cardiovascular Magnetic Resonance. 2017;19(1):43–43.

199. Kotecha T, Martinez-Naharro A, Boldrini M, Knight D, Hawkins P, Kalra S, et al. Automated Pixel-Wise Quantitative Myocardial Perfusion Mapping by CMR to Detect Obstructive Coronary Artery Disease and Coronary Microvascular Dysfunction: Validation Against Invasive Coronary Physiology. JACC Cardiovascular imaging. 2019 Oct;12(10):1958–69.

200. Ferreira VM, Piechnik SK, Dall'Armellina E, Karamitsos TD, Francis JM, Ntusi N, et al. T1 Mapping for the Diagnosis of Acute Myocarditis Using CMR: Comparison to T2-Weighted and Late Gadolinium Enhanced Imaging. JACC: Cardiovascular Imaging. 2013;6(10):1048–58.

201. Ntusi NAB, Piechnik SK, Francis JM, Ferreira VM, Matthews PM, Robson MD, et al. Diffuse Myocardial Fibrosis and Inflammation in Rheumatoid Arthritis. JACC: Cardiovascular Imaging. 2015;8(5):526–36.

202. Bohnen S, Prüßner L, Vettorazzi E, Radunski UK, Tahir E, Schneider J, et al. Stress T1-mapping cardiovascular magnetic resonance imaging and inducible myocardial ischemia. Clinical Research in Cardiology. 2019 Aug 1;108(8):909–20.

203. Burrage MK, Shanmuganathan M, Masi A, Hann E, Zhang Q, Popescu IA, et al. Cardiovascular magnetic resonance stress and rest T1-mapping using regadenoson for detection of ischemic heart disease compared to healthy controls. International Journal of Cardiology. 2021 Mar;15(333):239–45.

204. Salerno M, Janardhanan R, Jiji RS, Brooks J, Adenaw N, Mehta B, et al. Comparison of methods for determining the partition coefficient of gadolinium in the myocardium using T_1 mapping. Journal of Magnetic Resonance Imaging. 2013 Jul 1;38(1):217–24.

205. Kawel N, Nacif M, Zavodni A, Jones J, Liu S, Sibley CT, et al. T1 mapping of the myocardium: Intra-individual assessment of post-contrast T1 time evolution and extracellular volume fraction at 3T for Gd-DTPA and Gd-BOPTA. Journal of Cardiovascular Magnetic Resonance. 2012 Apr 28;14(1):26.

206. Schelbert EB, Testa SM, Meier CG, Ceyrolles WJ, Levenson JE, Blair AJ, et al. Myocardial extravascular extracellular volume fraction measurement by gadolinium cardiovascular magnetic resonance in humans: Slow infusion versus bolus. Journal of Cardiovascular Magnetic Resonance. 2011 Dec 4;13(1):16.

207. Weingärtner S, Meßner NM, Budjan J, Loßnitzer D, Mattler U, Papavassiliu T, et al. Myocardial T1-mapping at 3T using saturation-recovery: reference values, precision and comparison with MOLLI. Journal of cardiovascular magnetic resonance : official journal of the Society for Cardiovascular Magnetic Resonance. 2016 Nov 18;18(1):84.

208. Werys K, Dragonu I, Zhang Q, Popescu I, Hann E, Puchta H, et al. Total Mapping Toolbox (TOMATO): An open source library for cardiac magnetic resonance parametric mapping. SoftwareX. 2020 Jan 1;11:100369.

209. Hann E, Popescu IA, Zhang Q, Gonzales RA, Barutçu A, Neubauer S, et al. Deep Neural Network Ensemble for On-the-Fly Quality Control-Driven Segmentation of Cardiac MRI T1 Mapping. Medical Image Analysis. 2021 Mar 1;71:102029.

210. Lieu HD, Shryock JC, von Mering GO, Gordi T, Blackburn B, Olmsted AW, et al. Regadenoson, a selective A2A adenosine receptor agonist, causes dose-dependent increases in coronary blood flow velocity in humans. Journal of Nuclear Cardiology. 2007;14(4 SPEC. ISS.):514–20.

211. Piechnik SK, Chiarelli PA, Jezzard P. Modelling vascular reactivity to investigate the basis of the relationship between cerebral blood volume and flow under CO2 manipulation. NeuroImage. 2008 Jan 1;39(1):107–18.

212. Grubb RL, Raichle ME, Eichling JO, Ter-Pogossian MM. The Effects of Changes in PaCO2 Cerebral Blood Volume, Blood Flow, and Vascular Mean Transit Time. Stroke. 1974 Sep 1;5(5):630–9.

213. van Dijk R, Kuijpers D, Kaandorp TAM, van Dijkman PRM, Vliegenthart R, van der Harst P, et al. Effects of caffeine intake prior to stress cardiac magnetic resonance perfusion imaging on regadenoson- versus adenosine-induced hyperemia as measured by T1 mapping. International Journal of Cardiovascular Imaging. 2017 Nov 1;33(11):1753–9.

214. Caballeros M, Bartolomé P, Fernández González Ó, Greiser A, García Del Barrio L, Pueyo J, et al. Effect of contrast dose in the quantification of myocardial extra-cellular volume in adenosine stress/rest perfusion cardiac magnetic resonance examinations. Acta Radiologica. 2017 Jul 1;58(7):809–15.

215. Robson MD, Piechnik SK, Tunnicliffe EM, Neubauer S. T1 measurements in the human myocardium: The effects of magnetization transfer on the SASHA and MOLLI sequences. Magnetic Resonance in Medicine. 2013;70(3):664–70.

216. Heidenreich JF, Weng AM, Donhauser J, Greiser A, Chow K, Nordbeck P, et al. T1- and ECV-mapping in clinical routine at 3 T: Differences between MOLLI, ShMOLLI and SASHA. BMC Medical Imaging. 2019 Aug 1;19(1):59.

217. Gottbrecht M, Kramer CM, Salerno M. Native T1 and Extracellular Volume Measurements by Cardiac MRI in Healthy Adults: A Meta-Analysis. Radiology. 2019 Feb 1;290(2):317–26.

218. Nickander J, Themudo R, Sigfridsson A, Xue H, Kellman P, Ugander M. Females have higher myocardial perfusion, blood volume and extracellular volume compared to males – an adenosine stress cardiovascular magnetic resonance study. Scientific Reports. 2020 Dec 25;10(1):10380.

219. Teixeira T, Hafyane T, Stikov N, Akdeniz C, Greiser A, Friedrich MG. Comparison of different cardiovascular magnetic resonance sequences for native myocardial T1 mapping at 3T. Journal of Cardiovascular Magnetic Resonance. 2016 Oct 4;18(1):1–12.

220. Le DE, Bin JP, Coggins MP, Wei K, Lindner JR, Kaul S. Relation between myocardial oxygen consumption and myocardial blood volume: A

study using myocardial contrast echocardiography. Journal of the American Society of Echocardiography. 2002;15(9):857–63.

221. Wilson RF, Wyche K, Christensen B V, Zimmer S, Laxson DD. Effects of adenosine on human coronary arterial circulation. Circulation. 1990;82(5):1595–606.

222. Zhang Q, Werys K, Popescu IA, Biasiolli L, Ntusi NAB, Desai M, et al. Quality assurance of quantitative cardiac T1-mapping in multicenter clinical trials – A T1 phantom program from the hypertrophic cardiomyopathy registry (HCMR) study. International Journal of Cardiology. 2021 Jan;

223. Zhao G, Linke A, Xu X, Ochoa M, Belloni F, Belardinelli L, et al. Comparative profile of vasodilation by CVT-3146, a novel A2A receptor agonist, and adenosine in conscious dogs. Journal of Pharmacology and Experimental Therapeutics. 2003 Oct 1;307(1):182–9.

224. Vasu S, Bandettini WP, Hsu LY, Kellman P, Leung S, Mancini C, et al. Regadenoson and adenosine are equivalent vasodilators and are superior than dipyridamole- a study of first pass quantitative perfusion cardiovascular magnetic resonance. Journal of Cardiovascular Magnetic Resonance. 2013 Sep 24;15(1):85.

225. Rodrigues JCL, Amadu AM, Dastidar AG, Szantho GV, Lyen SM, Godsave C, et al. Comprehensive characterisation of hypertensive heart disease left ventricular phenotypes. Heart. 2016 Oct 15;102(20):1671–9.

226. Arnold JR, Karamitsos TD, Bhamra-Ariza P, Francis JM, Searle N, Robson MD, et al. Myocardial Oxygenation in Coronary Artery Disease. Journal of the American College of Cardiology. 2012;59(22):1954–64.

227. Uren NG, Camici PG, Melin JA, Bol A, De Bruyne B, Radvan J, et al. Effect of aging on myocardial perfusion reserve. Journal of Nuclear Medicine. 1995;36(11):2032–6.

228. Kuijpers D, Janssen CHC, van Dijkman PRM, Oudkerk M. Dobutamine stress MRI. Part I. Safety and feasibility of dobutamine cardiovascular magnetic resonance in patients suspected of myocardial ischemia. Eur Radiol. 2004 Oct;14(10):1823–8.

229. Monmeneu Menadas JV, Lopez-Lereu MP, Estornell Erill J, Garcia Gonzalez P, Igual Muñoz B, Maceira Gonzalez A. Pharmacological stress cardiovascular magnetic resonance: feasibility and safety in a large multicentre prospective registry. European Heart Journal - Cardiovascular Imaging. 2016 Mar 1;17(3):308–15.

230. van Assen M, van Dijk R, Kuijpers D, Vliegenthart R, Oudkerk M. T1 reactivity as an imaging biomarker in myocardial tissue

characterization discriminating normal, ischemic and infarcted myocardium. International Journal of Cardiovascular Imaging. 2019 Jul;35(7):1319–25.

231. Bohnen S, Prüßner L, Vettorazzi E, Radunski UK, Tahir E, Schneider J, et al. Stress T1-mapping cardiovascular magnetic resonance imaging and inducible myocardial ischemia. Clinical Research in Cardiology. 2019 Aug;108(8):909–20.

232. Lubbers DD, Janssen CHC, Kuijpers D, van Dijkman PRM, Overbosch J, Willems TP, et al. The additional value of first pass myocardial perfusion imaging during peak dose of dobutamine stress cardiac MRI for the detection of myocardial ischemia. International Journal of Cardiovascular Imaging. 2008 Jan;24(1):69–76.

233. Gebker R, Jahnke C, Manka R, Hamdan A, Schnackenburg B, Fleck E, et al. Additional value of myocardial perfusion imaging during dobutamine stress magnetic resonance for the assessment of coronary artery disease. Circulation Cardiovascular imaging. 2008;1(2):122–30.

234. Henzlova MJ, Duvall WL, Einstein AJ, Travin MI, Verberne HJ. ASNC imaging guidelines for SPECT nuclear cardiology procedures: Stress, protocols, and tracers. J Nucl Cardiol. 2016 Jun 1;23(3):606–39.

235. Schelbert HR. On the Relativity of Dipyridamole and Dobutamine Flows. J Nucl Cardiol. 2021 Feb 1;28(1):46–9.

236. Barbato E, Bartunek J, Wyffels E, Wijns W, Heyndrickx GR, De Bruyne B. Effects of intravenous dobutamineon coronary vasomotion in humans. Journal of the American College of Cardiology. 2003 Nov 5;42(9):1596–601.

237. Miyashiro JK, Feigl EO. Feedforward control of coronary blood flow via coronary beta-receptor stimulation. Circulation Research. 1993 Aug 1;73(2):252–63.

238. Ghaleh B, Béa M-L, Dubois-Randé J-L, Giudicelli J-F, Hittinger L, Berdeaux A. Endothelial Modulation of β-Adrenergic Dilation of Large Coronary Arteries in Conscious Dogs. Circulation. 1995 Nov 1;92(9):2627–35.

239. Nabel EG, Selwyn AP, Ganz P. Paradoxical narrowing of atherosclerotic coronary arteries induced by increases in heart rate. Circulation. 1990 Mar 1;81(3):850–9.

240. Krivokapich J, Huang S-C, Schelbert HR. Assessment of the effects of dobutamine on myocardial blood flow and oxidative metabolism in normal human subjects using nitrogen-13 ammonia and carbon-11

acetate. The American Journal of Cardiology. 1993 Jun 1;71(15):1351–6.

241. Bartunek J, Wijns W, Heyndrickx GR, de Bruyne B. Effects of Dobutamine on Coronary Stenosis Physiology and Morphology. Circulation. 1999 Jul 20;100(3):243–9.

242. Marwick TH, D'Hondt AM, Mairesse GH, Baudhuin T, Wijns W, Detry JM, et al. Comparative ability of dobutamine and exercise stress in inducing myocardial ischaemia in active patients. Heart. 1994 Jul 1;72(1):31–8.

243. Dagianti Armando, Penco Maria, Agati Luciano, Sciomer Susanna, Dagianti Alessandra, Rosanio Salvatore, et al. Stress echocardiography: Comparison of exercise, dipyridamole and dobutamine in detecting and predicting the extent of coronary artery disease. Journal of the American College of Cardiology. 1995 Jul 1;26(1):18–25.

244. Petropoulakis PN, Pavlides GS, Manginas AN, Vassilikos VS, Cokkinos DV. Intracoronary flow velocity measurements in adjacent stenotic and normal coronary arteries during incremental intravenous dobutamine stress and intracoronary adenosine injection. Catheterization and Cardiovascular Interventions. 1999;48(1):1–9.

245. Brown LAE, Saunderson CED, Das A, Craven T, Levelt E, Knott KD, et al. A comparison of standard and high dose adenosine protocols in routine vasodilator stress cardiovascular magnetic resonance: dosage affects hyperaemic myocardial blood flow in patients with severe left ventricular systolic impairment. Journal of Cardiovascular Magnetic Resonance. 2021 Mar 18;23(1):37.

246. Skopicki HA, Abraham SA, Picard MH, Alpert NM, Fischman AJ, Gewirtz H. Effects of Dobutamine at Maximally Tolerated Dose on Myocardial Blood Flow in Humans With Ischemic Heart Disease. Circulation. 1997 Nov 18;96(10):3346–52.

247. Pelletier-Galarneau M, Ferro P, Patterson S, Ruddy TD, Beanlands RS, deKemp RA. Comparison of myocardial blood flow and flow reserve with dobutamine and dipyridamole stress using rubidium-82 positron emission tomography. J Nucl Cardiol. 2021 Feb 1;28(1):34–45.

248. Wu XS, Ewert DL, Liu YH, Ritman EL. In vivo relation of intramyocardial blood volume to myocardial perfusion. Evidence supporting microvascular site for autoregulation. Circulation. 1992 Feb 1;85(2):730–7.

249. Nickander J, Themudo R, Thalén S, Sigfridsson A, Xue H, Kellman P, et al. The relative contributions of myocardial perfusion, blood volume and extracellular volume to native T1 and native T2 at rest and during

adenosine stress in normal physiology. Journal of Cardiovascular Magnetic Resonance. 2019 Nov;21(1):73–73.

250. Messroghli DR, Moon JC, Ferreira VM, Grosse-Wortmann L, He T, Kellman P, et al. Clinical recommendations for cardiovascular magnetic resonance mapping of T1, T2, T2* and extracellular volume: A consensus statement by the Society for Cardiovascular Magnetic Resonance (SCMR) endorsed by the European Association for Cardiovascular Imaging. J Cardiovasc Magn Reson. 2017;19(1):75–75.

251. Wilson RF, Laughlin DE, Ackell PH, Chilian WM, Holida MD, Hartley CJ, et al. Transluminal, subselective measurement of coronary artery blood flow velocity and vasodilator reserve in man. Circulation. 1985 Jul;72(1):82–92.

252. Bjornsson TD, Mahony C. Clinical pharmacokinetics of dipyridamole. Thromb Res Suppl. 1983;4:93–104.

253. Kuijpers D, Prakken NH, Vliegenthart R, van Dijkman PRM, van der Harst P, Oudkerk M. Caffeine intake inverts the effect of adenosine on myocardial perfusion during stress as measured by T1 mapping. International Journal of Cardiovascular Imaging. 2016 Oct;32(10):1545–53.

254. Piechnik SK, Neubauer S, Ferreira VM. State-of-the-art review: stress T1 mapping—technical considerations, pitfalls and emerging clinical applications. Magnetic Resonance Materials in Physics, Biology and Medicine. 2018 Feb;31(1):131–41.

255. Vasu S, Bandettini WP, Hsu LY, Kellman P, Leung S, Mancini C, et al. Regadenoson and adenosine are equivalent vasodilators and are superior than dipyridamole- a study of first pass quantitative perfusion cardiovascular magnetic resonance. Journal of Cardiovascular Magnetic Resonance. 2013 Sep;15(1):85–85.

256. Johnson NP, Gould KL. Regadenoson Versus Dipyridamole Hyperemia for Cardiac PET Imaging. JACC: Cardiovascular Imaging. 2015 Apr 1;8(4):438–47.

257. Tadamura E, Iida H, Matsumoto K, Mamede M, Kubo S, Toyoda H, et al. Comparison of myocardial blood flow during dobutamine-atropine infusion with that after dipyridamole administration in normal men. Journal of the American College of Cardiology. 2001 Jan 1;37(1):130–6.

258. Jagathesan R, Barnes E, Rosen SD, Foale RA, Camici PG. Comparison of myocardial blood flow and coronary flow reserve during dobutamine and adenosine stress: implications for pharmacologic stress testing in coronary artery disease. J Nucl Cardiol. 2006 May 1;13(3):324–32.

259. Murthy VL, Bateman TM, Beanlands RS, Berman DS, Borges-Neto S, Chareonthaitawee P, et al. Clinical Quantification of Myocardial Blood Flow Using PET: Joint Position Paper of the SNMMI Cardiovascular Council and the ASNC. J Nucl Cardiol. 2018 Feb 1;25(1):269–97.

260. Everaars H, van Diemen PA, Biesbroek PS, Hopman LHGA, Bom MJ, Schumacher SP, et al. Comparison between cardiac magnetic resonance stress T1 mapping and [15O]H2O positron emission tomography in patients with suspected obstructive coronary artery disease. European Heart Journal - Cardiovascular Imaging. 2021 May 13;(jeab073).